ISTANBUL TECHNICAL UNIVERSITY ★ GRADUATE SCHOOL

DEGRADATION OF INDUSTRIAL MICROPOLLUTANTS WITH SULFATE RADICAL–BASED ADVANCED OXIDATION PROCESSES

Ph.D. THESIS

Bahareh MONTAZERI

Department of Environmental Engineering

Environmental Science and Engineering Programme

JUNE 2021

ISTANBUL TECHNICAL UNIVERSITY ★ GRADUATE SCHOOL

**DEGRADATION OF INDUSTRIAL MICROPOLLUTANTS WITH
SULFATE RADICAL–BASED ADVANCED OXIDATION PROCESSES**

Ph.D. THESIS

Bahareh MONTAZERI
(501152711)

Department of Environmental Engineering

Environmental Science and Engineering Programme

Thesis Advisor: Prof. Dr. İdil ARSLAN ALATON

JUNE 2021

İSTANBUL TEKNİK ÜNİVERSİTESİ ★ LİSANSÜSTÜ EĞİTİM ENSTİTÜSÜ

SÜLFAT RADİKAL-BAZLI İLERİ OKSİDASYON PROSESLERİYLE ENDÜSTRİYEL MİKROKİRLETİCİLERİN BOZUNMASI

DOKTORA TEZİ

Bahareh MONTAZERI
(501152711)

Çevre Mühendisliği Anabilim Dalı

Çevre Bilimleri ve Mühendisliği Programı

Tez Danışmanı: Prof. Dr. İdil ARSLAN ALATON

HAZIRAN 2021

Bahareh MONTAZERI, a Ph.D. student of ITU Graduate School student ID 501152711, successfully defended the dissertation entitled "DEGRADATION OF INDUSTRIAL MICROPOLLUTANTS WITH SULFATE RADICAL–BASED ADVANCED OXIDATION PROCESSES", which she prepared after fulfilling the requirements specified in the associated legislations, before the jury whose signatures are below.

Thesis Advisor :   **Prof. Dr. İdil ARSLAN ALATON**   ……………….
Istanbul Technical University

Jury Members :   **Prof. Dr. Tuğba ÖLMEZ HANCI**   ……………….
Istanbul Technical University

        Prof. Dr. Mehmet ÇAKMAKÇI   ……………….
Yildiz Technical University

        Prof. Dr. Süreyya MERIÇ   ……………….
Namik Kemal University

        Doç. Dr. Didem OKUTMAN TAŞ   ……………….
Istanbul Technical University

Date of Submission : 1 May 2021
Date of Defense   : 22 June 2021

v

To those who have lost their lives and loved ones to Covid-19;

FOREWORD

June 2021   Bahareh MONTAZERI
                                                           (Environmental Engineer)

x

TABLE OF CONTENTS

ABBREVIATIONS

2,4-DCA	**:**	2,4-dichloroaniline
3,5-DCP	**:**	3,5-dichlorophenol
Al	**:**	Aluminum
AOP	**:**	Advanced Oxidation Processes
CAs	**:**	Chloroanilines
CPs	**:**	Chlorophenols
DOC	**:**	Dissolved Organic Carbon
DW	**:**	Distilled Water
eV	**:**	electron Volt
Fe	**:**	Iron
H$_2$O$_2$	**:**	Hydrogen Peroxide
HO$^{\bullet}$	**:**	Hydroxyl Radical
HPLC	**:**	High Performance Liquid Chromatography
IPR	**:**	Iprodione
LC-MS	**:**	Liquid Chromatography-Mass Spectrometry
PS	**:**	Persulfate
SO$_4$$^{\bullet-}$	**:**	Sulfate Radical
STS	**:**	Sodium Thiosulfate
SWW	**:**	Synthetic Tertiary Treated Urban Wastewater
TOC	**:**	Total Organic Carbon
UV-C	**:**	Ultraviolet-C
UV-C/PS	**:**	Ultraviolet-C-Activated Persulfate Oxidation Process
WWTP	**:**	Wastewater Treatment Plant
ZVA	**:**	Zero-Valent Aluminum
ZVA/PS	**:**	Zero-Valent Aluminum-Activated Persulfate Oxidation Process
ZVI	**:**	Zero-Valent Iron
ZVI/PS	**:**	Zero-Valent Iron-Activated Persulfate Oxidation Process

LIST OF TABLES

LIST OF FIGURES

xxii

DEGRADATION OF INDUSTRIAL MICROPOLLUTANTS WITH SULFATE RADICAL–BASED ADVANCED OXIDATION PROCESSES

SUMMARY

Occurrence of micropollutants in wastewaters from the industries poses a serious threat to the environment and many of these contaminants are recalcitrant and/or toxic and/or biologically non-degradable. Therefore, the major concern is to treat the wastewater before being discharge into the environment. Among all these industrial micropollutants, in particular 3,5-dichlorophenol (3,5-DCP) from chlorophenols (CPs), 2,4-dichloroaniline (2,4-DCA) from chloroanilines (CAs) and iprodione (IPR) from hydantoins, have been drawn specific attention due to their commercial importance as raw materials, potential toxicity and refractory nature. 3,5-DCP is directly released to the aquatic environment through various waste streams such as wood pulp bleaching processes. 2,4-DCA is extensively used in manufacturing of pigments, optical brighteners and pharmaceutical agents. IPR as a fungicide is used to prevent gray mold on crops; however, its usage has been banned recently by the European Food Safety Authority. Considering the wide spread usage of the above-mentioned micropollutants and their incomplete removal in conventional industrial and urban wastewater treatment plants; they may end up in the aquatic environment, becoming threats to wildlife. Sulfate radicals ($SO_4^{\bullet-}$)-based advanced oxidation processes (AOPs) have demonstrated that they have the potential to be efficiently applied in removing many organic pollutants from wastewater.

In the first part of this study, three persulfate (PS)-mediated AOPs including one homogenous photochemical oxidation processes; ultraviolet-C (UV-C)-activated PS oxidation process (UV-C/PS), and two heterogeneous catalytic oxidation processes; zero-valent iron-activated persulfate oxidation process (ZVI/PS) and zero-valent aluminum-activated persulfate oxidation process (ZVA/PS) were employed in order to investigate the three micropollutants removal in distilled water (DW) and examine the influence of initial PS concentration (0.00 mM-1.00 mM) and pH on the treatment performances. UV-C/PS treatment of 3,5-DCP for all studied PS concentrations resulted in complete 3,5-DCP removal and the 3,5-DCP degradation rate increased by increasing the initial PS concentration which can be explained by an increase in the steady-state concentration of $SO_4^{\bullet-}$ generation in reaction solution. Increasing the initial pH to values more than 7.5, resulted in rapid 3,5-DCP degradation. Maximum 3,5-DCP removal efficiency was as 59% by 120 min ZVI/PS (PS=1.00 mM; pH=5.0); however, complete 3,5-DCP removal was obtained by decreasing pH to more acidic value after 20 min ZVI/PS (PS=0.50 mM; pH=3.0) treatment. ZVA/PS could not provide complete 3,5-DCP removal after 120 min treatment such that for the highest tried PS concentration.(1.00 mM; pH=3.0) resulted in only 31% 3,5-DCP removal. 2,4-DCA degradation by UV-C/PS, at all studied initial PS concentrations and pH values resulted in complete pollutant removal. PS activation with ZVI resulted in complete 2,4-DCA removal for initial PS concentration exceeding 0.50 mM such that after 80 min ZVI/PS (PS=0.75 mM;

pH=5.0) treatment, complete 2,4-DCA was obtained; however, the required time to achieve complete 2,4-DCA with initial PS of 1.00 mM was longer (100 min) most probably as a result of $SO_4^{\bullet-}$ scavenging reaction with excess PS and/or ferrous ion. The highest 2,4-DCA removal (47%) by 120 min ZVA/PS (pH=3.0) treatment was obtained with initial PS concentration of 0.25 mM, below or beyond which the 2,4-DCA removal decreased. 2,4-DCA removal by 120 min ZVA/PS (PS=0.50 mM) treatment increased remarkably from 20% to 89% , when pH decreased from 3.0 to 1.5 suggesting that more acidic pH facilitated effective removal of 2,4-DCA due to ZVA corrosion. Complete IPR removal was achieved by UV-C/PS at all studied initial PS concentrations such that even with low PS (0.03 mM), complete IPR was obtained in 20 min. Increasing initial PS concentration in the range of 0.01 mM to 1.00 mM led to higher $SO_4^{\bullet-}$ concentrations and consequently faster IPR degradation rates. Alkaline hydrolysis of IPR was observed at initial pH of 9.0 and 11.0 during UV-C/PS treatment; however, complex pH effect on IPR degradation rate was observed at neutral and acidic pH values. ZVI/PS (pH=5.0) treatment of IPR, demonstrated that increasing initial PS concentration to more than 0.50 mM, appreciably improved ZVI/PS treatment of IPR. ZVA/PS was an efficient treatment only in IPR degradation such that even low PS concentrations (0.10 mM and 0.25 mM) with initial pH of 3.0 resulted in almost 80% IPR removal after 120 min treatment and for higher PS concentrations, complete IPR was obtained. In both heterogeneous treatments of all three model industrial micropollutants acidic pH values showed a better performance.

Those oxidation processes from treatability of the micropollutants in DW resulted in complete micropollutant removal, were investigated under selected PS and pH conditions to correlate each micropollutant removal with chloride ion (Cl⁻) release, metal ion release, dissolved organic carbon (DOC) removal and PS consumption. Experiments conducted in DW indicated that for all three model industrial micropollutants, complete removals were achieved by UV-C/PS accompanied with dechlorination and appreciable mineralizations. 3,5-DCP was completely degraded by UV-C/PS (PS=0.30 mM; pH=6.3) treatment in 40 min accompanied with 95% DOC removal that was achieved after 120 min treatment. Maximum Cl⁻ concentrations of 3.91 mg/L was obtained after 120 min UV-C/PS treatment of 3,5-DCP corresponding to practically 90% of the highest possible theoretical Cl⁻ release of 4.35 mg/L. Practically complete 2,4-DCA removal was achieved after 10 min UV-C/PS (PS=1.00 mM; pH=6.0); however, with the progress of the treatment, dechlorination and DOC removal were proceeded such that 93% DOC removal and Cl⁻ concentration of 3.64 mg/L were obtained after 40 min treatment. Beyond this treatment time, both DOC removal and dechlorination were practically stopped and remained constant probably due to PS depletion. IPR degradation was accompanied with rapid dechlorination and PS consumption. UV-C/PS (PS=0.30 mM; pH=6.2) treatment was also effective in IPR mineralization; 78% DOC was removed after 120 min treatment and maximum Cl⁻ concentrations of 1.50 mg/L was obtained at the end of the reaction. For all three studied industrial micropollutants, complete/near-complete removals were achieved by ZVI/PS accompanied with iron (Fe) release; however, their mineralizations were partially (21%-50% DOC removal) after 120 min treatment. ZVA/PS was only effective in IPR removal; however poor mineralization was obtained after 120 min treatment.

Treatability of the selected micropollutants was also examined in a synthetic tertiary treated urban wastewater (SWW) during the studied treatments due to the fact that

the presence of different water constituents in the reaction solution may inhibit the oxidation performance. Experimental results of three model industrial pollutants by the selected treatments (UV-C/PS and ZVI/PS) in SWW, revealed complete micropollutant removals; however, their mineralizations were partially and different compared to DW. UV-C/PS treatment of 3,5-DCP in DW that exhibited appreciable mineralization of 3,5-DCP, demonstrated worse treatment performance compared to ZVI/PS when applied in SWW (26% DOC removal and 41% DOC removal in SWW after 120 min treatment by UV-C/PS and ZVI/PS, respectively). Partial mineralizations of 2,4-DCA in SWW by 120 min UV-C/PS and ZVI/PS treatments were obtained as 57% and 35% DOC removals, respectively which were lower compared to DW revealing performance of both treatments decreased in complex medium. The experiments in DW exhibited the superior performance of the UV-C/PS for IPR mineralization (78% DOC removal after 120 min); however, the oxidation performance of UV-C/PS in SWW decreased appreciably and resulted in 24% DOC removal after 120 min. 40% DOC removal after 120 min was observed with ZVI/PS being the most efficient process in SWW. UV-C/PS treatment of all three selected micropollutants, was most negatively affected when apply in SWW most probably due to UV-C light absorption of SWW constituents hindering effective absorption by the target pollutant.

Vibrio fischeri (*V. fischeri*) and *Pseudokirchneriella subcapitata* (*P. subcapitata*) were employed as the organism tests to assess changes in acute toxicity during application of the studied treatments. Responses of the two mentioned test organisms were rather different; higher inhibition rates were observed on *P. subcapitata* than *V. fischeri*. While the percent relative inhibition of the original 3,5-DCP on *P. subcapitata* was almost 20%, the inhibitory effect increased after 80 min UV-C/PS treatment reaching to 47%. After 80 min ZVI/PS treatment of 3,5-DCP, the percent relative inhibition of treated samples on *P. subcapitata* did not change appreciably. The percent relative inhibition of the original 2,4-DCA on *P. subcapitata* was in the range of 20%-28%; however, the inhibitory effect increased and reached 72% after 120 min UV-C/PS treatment. The percent relative inhibition of original IPR samples on *P. subcapitata* was obtained as <10%; however, it reached 56% and 39% after 120 min UV-C/PS and ZVI/PS, respectively. During the application of selected treatments in DW, the genotoxicity of original micropollutants and their AOPs-treated samples were explored using a mutant strain of *Salmonella typhimurium* TA 1535; however, no significant genotoxic effect was observed.

At the final stage of this study, the type and nature of possible evolved degradation products during the selected treatments of three model industrial pollutants in DW were examined by ion chromatography, liquid chromatography and mass spectrometry analysis in order to gain a deeper insight into the formed radical reactions with the target pollutants. Hydroquinone, acetic acid and Cl$^-$ could be detected and quantified in the reaction solution during UV-C/PS and ZVI/PS treatments of 3,5-DCP. Aniline and acetic acid formations were evidenced during UV-C/PS treatment of 2,4-DCA accompanied with dechlorination; however only acetic acid was identified during ZVI/PS. LC analysis confirmed the formation of 2,4-DCA, hydroquinone, acetic acid and formic acids as the major aromatic and aliphatic degradation products of IPR during UV-C/PS while hydroquinone, lactic acid and acetic acid was evidenced for ZVI/PS treatment of IPR.

SÜLFAT RADİKAL-BAZLI İLERİ OKSİDASYON PROSESLERİYLE ENDÜSTRİYEL MİKROKİRLETİCİLERİN BOZUNMASI

ÖZET

Çeşitli endüstrilerden kaynaklanan ve atıksulara karışan mikrokirleticilerin bazı durumlarda zararlı, konvansiyonel arıtmaya dirençli ve/veya toksik davranış göstermeleri, çevresel açıdan çeşitli olumsuz etkilere neden olmakta ve insanların sağlığını ciddi boyutlarda tehdit etmektedir. Bu nedenlerden dolayı endüstriyel mikrokirleticilerin etkin bir şekilde arıtılmaları çevre kirliliği açısından öncelikli bir konu haline gelmiştir. Söz konusu mikrokirleticilerin arasında yer alan klorofenollerden 3,5-diklorofenol (3,5-DCP), kloroanilinlerden 2,4-dikloroanilin (2,4-DCA) ve hidantoin grubu pesitisitlerden iprodion (IPR) un yaygın olarak kullanımları, yüksek üretim miktarları ve toksik/inert yapıları nedeniyle ön plana çıkmıştır.

3,5-DCP kağıt hamuru ağartma işleminden, 2,4-DCA ise pigment, optik ağartıcı ve analjezik ilaç hammaddesi üretiminden kaynaklanan atıksularda mg/L mertebelerinde dahi bulunmaktadır. IPR ise domates, sarımsak, badem, üzüm, çilek ve yabanmersini gibi meyve, sebze ve yemiş mahsullerinde küf kontrolü amacıyla uygulnmakta, IPR üretimi ve kullanımından sulara ve atıksulara önemli konsantrasyonlarda (μg/L-mg/L) karışmaktadır. Kullanımı birkaç sene önce AB ülkelerinde ve Türkiye'de yasaklansa bile, arıtmaya ve bozunmaya dirençli yapısı nedeniyle atıksu ve sularda hala endişe verici konsantrasyonlarda rastlanmaktadır. Yukarıda sayıların endüstriyel aktivitelerden kaynaklanan atıksuların etkin bir şekilde arıtmı için son yıllarda çeşitli İleri Oksidasyon Prosesleri (İOP) uygulanmaya ve mevcut arıtma sistemlerine entegre edilmeye başlanmıştır. İOP arasında yer alan ve sülfat radikali ($SO_4^{\bullet-}$) üretimine dayanan ileri arıtma sistemleri, son zamanlarda su ve atıksularda bulunan toksik, inert ve/veya zor ayrışan, çoğunlukla endüstriyel kaynaklı atıksuların arıtımı için denenmeye başlanmış, konu ile ilgili arıtılabilirlik çalışmaları bilimsel literatürde yerini almıştır.

Doktora çalışmasının kapsamında seçilen üç model endüstriyel mikrokirletici için persülfat aktivasyonuna dayanan iç İOP kapsamlı bir şekilde araştırılmışt, söz konusu sülfat radikali üretimi bazlı İOP için ayrıtılı arıtılabilirlik, akut ve genotoksik etki ile ayrışma (ileri oksidasyon) ürünleri analizleri gerçekleştirilmiştir.

Deneysel çalışmanın ilk aşamasında, seçilen üç adet persülfat (PS)-bazlı İOP- bunlar; kısa ultraviyole (UV-C) ışıma ile aktive edilmiş PS'ın kullanıldığı bir homojen fotokimyasal İOP, ayrıca sıfır değerlikli demir (ZVI) ve sıfır değerlikli alüminyum (ZVA) ile aktive edilmiş PS'ın kullanıldığı iki tane heterojen kataktik oksidasyon prosesi- söz konusu model kirleticilerin saf sudaki çözeltileri üzerinde uygulanmıştır. Bu aşamada, söz konusu İOP'nin farklı pH değerlerinde (heterojen katalitik oksidasyon prosesleri için asidik pH değerleri çalışılmıştır) ve PS konsantrasyonlarında (0.0 -1.0 mM) hedef model mikrokirletici üzerindeki giderim verimleri ve hızları araştırılmıştır. Bu çalışma aşamasında, çözünmüş organik karbon

(ÇOK) değerleri ile Fe, Al ve Cl salınımıları da ölçülmüştür. Yapılan arıtılabilirlik çalışmaların sonucunda UV-C/PS fotokimyasal arıtma prosesinin pH değerlerine genel olarak fazla hassas olmadığı, PS konsantrasyonunun arttırılmasının mikrokirletici giderim verim ve hızlarınına olumlu etkisi olduğu anlaşılmıştır. Yüksek pH değerlerinde (pH = 9 ve 11) IPR hidrolizi ile doğrudan bozunma gözlenmiştir. ZVI/PS heterojen katalitik oksidasyon prosesi ile başarılı mikrokirletici giderimi elde ediliken, ZVA/PS heterojen katalitik oksidasyon prosesi ile seçilen çalışma aralıklarında her üç model mikrokirleticileri de %100 oranında giderilememiştir. Giderim hızları ve verimlerinde reaksiyon çözeltileri pH=5'ten pH=3'e düşürüldüğünde önemli bir iyileşme gözlenmiştir. Yapılan Cl analizleri, homojen fotokimyasal arıtma ile mikrokirletici giderimine paralel olarak yapıdan hızlı bir şekilde klorün ayrıldığını (oksidasyonla birlikte deklorinasyon) göstermiştir. Heterojen katalitik oksidasyon deneylerinde ise Fe ve Al salınım hızlarının, mikrokirletici arıtma performansı ile orantısal olarak arttığı görülmüştür. Mikrokirletici gideriminin yüksek olduğu arıtma deneylerinde (örneğin UV-C/PS) ÇOK giderim verimlerinin de oldukça yüksek olduğu (%60'a varan mertebeler) görülmüştir. ÇOK giderimleri, seçilen sülfat radikali bazlı İOP için 120 dk.lık bir arıtma süresinin sonunda %20-60 aralığında bulunmuştur.

Seçilen üç model mikrokirleticinin arıtılabilirliği ayrıca sentetik evsel atıksu (SWW) numuneleri hazırlanarak daha karmaşık bir su matrisinde incelenmiştir. Yapılan deneysel çalışmalar, UV-C/PS ve ZVI/PS arıtma prosesleri ile her üç mikrokirleticinin SWW ortamında da tamamen giderilebildiği, ÇOK giderimlerinin ise saf sudaki deneylerden farklı sonuçlandığını (azaldığı) göstermiştir. Her durumda UV-C/PS homojen fotokimyasal oksidasyon sisteminin heterojen katalitik oksidasyon proseslerine göre SWW matrisinden daha fazla olumsuz etkilendiği anlaşılmıştır.

Seçilen mikrokirleticlerin PS-bazlı İOP ile arıtma öncesi ve sonrasında gösterdikleri ekotoksikolojik etkileri sınamak üzere, deniz fotobakterisi *Vibrio fischeri* (*V. fischeri*) ve yeşil tatlısu mikroyosunu *Pseudokirchneriella subcapitata* (*P. subcapitata*) organizmaları ile akut toksisite, *Salmonella typhimurium* TA 1535 suşunun mutantı ile genotoksisite biyodeneyleri sırası ile SWW ve saf su ortamında gerçekleştirilmiştir. SWW ortamında yürütülen akut toksisite deneylerinde, seçilen organizmaların gösterdikleri tepki (% bağıl inhibisyon değerleri), model mikrokirleticiye ve arıtma prosesine göre farklılık göstermiş, toksik etki 3,5-DCP için %20 değerinden %72 değerine yükselirken, 2,4-DCA ve IPR arıtımı sırasında daha az artış (sırası ile %50 ve %60 mertebelerine yükseliş) göstermiştir. Genel olarak *P. subcapitata, V. fischeri* test organizmasına göre daha büyük hassasiyete (daha fazla akut toksik etkiye) neden olmuştur. Her üç model mikrokirletici için de arıtma öncesinde veya sonrasında *Salmonella typhimurium* TA 1535 suşunun kullanıldığı biyodeneylerde genotoksik bir etki görülmemiştir.

Deneysel çalışmanın son aşamasında, homojen fotokimyasal ve heterojen katalitik sülfat radikali üretimine dayanan, PS-bazlı İOP sırasında meydana gelen ayrışma (ileri oksidasyon) ürünlerinin türü ve konsantrasyonları tespit edilmiştir. Bunun için iyon kromatografi, likit kromatografi ve kütle spektrometrisi analizleri gerçekleştirilmiştir. 3,5-DCP'ün UV-C/PS ve ZVI/PS prosesleri ile arıtımında hidrokinon ve asetik asit bulunurken, 2,4-DCP'in UV-C/PS ve ZVI/PS prosesleri ile arıtımında sırası ile klorür, anilin, asetik ve formik asit saptanmıştır. IPR model kirleticisinin UV-C/PS prosesi ile arıtımında 2,4-DCA, hidrokinon, asetik ve formik

asit bulunurken, ZVI/PS ile arıtımında hidrokinon, laktik ve asetik asit tespit edilmiştir.

1. INTRODUCTION

Over the last few decades, the occurrence of micropollutants in the aquatic environment has become a global issue of increasing concern due to their potential harmful effects on health and the environment (Luo et al, 2014; Schwarzenbach et al, 2006). Around 300 million tons of synthetic compounds annually used in industrial and consumer products partially end up natural waters. Additional pollution comes from diffuse sources (agriculture), where 140 million tons of fertilizers and million tons of pesticides are applied each year (Schwarzenbach et al, 2006).

Micropollutants can be released into water bodies as a result of incomplete removal in conventional wastewater treatment plants as well as urban and agricultural run-offs (Miklos et al, 2018). Conventional wastewater treatment plants are designed to control a wide-ranging of substances, such as particulates, nutrients, carbonaceous substances and pathogens. Although these substances can be efficiently and consistently eliminated, the removal of micropollutants is often incomplete and insufficient (Luo et al, 2014). As a result, micropollutants are frequently released directly into receiving water bodies. Micropollutants are commonly present in waters at trace concentrations, ranging from a few ng/L to several μg/L (Luo et al, 2014) and the low concentration and diversity of micropollutants not only complicate the associated detection and analysis procedures but also create challenges for water and wastewater treatment processes (Song et al, 2017). Micropollutants consist of a vast and expanding array of anthropogenic and natural substances such as pharmaceuticals, personal care products, steroid hormones, industrial chemicals, pesticides and many other emerging compounds (Luo et al, 2014). Among these micropollutants industrial pollutants as well as and pharmaceutical compounds are most frequently detected pollutants in water supplies (Deblonde et al, 2011; Rodríguez-Delgado et al, 2016).

Chlorophenols (CPs), chloroanilines (CAs) and hydantoins as three main industrial micropollutants groups deserve special attention due to their high production/consumption rates. CPs have been widely employed in many industrial

processes as synthesis intermediates or as raw materials in the manufacturing of herbicides, fungicides, pesticides, insecticides, pharmaceuticals and dyes (Benitez et al, 2000). CAs are commonly formed during textile, dye and leather manufacturing processes and herbicide degradation(Liang et al, 2013). Hydantoins mainly been considered as anticonvulsant agents in pharmaceutical industries. For agricultural applications, hydantoins derivatives are being used as fungicides, herbicides and plant growth regulators (Shimizu, 1986). Due to worldwide use in industry and incomplete removal in the natural environment and conventional engineered treatment systems, the above-mentioned contaminants are continuously being discharged from wastewater treatment plants to the aquatic environment.

The occurrence of these micropollutants in the aquatic environment has been frequently linked with a number of negative effects, including short-term and long-term toxicity and antibiotic resistance of microorganisms (Luo et al, 2014). For example, CPs can inhibit the activity of nitrifiers in activated sludge treatment systems rendering their removal by conventional wastewater treatment plants rather inefficient (Kimura et al, 2016).

Considering the above mentioned issues, the efficient treatment of these micropollutants is a challenging task to protect human health and the environment. Advanced oxidation processes (AOPs) have been widely applied to degrade organic pollutants into less complex by-products and eventually mineralize into CO_2, H_2O and inorganic ions for many years (Du et al, 2020; Miklos et al, 2018; Wang and Zhuan, 2020). AOPs are based on the in situ formation of reactive species (free radicals) for the oxidation of a wide range of organic compounds. This includes processes based on hydroxyl radical ($HO^{\bullet}$), which constitute the majority of available AOPs; however, also processes rely on other oxidizing species such as sulfate radicals ($SO_4^{\bullet-}$) (Miklos et al, 2018). Although $HO^{\bullet}$ have proven to be capable of efficiently oxidizing industrial micropollutant (Apak and Hugül, 1996; Basu and Wei, 1998; Miklos et al, 2018), $SO_4^{\bullet-}$ are more selective oxidants than $HO^{\bullet}$ and also like $HO^{\bullet}$ have a strong oxidizing power (Lutze et al, 2015). Over the last few decades, significant research and development attention has been paid to $SO_4^{\bullet-}$-based processes typically generated from persulfate (PS) or peroxymonosulfate (PMS) (Anipsitakis and Dionysiou, 2004; Anipsitakis et al, 2006; Kolthoff and Miller, 1951; Wacławek et al, 2017). Most commonly, PS can be applied to generate

SO$_4^{\bullet-}$ by either homogeneous or heterogeneous activation. PS can be activated via heat (Tan et al, 2012), transition metals (Nie et al, 2015), UV light (Chen et al, 2016), metal oxides, transition metal ions and zero-valent metals (Li et al, 2017; Zhou et al, 2018) or other means, forming SO$_4^{\bullet-}$. Although SO$_4^{\bullet-}$ are capable of decomposing and or degrading even the non-biodegradable/recalcitrant organic compounds, major limitation of their full-scale have not been overcome yet (Rodríguez-Chueca et al, 2019); their capital and operating costs are still fairly high. Even in some cases the oxidation products are more toxic than the original pollutants (Lu et al, 2017; Rizzo, 2011). As a result, the control and optimization of AOPs remains a serious challenge, in particular for industrial wastewater treatments applications.

1.1 Aim of Study

There has been an ever-growing concern regarding the significant amount of refractory and/or toxic organic compounds associated with industrial wastewater; especially chloroaromatic compounds such as CPs, CAs, and so on that are well-known for their long persisting in the aqueous environment, their potential of toxicity and/or low rates of biodegradability. For these reasons, effective treatment of these micropollutants from industrial wastewater is necessary before being discharge into receiving water. Over the last years, SO$_4^{\bullet-}$-based AOPs have gain notable attention due to their high efficacy in degrading of a wide variety of recalcitrant compounds. Considering the necessary need to remove harmful micropollutants from industrial wastewater by effective treatments, the present study was aimed at investigating the potential of one homogeneous photochemical oxidation process named ultraviolet-C (UV-C)-activated PS oxidation process (UV-C/PS) and two heterogeneous catalytic oxidation processes including zero-valent iron-activated persulfate oxidation process (ZVI/PS) and zero-valent aluminum-activated persulfate oxidation process (ZVA/PS) for removal of three chloroaromatic compounds named 3,5-dichlorophenol (3,5-DCP), 2,4-dichloroaniline (2,4-DCA) and iprodione (IPR), being chosen as representatives of CPs, CAs and hydantoins, respectively. The oxidation systems were selected from different types (one homogeneous photochemical and two heterogeneous catalytic oxidation processes) since each oxidation type offers its own advantages; photochemical oxidation process have demonstrated more efficient

pollutant and organic carbon removals while employing heterogeneous catalytic oxidation processes would enable catalyst separation and reuse in real treatment applications. To the best author's knowledge the removal of the above mentioned model industrial micropollutants from aqueous phase by $SO_4^{\bullet-}$-based AOPs has not been explored up to now.

The first part of study was devoted to treatability investigation of each micropollutant in pure water (distilled water; DW) under different operating condition. Those experiments resulted the highest target pollutants removal during specific treatment time, were selected to correlate each pollutant removal with several important environmental process parameters (such as dissolved organic carbon (DOC), PS consumption and etc.). Owing to the fact that presence of different water constituents (organic as well as inorganic substances) in the reaction system may change dramatically the performance of selected treatments, it is imperative to examine their performance before being applied to real wastewater matrices. Therefore in the second part of study, the efficiency and performance of selected processes from treatability experiments in DW (baseline experiments) were investigated in a synthetic tertiary treated urban wastewater (SWW) under selected conditions.

It should be taken into account that the ability of AOPs to structurally transform a chemical leads to the potential contaminant with new chemical toxicity; therefore there is always the probability of decomposed compounds/intermediates that could have more toxic potential compared to the original/parent pollutant. Consequently, toxicity tests as integral tools can be employed in order to examine the ecotoxicologically safety of a treatment process. Hence, one stage of study was aimed to examine the toxic potency of the original pollutants and their possible evolved intermediates during the selected treatments.

Furthermore, during the application of AOPs, the main concern, relates to the formation of various intermediates as a consequence of the formed radicals that may trigger complex reaction pathways. Therefore, during the treatments, the disappearance of the original industrial pollutant may not imply that the treatments are efficient and hence further measurements such as some conventional environmental parameters including DOC, metal ion content (in case of catalytic treatments) as well as investigation of type and nature of possible evolved

4

degradation products can be conducted to assess the efficiency and the safe use potential of the treatments. Hence, eventually at the final stage of study, possible evolved degradation products of three model industrial micropollutants through selected treatments from baseline experiments were examined by LC analysis.

1.2 Scope of Study

As aforementioned, the main objective of this study was to investigate the potential of three PS oxidation processes for removal of three model industrial pollutants. For this purpose, baseline experiments carried out in DW spiked with 2 mg/L each industrial micropollutant separately to investigate its removal under varying treatment conditions such as different initial PS concentration (0.00-1.00 mM) and pH at fixed reaction duration of 120 min. Although the selected initial concentration of each model industrial pollutant is appreciably higher than environmentally relevant concentrations being mostly reported in literatures (μg/L or ng/L), this concentration was chosen to ensure accurate analytical, kinetic and further toxicological assessments of each selected pollutant. The effect of process parameters (PS and pH) on performance of each treatment was assessed on the basis of each pollutant removal. Important environmental process parameters such as PS consumption, chloride ion release (Cl⁻) (due to the presence of chlorine atom in molecular structure of all three model industrial pollutants), DOC and iron (Fe)/aluminum (Al) release (in case of catalytic heterogeneous experiments) were also followed during the selected treatments of each model industrial pollutant to provide more information about major process parameters.

In the second part of this study, each model industrial pollutant removal in SWW was investigated through selected treatments from baseline experiments to elucidate its treatability and detoxification behavior in a more complex urban effluent matrix bearing a variety of organic and inorganic compounds that may influence the performance of selected treatments. It should be noted that although employing AOPs may result in appreciable target industrial pollutant removal, there is always a possibility for generation of more toxic intermediates than the parent pollutants. Detection and identification of each of these intermediates and assessment of their potential impact on human health are neither feasible nor practical. Bioassays have unique potential to evaluate water quality, independent of specific structural nature

of putatively present pollutants. Therefore, in the next stage in order to question the ecotoxicological safety of the selected treatments, changes in acute toxicity towards marine photobacteria *Vibrio fischeri* (*V. fischeri*) and the green microalgae *Pseudokirchneriella subcapitata* (*P. subcapitata*) were followed in the original and treated SWW spiked with 2 mg/L 3,5-DCP, 2,4-DCA and IPR separately. Since acute toxicity tests give preliminary idea about the inhibitory effect of three model industrial micropollutants and their degradation products, it should always be complemented by another bioassay targeting the genotoxic potency of the original micropollutants and their evolved intermediates. Therefore, in order to provide a complete toxicological study, the genotoxicity of original micropollutants and their evolved intermediates was assessed using standard genotoxicity assays, *Salmonella typhimurium* TA 1535 (*S. typhimurium* TA 1535) reverse mutation assay (Ames test).

Furthermore, it was particularly aimed at quantifying evolving (aromatic and aliphatic) degradation products via liquid chromatography (LC) in order to establish the degradation mechanism for the selected treatments of each industrial pollutant. For this purpose, changes in several degradation products expected from selected treatments (UV-C photolysis, UV-C/PS and ZVI/PS) of these model industrial pollutants were quantified and followed by LC analysis to propose a degradation pathway for each model industrial pollutant.
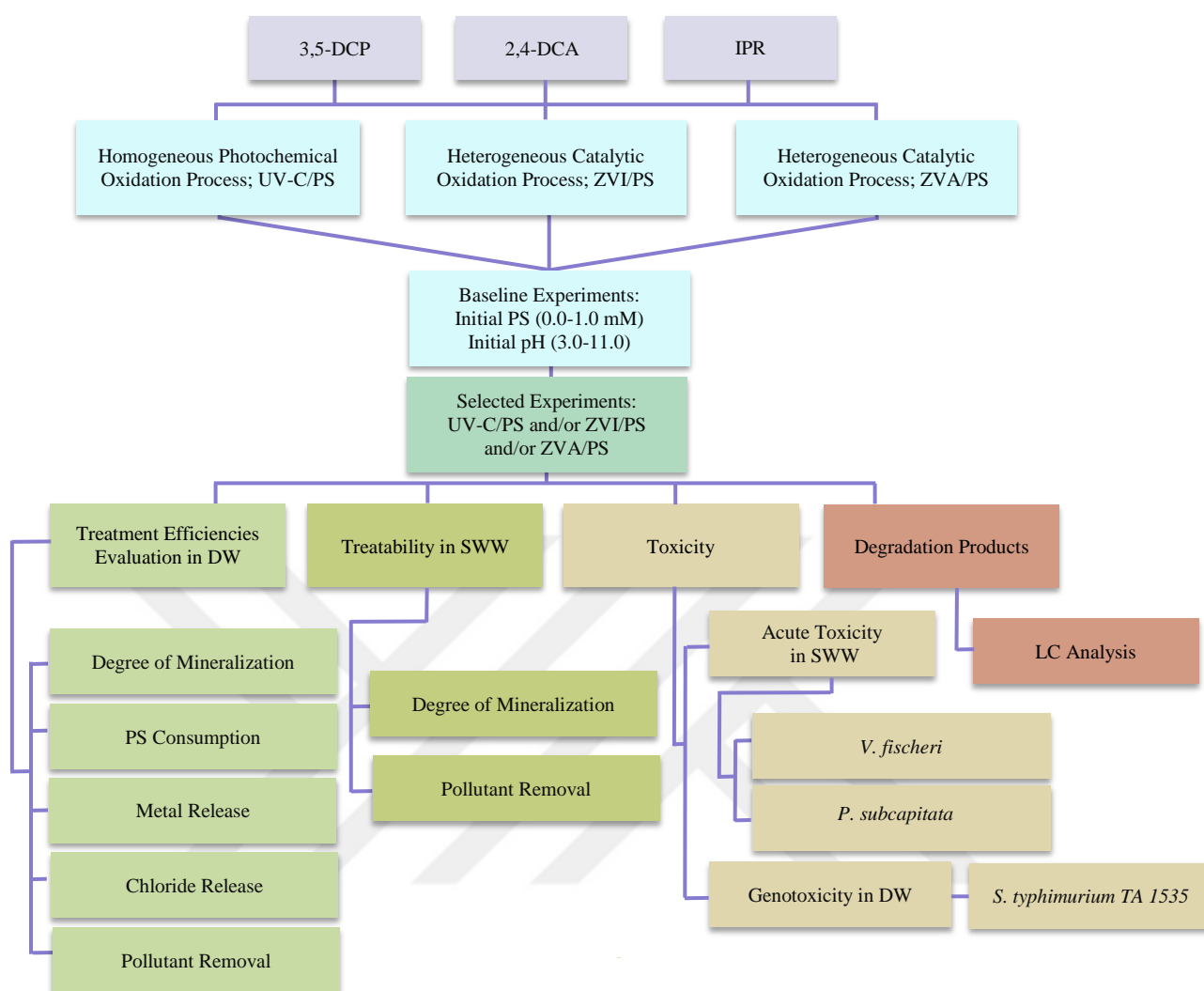
Figure 1.1 : The schematic diagram representing the scope of study.

2. THEORETICAL BACKGROUND

2.1 Industrial Micropollutants

As mentioned before, among a wide range of these ubiquitous micropollutants, most frequently types of them detected in water supplies are industrial pollutants as well as and pharmaceutical compounds (Deblonde et al, 2011; Rodríguez-Delgado et al, 2016). Generally, micropollutants can represent serious health hazards due to their moderate bioaccumulation and high toxicity. As a result, industrial wastewater treatments are necessary to eliminate potential toxic industrial pollutants but their efficiency are not yet clearly known (Deblonde et al, 2011).

2.1.1 Chlorophenols

CPs consist of the benzene ring, hydroxyl group (–OH) and one or more covalently bonded chlorine atoms. All CPs are solid at room temperature except 2-CP, which is a liquid. Generally, CPs dissolve weakly in water and their water solubility decreases with increasing number of chlorine atoms in their molecular structures (Czaplicka, 2004). CPs are considered weakly acidic; their acidity is slightly lower than that of phenols.

CPs are introduced into the environment as a result of several man-made activities and their share of world market are estimated around 10^8 kg annually (Czaplicka, 2004). As an intermediate, CPs are formed during wood pulp bleaching processes. CPs have been used as preservative agents for wood, paints, vegetable fibers and leather and as disinfectants because of their broad-spectrum antimicrobial properties, (Pera-Titus et al, 2004). The large scale production and heavy consumption of CPs and their derivatives generate wastewaters that contain these substances at high concentration.

In general, the fate and transport of a substance in the environment strictly rely on the value of the dissociation constant (K_a) which is related to the structure of the chemical compound as well as the partition coefficient (K_{ow}) in the octanol-water
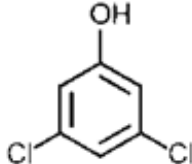
two phase system (Czaplicka, 2004; Pera-Titus et al, 2004). The dissociation constant of a CP as pK_a (pK_a=-log K_a) decreases, with the increase in chlorine atoms number in a molecule while their K_{ow} strongly increase with the number of chlorine atoms (Czaplicka and Kaczmarczyk, 2006). They can represent serious health hazards due to their moderate bioaccumulation and high toxicity, which increase with the increment of chlorination (Fattahi et al, 2007; Rodriguez et al, 1996).

Volatilization can be a major removal mechanism for those compounds with high vapor pressure and low solubility. Ionic strength, pressure, temperature, chemicals reaction, mixing the interfacial area available for transport and concentration can be considered as other factors influencing the rate and extent of volatilization (McCarty, 1980; Smith et al, 1980). Two useful indicators of a compound's potential for volatilization are the Henry's law constant and vapor pressure (McCarty, 1980; Smith et al, 1980). Smith et al. (1980) reported that highly volatile compounds typically have Henry's law constants greater than 4.6×10^{-3} m^3 atm/mole) and McCarty (1980) found compound with constant greater than 10^{-3} m^3 atm/mole were successfully removed by air stripping at 3000 m^3 air/m^3 water. Therefore based on the above mentioned, volatilization from water cannot be considered as an important process, except under condition of intense air-water contact. Due to most of CPs are toxic and hardly biodegradable, conventional wastewater treatment plants are not capable remove these pollutants from industrial wastewater and they are continuously being discharged into the receiving water bodies of the aquatic environment. These pollutants are subject to legislative control by the US Environmental Protection Agency (US EPA, 1998) and the Europe Union (EU) Directives. CPs are listed as "priority pollutants" by the US EPA in the Clean Water Act and by the EU in 2455/2001/EC (EC, 2001).

3,5-DCP was chosen as one of the three model industrial pollutants representing CPs. Wood pulp bleaching processes (Paasivirta et al, 1985) and the chlorination processes of water treatment (Sithole and Williams, 1986) result in direct release of 3,5-DCP to the environment through various waste streams. 3,5-DCP may be also formed and released to the environment via biodegradation in sediment of tri-, tetra- and penta-CPs through dechlorination process (Villemur, 2013). The structural formula and some physicochemical properties of 3,5-DCP are shown in Table 2.1.

3,5-DCP has a vapor pressure of 0.00842 mm Hg (Tugcu et al, 2017) and Henry's law constant of 2.4×10^{-7} m^3 atm/mole at 25 ºC (Mitchell et al, 2013; Trapp et al, 2000). Hence, this compound cannot be considered as highly volatile compound. 3,5-DCP has log K_{ow} of 3.62 and it does not sorb strongly (Trapp et al, 2000). 3,5-DCP exhibits a range of toxic mode of actions in eukaryotes, whereof it is used in herbicide production due to its quite high toxic potency to aquatic primary producers. 3,5-DCP can cause growth inhibition in primary producers and as a consequence of its toxic properties, it is normally used as positive controls in toxicity testing guidelines and studies with algae and aquatic plants (Xie et al, 2018).

Table 2.1 : Structural formula and selected physicochemical properties of 3,5-DCP.

3,5-DCP	
Molecular formula	$C_6H_4Cl_2O$
Molecular weight (g/mol)	163
TOC equivalent (g TOC/g 3,5-DCP)	0.44
pK_a[a]	8.14
Log K_{ow}[b]	3.62
Water solubility (g/L)	5.4 (25 ºC)
Structural formula	

[a](Dean, 1997).
[b](Mitchell et al, 2013).

The IC$_{50}$ of 3,5-DC (IC$_{50}$ is defined as the concentration of a substance required for 50% inhibition) to *Chlorella vulgaris* was 1.477 mg/L (Yen et al, 2002). The LC$_{50}$ of 3,5-DCP (LC$_{50}$ is defined as lethal concentration is the concentration of a substance that will lead to the deaths of 50% of the population) to *Daphnia pulex* and *Tilapia zilli* were reported 2.09 mg/L and 1.123 mg/L, respectively (Yen et al, 2002). The position of chlorine on the benzene ring seems to affect the toxicity CPs. When

position 3 and 5 or position 3 and 4 on the phenol ring was substituted with chlorine atoms such as 3,5-DCP, the chemicals were more toxic to *Daphnia pulex* and *Tilapia zilli* (Yen et al, 2002).
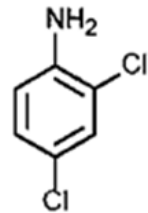
2.1.2 Chloroanilines

CAs have been among the most important industrially produced amines. CAs as chlorinated derivatives of aniline are formed as intermediates of manufacture of dyes pesticides, dyes, plastic and drugs (Zhang et al, 2011). CAs are introduced into the environment directly as industrial effluents and indirectly as biodegradation of broadly used herbicides, like acylanilide and phenylcarbamate (Cravedi et al, 2001; Padmanabhan et al, 2006). CAs can also be formed during surface water disinfection employing chlorine in the presence of high ammonia concentrations (Jurado-Sanchez et al, 2012). The analysis of the data obtained from a drinking water treatment plant in Spain revealed that 3-CA and 3,4-DCA were identified and quantified at low levels (up to 18 ng/L) in raw water (prior to any treatment) but their concentrations increased around 10 times after chloramination such that nine new amines compounds were formed for the first time including 4-CA, 2,4,6-trichloroaniline (TCA), 3,4,5-TCA (Jurado-Sanchez et al, 2012). CAs including all three mono- CA, 2,3-DCA, 2-chloro-4-methylaniline, 3,4-DCA, and 2,6-DCA, have been detected in industrial wastewaters in concentrations as high as 11.9 mg/L (Lacorte et al, 1999). Jen et al. (2001) even measured 2-CA concentration of 230 mg/L in wastewater from a polymer manufacturer (Jen et al, 2001). As a result of their incomplete removal in conventional industrial wastewater treatment plants; they may end up in the aquatic environment. For example, German waters load with all three isomeric mono- CAs was estimated at about 7 metric tons per year; measured concentrations of them in Rhine river and its tributaries were in a range of about 0.1 µg/L to 1 µg/L (Könnecker et al, 2003).

Intensive applications of CAs in agriculture and industries result in their accumulation in the environment such as agricultural water/soil, industrial wastewater as well as sludge (Hongsawat and Vangnai, 2011) and consequently impose serious risk to aquatic lives. Research demonstrated that several aromatic amines could cause damage to DNA and were highly toxic to aquatic life (Katsumata et al, 2012). CAs are suspected carcinogens and are highly toxic to aquatic life (Padmanabhan et al, 2006). Due to their toxicity and persistence in aquatic

environments (Boon et al, 2001), they are classified as the priority pollutants (Federal Register, 1979). 2,4-DCA was selected as the second model industrial pollutant from CAs and its structural formula and some physicochemical properties are shown in Table 2.2. 2,4-DCA is widely used in manufacturing of pigments, optical brighteners and pharmaceutical agents. In agriculture, it is mainly employed in manufacturing of fungicides, manufacturing of herbicides and manufacturing of insecticides (Kádár et al, 2001; Miller et al, 1980; Pascal-Lorber et al, 2003). As a result of its widespread usage in industries, this compound is one of the most environmental pollutants, particularly in wastewater (Kilemade and Mothersill, 2000). 2,4-DCA was frequently found in surface water, which would be harmful to aquatic life and human health (Cravedi et al, 2001). For instance, 2,4-DCA was detected in Rhine and Meuse river water samples with maximum concentrations 0.15 µg/L and 0.32 µg/L, respectively (Wegman and De Korte, 1981).

Table 2.2 : Structural formula and selected physicochemical properties of 2,4-DCA.

2,4-DCA	
Molecular formula	$C_6H_5Cl_2N$
Molecular weight (g/mol)	162
TOC equivalent (g TOC/g 2,4-DCA)	0.44
pK_a[a]	2.50
Log K_{ow}[a]	2.78
Water solubility (g/L)	<1 (25 ºC)
Structural formula	

[a](Causserand et al, 2005).
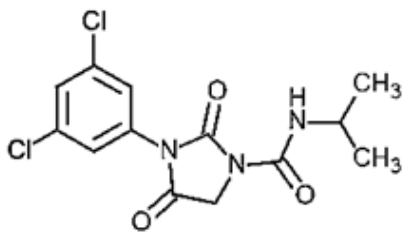
2,4-DCA has a vapor pressure of 0.015 mm Hg at 25 ºC and Henry's law constant of 1.6×10^{-6} m^3 atm/mole (Meylan and Howard, 1991). This Henry's law constant

indicates that 2,4-DCA is not very volatile. Based on relatively low values for Henry's law constant and the K_{ow}, it can be concluded that sorption and evaporation are unlikely to be important loss processes for 2,4-DCA. Hydrolysis of 2,4-DCA is not thought to be of any significance since the covalent bond of a substituent attached to an aromatic ring is resistant to this process because of the high negative charge-density of the aromatic nucleus (Crossland, 1990). A bioconcentration factor of 94.7 suggests bioconcentration in aquatic organisms is moderate (Cravedi et al, 2001; Pascal-Lorber et al, 2003). 2,4-DCA is known to be toxic to fish (Schafers and Nagel, 1991) and mammals (Valentovic et al, 1995). Nevertheless, scarce data exist on the metabolic fate of this chemical in fish. The EC_{50} of 2,4-DCA (EC_{50} is defined as the concentration of a substance that gives 50% maximal response) to *Daphnia magna* was 0.604 mg/L for 48 h contact time (Ashauer et al, 2011).

2.1.3 Hydantoins

Hydantoin is a five-membered ring heterocyclic compound with the formula $CH_2C(O)NHC(O)NH$ (Shimizu, 1986). In general, hydantoins refers a class of chemical compounds with the same ring structure as the parent. The basic chemistry of the hydantoin was studied by Meusel and Gütschow (2004). Hydantoins are weak acids which owe their acidic character to dissociation of the proton bonded to the 3-nitrogen atom. Hydantoin with the dissociation constant of $pK_a=9.12$, acts as a weak acid of approximately the same strength as hydrocyanic acid or phenol (Meusel and Gütschow, 2004). In pharmaceuticals, derivatives of hydantoin such as phenytoin and fosphenytoin are used as anticonvulsants in the treatment of seizure disorders (Meusel and Gütschow, 2004). One of the most important of hydantoins derivatives is IPR which has found wide use in agricultural productions as fungicide. IPR, 3-(3,5-dichlorophenyl)-N-isopropyl-2,4-dioxoimidazolidine-1-carboxamide, is a dicarboximide fungicide with protective and curative action, has a significant role in the control of *Sclerotinia, Botrytis, Rhizoctonia* and other fungal diseases in plants. Table 2.3 shows the structure formula and some physicochemical properties of IPR. It is mainly used in agriculture to prevent gray mold on crops, such as strawberries and blackberries (Grabke et al, 2014), grapes (Loutfy et al, 2015), almond (Yi et al, 2003), tomatoes (Cabras et al, 1985; Omirou et al, 2009) and white roots on garlics (Camiletti et al, 2016; Miñambres et al, 2010). IPR is also widely used on golf greens to protect turfgrass form fungal diseases (Strömqvist and Jarvis, 2005).

Table 2.3 : Structural formula and selected physicochemical properties of IPR.

IPR	
Molecular formula	$C_{13}H_{13}Cl_2N_3O_3$
Molecular weight (g/mol)	330
TOC equivalent (g TOC/g IPR)	0.47
Log K_{ow}[a]	3.0
Water solubility (g/L)	0.012 (20 ºC)
Structural formula	

[a](Hepperle et al, 2015)

In the agriculture sector of the US, 930,000 to 1,730,000 pounds of IPR active ingredient were applied annually (US EPA, 1998). In Japan massive fungicide usages have been reported such that the IPR usage amounts gradually increased from 1982 reaching a peak of 203 tons/year in 1990 (Kaonga et al, 2018). IPR has a vapor pressure of 2.7×10^{-7} mm Hg at 25 ºC and Henry's law constant of 9.02×10^{-9} m^3 atm/mole (US EPA, 1998). Due to its relatively low vapor pressure, IPR volatilization is not expected as an important IPR loss process. IPR is relatively mobile in the aquatic and soil environment (US EPA, 1998). IPR is not chemically stable since it is hydrolyzed in the environment, and its relatively low soil adsorption coefficient (K_{oc}; 400 ml/g) results in high soil mobility reaching groundwater (Zhang et al, 2020). Besides, through its application by spray drift, its residues have also been reported in surface waters (Derbalah et al, 2003; Sequinatto et al, 2013). A recent European Food Safety Authority (EFSA) study reported that the EC identified a high long-term risk of IPR to aquatic organisms (EFSA, 2016) and its re-approval was not granted by the EC under regulation 2017/2091 (EC, 2017) and in Turkey as well (Ministry of Agriculture and Forestry, 2018).

2.2 Advanced Oxidation Processes

Chemical contamination of surface waters, mainly due to industrial and agricultural discharges (Cuerda-Correa et al, 2020), is a significant health risk. Although different biological and physicochemical treatments have been reported for industrial pollutants, they could only be removed partially owing to their resistant nature (Cuerda-Correa et al, 2020; Luo et al, 2014). In recent decades, AOPs have been reported extensively for the removal a vast range of micropollutants (Wacławek et al, 2017; Wang and Zhuan, 2020; Wang and Xu, 2012; Yang et al, 2019). In these processes, different reactive species mainly $HO^{\bullet}$ and $SO_4^{\bullet-}$ can decompose the structure of micropollutants (Lee et al, 2021). Under appropriate conditions, AOPs can oxidize recalcitrant/biologically resistant and toxic pollutants through generation of high reactive species (Dewil et al, 2017) although, formation of toxic by-products, poor and partial mineralization can be considered as some limitations associated with AOPs (Cuerda-Correa et al, 2020; Dewil et al, 2017).

The high operating costs related to the consumption of energy and chemicals can be considered as the most important limiting factors for their applicability in full-scale wastewater treatment plants; however, appreciable cost reduction can be obtained by employing these processes as pre-treatment or post-treatment stage for partial oxidation of non-biodegradable/ biologically persistent to form biodegradable reaction intermediates (Mirzaei et al, 2017).

AOPs can be categorized in homogeneous and heterogeneous processes (Figure 2.1) (Amor et al, 2019). The AOPs that use solid catalysts such as TiO_2 and ZnO are denominated heterogeneous processes, and other processes are known as homogeneous processes (Huang et al, 1993). AOPs generally cover O_3, H_2O_2 and PS as oxidants with assistance of light (Yang et al, 2019), catalyst (Xiao et al, 2020), ultrasonic insertion (Chen and Su, 2012) and thermal input(Liang and Su, 2009). O_3, H_2O_2 as conventional oxidants are mostly the source of $HO^{\bullet}$ generation. Recently, PS as an alternative oxidant has been used for the radicalic oxidation of a wide variety of recalcitrant and toxic compounds leading to reducing toxicity and increasing biodegradability (Amor et al, 2019). While employing mere oxidants such as H_2O_2 and PS is inefficient for the degradation/decomposing of high concentration of recalcitrant organic pollutants (Girit et al, 2015; Karci et al, 2012), the

introduction of UV irradiation, transition metals, zero-valent metals and O_3 into the process can effectively boost not only degradation rate but also mineralization rate.

As it can be seen in Figure 2.1, there are several combinations such as Fenton (H_2O_2/Fe^{2+}) (Mirzaei et al, 2017), photo-Fenton ($H_2O_2/UV/Fe^{2+}$) (Goi and Trapido, 2002), H_2O_2 combined with UV light (UV/ H_2O_2) (Lopez-Alvarez et al, 2016), peroxone (O_3/H_2O_2), peroxone combined with UV light (UV/O_3/H_2O_2) (Pérez-Lucas et al, 2020), and O_3/TiO_2 combined with UV light (Rajeswari and Kanmani, 2009). These AOPs cost effective processes and give rise to non-selective active species that can decompose a vast range of recalcitrant chemical compounds.
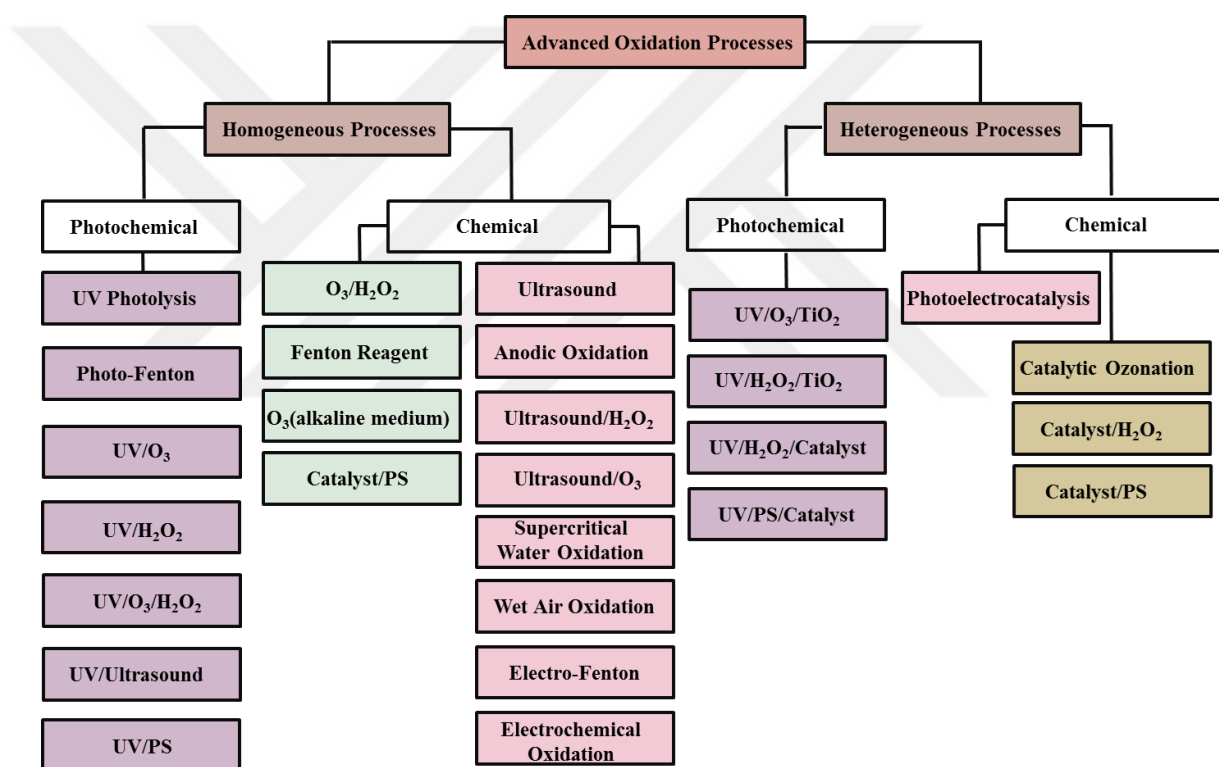
Figure 2.1 : Schematic representation and classification of AOPs.

Other AOPs such as supercritical water oxidation (Chang and Liu, 2007), wet air oxidation (Minière et al, 2018) and those AOPs employing ultrasound (Cravotto et al, 2010) have also been reported to be efficient processes to remove recalcitrant micropollutants. However, required high temperature and pressure by super critical water oxidation and wet air oxidation make these processes a non-viable option in economical point of view. In the same way, ultrasonic irradiation relying on the formation of, growth and subsequent collapse of micropubbles which leads high

energy release, has the drawback of inefficient conversion of energy in producing acoustic cavitation which hinders its scale-up to industrial application (Gogate and Pandit, 2004).

2.3 Sulfate Radical-Based Advanced Oxidation Processes

2.3.1 Definition and general principles

Recently $SO_4^{\bullet-}$-based AOPs have also received increasing attention due to being applied successfully to the treatment of wide range of recalcitrant pollutants from aqueous phase (Kronholm et al, 2000; Liang et al, 2009; Wacławek et al, 2017). $SO_4^{\bullet-}$ is generated mostly via two precursor salts named PS and PMS. PS could be found in the form of three salts for instance potassium, ammonia and sodium (Wacławek et al, 2017). $SO_4^{\bullet-}$ possesses equal or even higher redox potential (E^0=2.5–3.1 eV at room temperature depending on the pH) rather than $HO^{\bullet}$ (E^0=1.8-2.7 eV at room temperature depending on the pH) as well as $SO_4^{\bullet-}$ has longer half-life ($t_{1/2}$=30-40 µs) in comparison to $HO^{\bullet}$ ($t_{1/2}$=10^{-3} µs) (Buxton et al, 1988; Kolthoff and Miller, 1951). Consequently, $SO_4^{\bullet-}$ could be expected to show similar or better capacity in degrading the emerging contaminants.

2.3.2 Persulfate activation methods

The key during PS based oxidation is generation of highly reactive species with a potential to degrade pollutants. This can be achieved mainly by UV-C light, metal oxides, transition metal ions and zero-valent metals, sonolytic and radiolytic activation (Chen and Su, 2012; Chen et al, 2017; Criquet and Leitner, 2011; Li et al, 2015a; Zhou et al, 2018). PS activation involves a series of oxidizing processes through O–O bond-breaking due to its long bond distance (1.497 A˚) and low bond energy (140 kJ/mol) (Wacławek et al, 2017; Xiao et al, 2018).

As mentioned before, $SO_4^{\bullet-}$ is generated mostly via two precursor salts named PS and PMS. Most commonly, PS can be applied to generate $SO_4^{\bullet-}$ by either homogeneous or heterogeneous activation (Wacławek et al, 2017; Xiao et al, 2020).

2.3.2.1 Photochemical

UV-C activation of PS is one of the most direct ways to form $SO_4^{\bullet-}$ wherein one mole of PS undergoes UV-C photolysis (λ=254 nm) and is cleaved into two moles of $SO_4^{\bullet-}$ through the following equation (Dogliotti and Hayon, 1967);

$$S_2O_8^{2-} + h\nu \rightarrow 2SO_4^{\bullet-} \tag{2.1}$$

Maximum quantum yield of the above reaction in neutral solution is unity (Dogliotti and Hayon, 1967; Hori et al, 2005).

2.3.2.2 Zero-valent metals

Zero-valent iron

$SO_4^{\bullet-}$ can be produced by PS activation with assistance of zero-valent iron (ZVI) through the following equations (Hussain et al, 2014; Li et al, 2014a). The use of ZVI has recently received great attention due to their unique surface properties, high reactivity (E^0=-0.44 eV) and expected low impact on the environment considering of Fe's high abundance in the earth crust (Hussain et al, 2012; Li et al, 2014a; Pasinszki and Krebsz, 2020). PS can be activated by ZVI through the following equations;

$$Fe^0 + S_2O_8^{2-} \rightarrow Fe^{2+} + 2SO_4^{2-} \tag{2.2}$$

$$Fe^{2+} + S_2O_8^{2-} \rightarrow Fe^{3+} + SO_4^{2-} + SO_4^{\bullet-}; \; k = 27 \; M^{-1}s^{-1} \tag{2.3}$$

$$Fe^0 + S_2O_8^{2-} \rightarrow Fe^{2+} + 2SO_4^{2-} + 2SO_4^{\bullet-} \tag{2.4}$$

$$Fe_{(surf)}^{2+} + S_2O_8^{2-} \rightarrow Fe_{(surf)}^{3+} + SO_4^{2-} + SO_4^{\bullet-} \tag{2.5}$$
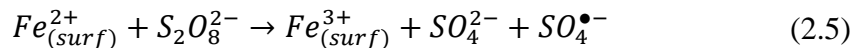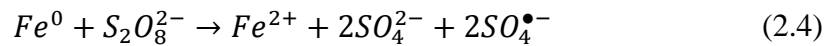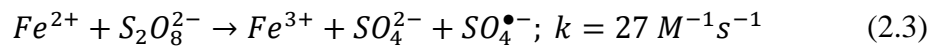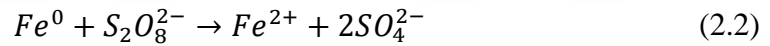
Ferrous ion generation and recycling of ferric ion at ZVI surface (equation 2.6) can overcome the disadvantage of $SO_4^{\bullet-}$ consumption by excessive ferrous ion (equation 2.7) and reduce the precipitation of iron hydroxides during reaction (Fernandez et al, 2004; Li et al, 2017).

$$2Fe^{3+} + Fe^0 \rightarrow 3Fe^{2+} \tag{2.6}$$

$$SO_4^{\bullet-} + Fe^{2+} \rightarrow Fe^{3+} + SO_4^{-2}; k = 4.6 \times 10^9 \; M^{-1}s^{-1} \; (22 \; °C) \tag{2.7}$$
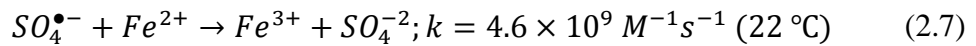
Although $SO_4^{\bullet-}$-based oxidation processes have shown promising results, the number of publications dealing with these oxidation processes are still much lower that for classical AOPs, and various aspects still need to be investigated to fully understand the degradation mechanisms (Dewil et al, 2017; Oller et al, 2011).

$SO_4^{\bullet-}$ react with water at all pH values forming $HO^{\bullet}$ through following equations. At pH<7, $SO_4^{\bullet-}$ are the dominant reactive species; whereas at neutral pH $HO^{\bullet}$ and $SO_4^{\bullet-}$ participate equally in reactions. At alkaline pH values, $HO^{\bullet}$ dominate over $SO_4^{\bullet-}$ in reactions (Kolthoff and Miller, 1951).

$$SO_4^{\bullet-} + H_2O \rightarrow HO^{\bullet} + SO_4^{2-} + H^+ \qquad (2.8)$$

$$SO_4^{\bullet-} + OH^- \rightarrow SO_4^{2-} + HO^{\bullet} \qquad (2.9)$$
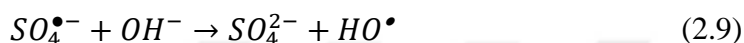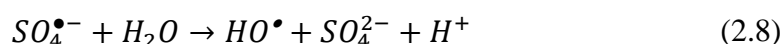
Zero-valent aluminum

Al is found as the most abundant metallic element in the earth's crust (Ren et al, 2018). Recently, zero-valent aluminum (ZVA) has gained increasing attention in the environmental field for contaminant removal due to its unique properties. ZVA acts nicely at acidic conditions (below pH of 4) and has high catalytic activity (Bokare and Choi, 2009; Liu et al, 2011; Nidheesh et al, 2018). $SO_4^{\bullet-}$ can be generated in aqueous phase through the reaction between ZVA and PS (equation 2.10).

$$2Al^0 + S_2O_8^{2-} + 6H^+ + 1.5O_2 \rightarrow 2SO_4^{\bullet-} + 3H_2O \qquad (2.10)$$
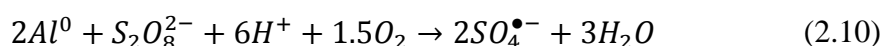
2.3.3 Inefficiency in persulfate oxidative processes

Inefficiency in PS oxidative processes involving radical intermediates can be ascribed to two general mechanisms, nonproductive reactions and radical scavenging (Crincoli et al, 2020). Nonproductive reactions are those reactions that do not yield radicals and consequently lead to oxidant depletion, and radical scavenging are the reactions between radicals and non-target chemical species. For instance, the formed $SO_4^{\bullet-}$ can be scavenged by PS, transition metals such as Fe^{2+} and Co^{2+} present in the reaction medium and $SO_4^{\bullet-}$ (equations 2.11-13) (Huie and Clifton, 1989; Wei et al, 2016; Yu et al, 2004).

$$S_2O_8^{2-} + SO_4^{\bullet-} \rightarrow S_2O_8^{\bullet-} + SO_4^{2-}; \; k = 6.1 \times 10^5 \; M^{-1}s^{-1} \qquad (2.11)$$

$$Fe^{2+} + SO_4^{\bullet-} \rightarrow Fe^{3+} + SO_4^{2-}; \; k = 3 \times 10^8 \; M^{-1}s^{-1} \qquad (2.12)$$

$$SO_4^{\bullet-} + SO_4^{\bullet-} \rightarrow S_2O_8^{2-}; \; k = 4 \times 10^8 \; M^{-1}s^{-1} \qquad (2.13)$$
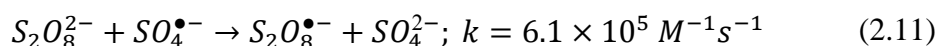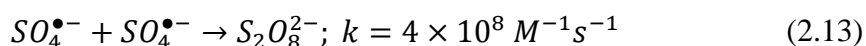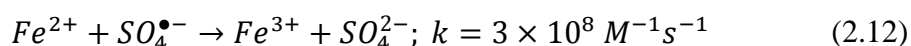
2.3.4 Applications of sulfate radical-based advanced oxidation processes in micropollutant treatments

2.3.4.1 Photochemical

Many scientific literatures have demonstrated that the UV activation of PS can effectively degrade a wide range of micropollutants. Table 2.4 listed the maximum degradations of several micropollutants through UV/PS. As it can be seen in Table 2.4, required PS concentrations for removal of micropollutants change with the types of micropollutant and its initial concentration, which brings the challenge for the treatment of real wastewater.

In the study of Yang et al. (2010), the activation of the three most common oxidant namely PS, PMS and H_2O_2 by UV-C was compared in term of azo dye Acid Orange 7 degradation. In that study, it was demonstrated that Acid Orange 7 could be decomposed under UV-C irradiation; however, its degradation rate was improved nearly 40% with the addition of above mentioned oxidants (Yang et al, 2010). The order of degradation rates of 20 mg/L Acid Orange 7 by employing three activated oxidants, was PS>H_2O_2>PMS (each initial oxidant concentrations were 0.57mM, 2.85 mM and 5.71 mM; and the initial pH values in the presence of PS, PMS and H_2O_2 were 6.3, 3.3 and 6.5, respectively) (Yang et al, 2010). Treatments by UV-C activation of PS and PMS often demonstrate different performance in dealing with different target micropollutants and in most of investigations, UV-C/PS exhibited more excellent organic pollutants oxidation ability than UV-C/PMS (Yang et al, 2019) most probably as a result of the quantum yield of radical formation. The apparent quantum yield for $SO_4^{\bullet-}$ in the UV/PMS system (λ=254 nm) was reported as only 0.52±0.01 at pH of 7 (Guan et al, 2011). In another related study (Mahdi-Ahmed and Chiron, 2014), UV-C/PS (PS=1 mM; pH=7) treatment efficiency of 1.66 mg/L ciprofloxacin was investigated in DW and compared with UV-C/PMS and UV-C/H_2O_2. The most effective process in ciprofloxacin removal was UV-C/PS, followed by UV-C/PMS and UV-C/H_2O_2 but their performances were opposite in wastewater. UV-C/PMS has shown better kinetic performances over UV-C/PS and

UV/H_2O_2 treatments for ciprofloxacin removal in wastewater mainly due to presence of bicarbonate ions which could activate PMS into $SO_4^{\bullet-}$ and due to the higher selectivity in reactivity of $SO_4^{\bullet-}$ with respect to $HO^{\bullet}$ in organic rich matrices (Mahdi-Ahmed and Chiron, 2014).

In another related study (Lau et al, 2007), the UV-C/PS (PS=2 mM) treatment of 18 mg/L butylated hydroxyanisole was investigated at pH values ranging 3 to 11. In that study, the kinetic rate constant for butylated hydroxyanisole degradation was increased in a stepwise manner such that low and high degradation rates of butylated hydroxyanisole were obtained under acidic condition with pH<5 and basic conditions with pH>10, respectively (Lau et al, 2007). After 60 min UV-C/PS (PS=2 mM; pH=7) treatment of butylated hydroxyanisole, complete mineralization of butylated hydroxyanisole and its associated intermediates took place simultaneously (Lau et al, 2007).

Table 2.4 : Recent studies on UV/PS treatments of micropollutants.

Micropollutants	Experimental Conditions	Treatment time (min)	Maximum micropollutant removal (%)	Reference
Sulfamethazine	Initial pollutant concentration=5.57 mg/L $[PS]_0$= 0.2 mM, pH_0=6.5 Irradiation source=low-pressure mercury lamp (15 W) Light intensity=n.d[a] Wavelength=254 nm	45	~90	(Gao et al, 2012)
2-Methylisoborneol	Initial pollutant concentration=0.04 mg/L $[PS]_0$=0.01 mM, pH_0=7.0 Irradiation source= low-pressure mercury lamp (6 W) Light intensity=1.79 mW/cm^2 Wavelength=254 nm	8.4	>90	(Xie et al, 2015)
2-CP, 3-CP, 4-CP	Initial each pollutant concentration=26 mg/L $[PS]_0$=10 mM, pH_0=4 Irradiation source=medium-pressure mercury vapor lamp (100 W) Light intensity=n.d[a] Wavelength=365 nm	90	100	(Fang et al, 2017)

Table 2.4 (continued) : Recent studies on UV/PS treatments of micropollutants.

Micropollutants	Experimental Conditions	Treatment time (min)	Maximum micropollutant removal (%)	Reference
Chloramphenicol	Initial pollutant concentration=10 mg/L $[PS]_0$=0.25 mM, pH_0=6.07 Irradiation source=low-pressure mercury lamp (4.9 W) Light intensity=2.43 mW/cm^2 Wavelength=254 nm	60	100	(Ghauch et al, 2017)
2,4-Di-tert-butylphenol	Initial pollutant concentration=5 mg/L $[PS]_0$=1 mM, pH_0=7.0 Irradiation source=low-pressure mercury lamp (75 W) Light intensity=not determined Wavelength=254 nm	30	85.6	(Wang et al, 2016)
Dichloroacetonitrile	Initial pollutant concentration=0.22 mg/L $[PS]_0$=0.2 mM, pH_0=6.0 Irradiation source=low-pressure mercury lamp (10 W) Light intensity=6.23 mW/cm^2 Wavelength=254 nm	180	99.8	(Hou et al, 2017)

Table 2.4 (continued) : Recent studies on UV/PS treatments of micropollutants.

Micropollutants	Experimental Conditions	Treatment time (min)	Maximum micropollutant removal (%)	Reference
Oxcarbazepine	Initial pollutant concentration=5 mg/L $[PS]_0$=1 mM, pH_0=11 Irradiation source=low-pressure mercury lamp (75 W) Light intensity=0.114 mW/cm^2 Wavelength=254 nm	120	~84	(Bu et al, 2016)
Oxytetracycline	Initial pollutant concentration=18.4 mg/L $[PS]_0$=1 mM, pH_0=7 Irradiation source=two low-pressure mercury lamp (15 W) Light intensity=0.1 mW/cm^2 Wavelength=254 nm	600	100	(Liu et al, 2016)
1H-benzotriazole, N,N-diethyl-mtoluamide, 3-Methylindole, Nortriptyline Hydrochloride	Initial 1H-benzotriazole concentration=0.119 mg/L Initial N,N-diethyl-mtoluamide concentration=0.191 mg/L Initial chlorophene concentration=0.219 mg/L Initial 3-methylindole concentration=0.131 mg/L Initial nortriptyline hydrochloride concentration=0.300 mg/L $[PS]_0$=50 μM, pH_0=7, Irradiation source=low-pressure mercury lamp (15 W), Light intensity=4.23 mW/cm^2, Wavelength=254 nm	30	~100	(Acero et al, 2018)

Table 2.4 (continued) : Recent studies on UV/PS treatments of micropollutants.

Micropollutants	Experimental Conditions	Treatment time (min)	Maximum micropollutant removal (%)	Reference
Lindane	Initial pollutant concentration=0.10 mg/L-2.00 mg/L $[PS]_0$=100 μM-1000 μM, pH_0=5.8-9.0 Irradiation source=two low-pressure mercury lamp (15 W) Light intensity=0.10 mW/cm^2 Wavelength=245 nm	120	96	(Khan et al, 2020)
Tetracycline	Initial pollutant concentration=5 mg/L $[PS]_0$=0.2 mM, pH_0=5-9 Irradiation source=low-pressure UV-C lamp (75 W) Light intensity=0.411 mW/cm2 Wavelength=254 nm	60	~100	(Xu et al, 2020a)
Carbamazepine	Initial pollutant concentration=1.0-10.0 mg/L $[PS]_0$=0.1 mM-0.6 mM, pH_0=5.0-9.0 Irradiation source=low-pressure UV-C lamp (75 W) Light intensity=0.411 mW/cm^2 Wavelength=254 nm	30	~99	(Xu et al, 2020b)

.

2.3.4.2 Zero-valent metals

Zero-valent iron

From previous studies, ZVI/PS has been proved to be effective for the degradation of 4-CP (Zhao et al, 2010a), acetaminophen (Deng et al, 2014), bentazon (Wei et al, 2016), metoprolol (Gao et al, 2020), acid orange 7 (Li et al, 2014b), sulfamethazine (Lin and Chen, 2018), aniline (Hussain et al, 2014), 4-CA (Hussain et al, 2012), naphthalene (Liang and Guo, 2010), trichloroethylene (Liang and Lai, 2008), 2,4-dinitrotoluene (Oh et al, 2010) and polyvinyl alcohol (Oh et al, 2009).

Oh et al. (2010) examined of 2,4-dinitrotoluene degradation through ZVI/PS and compared the results with activation of PS by Fe^{2+}. No 2,4-dinitrotoluene degradation was observed in the presence of mere PS. 2,4-dinitrotoluene degradation rate increased with increasing ZVI concentration mainly because of the enhanced PS activation with ZVI as a result of Fe^{2+} formation and consequently more generation of $SO_4^{\bullet-}$. While the ZVI/PS resulted in complete 2,4-dinitrotoluene removal, only limited 2,4-dinitrotoluene degradation (~20%) was achieved and the reaction delayed quickly by adding an equimolar concentration of Fe^{2+} instead of ZVI. By comparing the results of 2,4-dinitrotoluene degradation through ZVI/PS and PS activation by Fe^{2+}, it can be concluded that ZVI as an activating agent demonstrated more effective performance compared to Fe^{2+} in 2,4-dinitrotoluene removal since ZVI allows the slow and efficient release of Fe ions from its surface via corrosion (Oh et al, 2010).

In a study of Hussain et al. (2012), the degradation of 6.38 mg/L 4-CA by ZVI/PS (PS=2.5 mM) was investigated through batch experiments. Effects of ZVI concentrations (0.35 g/L to 5.0 mg/L), pH (2.0 to 11.0), temperature and (15 ℃ to 50 ℃) were examined in term of 4-CA removal. Obtained results revealed that the degradation of 4-CA increased with increasing ZVI due to increased activation of PS to produce $SO_4^{\bullet-}$. ZVI/PS treatment of 4-CA demonstrated better performance under acidic pH conditions (such as initial pH of 2.0 and 4.0) compared to alkaline conditions. Complete degradation of 4-CA was obtained in 12 min by ZVI/PS with initial pH of 4.0 (Hussain et al, 2012). Table 2.5 listed several recent studies on ZVI/PS treatments of micropollutants.

More recently, Wei et al. (2016) investigated the removal of a post-emergence herbicide namely bentazon by ZVI/PS. Several key factors affecting the ZVI/PS

treatment performance were examined; including initial bentazon (3.00 mg/L to 6.99 mg/L), PS (0.262 mM to 1.050 mM), and ZVI (0, 0.895 mM, 2.686 mM, 4.477 mM, and 6.267 mM; 50 mg/L-350 mg/L) concentrations, initial solution pH (3 to 11), temperature (15 ℃ to 55 ℃) and common ions in water (Wei et al, 2016). The formed $SO_4^{\bullet-}$ were mainly responsible for effective bentazon degradation. Complete bentazon removal was reported under the optimal ZVI (4.477 mM) and PS (0.262 mM) with initial bentazon concentration of 5.04 mg/L, at an initial pH 6–7 (Wei et al, 2016).

In another related study Girit et al. (2015) explored the use of commercial, air-stable ZVI nanoparticles for 20 mg/L bisphenol A treatment. In their study the effect of reaction pH over a range of 3 to 7, addition of H_2O_2 and PS oxidants with initial concentration of 1.25 and 2.5 mM, were studied for bisphenol A treatment by ZVI/PS. ZVI/PS provided an effective treatment system as a consequence of rapid $SO_4^{\bullet-}$ formation by a Fenton-like reaction between the released Fe^{2+} and PS (Girit et al, 2015). Complete bisphenol A degradation (in 5 min) accompanied with a significant mineralization (88% in 120 min) was achieved with ZVI/PS treatment (PS=1.25 mM; pH=5.0) (Girit et al, 2015).

Table 2.5 : Recent studies on ZVI/PS treatments of micropollutants.

Micropollutant	Experimental Conditions	Treatment time (min)	Maximum micropollutant removal (%)	Reference
2,4-DCP	Initial pollutant concentration=30 mg/L ZVI concentration=1.0 g/L $[PS]_0$=12.5 mM, pH_0=3.0	180	37.8	(Li et al, 2015b)
2,2′,4,4′-Tetrabromodiphenyl ether	Initial pollutant concentration=15 mg/L ZVI concentration=1 g/L $[PS]_0$=71.4 mM, pH_0=11.48	2880	64	(Wang et al, 2017)
Trichloroethylene	Initial pollutant concentration=19.7 mg/L ZVI/zeolite concentration=84 mg/L $[PS]_0$=1.5 mM, pH_0=7	120	98.8	(Huang et al, 2019)
Atrazine	Initial pollutant concentration=10 mg/L ZVI/graphene concentration=0.1 g/L $[PS]_0$=0.5 mM, pH_0=6.0	21	92.1	(Wu et al, 2018)
Trichloroethylene	Initial pollutant concentration=131.4 mg/L S-ZVI concentration=5 mM $[PS]_0$=5 mM, pH_0=2.32	30	90.68	(Dong et al, 2019)

Table 2.5 (continued) : Recent studies on ZVI/PS treatments of micropollutants.

Micropollutant	Experimental Conditions	Treatment time (min)	Maximum micropollutant removal (%)	Reference
Naproxen	Initial pollutant concentration=1.15 mg/L-5.75 mg/L ZVI concentration=14 mg/L-84 mg/L $[PS]_0$=0.1 mM-0.5 mM, pH_0=3.0-11.0	30	100	(Dong et al, 2020)
Phenol	Initial pollutant concentration=940 mg/L ZVI concentration=112 mg/L $[PS]_0$=420 mM, pH_0=3	10080	40	(Lominchar et al, 2018)
Reactive orange 107	Initial pollutant concentration=25 mg/L–100 mg/L ZVI concentration=0 g/L-1 g/L $[PS]_0$=2×10^{-4}M-0.01 M, pH_0=4-10	30	100	(Weng and Tao, 2018)
Reactive orange 107	Initial pollutant concentration=57 mg/L ZVI concentration=55.84 mg/L $[PS]_0$=1 mM, pH_0=3.5	180	100	(Rodriguez et al, 2014)
Direct Red 23	Initial pollutant concentration=16.3 mg/L ZVI concentration=0.5 g/L $[PS]_0$=0 mM-5 mM, pH_0=6.0 Temperature=4 ºC-55 ºC	30	100	(Weng and Tsai, 2016)

Zero-valent aluminum

It has been reported the ZVA/PS treatments are effective for the removal of a vast range of wastewater pollutants (Khatri et al, 2018) such as triton X-45 (Arslan-Alaton et al, 2017b), iopamidol (Arslan-Alaton et al, 2017c), bisphenol A (Dogan et al, 2016), trichloroethylene (Ren et al, 2018), etc.

In a former related study (Ren et al, 2018), ZVA/PS was investigated for the treatment of 26.28 mg/L trichloroethylene under different initial PS (0.20 mM to 4.00 mM) and ZVI (0.02 g/L to 0.20 g/L) concentrations and pH (3.00 to 10.00). In that study, approximately complete trichloroethylene degradation after 120 min ZVA/PS (PS=2.00 mM, pH=5.00) was achieved while the control experiments in the absence of either ZVA or PS showed less than 10% trichloroethylene degradation, which revealed a significant synergistic effect on the trichloroethylene degradation with the combination of ZVA and PS (Ren et al, 2018).

In another related study (Arslan-Alaton et al, 2017c), ZVA/PS treatment of iopamidol with initial concentration of 2 mg/L at initial pH of 3.0 was explored in different water matrices including DW, tap water, raw surface water and tertiary treated sewage effluent. Obtained results revealed that the ZVA/PS (PS=0.5 mM; pH=3) treatment could efficiently degraded iopamidol trough generation of $SO_4^{\bullet-}$ such that resulted in 95% iopamidol removal after 120 min. It should be mentioned here that, the efficiency of ZVA/PS depended on the type of water matrix. Efficiency of the process for Iopamidol removal reduced from 95% in DW to 29% in surface water. Iopamidol removal efficiency in wastewater was insignificant (Arslan-Alaton et al, 2017c).

ZVA/PS treatment of 2 mg/L triton X-45, an octylphenol polyethoxylate, was investigated in aqueous phase (Arslan-Alaton et al, 2017b). Results demonstrated that ZVA/PS was able to remove triton X-45 completely from water medium within 90 min. Poor triton X-45 removals in the absence of ZVA and PS were obtained (5%-38%). Activation of PS with ZVA substantially boosted triton X-45 degradation. Complete triton X-45 degradation occurred in DW with the ZVA/PS treatment after 90 min (ZVA=1 g/L; PS=0.5 mM; pH=3) (Arslan-Alaton et al, 2017b).

In the study of Dogan et al. (2016), activation of PS through ZVA was investigated for the removal of 20 mg/L (88 μM) aqueous bisphenol A. Complete bisphenol A

removal was achieved by using 1 g/L ZVA activated with 2.5 mM PS at pH=3 during ZVA/PS treatment. Oxidation with PS in the absence of ZVA did not cause bisphenol A degradation, whereas the mere ZVA treatment (in the absence of PS) at an initial reaction pH of 3, resulted in 33% bisphenol A removal. Mineralization efficiency of ZVA/PS was achieved as 90% at pH=3 (Dogan et al, 2016).

2.4 Toxicity

Toxicity of a substance is defined as its ability to adversely affect biological systems. This property is usually related to the time and degree of exposure, chemical concentration and the properties of the biological system involved (Czaplicka, 2004). Toxicity of a given substance is determined via standardized tests, with the use of selected model organisms and toxicity endpoints (like acute toxicity or lethality in selected organisms). In such standard tests, the effect is related to exposure concentrations in the surrounding medium and bioavailability (Schwarzenbach et al, 2006).

2.4.1 Necessity and importance of toxicity tests

Industrialization as well as the use of chemicals in agriculture generally lead to the release of many toxic compounds into water and cause many environmental problems (Jaffrezic-Renault and Dzyadevych, 2008) and the exposure of humans and animals to high toxic level of these compounds can cause harmful effects on living organisms such as long-term inhibition of growth/reproduction (Hassan et al, 2016). Therefore, detection of toxic compounds is crucial for overall safety of all biota on earth.

Besides, AOPs may have the risk of producing toxic transformation products during their application. The collective environmental parameters such as chemical oxygen demands (COD) and total organic carbon (TOC) remain insufficient to assess the biocompatability of AOP-treated effluents before discharge into receiving water bodies or transferred to a biological treatment. Several studies have already revealed that the partial mineralization of organic contaminants by different AOP, resulted information of more toxic intermediates at the end of treatment compared to the untreated water/wastewater (Mico et al, 2010; Neamtu et al, 2004; Olmez-Hanci et al, 2010). This major throwback makes the careful operation and monitoring of AOP

by means of toxicity bioassays necessary in order to evaluate the detoxification level achieved after an AOP. Toxicity screening is also useful for deciding on samples in which the inhibitory effect has changed enough to make performing biodegradability test.

Recently, different biological assays for toxicity assessment have been used and they rely on changes in the physiological response of living organisms which can be inferred on higher organisms and have many advantages such as rapid response, simplicity, specificity, sensitivity and cost effectiveness (Rizzo, 2011).

2.4.2 Bioassays

Generally, the analysis of toxic substances in environmental samples can be divided into two groups. In the first one, the toxic pollutants are identified and quantified based on chemical or physical analyses using high performance liquid chromatography (HPLC) and/or gas chromatography (GC) and/or atomic absorption spectroscopy (AAS). Despite of their high sensitivity and accuracy in the determination of the concentration of pollutants in environmental samples, these techniques have several disadvantages such as being time consuming (due to the need for sample preparation and pre-concentration), expensive (due to the need for skilled personnel) and incapable to give an indication of the cumulative toxicity of multiple contaminants in a sample (Hassan et al, 2016). The second group is bioassays such that the toxic chemicals are not clearly identified, but the measurements allow for the assessment of toxicity of environmental samples toward living organisms. Therefore, a bioassay can determine the relative potency or effectiveness of a given pollutant by comparing its effect on living organisms using appropriate controls (Sadick, 2002).

2.4.2.1 Luminescence inhibition test with *Vibrio fischeri*

Various biotesting methods have been developed to evaluate water toxicity (Zadorozhnaya et al, 2015) by studying the reaction of a living test-object exposed to an environmental sample. Luminescent marine bacteria *V. fischeri* also known formerly as *Photobacterium phosphoreum* are employed as a biotests-object. The Microtox acute toxicity test is one of the most extensively used methods. This approach has several advantages compared to other bioassays. For instance, it is rather uncomplicated and made of very few elements, test biota does not need

preculturing and it can be considered as a cost-effective test since the bacteria is stored in lyophilized state and consequently maintenance cost is eliminated and the culture has long term stability (Farré and Barceló, 2003; Rizzo, 2011; Zadorozhnaya et al, 2015). Microtox is applied as a biomonitoring tool for a wide range of ecotoxicological problems. Over 50% of all applications of the Microtox acute toxicity test are related to assessment of industrial–domestic wastes, leachate studies and also for evaluation of risks, in relation with a simulated oil spill (Zadorozhnaya et al, 2015).

V. fischeri, a kind of marine photobacterium, has been the most often used bacteria due to its high sensitivity towards a vast range of pollutants (Rizzo, 2011). The test relies on measurement of the bacterial luminescence when the microorganisms are exposed to toxic chemicals (Farré and Barceló, 2003). Due to the rapid response of *V. fischeri* to toxicants, it has been used extensively for toxicity measurements (Karci, 2014; Stolper et al, 2008; Zadorozhnaya et al, 2015).

In many previous AOPs studies, toxicity of target pollutant and their possible degradation product were assessed by *V. fischeri* considering the difficulties in detecting all possible oxidation by-products evolving during AOPs in different matrices. For instance, the acute toxicity of original 1,2,3-trichlorobenzene (100 µg/L) and its UV-C/PS (0.3 mM; pH=7.6-8.0) treated samples in two natural water samples (surface water and ground water) spiked with 1,2,3-trichlorobenzene (100 µg/L) were examined using the luminescence inhibition test with *V. fischeri* bacteria (Đurkić et al, 2020). In that study, it was found that for all the untreated natural water samples containing 1,2,3-trichlorobenzene, the inhibition of *V. fischeri* was negligible (13%). Slightly higher *V. fischeri* bioluminescence inhibitions were observed after UV-C/PS (14–23%), with higher inhibition noted for ground water than for surface water, most probably as a result of the products of natural organic matter transformation (Đurkić et al, 2020).

In another related study (Yang et al, 2017), acute toxicity to *V. fischeri* during UV-C/H_2O_2 (H_2O_2=1 mM) and UV-C/PS (PS=1 mM) treatments of 5.07 mg/L sulfamethoxazole were examined. Obtained results showed that with the degradation of sulfamethoxazole during UV-C/H_2O_2, the luminescence slightly increased; however, the luminescence of samples treated by UV-C/PS reduced by 65%,

indicating oxidation of $SO_4^{\bullet-}$ with sulfamethoxazole generated more toxic products than those of $HO^{\bullet}$ (Yang et al, 2017).

In the study of Frontistis (2019), the origin toxicity of 1 mg/L piroxicam in secondary treated effluent and UV-C/PS (PS=5 mg/L; pH=8.5) treated samples was evaluated using the bacterium *V. fischeri*. In that study, it was found that the presence of 1 mg/L of piroxicam does not significantly increase the inhibition of *V. fischeri* which is mainly related to the constituent of the secondary effluent. The inhibition of *V. fischeri* remains stable during the first 15 min, and it is then reduced but to a lower extent than correspondingly decreases piroxicam (Frontistis, 2019).

In the study of Yangin-Gomec et al (2018), the acute toxicity of the 2 mg/L aqueous iopamidol and its degradation products by ZVA/PS (PS=0.50 mM; pH=3) treatment were examined by *V. fischeri*. Obtained results demonstrated that neither the original nor the ZVA/PS treated iopamidol solutions demonstrated inhibitory effects towards *V. fischeri*. The percent relative inhibition of the original iopamidol toward *V. fischeri* was only 5% and fluctuated during ZVA/PS treatment, but remained always below 10% (Yangin-Gomec et al, 2018).

2.4.2.2 Growth inhibition test with *Pseudokirchneriella subcapitata*

Freshwater algae have been the test species in most phytotoxicity tests due to their relatively short life cycle, acting as surrogates for marine species and macrophytic species (Karci, 2014). One of most popular microalgal indicators studied most extensively by ecotoxicologists is *P. subcapitata* due to its sensitivity to various substances, particularly herbicides as well as metals. In toxicity tests based on employing *P. Subcapitata,* the inhibition of the green algal growth is used as the indicator of toxicity and at the end of the specified exposure time, the number of algae is calculated (Escher et al, 2011; Rizzo, 2011). Difficulty in culturing and, sometimes, lack of reproducibility can be considered as the main drawbacks of using algal methods (Chen et al, 2007).

Yangin-Gomec et al (2018) explored, the acute toxicity of the 2 mg/L aqueous iopamidol and its degradation products by ZVA/PS (PS=0.50 mM; pH=3) treatment by *P. subcapitata*. In that study, the toxic effect of original iopamidol solution was found 74% indicating that iopamidol was highly toxic towards *P. subcapitata*. During the first 30 min of ZVA/PS treatment, the relative inhibition of iopamidol

decreased from 74% to 29% when approximately 50% iopamidol was removed. Thereafter, the relative inhibition of 120 min ZVA/PS treated samples toward *P. subcapitata* increased ultimately to 93% indicating the presence of ZVA/PS degradation products being more toxic towards *P. subcapitata* than the untreated iopamidol solution (Yangin-Gomec et al, 2018).

Acute toxicity of 20 mg/L original aqueous triton X-45 and ZVI/PS (PS=2.5 mM; pH=5.0) treated samples were investigated by *P. subcapitata* in the study of Temiz et al. (2016). In that study, it was found that the relative inhibition of original TX-45 solution to *P. subcapitata* was low (12%); it increased to 22% after 20 min and quickly decreased to nondetectable levels beyond 40 min treatment (Temiz et al, 2016). The fluctuations observed in the toxicity responses could be attributed the formation and subsequent disappearance of several degradation products evolving during ZVI-activated PS oxidation such as polyethylene glycols ad mono-carboxylated polyethylene (Olmez-Hanci et al, 2014b).

In another related study (Arslan-Alaton et al. 2017b), the acute toxicity of 2 mg/L triton X-45 with and its ZVA/PS (PS=0.50 mM; pH=3) treated samples in DW and surface water were investigated by *P. subcapitata*. The percent relative inhibition values of 2 mg/L triton X-45 in DW and surface water samples towards *P. subcapitata* were found to be 35% and 39%, respectively. During the early stages of triton X-45 samples treatment by ZVA/PS, the relative inhibition of triton X-45 toward *P. subcapitata* increased from 35% to 44% and from 39% to 52% in DW and SW samples, respectively. After 120 min treatment, it dropped back to 40% and 25% in DW and SW samples, respectively (Arslan-Alaton et al, 2017b).

2.4.2.3 Genotoxicity test with *Salmonella typhimurium* TA 1535

AOPs should be carefully monitored and ecotoxicological investigations should be accompanied to investigate the formation of potentially toxic transformation products. Screening for mutagens in environmental complex mixtures using *S. typhimurium* strain has been accepted as a routine methodology in the monitoring processes (Černá et al, 1991; Węgrzyn and Czyż, 2003).

In study of Han et al. (2019), genotoxic potency of 1 mg/L tetrabromobisphenol A and its evolved intermediates during 60 min ozonation under different ozone concentration (10.42 μM, 25.00 μM, 41.67 μM and 83.33 μM; pH=7.0) was

investigated by the Ames test using *S. typhimurium* T100. The number of the revertant colonies of *S. typhimurium* T100 was counted, with 160±12 in blank control. While in the treated samples, the amount of the revertant colonies was in the range of 117±6-193±17, with no significant increase as compared with that in blank control. The result indicated that the water samples were all with no mutagenicity and genotoxicity. None of the products generated during the degradation of tetrabromobisphenol A induced a base substitution mutation (Han et al, 2019).

In another related study (Muneer et al. 2020), the mutagenicity evaluation of original 50 mg/L reactive yellow 145 dye and its treated samples by UV-C/H_2O_2 ($H_2O_{2=}$1 ml/L) was performed using the Ames test with *S. typhimurium* TA98 and *S. typhimurium* TA100. Obtained results demonstrated that the mutagenicity of dye solutions was reduced to 78.25% (in case of *S. typhimurium* TA98), while 82.53% (in case of *S. typhimurium* TA100) using UV-C/H_2O_2. Results suggested that UV-C/H_2O_2 can efficiently be used to degrade and detoxify the textile wastewater (Muneer et al, 2020).

2.4.3 Application of toxicity tests in advanced oxidation treatments of micropollutants

Table 2.6 demonstrates recent studies concerning the ecotoxicological characterization of AOPs for the removal of several micropollutants. In published studies, toxicity was generally taken as the overall toxicity of the solution for instance the mixture of transformation products as well as parents compounds) toward the species.

Table 2.6 : Recent studies on toxicity changes during UV-C/PS, ZVI/PS and ZVA/PS treatments of several micropollutants.

Micropollutant	AOP	Experimental Conditions	Evaluation of toxic effect	Reference
Indomethacin	UV-C/PS	Initial pollutant concentration=7.16 mg/L $[PS]_0$=20 µM, pH_0=7 Irradiation source=low-pressure mercury lamp (22 W) Light intensity=1.250 mW/cm^2 Wavelength=254 nm	*V. fischeri*	(Li et al, 2018)
Triton X-45	ZVI/PS	Initial pollutant concentration=20 mg/L ZVI concentration=1 g/L $[PS]_0$=2.5 mM, pH_0=5.0	*V. fischeri* *P subcapitata.*	(Temiz et al, 2016)
Bisphenol A	ZVI/PS	Initial pollutant concentration=20 mg/L ZVI concentration=1 g/L $[PS]_0$=2.5 mM, pH_0=5	*V. fischeri* *P subcapitata.*	(Girit et al, 2015)
Triton X-45	ZVA/PS	Initial pollutant concentration=2 mg/L ZVA concentration=1 g/L $[PS]_0$=0.5 mM, pH_0=3	*V. fischeri* *P subcapitata*	(Arslan-Alaton et al, 2017b)
Suladiazine	ZVI/PS	Initial pollutant concentration=5 mg/L ZVI concentration=1 mM $[PS]_0$=0.5 mM, pH_0=4.0	*V. fischeri.*	(Guo et al, 2020)

Table 2.6 (continued) : Recent studies on toxicity changes during UV-C/PS, ZVI/PS and ZVA/PS treatments of several micropollutants.

Micropollutant	AOP	Experimental Conditions	Evaluation of toxic effect	Reference
Iopamidol	UV-C/PS	Initial pollutant concentration=2 mg/L $[PS]_0$=0.2 mM, pH_0=7 Irradiation source=ten fluorescent lamps (each 8 W) Light intensity=0.26 mW/cm^2 Wavelength=254 nm	*V. fischeri* *P subcapitata*	(Arslan-Alaton et al, 2018a)
Naphthenic acids	UV/PS	Initial pollutant concentration=4.0 mg/L-30.8 mg/L $[PS]_0$=0.5 mM-4.0 mM, pH_0=8.4 Irradiation source=medium pressure mercury lamp (1k W) Light intensity=3.5 mW/cm^2 Wavelength>200 nm	*V. fischeri*	(Fang et al, 2019)
Losartan potassium, Furosemide, Caffeine, Carbendazim	UV-C/PS	Initial Losartan potassium concentration=4.61 mg/L Initial Furosemide concentration=3.31 mg/L Initial Caffeine concentration=1.94 mg/L Initial Carbendazim concentration=1.91 mg/L $[PS]_0$=1 mM, pH_0=3-9 Irradiation source= low-pressure mercury lamp (10 W) Light intensity=0.241mW/cm^2 Wavelength=254 nm	*V. fischeri*	(Starling et al, 2019)

2.5 Degradation Products of the Selected Model Industrial Micropollutants

Although for most applications of AOPs successful results in industrial micropollutants removal have been documented from previous related studies (Khatri et al, 2018; Rodríguez-Chueca et al, 2019), it is already known that intermediates/degradation products being more toxic compared to the parent pollutant may form during AOPs applications (Olmez-Hanci et al, 2014b; Rizzo, 2011). Hence, it is essential to identify and monitor degradation products of three model industrial pollutants and their evolution during UV-C, UV-C/PS and ZVI/PS and to explore the degradation products to establish a possible reaction pathway of each treatment process in order to decide which AOPs should be preferred for the effective and sustainable treatment of each model industrial pollutant.

2.5.1 Chlorophenols

2.5.1.1 Photolytic and photochemical treatments

CPs have been listed as priority pollutants due to their high toxicity and hard biodegradability (Zhou et al, 2011). It should be mentioned here that during the application of AOPs, the main concern, relates to the formation of various degradation products as a consequence of reactions of radicals with CPs and their degradation products may have biological activity/toxicity similar to or different from their parent compounds (Sharma et al, 2018).

Generally, in the UV region, the molar absorptivity of CPs is known to be relatively high (Trapido et al, 1997) and can be degraded successfully. Photodegradation products of CPs have been reported in previous related studies (Czaplicka, 2006; Czaplicka and Kaczmarczyk, 2006). The CPs are mainly converted into hydroxybenzenes and less-chlorinated phenols through photolytical dechlorination (Czaplicka and Kaczmarczyk, 2006). For example, Czaplicka and Kaczmarczyk (2006) investigated the photolysis of 3-CP and identified resorcinol and 3-chloro-1,4-benzenediol in solution irradiated for 120 min at 254 nm (Czaplicka and Kaczmarczyk, 2006). 2,4-DCP photodegradation products have been reported in several studies in which direct photolysis of this compound leads to formation of mono-CPs, chlorinated cyclopentadienyl, chlorohydroquinones (Czaplicka, 2006; Gsponer et al, 1987; Pandiyan et al, 2002).

Among the AOPs, UV/PS, the UV-activated hydrogen peroxide (UV/H_2O_2) have been extensively studied in the scientific literature for CPs degradation where the formation of chlorohydroquinone, chlorobenoquinone, chlorocatechol, hydroquinone, catechol, phenol and low molecule weight organic acids were identified during application of these processes. Table 2.7 presents the studies aiming identification and monitoring of evolved degradation products during these processes.

2.5.1.2 Heterogeneous catalytic treatments

The formation of intermediates during the degradation of CPs through Fenton (Du et al, 2007) and photo-Fenton processes (Basu and Wei, 1998; Karci et al, 2012), ZVI/H_2O_2 (Lente and Espenson, 2004) and using Cu–Al hydrotalcite/clay composite with H_2O_2 (Zhou et al, 2011) were investigated in previous studies. In each process, the breakdown pathway can proceed through direct addition of HO$^{\bullet}$ onto the aromatic ring of the respective CPs resulted in the generation of hydroxylated chlorophenolic intermediates or HO$^{\bullet}$ could attack onto the C atom being occupied by the chlorine group resulted in chloride ion (Cl^-) (Karci, 2014) . In recent years CPs degradation by PS activation methods has also been explored (Liu et al, 2015; Pang et al, 2019; Yeber et al, 2010; Zhou et al, 2018) for the free radical-mediated oxidation. The formation of intermediates during 2,4-DCP treatment by ZVI/PS was studied by Li at al. (2017). According to their study, the formation of some intermediates including 4-CP, 2-CP, phenol, 2-chloro-1,4-benzenediol, 4-chloro-1,2-benzenediol, hydroquinone and catechol were observed (Li et al, 2017). Table 2.8 presents the studies aiming identification and monitoring of evolved degradation products during heterogeneous catalytic treatments

Table 2.7 : A list of CPs degradation products evolving during application of homogeneous photochemical treatments.

Compounds	Treatment Methods	Experimental Conditions	Transformation Products	Reference
2-CP 3-CP 4-CP	UV/PS	Initial pollutant concentration=26 mg/L $[PS]_0$=10 mM, pH_0=4.0 Irradiation source=100 W medium pressure mercury vapor lamp Light intensity=12.7 mW/cm^2	2,4,5-trichlorophenol(TCP) 2,6-DCP 2,4-DCP 2,3-DCP 2,3,5,3',5'-pentachlorobiphenyl	(Fang et al, 2017)
2,4-DCP	UV/H$_2$O$_2$	Initial pollutant concentration=30 mg/L $[H_2O_2]_0$=0.18–1.1 mM, pH_0=3 Irradiation source=Low pressure mercury lamp (15 W) Light intensity=n.d[a]	4,6-Dichlorocatechol 2,5-Dichlorohydroquinone 4-Chloro-1-naphthalenole 1-Chloro-2,6-dimethoxynaphthalene	(Kucharska and Naumczyk, 2009)
4-CP	UV-C/H$_2$O$_2$	Initial pollutant concentration=130 mg/L $[H_2O_2]_0$=30 mM, pH_0=7 Irradiation source=low pressure mercury UV-C lamp Light intensity=4.4 mW/cm^2	Hydroquinone Benzoquinone 4-Chlorocatechol Phenol	(Peternel et al, 2012)

Table 2.8 : A list of CPs degradation products evolving during application of heterogeneous catalytic treatments.

Compounds	Treatment Methods	Experimental Conditions	Transformation Products	Reference
3,5-DCP	Cu–Al hydrotalcite/clay composite with H_2O_2	Initial pollutant concentration=326 mg/L Catalyst concentration=1 g/L $[H_2O_2]_0$=40 mM, pH_0=2.77–7.87	2,6-Dichloro-1,4-benzoquinone	(Zhou et al, 2011)
2,4-DCP	Magnetic nanoparticles and graphene oxide with PS	Initial pollutant concentration=10-80 mg/L Catalyst concentration=100-400 mg/L $[PS]_0$=0.05-1.0 mM, pH_0=3-9	4-CP Cyclohexanol Crotonic acid Butane 2-Methylbutane	(Pang et al, 2019)
2,4-DCP	Zero-valent copper/PS or PMS	Initial pollutant concentration=5 mg/L Catalyst concentration=50 mg/L $[PS]_0$ or $[PMS]_0$=0.5 mM pH_0=3.1	4-Chlorocatechol 2-Chlorohydroquinine Chlorobenzoquinone 4-Benzoquinone, 4-CP 2-CPhlorophenol Phenol Catechol Resorcinol Hydroquinone Maleic acid, Fumaric acid	(Zhou et al, 2018)

2.5.2 Chloroanilines

2.5.2.1 Photolytic and photochemical treatments

CAs are common water pollutants which are formed during textile, dye and leather manufacturing processes (Latorre et al, 1984) and are considered as toxic and recalcitrant compounds in industrial wastewater that must be efficiently removed. 2,4-DCA, an important CA, is widely used as an intermediate in industrial synthesis (Pascal-Lorber et al, 2003). CAs represent a considerable long-term threat to aquatic and, human life because of their hydrophobic (bioaccumulative) properties and high acute/chronic toxicity (Kilemade and Mothersill, 2000). Among various methods to remove CAs from aqueous phase, AOPs have shown successful results in CAs degradation (Liang et al, 2013; Mailhot et al, 2004; Winarno and Getoff, 2002a). So far several studies have been focusing on identification and monitoring of evolved transformation/degradation products during CAs removal through AOPs (Kádár et al, 2001; Mailhot et al, 2004; Nitoi et al, 2015; Yuan et al, 2015).

Photochemistry of 4-CA which had previously been investigated in previous transformation product studies (Grabner and Richard, 2005; Othmen et al, 2000; Ratti et al, 2015) showed that the main photointermediate in polar solvents was detected a carbene named 4-iminocyclohexa-2,5-dienylidene as a result of dechlorination of excited state species of 4-CA. The carbene could subsequently react to stable products along four different pathways, namely through (i) coupling with another equivalent of the substrate, (ii) addition of molecular oxygen followed by substrate addition, (iii) hydrogen abstraction and (iv) addition of H_2O. For example, in the study of Ratti et al. (2015), UV-C photolysis of 4-CA was investigated in the pH range of 2.0 to 9.0. In that study, degradation product analyses revealed the formation of coupling products including dimers, trimers, and tetramers of partially de-chlorinated 4-CA predominantly via pathways (i) and (ii). Many of the coupling products were detected at high peak intensities such as 4-hydroxy-4′-chlorodiphenylamine (Ratti et al, 2015).

It should be noted here that the main photochemical reaction of DCAs is photohydrolysis (Othmen and Boule, 1999). Photodegradation products of 2,4-DCA was investigated in study of Othmen and Boule (1999) at 290 nm and the main primary photoproduct was identified as 2-amino-5-chlorophenol. Another

photoproduct was identified 2-amino-7-chlorophenoxazin-3-one in presence of oxygen (Othmen and Boule, 1999).

2.5.2.2 Heterogeneous catalytic treatments

So far, AOPs have been successfully applied for degradation of CAs (Kádár et al, 2001; Meinero and Zerbinati, 2006). CA degradation through heterogeneous catalytic treatment system has been investigated in previous studies (Hofmann et al, 2005; Liang et al, 2013; Mailhot et al, 2004). However, there are only limited studies focusing on CA degradation pathways through AOPs (Hussain et al, 2012; Liang et al, 2013). Hussain et al. (2012) investigated formation of intermediates during ZVI/PS (PS= 2.5 mM) treatment of 0.05 mM 4-CA in the acidic pH range 2.0 to 4.0. In that study, aniline, N-(4-chlorophenyl)-p-phenylene di-imine, 1-(4-Chlorophenyl)-3-phenlurea and 5-chloro-2-((4-chlorophenyl) diazenyl) phenol were identified as intermediate products during 4-CA oxidation through ZVI/PS (Hussain et al, 2012).

2.5.3 Hydantoins

2.5.3.1 Photolytic and photochemical treatments

Limited information is currently available describing photolytic and photochemical degradation of IPR (Burrows et al, 2002; Lassalle et al, 2014; Lopez-Alvarez et al, 2016; Schwack and Bourgeois, 1989; Schwack et al, 1995). In the study of Lassalle et al. (2014), identification of evolved intermediates from photolytic degradation of IPR was investigated. Dechlorination has been reported as one of the stage of IPR degradation followed by hydroxyl group replacement (Lassalle et al, 2014). This degradation pathway also reported in previous related study where IPR and its possible degradation pathway was investigated in presence of H_2O_2 (Lopez-Alvarez et al, 2016) and release of Cl^- as early stage of IPR degradation, suggesting the $HO^{\bullet}$ attack into the carbon-chloride bond. In the study of Lassalle et al (2014), the main dissociation pathways of protonated IPR was proposed through propene and isopropyl isocyanate eliminations to provide intermediates with the formula $C_{10}H_8Cl_2N_3O_3$ and $C_9H_7Cl_2N_2O_2$, respectively. Therefore five intermediates were reported, namely; three photoproducts were from elimination of one or two chlorine atoms, followed by hydroxyl or hydrogen addition, while two products were cyclic isomers of IPR (Lassalle et al, 2014).

Schwack et al. (1995) examined the photodegradation of IPR in isopropyl alcohol (3 g/L). A high pressure mercury lamp (150 W) was used and The UV light was filtered by glass filters WG 295 (λ>280 nm). In that study, the main reaction consisted of the successive dehalogenations of IPR. To a minor extent an intermediate with the formula $C_{16}H_{20}ClN_3O_4$ was also reported as a combination product of a radical formed by homolytic cleavage of the C-Cl bond of IPR with an isopropyl alcohol radical (Schwack et al, 1995).

2.5.3.2 Heterogeneous catalytic treatments

Degradation of IPR using a photocatalytic reactor with TiO_2-coated thin-film was investigated in the study of Bessergenev et al. (2017) using UV-C lamp source. Initial IPR concentration was 5 mg/L and initial pH was 3, 6 and 9. Complete degradation of IPR was reported in the presence of TiO_2 after 20 min showing significant photocatalytic degradation effect on IPR decay while only 30% IPR removal was observed by UV-C photolysis after 15 min. TOC removal was not studied at that study and author just reported IPR removed mainly by the oxidation of $HO^\bullet$ whose production was related to the radiation intensity on the surface of TiO_2 (Bessergenev et al, 2017).

3. MATERIALS AND METHODS

3.1 Materials

3.1.1 Chemicals and Reagents

3,5-DCP, 2,4-DCA and IPR were purchased from Sigma-Aldrich (purity >98%) and used as received. Potassium persulfate (formula: $K_2S_2O_8$; molecular weight: 270 g/mol), hydroquinone (formula: $C_6H_6O_2$; molecular weight:110 g/mol), benzoquinone (formula: $C_6H_4O_2$; molecular weight:108 g/mol), phenol (formula: C_6H_6O; molecular weight: 94 g/mol), 4-CP (formula: C_6H_5ClO; molecular weight: 129 g/mol), aniline (formula: C_6H_7N; molecular weight: 93 g/mol), nitrobenzene (formula: $C_6H_5NO_2$; molecular weight: 123 g/mol) and phthalic acid (formula: $C_8H_6O_4$; molecular weight: 166 g/mol) were all purchased from Sigma-Aldrich. Lactic acid (formula: $C_3H_6O_3$; molecular weight: 90 g/mol), acetic acid (formula: $C_2H_4O_2$; molecular weight: 60 g/mol) and formic acid (formula: CH_2O_2; molecular weight: 46 g/mol) were purchased from Merck. Catechol (formula: $C_6H_6O_2$; molecular weight: 110 g/mol) was obtained from Acros Organics. Methanol, acetic acid and sulfuric acid for mobile phase preparation were supplied to prepare HPLC mobile phase. Commercial nano-scale ZVI (average particle size 50 nm; BET surface area 20-25 m^2/g; purity>99.5%) was obtained from Nanofer Star, Nano Iron (Czech Republic). High purity (>99.5%) ZVA nanoparticles (average particle size 100 nm; specific surface area 10-20 m^2/g) were purchased from US Research Nanomaterials, Inc. (Houston, USA). All aqueous solutions were prepared in DW.

3.1.2 The synthetic urban wastewater sample

In order to examine oxidation performance of each model industrial micropollutant under real environmental conditions, a synthetic urban wastewater surrogating a tertiary treated urban effluent in terms of nutrients content, was prepared. The composition of the synthetic urban wastewater comprised of different organic and inorganic components with the following composition; $(NH_4)_2SO_4$ (12 mg/L), tryptone (50 mg/L), meat extract (50 mg/L), yeast extract (7.5 mg/L), urea (7.5

mg/L), K_2HPO_4 (10 mg/L), $CaCl_2.2H_2O$ (1 mg/L), $MgSO_4.7H_2O$ (1 mg/L) (Bellucci et al, 2013; Imai et al, 2002).

Besides the above mentioned components, the synthetic urban wastewater was also supplemented by 4 mg/L humic acid, as a complex organic compound to render the SWW composition more complex as is being typical for urban effluent which is generally containing a mixture of industrial wastewater, domestic wastewater and run-off rain water. The pH of this synthetic urban wastewater was around 6.8. The synthetic urban wastewater was diluted at a ratio of 1:5 (w:w) to obtain a final DOC of approximately 10 mg/L which is reported as a typical DOC corresponding to tertiary treated effluent (Bernabeu et al, 2011). Table 3.1 shows environmental characteristic of synthetic urban wastewater.

Table 3.1 : Environmental characteristic of synthetic urban wastewater.

Parameters	Values
COD (mg O_2/L)	145±7
BOD$_7$ (mg O_2/L)	88±4
DOC[a] (mg/L)	52±3
TSS (mg/L)	17±1
TP (mg P/L)	2.4
NH$_3$-N (mg N/L)	4.3
Conductivity (µs/cm)	522
Color (pt-Co Unit)	116
pH	6.8±0.2

[a]DOC (TOC filtered through 0.22 µm PVDF syringe filter).

TOC is total oxidizable carbon converted into CO_2 by oxidation. DOC is organic carbon determined by the analysis of aqueous samples that have been filtered through 0.22 µm PVDF syringe filters (St-Jean, 2003). Environmental parameter of DOC has only been addressed in this study.

Urban wastewater is considered domestic wastewater or the mixture of domestic wastewater with industrial waste water and/or run-off rain water. Urban wastewater contains a diverse and expanding number of anthropogenic and natural compounds including industrial chemicals, compounds present in personal care products, pharmaceuticals, their metabolites, and transformation products formed during wastewater treatment (Fatta-Kassinos et al, 2016).

3.2 Experimental Procedures

3.2.1 Ultraviolet-C and Ultraviolet-C-activated persulfate oxidation processes

All UV-C and UV-C/PS experiments were conducted in a 500 mL-capacity three-neck quartz flask (h=10 cm; r=4 cm) placed at the center of the photochemical reaction chamber where the reaction solution was stirred from the reactor bottom at 100 rpm. The photochemical reaction chamber was a LZC-ORG model (Luzchem Research Inc., Canada) photoreactor (dimensions: 32×33×21 cm) equipped with a digitally controlled thermometer and a magnetic stirrer (Figure 3.1). The chamber comprised an air cooling fan to control the temperature in the reaction chamber. The air flow design of the chamber stabilizes the temperature about 3-4 ℃ above room temperature. A maximum of ten fluorescent UV-C lamps (8 W each) could be placed on the reactor walls of the reaction chamber. The spectral distribution of the UV-C lamps had a Gaussian shape with a central wavelength at 254 nm. The average radiation flux was measured 0.5 W/L with a UV-meter (Smart Sensor–AR823) when all lamps were turn on.
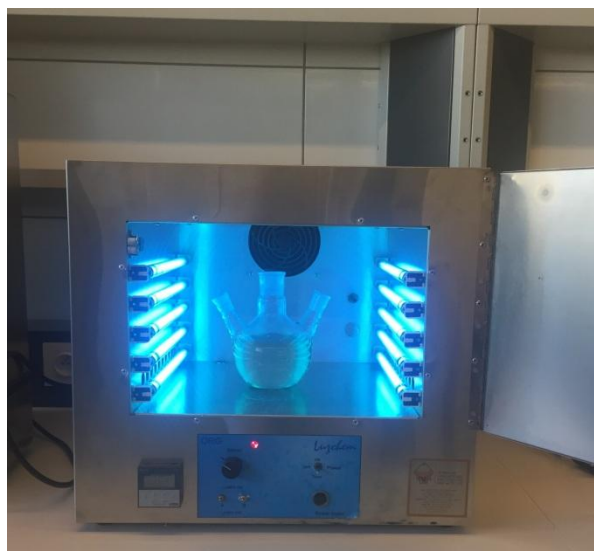
Figure 3.1 : The photoreactor being used through UV-C and UV-C/PS treatment runs.

All preliminary experiments were conducted in DW with initial concentration 2 mg/L for each industrial model pollutant. Although such initial concentration is appreciably higher than environmentally relevant concentrations being mostly reported in literatures (Kreuger, 1998; Stamatis et al, 2010), this concentration was chosen to ensure accurate analytical, kinetic and toxicological assessments of selected model industrial pollutants.

Photochemical treatment experiments were conducted in DW which spiked with 2 mg/L of each model industrial micropollutant separately. At the beginning a predetermined PS was added if necessary to the reaction solution and mixed well until being completely dissolved. Then, the reaction solution was inserted into the reaction chamber and samples were taken at regular time intervals for up to 120 min for analytical and instrumental analyses.

3.2.2 Zero-valent iron and zero-valent aluminum-activated persulfate oxidation processes

All ZVI/PS and ZVA/PS experiments were carried out in 500 mL-capacity borosilicate glass beakers under continuous stirring at 150 rpm to maintain the oxygen content of reaction solution near saturated level and distribute ZVI and ZVA particles properly in the reaction solution.

Prior to each ZVI/PS and ZVA/PS experiment, the initial pH of the solutions was adjusted to the desired value by adding 1-4 N H_2SO_4 solutions. The selection of the

working conditions was based on former related studies in which more effective performances of Fenton/Fenton-like reactions were reported under acidic pH conditions (Hussain et al, 2014; Hussain et al, 2012; Xiao et al, 2020). Thereafter, 1 g/L of ZVI (or 1 g/L of ZVA) was added to the reaction solution and finally the oxidant PS was introduced to start reaction. Samples were taken at regular time intervals and filtered through 0.22 µm PVDF syringe filters (GVS, USA) to remove ZVI (or ZVA) particles. Besides, the pH of the samples was increased to range of 7.0 to 7.5 (pH of all IPR samples was increased maximum to 7.0 because of IPR hydrolysis) by adding 1-4 N NaOH solutions to remove dissolved Fe in the form of ferric hydroxide flocs to stop Fenton/Fenton-like reactions (Messele et al, 2019; Xiao et al, 2020).

3.3 Analytical Procedures

3.3.1 The model industrial micropollutants and their aromatic degradation products

Three model industrial micropollutants and their expected degradation products were monitored with a HPLC (Agilent 1100 Series, Agilent Technologies, USA) coupled with a diode array detector (G1315A, Agilent Series). Measurements were done at wavelengths of 285 nm, 240 nm, 210 nm, 260 nm, 254 nm and 280 nm for 3,5-DCP, 2,4-DCA, IPR, nitrobenzene, aniline and 4-CP, respectively with a Nova-Pak C18 (3.9 mm × 150 mm, 4 µm, Waters, USA) as reversed phase column. The mobile phase consisted of 70% methanol and 30% ultrapure water at a flow rate of 1 mL/min. The injection volume in HPLC analysis and temperature of the column were set as was set as 100 µL and 25°C, respectively. Detection and quantification limits were determined as 0.06 mg/L and 0.21 mg/L for 3,5-DCP, 0.03 mg/L and 0.12 mg/L for 2,4-DCA, 0.03 mg/L and 0.10 mg/L for IPR, 0.16 mg/L and 0.55 mg/L for nitrobenzene, 0.05 mg/L and 0.16 mg/L for aniline, 0.04 mg/L and 0.14 mg/L for 4-CP, respectively.

The mobile phase used for the determination of hydroxylated degradation products of 3,5-DCP, 2,4-DCA and IPR (phenol, hydroquinone, p-benzoquinone and catechol) as well as phthalic acid consisted of 79.2% ultrapure water, 19.8% methanol and 1% acetic acid run at a flow rate of 0.8 mL/min. Diode array detection was performed at 270 nm, 290 nm, 245 nm, 276 nm and 254 nm for phenol, hydroquinone, *p-*

benzoquinone, catechol and phthalic acid qualifications, respectively. The LC column (Nova-Pak C18, 3.9 mm × 150 mm, 4 μm, Waters, USA) temperature and injection volume were set as 40°C and 40μL, respectively. Limits of detection and quantification were determined as 0.06 mg/L and 0.20 mg/L for phenol, 0.01 mg/L and 0.04 mg/L for hydroquinone, 0.70 mg/L and 2.34 mg/L for *p*-benzoquinone, 0.10 mg/L and 0.34 mg/L for catechol, respectively.

Moreover, the analysis of IPR degradation products during UV-C and UV-C/PS treatments was performed using a LC (Shimadzu LC20AD) coupled with mass spectrometry (LC-MS) at Boğaziçi University. A Nova-Pak C18 (3.9 mm × 150 mm, 4 μm, Waters, USA) was utilized as a stationary phase, while the mobile phase was a mixture of methanol/water in 70/30 (v/v) ratio. Possible transformation products were picked from full-scan spectra of the samples.

3.3.2 Carboxylic acids

For carboxylic acids (acetic acid, formic acid and lactic acid), the quantitative analysis was carried out with a Prominence LC-20A series HPLC system. The analytical column (SHIM-PACK SCR-101H; 300mm×7.9mm×10μm) was maintained at 60°C and the mobile phase was 0.025% (v/v) H_2SO_4 run at a flow rate of 0.7 mL/min. Analytical methods were validated in the concentration range of 0.3125 mg/L to 100 mg/L. nine points calibration curves showed good linearity values (R^2) of > 0.9999.

3.3.3 Residual persulfate

Residual PS concentrations were determined by colorimetric method (Villegas et al, 1963) and Jenway 6300 spectrophotometer instrument (wavelength 320~1000 nm, accuracy ±1% transmittance, ±0.01 absorbance at 1.000 Absorbance, light source: Tungsten Halogen lamp, designed in UK) was employed to measure the total PS concentration in the samples at 615 nm wavelength.

3.3.4 Iron and aluminum release

In order to measure Fe and Al content of each treated samples by ZVI/PS and ZVA/PS, 40 ml sample aliquots were taken at regular time intervals. The samples were filtered through 0.22 μm PVDF syringe filters and immediately quenched by adding 2 ml of freshly prepared Sodium sulphite (Na_2SO_3) 10% (w/v) at an

equimolar ratio to the determined PS concentration instead of the routine pH-re-adjustment procedure. Fe and Al release were measured by the inductively coupled plasma mass spectrometry (ISO 17294-2, 2003).

3.3.5 Chloride release

Cl^- analysis was conducted by Ion Chromatography (Dionex Corporation, Sunnyvale, CA, USA) equipped with a conductivity detector and an analytical column (AS14A). Samples were filtered through 0.22 μm PVDF filters (Millipore) and stored at 4°C until quantification. The IC was operated in auto-suppression mode with a 1 mM $NaHCO_3$/8 mM Na_2CO_3 eluent mixture at a flow rate of 1.0 mL/min.

3.4 Other Procedures

The organic carbon content of the samples (DOC and TOC) was measured on a Shimadzu V_{PCN} analyzer (Japan) equipped with an autosampler according to the combustion method and an Orion 720^+ model pH-meter (Thermo Scientific, USA) was employed to measure pHs of samples. The SWW sample was characterized in terms of conventional environmental parameters (APHA, 2012).

3.5 Bioanalytical Procedures

3.5.1 Acute toxicity experiments in synthetic tertiary treated urban wastewater

3.5.1.1 Luminescence inhibition test with photobacteria *Vibrio fischeri*

Among a wide variety of bioassays, the marine bioluminescent bacterium, *V. fischeri* is the most used microorganism (Rizzo, 2011) due to high sensitivity towards a wide range of pollutants and ease of usage (Dalzell et al, 2002; Parvez et al, 2006). *V. fischeri* toxicity test relies on the change in the bacterial luminescent when the microorganisms are exposed to toxic chemicals (Farré and Barceló, 2003).

Acute toxicity changes during photolytic, homogeneous photochemical and heterogeneous catalytic treatments of each model industrial micropollutants were measured by using a commercial assay kit marketed as BioTox^{TM} (Finland) (ISO 11348-3, 2007). The inhibition of light emission by cultures of *V. fischeri* is determined by means of a batch test. This is accomplished by combining specified volumes of the test sample or the diluted sample with the luminescent bacteria

suspension in a test tube. The test criterion is the luminescence, measured after a contact time of 15 min by a spectrophotometer. Prior to the assay the pH of all samples was adjusted to 7.0±0.2 with 1-4 N NaOH or 1-4 N H_2SO_4 solutions and any possible solid particles were removed via 0.22µm filtration. The sample solutions were oxygenated by stirring overnight and a chloride concentration 2% (w/v) was prepared in each sample through adding NaCl. In order to eliminate the positive effect of PS on the toxicity test results, any unreacted (remaining) PS in the samples was decomposed by adding sodium thiosulfate (STS) with a stoichiometry of 2 mol STS per mol of PS in each 20 mL of sample (2 mg STS in each 20 mL of sample for photochemical experiments and 9.5 mg STS in each 20 mL of sample for heterogeneous catalytic experiments) (Olmez-Hanci et al, 2014a).

Freeze-dried photobacteria and all samples vials were placed in a chilling/heating dry bath device (EchoTherm^{TM}) at 4 ºC for 30 min and then after its temperature increased to 15 ºC for another 30 min. 500 µL of each sample was mixed with 500 µL luminescent bacterial suspension (dilution ratio=50%, v/v) in each test vials and put in the luminometer (Luminoskan TL Plus, Thermo Lab Systems, Finland). The relative inhibition of light emitted by the V. fischeri photobacteria was measured in relative luminescence units (RLU) after 15 min contact time at 15 ºC. The percent relative inhibition was calculated relative to a control by the following equation;

$$Relative\ inhibition(\%) = 100 \times (RLU_c - RLU_t)/(RLU_c) \qquad (3.1)$$

Where RLU_t is the average RLU of *V. fischeri* photobacteria exposed to samples at time t and RLU_c refers to the average RLU of *V. fischeri* photobacteria exposed to the controls.

3.5.1.2 Growth inhibition test with microalgae *Pseudokirchneriella subcapitata*

Algaltoxkit F^{TM} (MicroBioTests, Inc., Gent, Belgium) was used to measure the acute toxicity towards the freshwater microalgae *P. subcapitata* (ISO 8692, 2012). Exponentially growing test organisms were exposed to the original micropollutants and their treated samples in batch cultures over a period of 72 h. The initial biomass concentration must be adequately low to allow exponential growth during the incubation period without risk of nutrient depletion. Besides that, Initial biomass concentration should not exceed 0.5 mg/L as dry weight. Algal biomass is defined as

the dry weight per volume (e.g. mg algae/L) test solution. However, dry weight is difficult to measure and therefore surrogate parameters are used. Controls and treated samples were inoculated with a predetermined volume of concentrated suspension algae to supply 1×10^4 cell/mL as initial concentrations. Three replicates were prepared for each control and treated sample. After inoculation, the vessels containing replicates were shaken and placed in the culturing apparatus under continuous fluorescent illumination (sideway illumination=10000 lx). The replicates should be maintained at a temperature in the range of 23 ºC±2 ºC. The cell densities of the replicates were measured after each 24 h interval up to 72 h. For each sample replicate, the algal biomass concentration was calculated by the measured optical density in a cuvette with 10 cm path-length employing a Jenway 6300 spectrophotometer instrument 670 nm.

The specific growth rate, μ (h^{-1}), for each control and treated batch replicate, was calculated using the following equation;

$$\mu = (ln\ N_L - ln\ N_0)/(t_L - t_0) \tag{3.2}$$

Where N_0 is the initial cell density; N_L is the measured cell density at time t_L (h); t_0 (h) is the time of test start; t_L (h) is the time of test termination.

Percent relative inhibition was calculated by the following equation;

$$Relative\ inhibition(\%) = 100 \times (\mu_c - \mu_i)/\mu_c \tag{3.3}$$

Where μ_i (h^{-1}) is the growth rate for test batch i and μ_c (h^{-1}) is the mean growth rate for the control batches. The untreated SWW sample was used as the control of the bioassay.

3.5.2 Genotoxicity experiments in pure water: Ames mutation test

The microbial mutagenicity Ames test is a simple, rapid and robust bacterial bioassay accomplished in vitro to evaluate the mutagenicity of various environmental samples such as pesticides, drugs, dyes, reagents, and other substances which are easily solubilized in a liquid suspension and since 1989 has been included as a proposed mutagenicity test in the standard methods for examination of water and wastewater (Gupta et al, 2009).

The mutagenicity assay was performed using a mutant strain of *S. typhimurium* TA 1535 according to the standard Ames practice. *S. typhimurium* TA 1535 is susceptible to additional mutations because of deficiencies in the repair mechanisms; also, it is more permeable to the possible mutagens. In this assay, cells are cultivated on histidine-free culture media; therefore, only cells regaining the ability to synthesize histidine survive. Regaining this ability can be spontaneous or mutagen-driven. A certain compound is accepted as mutagen only the rate of mutation caused by this compound is twice the rate of spontaneous mutation rate.

Before starting Ames test, histidine auxotrophy and rfa mutation must be checked. In order to check histidine auxotrophy, firstly, *S. typhimurium* TA 1535 cells were streaked on nutrient agar plate and the plate in incubated at 37 °C for 24 h. Then, a single colony was transferred to nutrient broth and culture was cultivated overnight. After reaching to optical density of 1.0 at 600 nm, culture was streaked on minimal glucose agar (MGA) plate which contains no histidine and plate was cultivated at 37 °C for 48 h. No growth was observed on MGA plate after incubation.

One of the mutations namely rfa, causes partial loss of the lipopolysaccharides barrier that coats the surface of the bacteria and increases permeability to large molecules (Mortelmans and Zeiger, 2000). In order to screen rfa mutation, 100 µL of culture with optical density of 1.0 (at 600 nm) was spread on histidine-biotin agar (HBA) plate. Then, Whatman disks immersed into 1 mg/mL crystal violet (CV) solution were placed on the plate surface. Plates were incubated at 37 °C for 48 h. After incubation, zones with no microbial growth were observed around disks (Figure. 3.2). No inhibition zone was observed around control disk, while the inhibition zone around the CV disk was indicated with arrow.
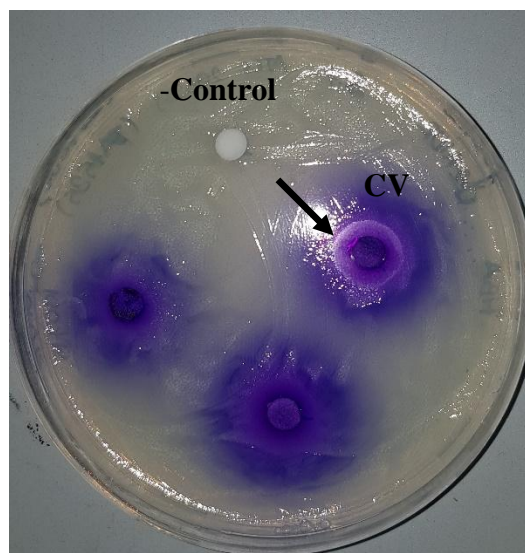
Figure 3.2 : HBA plate after incubation.

In Ames test, DW was used as negative control while sodium azide (NaN$_3$) was used as positive control for *S. typhimurium* TA 1535. Single colony from a fresh plate was transferred to 20 mL of 2.5% nutrient broth and incubated at 37 ℃ for 14 h and 210 rpm. On the next day, MGA plates with 20 mL media were prepared. Top agar was molten and its temperature was set to 50 ℃. Then top agar mixture was prepared with 1.6 mL of top agar, 100 µL of cell culture and 80 µL of histidine-biotin solution per plate. After that, it was mixed with 100 µL of sample (or sterile DW for negative control). Sodium azide concentration was adjusted to 5 µg/plate. The mixture was poured on MGA plate surface and spread the surface by gently shaking the plate. Ames test was performed as triplicate per sample. All plates were incubated at 37 ℃ for 48 h and colony formations were observed.

4. RESULTS AND DISCUSSION

4.1 Treatability of the Model Industrial Micropollutants in Distilled Water

Generally the performance of photochemical oxidation processes as well as heterogeneous catalytic oxidation processes in aqueous pollutant removal, is affected by various variables such as initial oxidant concentration, pH and treatment time (Gao et al, 2012; Hayat et al, 2019; Hussain et al, 2014; Hussain et al, 2012; Ren et al, 2019; Sharma et al, 2015). Assessment of all these variables is too time-consuming and complicated, so considering those variables can play a significant role on treatment performance is important. In this section, the result of treatability of three models micropollutant in DW aiming at investigation of the effect of initial PS concentration and pH were explained and discussed.

4.1.1 3,5-Dichlorophenol

4.1.1.1 Ultraviolet-C-activated persulfate oxidation processes

In order to evaluate the individual/combined/synergistic effects of PS and UV-C light, control experiments were conducted (PS only; UV-C only). The experiment performed with PS only at an initial concentration of 1.00 mM and a pH of 6.3 indicated that 3,5-DCP (2 mg/L) could not be oxidized by using PS without activation (data are shown in appendix A), as expected, due to its limited reduction potential compared to $HO^{\bullet}$ and $SO_4^{\bullet-}$. On the other hand, complete 3,5-DCP degradation was achieved by UV-C photolysis after 80 min indicating that direct UV-C photolysis was very effective in terms of 3,5-DCP degradation as has already been reported in earlier studies (Boule et al, 1984; Hwang et al, 1986; Karci et al, 2013b).

Effect of initial persulfate concentration

Figure 4.1 shows the effect of initial PS concentration on normalized 3,5-DCP concentration decay at the natural pH of aqueous 3,5-DCP solution (pH=6.3). 3,5-DCP degradation could be fitted into pseudo-first-order kinetics with high correlation

coefficients ($R^2 \geq 0.98$) and the calculated 3,5-DCP apparent degradation rate coefficients (k values, in min^{-1}) were also provided in Figure 4.1 as a figure insert. From Figure 4.1 it is evident that 3,5-DCP decay rates increased with increasing initial PS concentrations which can be described by an increase in the steady-state concentration of $SO_4^{\bullet-}$. According to Figure 4.1, complete 3,5-DCP degradation was obtained after 60 min, 20 min and 2 min at initial PS concentrations of 0.02 mM, 0.10 mM and 1.00 mM, respectively. In a former related study (Antonaraki et al, 2002), the photochemical degradation of CPs under UV-C light in the presence of 0.1 M H_2O_2 was investigated and similar apparent degradation rate constants were obtained. It was also found that when two chlorine substituents exist in the *meta* positions of the phenolic ring, the photodecomposition rate accelerates significantly which can be ascribed to the stronger activation of the free positions compared to mono-CPs (Antonaraki et al, 2002).

Figure 4.1 : Changes in normalized 3,5-DCP concentration UV-C and UV-C/PS treatments in DW at varying initial PS concentrations. 3,5-DCP=2 mg/L; UV-C intensity=0.5 W/L; pH=6.3. Figure 4.1 insert shows the calculated apparent degradation rate constants for 3,5-DCP (in min^{-1}) varying with the initial PS concentrations for 0.00-0.10 mM PS.

In another related study (Chen et al, 2017), the degradation of 2,4-DCP, one of 3,5-DCP's isomers, was investigated using the UV-C/PS treatment process at different

initial PS concentrations in the range of 0.10 mM to 0.90 mM to follow 2,4-DCP degradation kinetics. 2,4-DCP abatement rates increased with increasing PS concentration and no inhibition was observed at elevated (excessive) PS concentrations revealing that no free radical scavenging effects were observed in the studied PS concentration range (Chen et al, 2017). As summary, Table 4.1 presents pseudo-first-order rate coefficients and 3,5-DCP percentage removal after 120 min UV-C photolysis and UV-C/PS treatments at varying initial PS concentrations.

Table 4.1 : The pseudo-first-order rate coefficients and 3,5-DCP removal percentage after 120 min UV-C photolysis and UV-C/PS treatments at varying initial PS concentrations. 3,5-DCP=2 mg/L; pH=6.3; UV-C intensity=0.5 W/L.

PS Concentration (mM)	k (min^{-1})	3,5-DCP Removal (%)
0.000	0.0549	100
0.020	0.0669	100
0.030	0.0853	100
0.050	0.0786	100
0.075	0.1214	100
0.100	0.3105	100

Effect of initial pH

In order to investigate the effect of initial pH on 3,5-DCP degradation with the UV-C/PS treatment process, separate experiments were conducted at an initial PS concentration of 0.03 mM and initial pH values were adjusted to 3.0, 5.0, 6.6, 7.5, 9.0 and 11.0 for this set of experiment. Figure 4.2 displays the effect of varying initial solution pH on 3,5-DCP degradation. From Figure 4.2 it is evident that the degradation efficiency of 3,5-DCP decreased with increasing pH from 3.0 to 6.6; parallel to which observation the apparent degradation rate constant decreased from 0.1211 min^{-1} to 0.0853 min^{-1}. However, upon further increase of the initial reaction pH from 6.6 to 7.5, 9.0 and 11.0, the apparent 3,5-DCP degradation rate re-increased remarkably. Complete 3,5-DCP degradation was achieved within less than 5 min at

initial solution pHs of 7.5, 9.0 and 11.0. Table 4.2 presents pseudo-first-order rate coefficients and 3,5-DCP percentage removal after 120 min UV-C/PS treatments at varying initial pHs. It might be argued that under acidic conditions (pH=3.0), additional $SO_4^{\bullet-}$ could be formed through the reactions shown in equations 4.1 and 4.2 that lead to higher $SO_4^{\bullet-}$ concentrations and consequently faster 3,5-DCP degradation rates compared to high pH environments (Neta et al, 1988);

$$S_2O_8^{2-} + H^+ \rightarrow HS_2O_8^- \tag{4.1}$$

$$HS_2O_8^- \rightarrow SO_4^{\bullet-} + SO_4^{2-} + H^+ \tag{4.2}$$

Figure 4.2 : Changes in normalized 3,5-DCP concentration during UV-C/PS treatments in DW at different initial pH values. 3,5-DCP=2 mg/L; PS=0.03 mM; UV-C intensity=0.5 W/L.

On the other hand, increasing the initial solution pH to >7.5 resulted in a rapid dissociation of 3,5-DCP (pK_a of 3,5-DCP=8.18) which might change its reactivity towards electrophilic attack free radical oxidation (Dean, 1997). In fact, ionization of 3,5-DCP to its deprotonated form is expected to enhance electrophilic attack by oxidizing species. Chen et al. (2016) also investigated the UV-C/PS oxidation of 6 µM 2,4-DCP in water with 0.90 mM PS at different initial pH values varying from 5 to 8. In that study, the highest apparent 2,4-DCP degradation rate constant being

calculated as 0.00351 min^{-1} was obtained at pH=7, below and beyond which it slightly decreased (Chen et al, 2016). In another study, the degradation of antipyrine by UV/PS treatment at pH=2.5-11.5 was investigated. It could be shown that by increasing initial pH from 2.5 to 11.5, the apparent degradation rate constant of antipyrine increased constantly from k=1.346 h^{-1} to k=2.005 h^{-1} (Tan et al, 2013). From all of these studies, it can be generally concluded that the effect of pH on UV/PS oxidation of pollutants may vary and is pH- as well as pollutant-dependent.

Table 4.2 : The pseudo-first-order rate coefficients and 3,5-DCP removal percentage after 120 min UV-C/PS treatments at varying initial pHs. 3,5-DCP=2 mg/L; PS=0.03 mM; UV-C intensity=0.5 W/L.

pH	k (min^{-1})	3,5-DCP Removal (%)
3.0	0.1211	100
5.0	0.0891	100
6.6	0.0853	100

4.1.1.2 Zero-valent iron-activated persulfate oxidation process

In order to investigate the capability of ZVI (1 g/L) in 3,5-DCP degradation, a control experiment was conducted with an initial concentration of 2 mg/L 3,5-DCP at initial pH of 5.0 in DW in the absence of PS. There was no 3,5-DCP removal in solutions in PS absent (ZVI only), indicating that ZVI alone could not cause 3,5-DCP degradation. The results were in agreement with the observations of Zhao et al. (2016) who investigated bisphenol A and phosphate in ZVI and ZVI/PS with ZVI concentration in the range of 0.1 g/L to 0.5 g/L (Zhao et al, 2016).

Effect of initial persulfate concentration

Figure 4.3 depicts the effect of initial PS concentration in the range of 0.10 mM to 1.00 mM on normalized 3,5-DCP concentration (pH=5.0). As can be seen from Figure 4.3, an induction phase (<40 min) was evident for all studied PS concentrations during ZVI/PS treatments. 3,5-DCP removal started after 40 min with different abatement rates. According to Figure 4.3, no 3,5-DCP removal was achieved for 0.10 mM PS and the obtained removal efficiency was rather negligible

(5%) for 0.25 mM PS. Starting from 0.25 mM PS, 3,5-DCP removal efficiencies increased with increasing PS concentrations. Maximum removal efficiencies after 120 min of treatment were obtained as 11%, 27% and 59% for 0.50 mM PS, 0.75 mM PS and 1.00 mM PS, respectively.

Figure 4.3 : Changes in normalized 3,5-DCP concentration during ZVI/PS treatments in DW at varying initial PS concentrations. 3,5-DCP=2 mg/L; ZVI=1 g/L; pH=5.0.

This effect could be attributed to the formation of more $SO_4^{\bullet-}$ generation as a result of PS activation by ZVI. Generally, increment in PS could lead to more generation of $SO_4^{\bullet-}$. On the other hand, it has also been reported in several literatures (Barzegar et al, 2018; Luo et al, 2019) that higher PS concentration could have negative effect on the concentration of $SO_4^{\bullet-}$ through scavenging reactions. However, during ZVI/PS treatment of 3,5-DCP in the range of 0.10 mM to 1.00 mM PS, no inhibitory effect of excess PS was observed.

Effect of initial pH

It has already been demonstrated that the solution pH is a critical factor affecting the performance of the ZVI/PS treatment in the degradation of contaminants due to its function in control of the activity of the free radicals, the catalytic activity, and Fe species (Barzegar et al, 2018; Wei et al, 2016). From previous studies, it was

reported that acidic environment could better promote the ZVI/PS system reaction (Gao et al, 2020; Hussain et al, 2014; Hussain et al, 2012; Zhao et al, 2010a) most probably due to accelerated ZVI corrosion that facilitates Fe^{2+} formation. Hence, in order to investigate the pH effect on 3,5-DCP degradation during ZVI/PS treatment, pH values of 3.0 and 5.0 and a PS concentration of 0.50 mM were tested. From Figure 4.4, it is apparent that 3,5-DCP removals were enhanced when the initial solution pH was decreased from 5.0 to 3.0 during ZVI/PS treatment because the acidic condition (in this case pH=3.0) is favorable for the formation and maintain of Fe^{2+} that play an important role in producing $SO_4^{\bullet-}$ (Wei et al, 2016; Xiao et al, 2020).

The overall percent 3,5-DCP removal efficiency was obtained as 11% at pH 5.0 after 120 min, whereas complete removal of 3,5-DCP was realized at pH 3.0 for a treatment period of 20 min. The results of the present study were also in agreement with previous findings. For example, pH 3.0 was shown to be the most favorable pH for bentazon degradation with ZVI/PS system over a wide range of studied pH from 3.0 to 11.0 (Wei et al, 2016).

△ pH 3.0   ◇ pH 5.0

Figure 4.4 : Changes in normalized 3,5-DCP concentration during ZVI/PS treatments in DW at different initial pH values. 3,5-DCP=2 mg/L; PS=0.50 mM; ZVI=1 g/L.

65

4.1.1.3 Zero-valent aluminum-activated persulfate oxidation process

In order to investigate the effect of ZVA (1 g/L) on 3,5-DCP removal, a control experiment was run with an initial concentration of 2 mg/L 3,5-DCP at initial pH of 3.0 in DW in the absence of PS. Obtained results (data are shown in Appendix A) indicated that 3,5-DCP removal was limited to 22%. From the result, it can be concluded that mere ZVA (in the absence of PS) was not effective in terms of 3,5-DCP degradation. Similar trends for low and slow micropollutant removals by mere ZVA have been already presented in the previous studies (Arslan-Alaton et al, 2017a; Yangin-Gomec et al, 2018). In the study by Arslan-Alaton et al. (2017a), Bisphenol A degradation was explored employing ZVA in acidic condition (pH=3.0) and in the absence of H_2O_2 or PS. The results demonstrated that the Bisphenol A degradation after 120 min was limited to less than 10% while by addition only 0.25 mM PS, complete Bisphenol A was achieved in 40 min. indicating the presence of an oxidizing agent is substantial for effective Bisphenol A degradation (Arslan-Alaton et al, 2017a).

Effect of initial persulfate concentration

The effect of initial PS concentration in the range of 0.10 mM to 1.00 mM on normalized 3,5-DCP concentration was investigated during ZVA/PS (pH=3.0). According to the data presented in Figure 4.5, the highest 3,5-DCP abatement of 31% was reached with 1.00 mM of PS. The other examined PS concentrations (0.10-0.75 mM) exhibited quite similar degradation rates, which did not exceed 21% removal of 3,5-DCP (Figure 4.5).

In the present study, ZVA/PS treatment was found to be inefficient for the complete removal of 3,5-DCP. Although activation of PS with ZVA was not suitable for the investigated micropollutant oxidation, full degradation of bisphenol A and 95% removal of iopamidol under similar reaction conditions were reported in the literature (Arslan-Alaton et al, 2017a; Arslan-Alaton et al, 2017c).
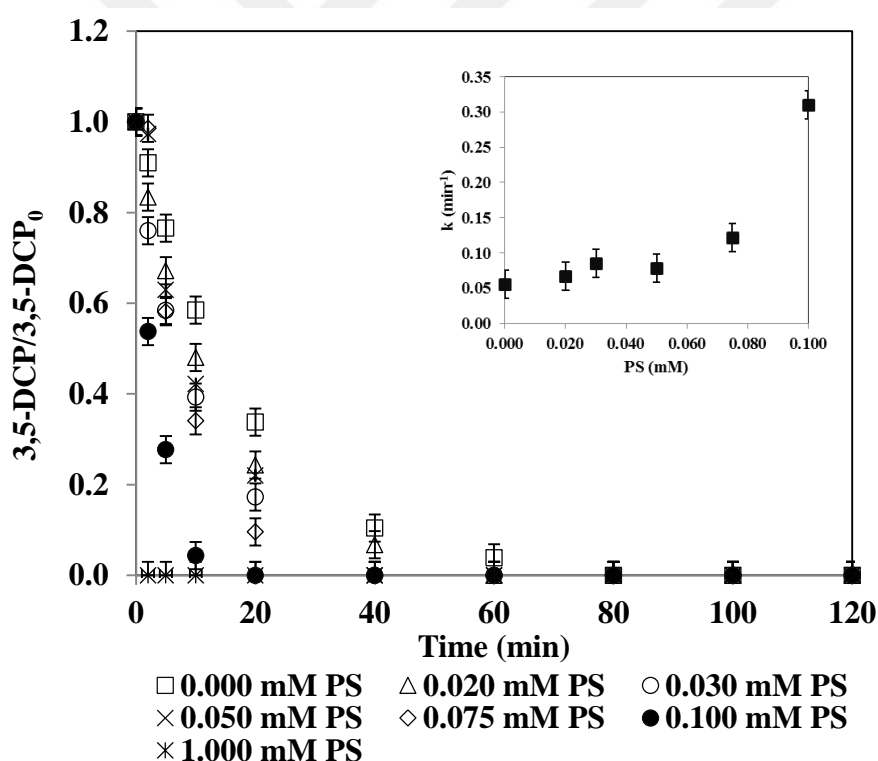
Figure 4.5 : Changes in normalized 3,5-DCP concentration during ZVA/PS treatments in DW at varying initial PS concentrations. 3,5-DCP=2 mg/L; ZVA=1 g/L; pH=3.0.

Effect of initial pH

The effect of solution pH on 3,5-DCP degradation was investigated with initial solution pH of 1.5 and 3.0 During ZVA/PS treatment of 3,5-DCP (PS=0.50 mM). Due to inherent activity/reactivity of ZVA, these particles might be easily covered with a hydrated alumina layer (with Al_2O_3+ Al(oxy) hydroxide) (Arslan-Alaton et al, 2017c; Bokare and Choi, 2009). Several studies have shown that extremely acidic conditions or an acid washing procedure should be applied in order to dissolve and hence get rid of the oxide layers on the ZVA nanoparticles to promptly initiate Fenton/Fenton-like reactions (Arslan-Alaton et al, 2017a; Arslan-Alaton et al, 2017c; Bokare and Choi, 2009; Ren et al, 2019). Thus, pH of the reaction solution plays a crucial role in the degradation of micropollutants by ZVA/oxidant treatment systems.

In order to investigate the effect pH on 3,5-DCP degradation, 0.50 mM of PS and pH values of 1.5 and 3.0 were selected. The effect of initial pH on PS activation with ZVA is delineated in Figure 4.6. Obviously, there was a general trend of increasing 3,5-DCP abatement with decreasing initial pH (Figure 4.6). 3,5-DCP removal efficiency after 120 min ZVA/Ps treatment, was enhanced from 20% to 77% (Figure

4.6) when reaction pH was reduced from 3.0 to 1.5. However, still complete degradation of the investigated micropollutants was not realized. The higher removal efficiencies obtained at pH 1.5 might be due to fast dissolution of the oxide layer on ZVA nanoparticles that facilitated surface oxidation reactions. It should be pointed out that during the corrosion of ZVA nanoparticles under acidic conditions, pH might be increased due to the formation of Al^{3+} and hydroxide ions (Bokare and Choi, 2009). As Bokare and Choi (2009) indicated, as long as solution pH remains < 4 during the reaction, ZVA dissolution and hence oxidation reactions will continue even in the absence of PS activation. In the present study, an overall, a slight increase in the solution pH from 1.5 to 2.0 and from 3.0 to 3.4 was observed due to the following redox reaction, equation 4.3 (Bokare and Choi, 2009);

$$2Al^0 + 1.5\,O_2 + 3H_2O \rightarrow 2\,Al^{3+} + 6OH^- \qquad (4.3)$$
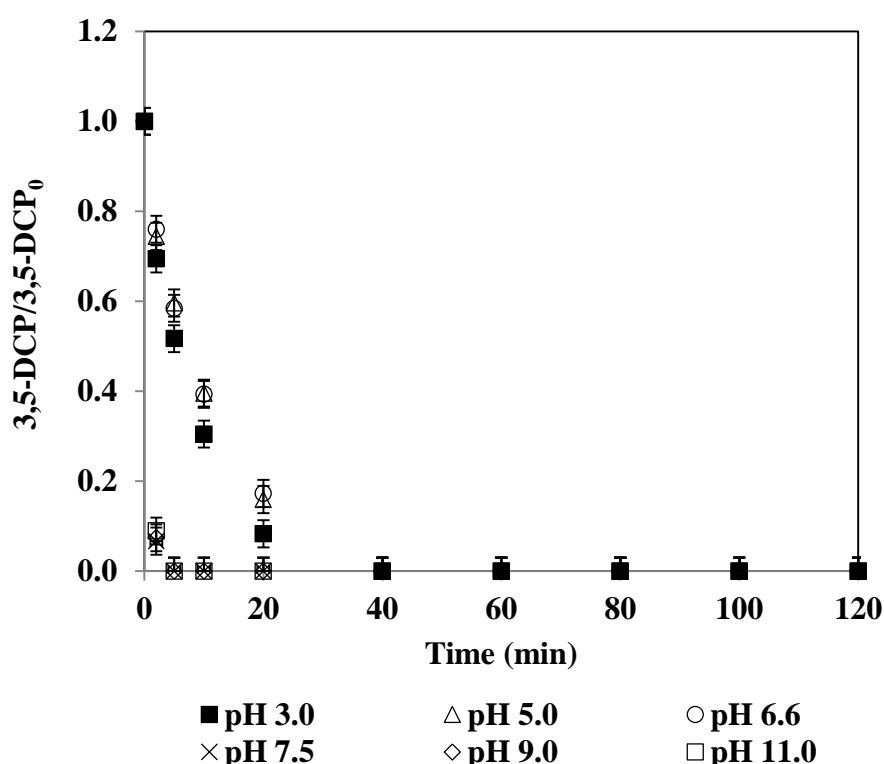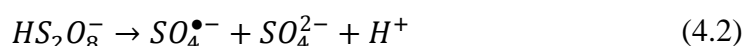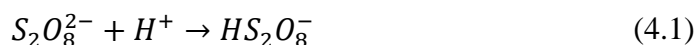

△ pH 1.5 ◇ pH 3.0

Figure 4.6 : Changes in normalized 3,5-DCP concentration during ZVA/PS treatments in DW at different initial pH values. 3,5-DCP=2 mg/L; PS=0.50 mM; ZVA=1 g/L.

4.1.2 2,4-Dichloroaniline

4.1.2.1 Ultraviolet-C-activated persulfate oxidation processes

First of all, two control experiments (only PS; only UV-C) were conducted in order to realize whether mere PS and mere UV-C irradiation could result in any reduction in 2,4-DCA concentration during 120 min with initial pH of 6.0. It should be mentioned here that, the initial PS concentration 1.00 mM was the highest initial PS concentration being used in this experimental part. The findings demonstrated that PS without UV-C irradiation resulted in poor 2,4-DCA removal (5%) with initial 2,4-DCA concentration 2 mg/L after 120 min treatment (data are shown in appendix A) which was expected due to PS has a lower reduction potential (E^0=2.1 eV at room temperature depending on the pH) (Araújo et al, 2018) in comparison to $SO_4^{\bullet-}$ (E^0=2.5–3.1 eV at room temperature depending on the pH) (Kolthoff and Miller, 1951). However, as it can be seen in Figure 4.7 complete 2,4-DCA was achieved only after 20 min UV-C photolysis. In a similar related study, direct photolysis of 13 mg/L 4-CA led to complete transformation within less than 20 min (Ratti et al, 2015). In that study direct photolysis of 4-CA led to the heterolytic dechlorination of excited state species of 4-CA. Excited states of CAs have been suggested to be generated as a result of their UV absorption (Othmen et al, 2000; Ratti et al, 2015). Consequently, in these excited state, CAs can undergo intramoleculat transformation and stabilize states with different electron distribution, in turn decomposing to radical or macular products (Ratti et al, 2015).

Effect of initial persulfate concentration

Figure 4.7 shows the effect of initial PS concentration on normalized 2,4-DCA concentration at the natural pH of aqueous 2,4-DCA solution (pH=6.0). From Figure 4.7, it could be seen that the combination of PS with UV-C irradiation at all studied initial PS concentrations enhanced the 2,4-DCA removal. This increase in the 2,4-DCA removal can be attributed to $SO_4^{\bullet-}$ being generated in the reaction solution due to the photohomolysis of PS according to equation 2.1. It should also mentioned here that 2,,4-DCA degradations by UV-C/PS at different initial PS concentrations, were too fast such that there were not enough data to be fitted into pseudo-first-order kinetics.

Figure.4.7.: Changes in normalized 2,4-DCA concentration during UV-C and UV-C/PS treatments in DW at varying initial PS concentrations. 2,4-DCA=2 mg/L; UV-C intensity=0.5 W/L; pH=6.0.

Effect of initial pH

The effect of initial pH of aqueous 2,4-DCA solution on the normalized 2,4-DCA concentration is represented in Figure 4.8 The initial pH values of 3, 5, 7, 9 and 11 were chosen as the representative of acidic, neutral and alkaline media, respectively and initial 2,4-DCA and PS concentrations were considered 2 mg/L and 0.10 mM, respectively. It should be mentioned here the pH of all three target model micropollutants was not buffered to avoid scavenging of the formed radicals by inorganic constituents being generally present in buffer solution (Kang et al, 2009).

As it can be seen from Figure 4.8, for all examined pHs, the normalized 2,4-DCA concentrations decreased with increasing the initial solution pH. In fact with increasing the initial solution pH in the range of 3.0 to 11.0, rapid decomposition of 2,4-DCA was observed.
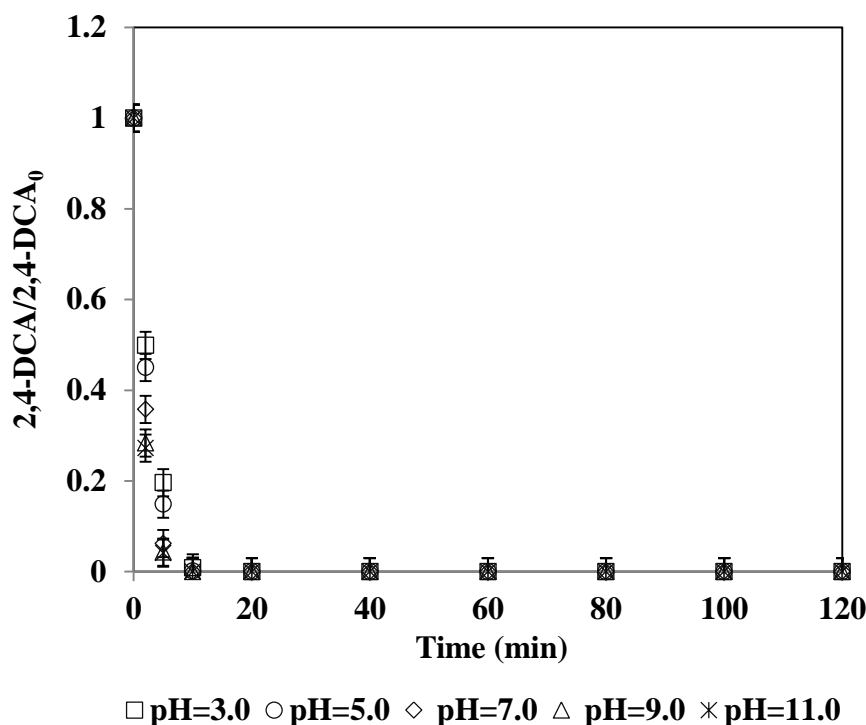
Figure 4.8 : Normalized 2,4-DCA concentration decay during UV-C/PS treatments in DW at different initial pH values. 2,4-DCA=2 mg/L; PS=0.10 mM; UV-C intensity=0.5 W/L.

4.1.2.2 Zero- valent iron-activated persulfate oxidation process

In order to examine the effect of ZVI (1 g/L) on 2,4-DCA removal, a control experiment was carried out in with an initial 2,4-DCA concentration of 2 mg/L at initial pH of 5.0 in the absence of PS. The results (data are shown in Appendix A) indicated that poor removal was obtained under above mentioned conditions indicting that ZVI was not effective in 2,4-DCA removal in the absent of the PS as an oxidant. This finding is in accordance with other studies that find poor pollutant removals by only ZVI (Kim et al, 2018; Oh et al, 2010; Zhao et al, 2016).

Effect of initial persulfate concentration

Figure 4.9 exhibits the effect of initial PS concentration in the range of 0.10 mM to 1.00 mM on normalized 2,4-DCA concentration (pH=5.0). As can be seen from Figure 4.9, the degradation of 2,4-DCA was clearly enhanced by increasing the initial PS concentration from 0.10 mM to 0.75 mM. Percent 2,4-DCA removal efficiencies obtained at the end of 120 min for initial PS concentrations of 0.10 mM , 0.25 mM and 0.50 mM, were 15%, 23% and 91%, respectively. Complete 2,4-DCA degradation was achieved after 80 min treatment with 0.75 mM PS. On the other

hand, when the initial PS concentration increased from 0.75 mM to 1.00 mM, the time required for complete 2,4-DCP removal increased from 80 min to 100 min.
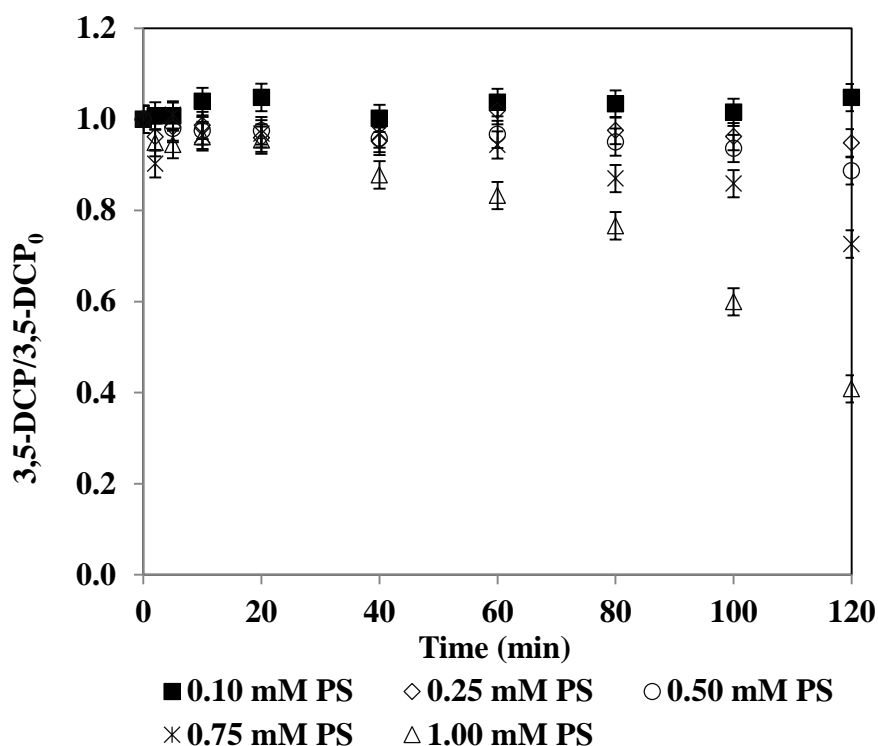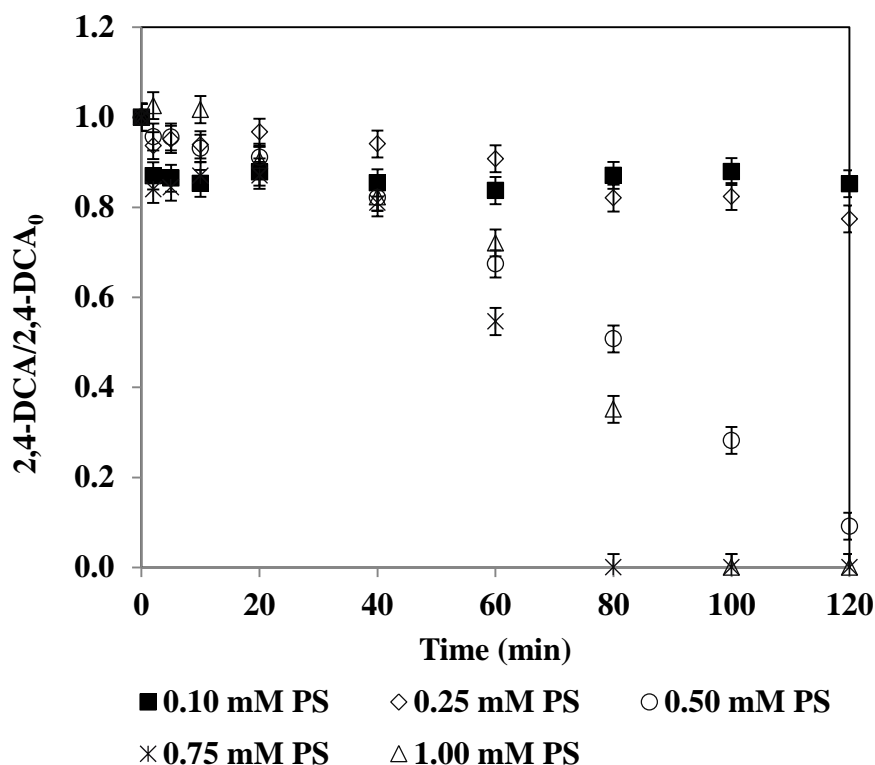

Figure 4.9 : Changes in normalized 2,4-DCA concentration during ZVI/PS treatments in DW at varying initial PS concentrations. 2,4-DCA=2 mg/L; ZVI=1 g/L; pH=5.0.

This effect might be caused due to several reasons such as $SO_4^{\bullet-}$-scavenging reaction with excessive PS and/or Fe^{2+} concentrations rather than with the target pollutant or radical recombination reactions through equations 2.11-13. Similar results were also presented for ZVI/PS treatment of bentazon, where PS increment from 0.787 mM to 1.050 mM resulted in decrease reaction rate constant from 0.0753 min^-1 to 0.0182 min^{-1} (Wei et al, 2016). Another study by Hayat et al. (2019) dealing with degradation of imidacloprid by ZVI/PS, reported that increasing PS concentration from 2.5 mM to 10 mM (30 ppm of compound was used) led to reduction in degradation from 88 to 58.82% after 180 min (Hayat et al, 2019).

Effect of initial pH

Figure 4.10 depicts the effect of initial pH solution on normalized 2,4-DCA concentration during ZVI/PS with an initial PS concentration of 0.50 mM. 91% 2,4-DCAremoval was evidenced after 120 min by ZVI/PS treatment at pH 5.0. Decreasing the pH from 5.0 to 3.0 accelerated the 2,4-DCA degradation rate and

100% removal was achieved after 10 min ZVI/PS treatment. This can be explained that the acidic conditions favor rapid corrosion of ZVI and therefore under more acidic conditions, extra $SO_4^{\bullet-}$ could be generated, which may induced the increased degradation (Hayat et al, 2019).
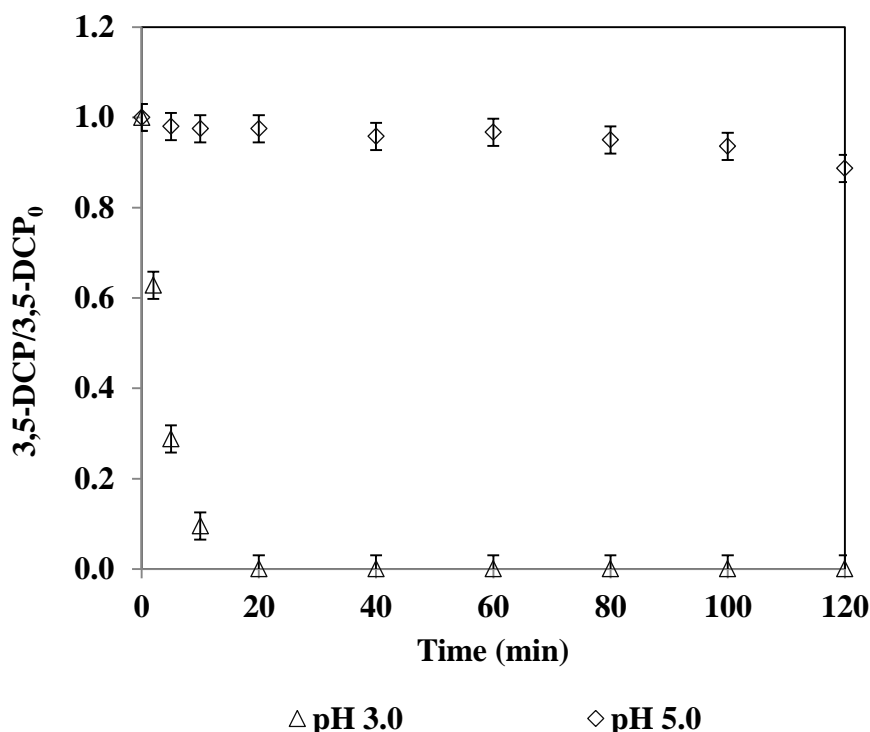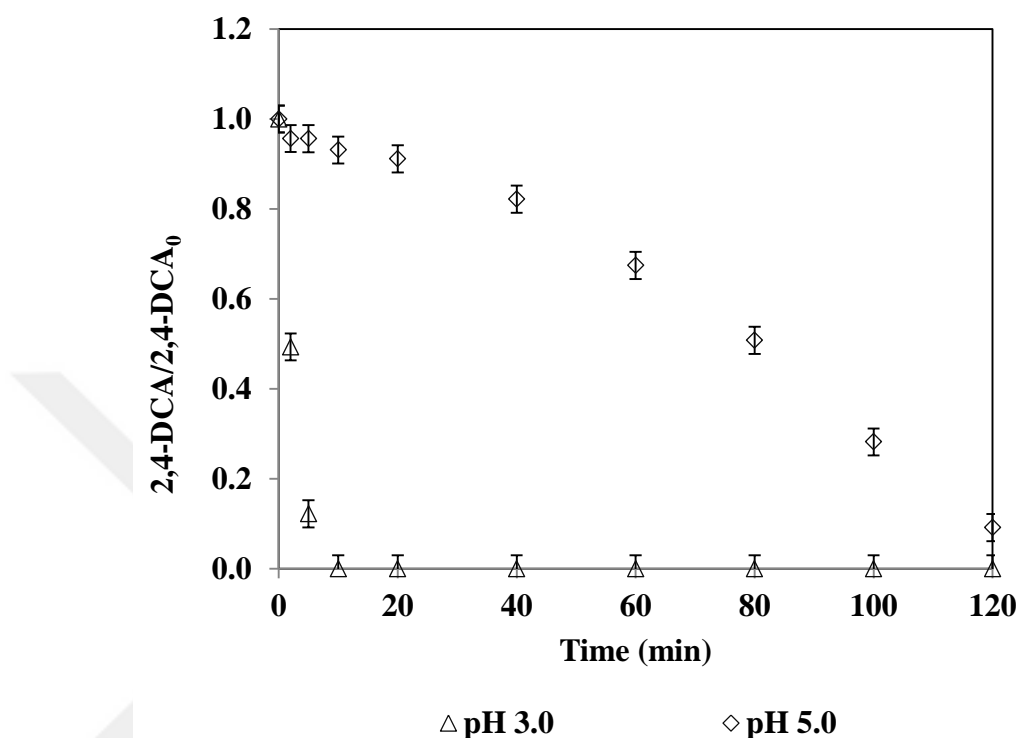

Figure 4.10 : Changes in normalized 2,4-DCA concentration during ZVI/PS treatments in DW at different initial pH values. 2,4-DCA=2 mg/L; PS=0.50 mM; ZVI=1 g/L.

Generally, the optimum pH of the Fenton and Fenton-like reactions was reported as 3.0±0.2 (Zhang et al, 2005) The reaction pH mainly affects the speciation of dissolved metal species as well as the activity/decomposition rate of the oxidants (Zhang et al, 2005). Based on the data obtained in this study, it could be concluded that the acidic reaction conditions were much better for the formation and maintaining of ferrous ion that plays an important role in $SO_4^{\bullet-}$ production (Wei et al, 2016). It should be also emphasized here that the surface properties of ZVI (the speciation of iron oxides/hydroxides on the ZVI surface) might change during the ZVI/oxidant treatment systems due to the reaction pH (Li et al, 2014a; Li et al, 2015b).

4.1.2.3 Zero-valent aluminum-activated persulfate oxidation process

A control experiment was carried out with an initial concentration of 2 mg/L 2,4-DCA at initial pH of 3.0 in DW in the absence of PS, in order to examine the effect of ZVA (1 g/L) on 2,4-DCA removal. Results (data are shown in Appendix A) revealed that 2,4-DCA removal by ZVA was poor and mere ZVA (in the absence of PS) was not effective in terms of 2,4-DCA degradation. Similar trends for poor micropollutant removals by mere ZVA have been already presented in the previous studies (Arslan-Alaton et al, 2017a; Yangin-Gomec et al, 2018).

Effect of initial persulfate concentration

Figure 4.11 delineates the effect of initial PS concentration (in the range of 0.10-1.00 mM) on normalized 2,4-DCA concentration was investigated during ZVA/PS (pH=3.0). As can be seen from Figure 4.11, the most efficient 2,4-DCA degradation (47%) was achieved at the initial PS concentration of 0.25 mM after 120 min ZVA/PS treatment. Further increase of the initial PS concentration did not enhance the 2,4-DCA degradation. All the tested PS concentrations, besides 0.25mM PS, exhibited similar elimination trends for 2,4-DCA in range of 22% to 33%. In the study of Ren et al. (2019) where trichloroethylene (0.20 mM in DW) removal by ZVA/PS at varying concentrations of PS (from 2 mM to 20 mM) was investigated (Ren et al, 2019); the trichloroethylene elimination rate constant initially increased from 0.0076 min^{-1} to 0.0317 min^{-1} and thereafter decreased to 0.0307 min^{-1} with an optimum PS concentration of 15 mM (Ren et al, 2019). These results support the presence of a pollutant-specific optimum initial PS concentration (in the present case 0.25 mM PS) in PS-activation oxidation processes, since excessive $SO_4^{\bullet-}$ concentrations might trigger self-quenching and re-combination reactions as previously given in the equations 2.11 and 2.13. In the present study, ZVA/PS treatment was found to be inefficient for the complete removal of 2,4-DCA. Although activation of PS with ZVA was not suitable for the investigated micropollutants oxidation, full degradation of bisphenol A and 95% removal of iopamidol under similar reaction conditions were reported in the literature (Arslan-Alaton et al, 2017a; Arslan-Alaton et al, 2017c).
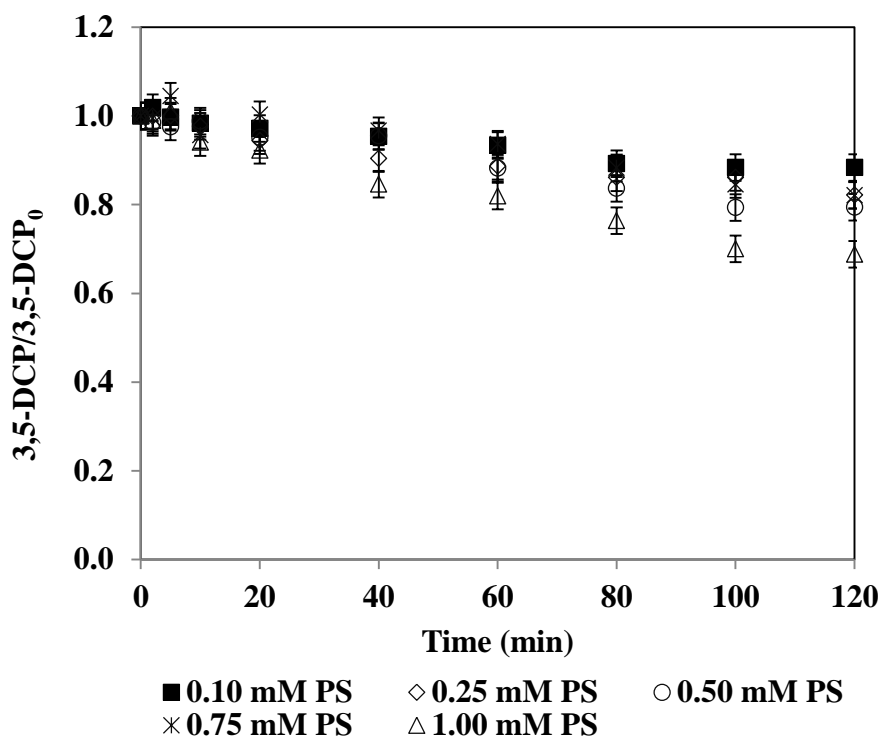
Figure 4.11 : Changes in normalized 2,4-DCA concentration during ZVA/PS treatments in DW at varying initial PS concentrations. 2,4-DCA=2 mg/L; ZVA=1 g/L; pH=3.0.

Effect of initial pH

In order to examine the effect pH on 2,4-DCA degradation, 0.50 mM of PS and pH values of 1.5 and 3.0 were chosen. The effect of initial pH on normalized 2,4-DCA is delineated in Figure 4.12. As can be seen from Figure 4.12, decreasing pH from 3.0 to 1.5, increased appreciably 2,4-DCA removal which can be explained by an increase in the concentration of $SO_4^{\bullet-}$ as a result of the enhanced corrosion of ZVA in more acidic condition (Bokare and Choi, 2009). In previous related studies it could be demonstrated that the removal of aqueous organic pollutants such as acetaminophen, phenol and bisphenol A was severely dependent on solution pH (Liu et al, 2011; Zhang et al, 2012). For example, acetaminophen removal using ZVA acid system in the pH range of 1.5 to 3.5, decreased with increasing initial pH such that its removal after 16 h treatment decreased from 99% at pH 1.5 to 46% at pH 2.5 (Zhang et al, 2012).
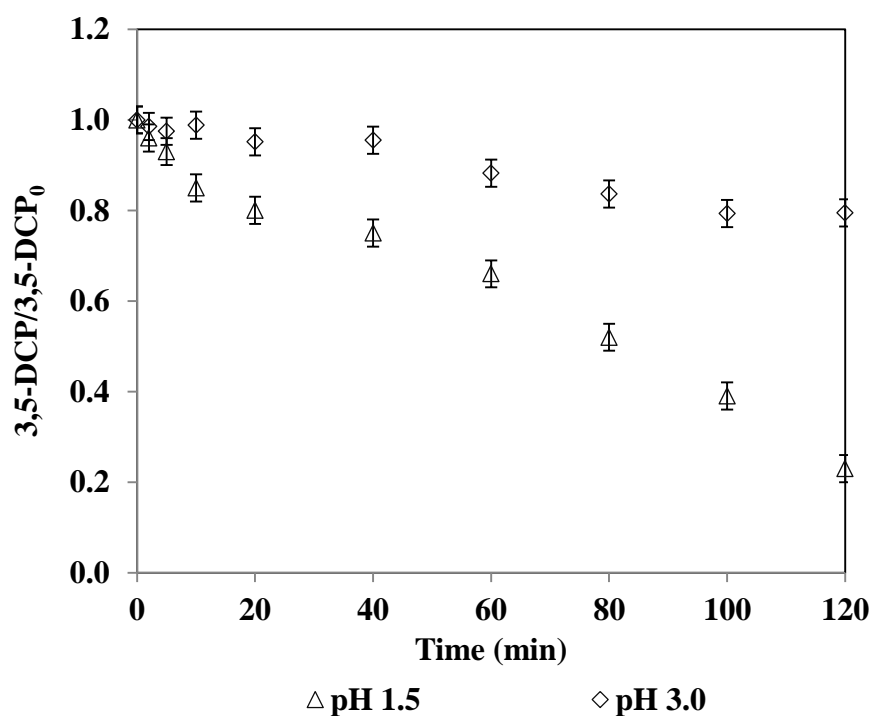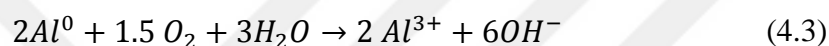
Figure 4.12 : Changes in normalized 2,4-DCA concentration during ZVA/PS treatments in DW at different initial pH values. 2,4-DCA=2 mg/L; PS=0.50 mM; ZVA=1 g/L.

4.1.3 Iprodione

4.1.3.1 Ultraviolet-C-activated persulfate oxidation processes

The control experiment performed by PS (mere PS oxidation) at concentration of 1.0 mM and pH of 6.2 indicated that IPR (2 mg/L) could not be removed by PS alone (data are shown in Appendix A). On the other hand, UV-C photolysis (in the absence of PS) resulted more than 97% IPR removal after 120 min indicating that direct UV-C photolysis was very effective in terms of IPR removal. The degradation of hydantoin pesticides including IPR by photolysis has already been examined in former study. Unlike UV-C, near-UV photolysis of IPR resulted in only 50% removal even after 180 min treatment (Lassalle et al, 2014).

Effect of initial persulfate concentration

Figure 4.13 presents the effect of varying initial PS concentrations on normalized IPR abatements. The Figure insert shows corresponding first-order IPR abatement rate coefficients (k values, in min^{-1}) obtained for this set of experiments with high correlation coefficients ($R^2 \geq 0.96$). From Figure 4.13 it is also evident that IPR

degradation rates increased with increasing initial PS concentration which can be explained by an increase in the steady-state concentration of $SO_4^{\bullet-}$. In this study, the free radical scavenging (inhibitory) effect of excessive PS concentrations was not observed for the 0.00-1.00 mM PS concentration range most probably because the highest PS concentration (1.00 mM) did not reach the critical level at which the competitive reaction of excessive PS and IPR with $SO_4^{\bullet-}$ reduced the target pollutant oxidation rate. As has been reported previously, optimum PS concentrations are case-specific (Frontistis, 2019).
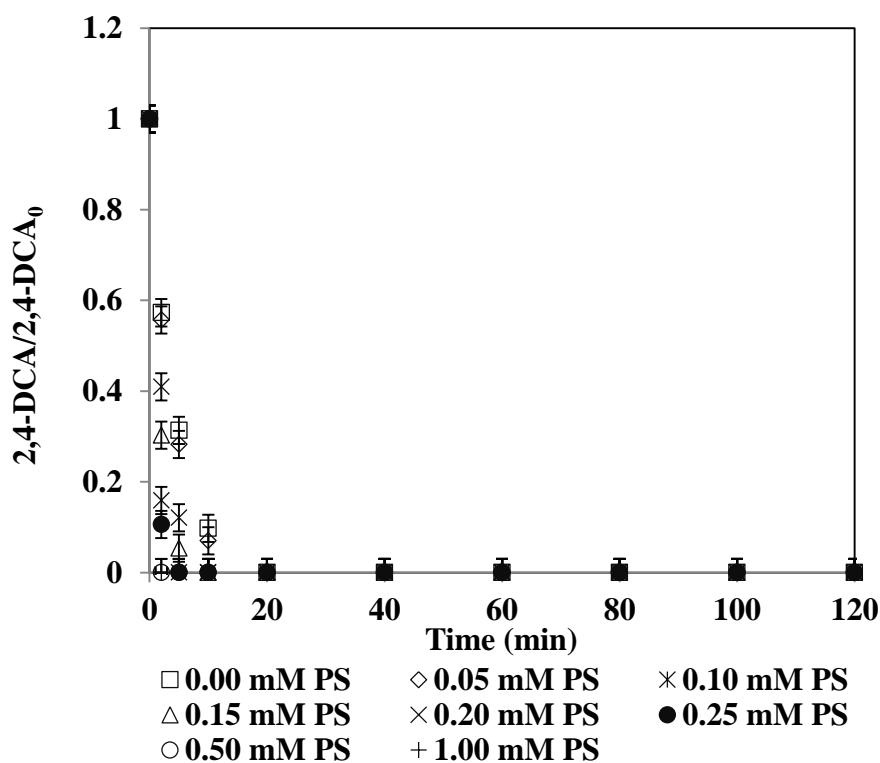

Figure 4. 13: Changes in normalized IPR concentration during UV-C and UV-C/PS treatments in DW at varying initial PS concentrations. IPR=2 mg/L; UV-C intensity=0.5 W/L; pH=6.2. Figure 4.13 insert shows the calculated apparent degradation rate constants for IPR (in min^{-1}) varying with the initial PS concentrations for 0.00-0.05 mM PS.

From Figure 4.13 it is also evident that 94% and 100% IPR removals were obtained after 20 min UV-C/PS treatment at initial PS concentrations of 0.02 mM and 0.03 mM, respectively. For the treatment of IPR in the presence of 0.05 and 0.10 mM PS, complete IPR removals were obtained in 10 min and 5 min, respectively. IPR abatements could be fitted to first-order kinetics and analysis of the first-order abatement rate constants (k values; in min^{-1}) indicated that an appreciable improvement in the photochemical oxidation rate of IPR occurred in the presence of

77

PS increasing about four times in the presence of 0.03 mM PS as compared with UV-C photolysis rates. Table 4.3 presents pseudo-first-order rate coefficients and IPR percentage removal after 120 min UV-C photolysis and UV-C/PS treatments at varying initial PS concentrations.

In former related study (Bessergenev et al, 2017), photolysis and heterogeneous photocatalytic oxidation of IPR has been reported under near-UV and visible light irradiation. Over 80% IPR could be removed by photolysis while titania-mediated, photocatalytic degradation of IPR resulted in more than 95% IPR removal as a consequence of $HO^\bullet$ formation. In that study, a five-fold increment was evidenced when IPR was degraded by $HO^\bullet$-based, heterogeneous photocatalytic treatment.

Table 4.3 : The pseudo-first-order rate coefficients and IPR removal percentage after 120 min UV-C photolysis and UV-C/PS treatments at varying initial PS concentrations. IPR=2 mg/L; pH=6.2; UV-C intensity=0.5 W/L.

PS Concentration (mM)	k (min^{-1})	IPR Removal (%)
0.00	0.0330	98
0.01	0.0504	100
0.02	0.1392	100
0.03	0.2346	100
0.05	0.4179	100
0.10	0.8485	100

Effect of initial pH

In order to investigate the effect of pH on IPR degradation with the UV-C/PS treatment process, separate experiments were conducted at an initial PS concentration of 0.02 mM and initial pH values of 3, 5, 6, 7, 9 and 11. It should be pointed out here that at pH 9 and 11 IPR was rapidly decomposed (data not shown) due to the alkaline hydrolysis of IPR that has already been reported in former study (Belafdal et al, 1986; Campos et al, 2015). Therefore, experimental findings were only presented for the pH range of 3 to 7 range for the degradation of IPR at varying

initial pH values. Figure 4.14 depicts normalized IPR abatements during UV-C/PS treatment with 0.02 mM PS at varying pHs with an insert figure presenting the calculated first-order IPR abatement rate coefficients. As can be seen from the insert of Figure 4.14, IPR degradation rate increased with the increasing pH from 3.0 to 6.0 being highest at pH 6.0 (k=0.1392 min^{-1}). Upon further increase of the initial reaction pH from 6.0 to 7.0, the IPR abatement rate coefficient decreased to 0.0825 min^{-1}. A similar finding was reported by Gao et al. (2012) who studied the UV-C/PS oxidation of sulfamethazine in water. Herein, the highest sulfamethazine degradation rate (k=7.50×10^{-2} min^{-1}) was observed at pH 6.5, below or beyond which the rate constant decreased (for 0.02 mM sulfamethazine, 0.2 mM PS) (Gao et al, 2012).
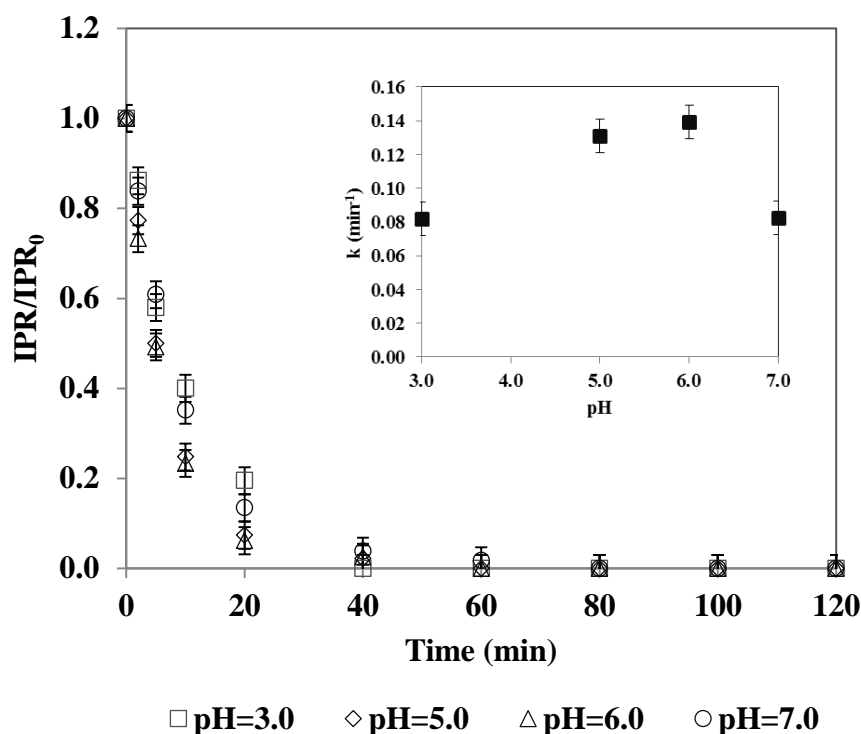
Figure 4.14 : Changes in normalized IPR concentration during UV-C/PS treatments in DW at different initial pH values. IPR=2 mg/L; PS=0.02 mM; UV-C intensity=0.5 W/L. Figure 4.14 insert shows the calculated apparent degradation rate constants for IPR (in min^{-1}) varying with the initial pH of 3.0-7.0.

On the other hand, Lin et al. (2011) found that the pseudo-first-order degradation rate constants of phenol degradation via UV-C/PS continuously increased from 0.142 min^{-1} at pH 3.0, through 0.157 min^{-1} at pH 7.0 and to 0.164 min^{-1} at pH 11.0, at initial phenol and PS concentrations of 0.5 mM and 84.0 mM, respectively (Lin et al, 2011). The rather complex pH effect observed during UV-C/PS treatment of different organic pollutants might be related to the total free radical concentration

and relative speciation of different free radicals at varying pH (Gao et al, 2012). It is also well-known that the solution pH has an important effect on the speciation of pollutants, which might change its reactivity towards free radical oxidation (electrophilic attack) with the reactivity of chemicals increasing with an increasing degree of de-protonation/ionization (Wang and Wang, 2018). That the UV-C/PS process is more sensitive to PS concentration than to pH was already reported in former study and also evidenced in the present study (Fang et al, 2018; Liang et al, 2007; Lopez-Alvarez et al, 2016). Figures 4.13 and 4.14 indicate that the effect of pH on IPR removal rate was not as pronounced as the effect of initial PS concentration; obviously, UV-C/PS oxidation of IPR was more sensitive to initial PS concentration than to pH. In a former related study (Lopez-Alvarez et al, 2016) where the influence of both parameters pH and H_2O_2 concentration on UV-C/H_2O_2 treatment of IPR removal was examined. It could be demonstrated that IPR degradation was strongly influenced by varying the initial H_2O_2 concentration while the solution pH did not affect IPR removal rates. These findings are in accord with the results of the current experimental study. As a summary, Table 4.4 presents pseudo-first-order rate coefficients and IPR percentage removal after 120 min UV-C/PS treatments at varying initial pHs.

It should be also mentioned that the pH values gradually decreased as the photochemical degradation of IPR progressed most probably due to carboxylic acid formation during its treatment. pH data is provided in Appendix B and given in Figure B1.

Table 4.4 : The pseudo-first-order rate coefficients and IPR removal percentage after 120 min UV-C/PS treatments at varying initial pHs. IPR=2 mg/L; PS=0.02 mM; UV-C intensity=0.5 W/L.

pH	k (min^{-1})	IPR Removal (%)
3.0	0.0817	100
5.0	0.1309	100
6.0	0.1392	100
7.0	0.0825	100

4.1.3.2 Zero-valent iron-activated persulfate oxidation process

No appreciable IPR removal was found with mere ZVI (in the absence of PS) during 120 min (data are shown in Appendix A) suggesting that the degradation of IPR by only ZVI was insignificant and highlighting the role of PS as an oxidant in IPR removal.

Effect of initial persulfate concentration

Figure 4.15 depicts the effect of initial PS concentration in the range of 0.10 mM to 1.00 mM on normalized IPR during ZVI/PS (pH=5.0). As can be seen from Figure 4.15, poor IPR removal was observed after 120 min ZVI/PS treatment with initial PS concentrations of 0.10 mM and 025 mM. However, by increasing initial PS concentrations to 0.50 mM and 0.75 mM, complete IPR removal was achieved for both examined PS concentrations after 120 min ZVI/PS treatment. Eventually, as the initial PS concentration rose from 0.75 mM to 1.00 mM, the required time for complete IPR degradation decreased from 120 min to only 80 min, revealing that a higher PS concentration favored IPR degradation.
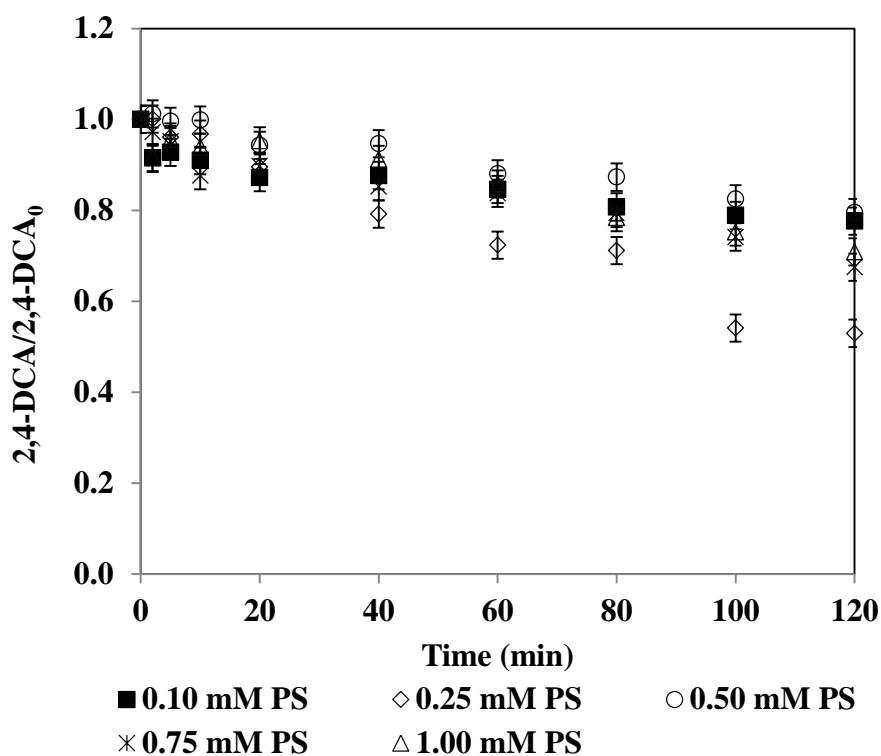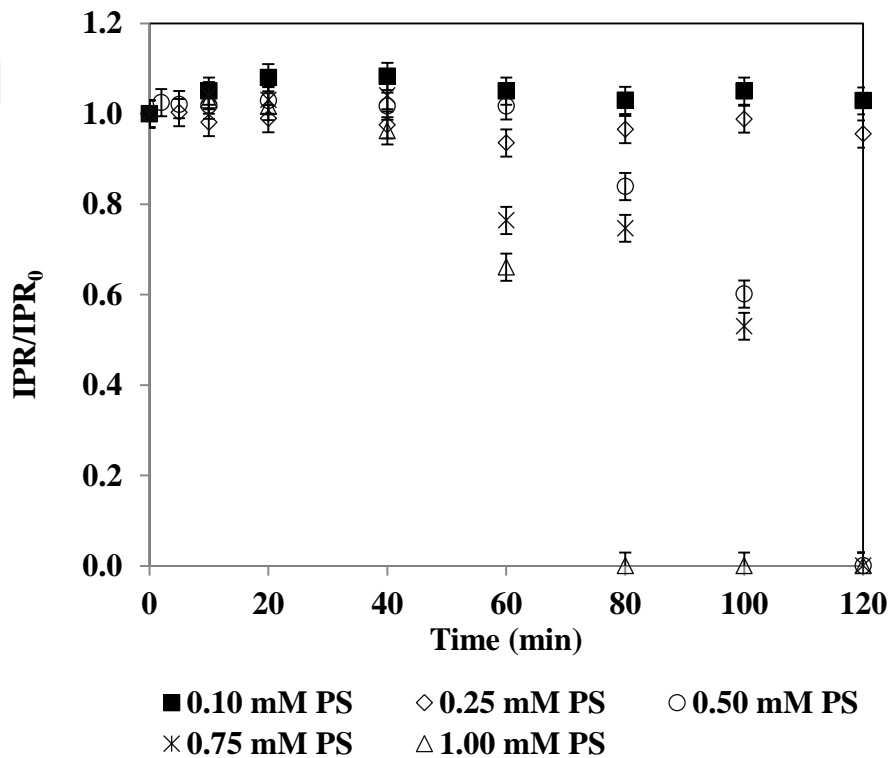

Figure 4.15 : Changes in normalized IPR concentration during ZVI/PS treatments in DW at varying initial PS concentrations. IPR=2 mg/L; ZVI=1 g/L; pH=5.0.

This increment in IPR degradation could be ascribed to the greater decomposition of PS to produce more $SO_4^{\bullet-}$. It should also be mentioned that no inhibitory effect as a result of excessive oxidizing agent concentration (PS), was observed in the PS studied range (0.10 mM- 1.00 mM). In a former related study (Gao et al, 2020), the effect of initial PS concentration on metoprolol degradation was investigated in the range of 0.25 mM PS to 4.00 mM PS. In that study, the degradation of metoprolol increased from 40.2% to 96.3% as the PS concentration rose from 0.50 to 3.00 mM. However, further increment of the initial PS concentration to 4.00 mM, no change in metoprolol degradation was observed probably due to the side reaction between $SO_4^{\bullet-}$ and excess PS and the self-combination of $SO_4^{\bullet-}$, causing an insignificant improvement during the process (Gao et al, 2020).

Effect of Initial pH

In order to investigate the pH effect on IPR degradation during ZVI/PS treatment, pH values of 3.0 and 5.0 with a determined PS concentration of 0.50 mM were examined. From Figure 4.16, the complete IPR removal was observed only after 10 min ZVI/PS treatment at initial pH of 3.0 while no IPR removal was observed even at 60 min treatment at initial pH 0f 5.0. With the progress of treatment from 60 min, IPR removal percentage reached 16% and 40% after 80 min and 100 min, respectively at initial pH of 5.0. Eventually, as can be seen in Figure 4.16, complete IPR was obtained after 120 min AVI/PS treatment at initial pH of 5.0. Hence, IPR removals were enhanced remarkably when the initial solution pH was decreased from 5.0 to 3.0 during ZVI/PS treatment because the more acidic condition (in this case pH=3.0) led to the rapid corrosion of ZVI and Fe^{2+} release and consequently more $SO_4^{\bullet-}$ generation (Gao et al, 2020; Zhao et al, 2010a). The results were in agreement with the study of Goa et al. (2020) who studied ZVI/PS treatment of metoprolol in the pH range of 3.0 to 11.0. In that study, the maximum degradation efficiency of 99.5% was achieved at pH 3 and almost 88.7% of metoprolol was degraded within the first 5 min. With increasing the pH from 5 to 9, the degradation of metoprolol slightly reduced from 95.9% to 83.8% (Gao et al, 2020).
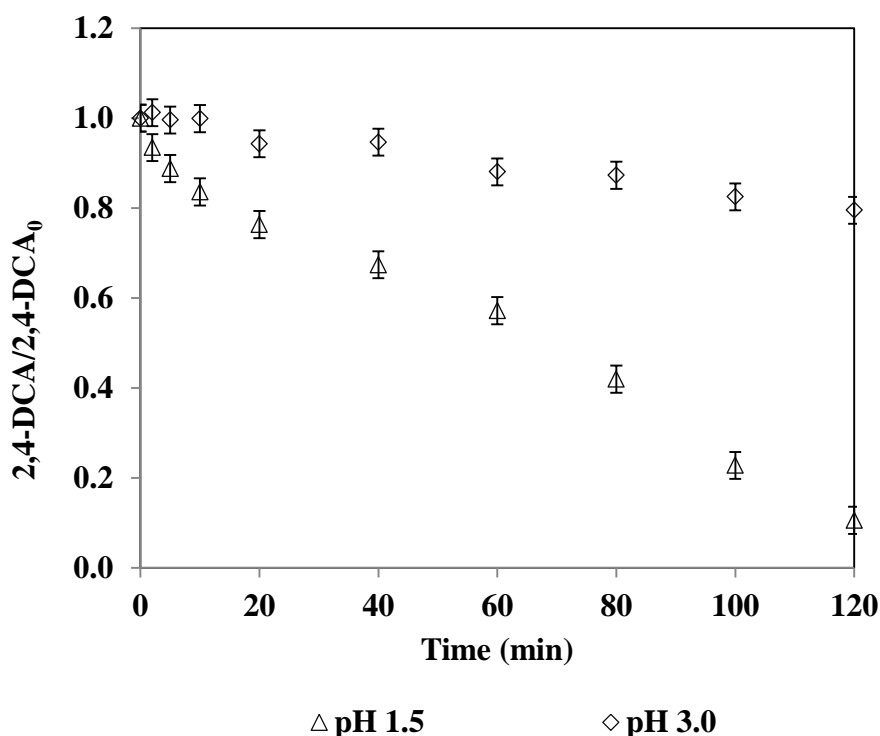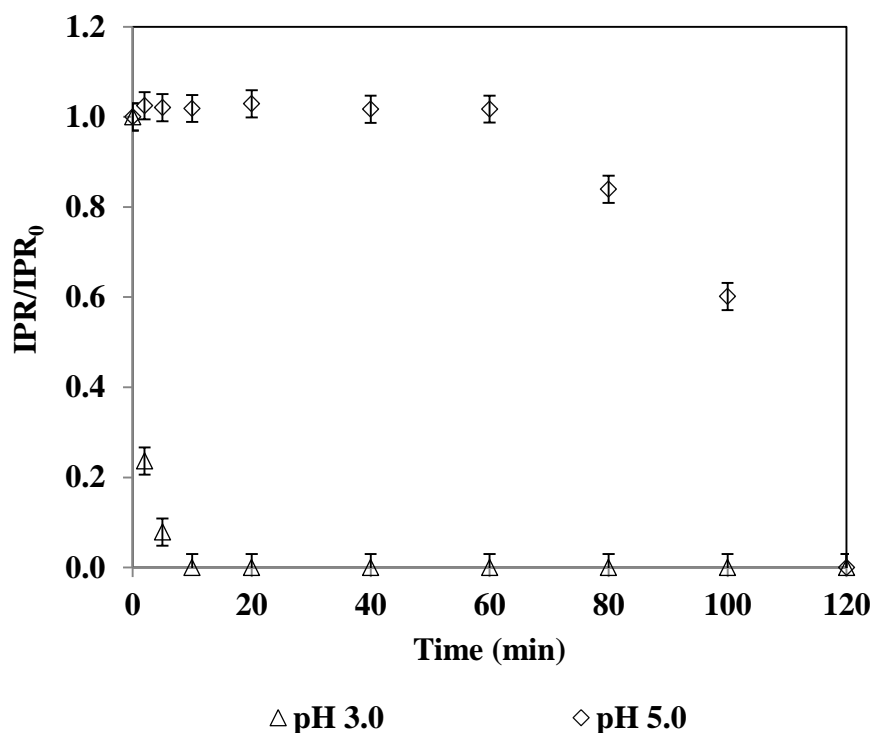
Figure 4.16 : Changes in normalized IPR concentration during ZVI/PS treatments in DW at different initial pH values. IPR=2 mg/L; PS=0.50 mM; ZVI=1 g/L.

4.1.3.3 Zero-valent aluminum-activated persulfate oxidation process

In order to investigate the effect of ZVA (1 g/L) on IPR removal, a control experiment was conducted with an initial concentration of 2 mg/L IPR at initial pH of 3.0 in DW in the absence of PS. Obtained results (data are shown in Appendix A) indicated that IPR removal was limited to 35% after 120 min ZVA treatment.

Effect of initial persulfate concentration

The effect of initial PS concentration in the range of 0.10 mM PS to 1.00 mM PS on IPR was explored during ZVA/PS treatment at initial pH of 3.0. As can be seen from Figure 4.17, percentage of IPR removal efficiencies obtained at 120 min ZVA/PS for both initial PS concentrations of 0.10 mM and 0.25 mM were around 80%. However, by increasing initial PS concentration to the range of 0.50 mM to 1.00 mM complete degradation of IPR was observed at 120 min.
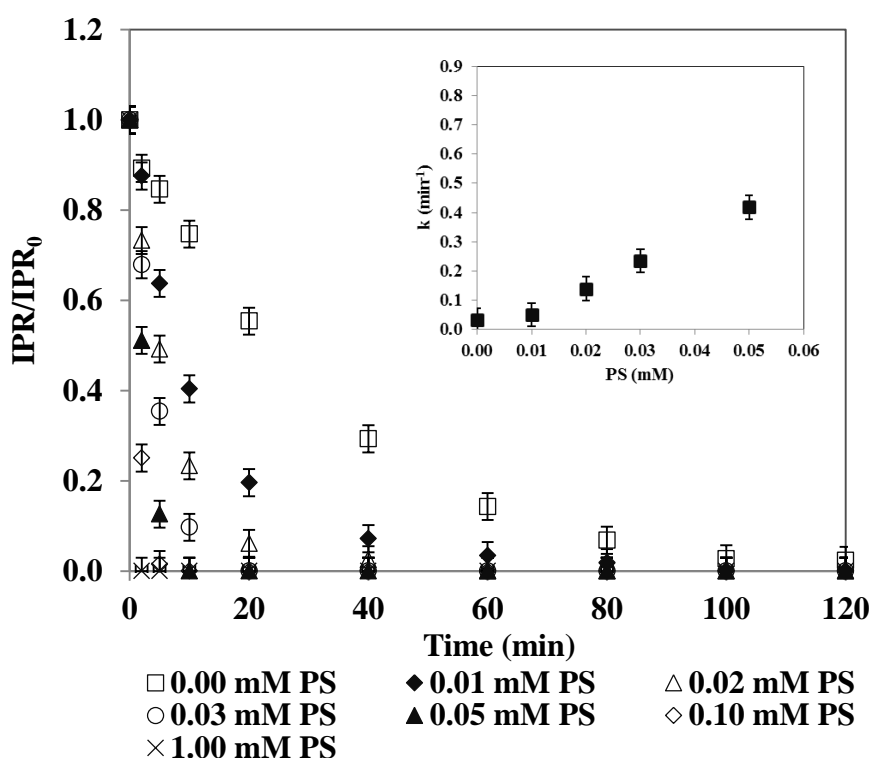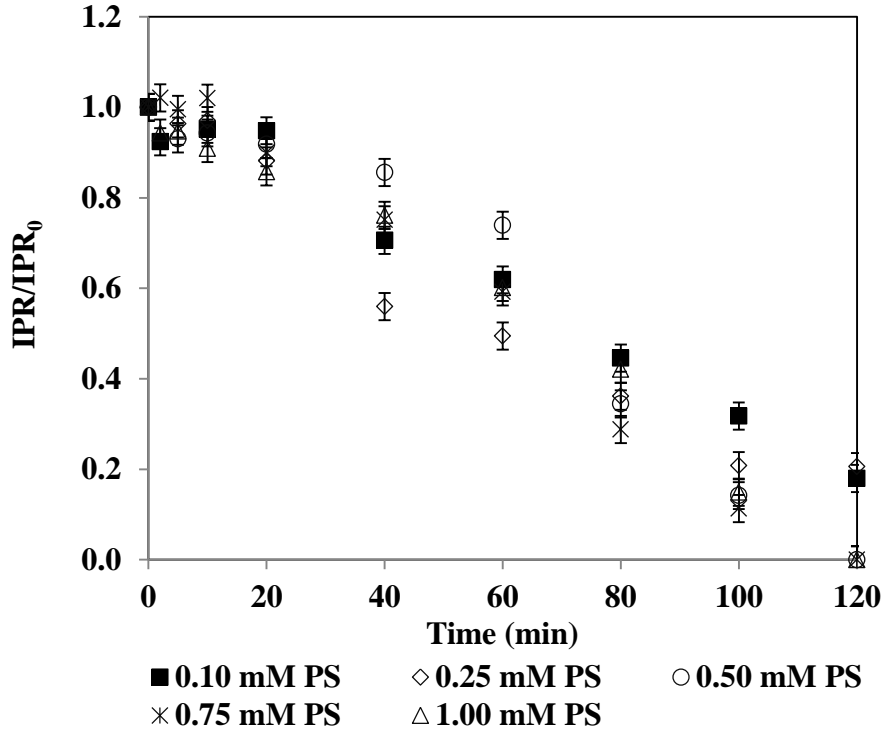
Figure 4.17 : Changes in normalized IPR concentration during ZVA/PS treatments in DW at varying initial PS concentrations. IPR=2 mg/L; ZVA=1 g/L; pH=3.0.

Effect of initial pH

Since solution pH can play an important role in pollutant removal during heterogeneous catalytic AOPs, particularly those involving metals/metal ions/oxides (Arslan-Alaton et al, 2017c; Bokare and Choi, 2009; Nidheesh et al, 2018), the effect of pH on IPR degradation during ZVA/PS treatment was investigated with initial pH of 1.5 and 3.0. Figure 4.18 depicts the effect of initial pH on ZVA/PS treatment of IPR degradation with an initial PS concentration of 0.50 mM. As it can be seen in Figure 4.18, IPR degradation was relatively faster at pH=1.5 compared to pH=3.0 during the first 60 min ZVA/PS treatment. This can be attributed to the fact that the reactivity of ZVA might be enhanced through rapid corrosion of ZVA and continuous activation of passive layer in the solution with higher H^+ concentration (pH=1.5). However, with the progress of treatment (after 60 min), both treatments resulted in similar IPR abatements.
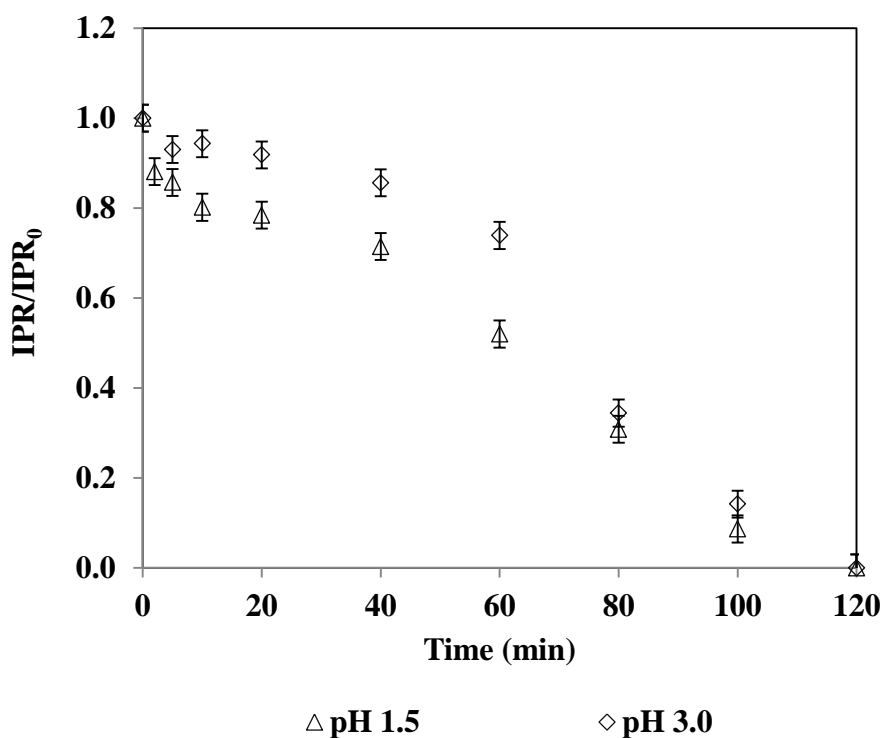
Figure 4.18 : Changes in normalized IPR concentration during ZVA/PS treatments in DW at different initial pH values. IPR=2 mg/L; PS=0.50 mM; ZVA=1 g/L.

4.2 Selected Oxidation Processes

In order to gain an insight to the treatments mechanism and examine their performances, several treatments were chosen from preliminary experiments under selected conditions (Table 4.5) and compared in terms of each micropollutant removal, DOC removal, PS consumption rate, dechlorination (Cl$^-$ release), etc.

Low mineralization of micropollutants during AOPs may lead to the formation of more resistant degradation products compared to the initial micropollutants and therefore require more time or chemicals for complete mineralization (Tufail et al, 2020). Herein, during the selected treatment applications, the degree of mineralization was followed in terms of the DOC parameter (as DOC removal). It should also be considered that, direct application of zero-valent iron/aluminum-based AOPs in wastewater treatment technology, is accompanied with Fe/Al release into the environment. Hence, during application of the selected catalytic oxidation processes, the assessment of these ions in the reaction solution is very essential and in this study, metal ion (Fe/Al) release in case of catalytic oxidation processes was also followed.

Table 4.5 : Initial reaction conditions of selected treatment-processes for each model industrial micropollutant in DW.

Pollutant	Selected processes	Reaction conditions and treatment time
3,5-DCP	UV-C	3,5-DCP=10 mg/L; pH=6.3; t=120 min
	UV-C/PS	3,5-DCP=10 mg/L; PS=0.30 mM; pH=6.3; t=120 min
	ZVI/PS	3,5-DCP=10 mg/L; PS=2.50 mM; pH=3.0; t=120 min
2,4-DCA	UV-C	2,4-DCA=10 mg/L; pH=6.0; t=120 min
	UV-C/PS	2,4-DCA=10 mg/L; PS=1.00 mM; pH=6.0; t=120 min
	ZVI/PS	2,4-DCA=10 mg/L; PS=2.50 mM; pH=3.0 and pH=5.0; t=120 min
IPR	UV-C	IPR=10 mg/L; pH=6.2; t=120 min
	UV-C/PS	IPR=10 mg/L; PS=0.30 mM; pH=6.2; t=120 min
	ZVI/PS	IPR=10 mg/L; PS=2.50 mM; pH=3.0; t=120 min
	ZVA/PS	IPR=10 mg/L; PS=2.50 mM; pH=3.0; t=120 min

4.2.1 3,5-Dichlorophenol

4.2.1.1 Photolysis and homogeneous photochemical processes

Figure 4.19 presents changes in normalized 3,5-DCP (a), DOC (b) and Cl$^-$ (c) concentrations during UV-C and UV-C/PS treatments (3,5-DCP=10 mg/L; PS=0.30 mM; pH=6.3). As is obvious from Figure 4.19 (a), the target compound was completely removed after 40 min by UV-C/PS treatment, whereas 3,5-DCP degradation by mere UV-C photolysis was appreciably slower achieving complete degradation of 3,5-DCP in 100 min. PS consumption was also evaluated for UV-C/PS treatment to examine whether the oxidant is efficiently used during the UV-C/PS oxidation (insert in Figure 4.19 (a)). Apparently, complete PS consumption was reached after 80 min treatment which was later than the time observed for complete 3,5-DCP degradation (40 min). It can be inferred that the residual (unreacted) PS was

further used for the degradation of the oxidation intermediates, leading to 95% DOC removal by the UV-C/ PS process after 120 min treatment. Similar results were previously reported for 3,4-DCP degradation with the UV-C/PS treatment process, where 96% DOC removal was achieved after 60 min treatment.
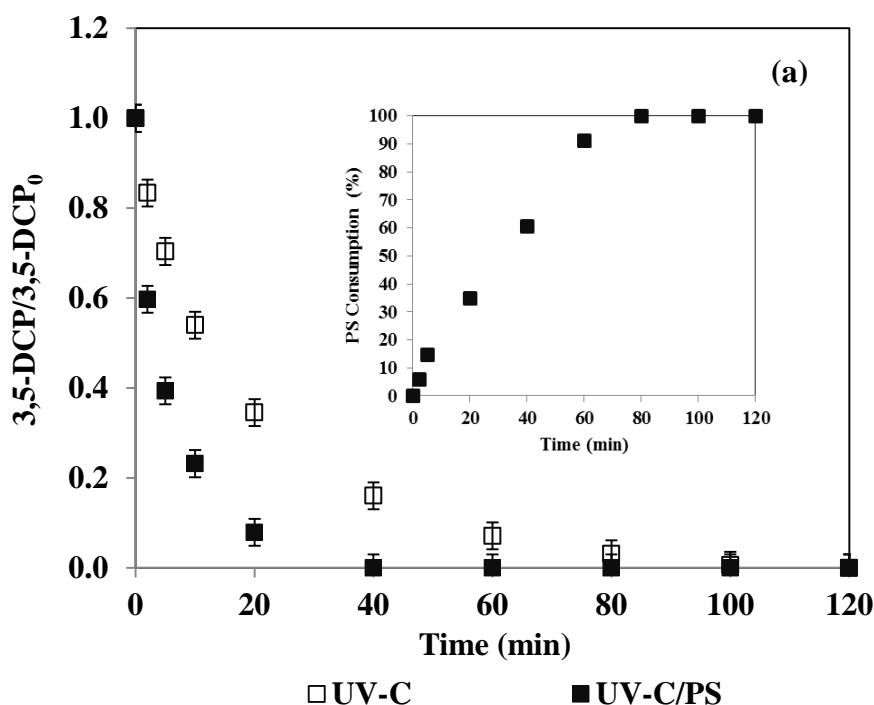
Figure 4.19 : Changes in normalized 3,5-DCP (a), DOC (b) and Cl⁻ (c) concentrations during UV-C and UV-C/PS treatments of 3,5-DCP in DW. The theoretically expected maximum Cl⁻ concentration after full oxidation of 3,5-DCP is 4.35 mg/L. 3,5-DCP=10 mg/L; PS=0.30 mM; DOC for 10 mg/L 3,5-DCP=4.42 mg/L; UV-C intensity=0.5 W/L; pH=6.3. Figure 4.19 (a) insert shows the calculated PS consumptions (%) during UV-C/PS treatment of 10 mg/L 3,5-DCP in DW.
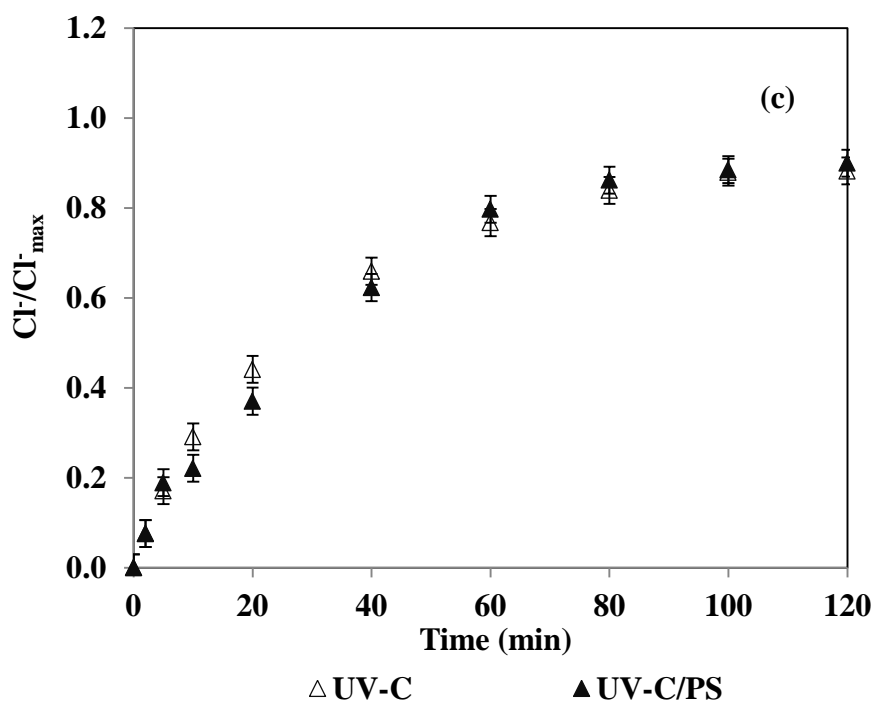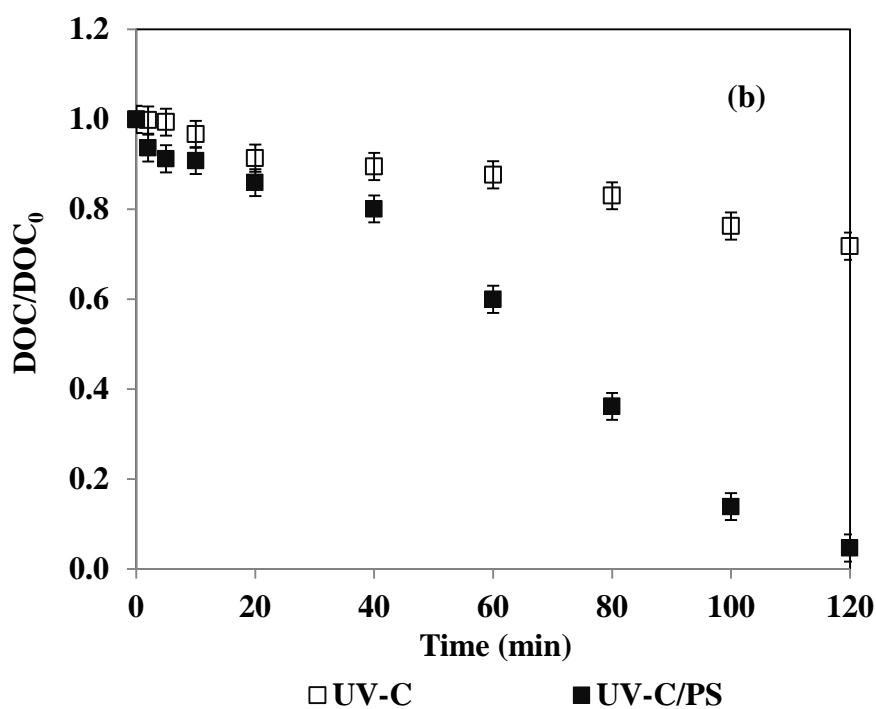
Figure 4.19 (continued) : Changes in normalized 3,5-DCP (a), DOC (b) and Cl- (c) concentrations during UV-C and UV-C/PS treatments of 3,5-DCP in DW. The theoretically expected maximum Cl- concentration after full oxidation of 3,5-DCP is 4.35 mg/L. 3,5-DCP=10 mg/L; PS=0.30 mM; DOC for 10 mg/L 3,5-DCP=4.42 mg/L; UV-C intensity=0.5 W/L; pH=6.3. Figure 4.19 (a) insert shows the calculated PS consumptions (%) during UV-C/PS treatment of 10 mg/L 3,5-DCP in DW.

According to Figure 4.19 (b), UV-C photolysis resulted in poor DOC (28%) removal efficiencies after 120 min, which is not surprising, since UV-C photolysis is usually not capable of fully degrading organic pollutants and their transformation products to mineralization end products. Based on the obtained findings, it may be concluded that UV-C/PS was much more efficient in terms of 3,5-DCP degradation and DOC removal. The above results were also in agreement with previous studies where $SO_4^{\bullet-}$ -based AOPs have proven to be more successful in terms of degradation of organic compounds as compared to mere UV-C photolysis (Chen et al, 2018). It has previously been shown that the degradation of CPs is associated with the release of organically bound Cl atoms in the form of free Cl^- ions to the reaction solution during their treatment (Karci et al, 2012). Figure 4.19 (c) presents Cl^- release during UV-C and UV-C/PS treatment of 10 mg/L 3,5-DCP at an initial PS concentration of 0.30 mM at pH 6.3. From Figure 4.19 (c) it is obvious that for both treatments similar trends were observed for Cl^- release. Peak Cl^- concentrations of 3.84 m/L and 3.91 mg/L were obtained at the end of 3,5-DCP treatment with UV-C and UV-C/PS, respectively, corresponding to practically 88% and 90% of the highest possible theoretical Cl^- release of 4.35 mg/L. Karci et al. (2012) also reported an abrupt release of the Cl^- that proceeded simultaneously to 2,4-DCP oxidation by UV-C/H_2O_2. Cl^- release was practically complete within 20 min reaching asymptotic values of 0.66 mM until the end of 100 min treatment time (Karci et al, 2012).

4.2.1.2 Heterogeneous catalytic experiment

Zero-valent iron-activated persulfate oxidation process

Figure 4.20 depicts changes in normalized 3,5-DCP (a) and DOC (b) concentrations during ZVI/PS (PS=2.50 mM; pH=3.0) treatment and the insert in Figure 4.20 (a) depicts the calculated PS consumptions (%) during the treatment of 10 mg/L 3,5-DCP in DW. According to Figure 4.20 (a) and (b), 3,5-DCP could be completely degraded within short treatment periods (<10 min) accompanied with partially DOC removal (47%). As it can be seen from the insert in Figure 4.20 (a), most of the PS (~70%) was consumed during the first 10 min ZVI/PS treatment delineating the contribution of $SO_4^{\bullet-}$ in complete 3,5-DCP as well as partially DOC removals. However, after 10 min ZVI/PS treatment, DOC removal did not significantly change and slightly increased from 47% to 50% after 120 min treatment. This was consistent with the study reported by Temiz et al. (2016), who found that 20 mg/L triton X-45

degradation by ZVI/PS (PS=2.5 mM; pH=5.0) occurred promptly and rapidly, whereas its mineralization was very complicated and involved the intermediacy of aromatic intermediates that were much more difficult to oxidize than the original pollutant triton X-45 (Temiz et al, 2016).

The degree of Fe release and PS consumption was also followed after 120 min ZVI/PS (PS=0.50 mM, pH=3.0) treatment of 2 mg/L 3,5-DCP and a positive correlation existed between enhanced 3,5-DCP removal and ZVI-activated PS consumption accompanied with a parallel Fe release. From obtained experimental findings, complete 3,5-DCP removal was achieved accompanied with 50 mg/L Fe release in the bulk reaction as well as complete PS consumption after 120 min ZVI/PS treatment revealing the efficient interaction between the ZVI surface and PS that resulted in Fe release through equations 2.2-5. Not surprisingly, Fe concentration was only 0.51 mg/L for 3,5-DCP treatment with mere ZVI with initial pH of 5.0; however, by addition of only 0.50 mM PS it reached 22 mg/L. It should be noted here that it is possible to remove soluble Fe by >95% by precipitation in the form of solid Fe (III) hydroxide after pH increment above 7.0. A similar increase in released Fe concentrations after PS addition was also observed in the study by Dogan et al. (2016) where bisphenol A degradation with ZVI/air/H^{+} and ZVI/PS treatments was investigated (Dogan et al, 2016). It was shown that in the presence of PS, dissolution of Fe increased from 25 to 200 mg/L (conditions: bisphenol A=20 mg/L, PS=2.5 mM, ZVI=1 g/L, pH 3.0) (Dogan et al, 2016).
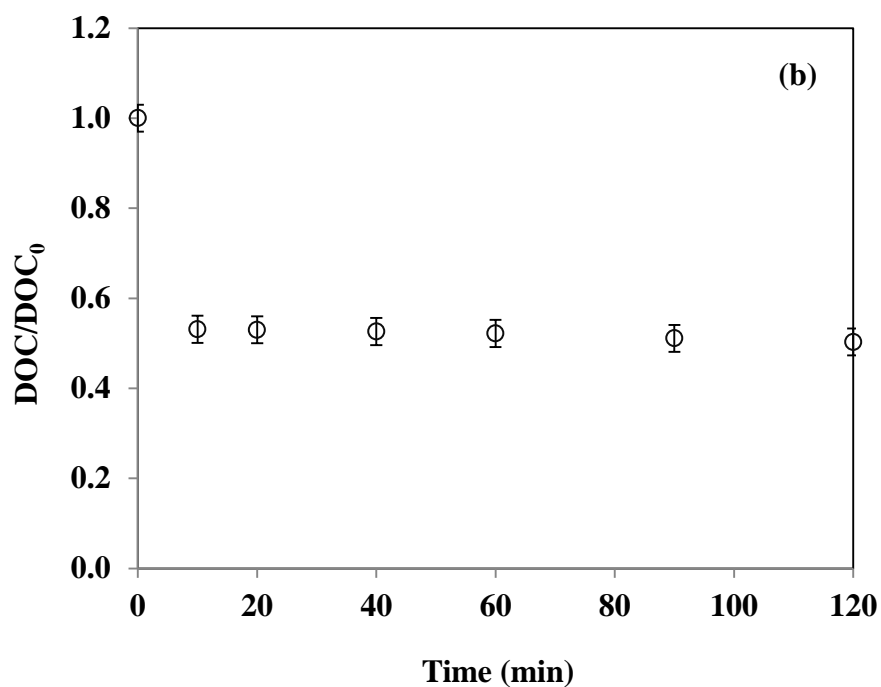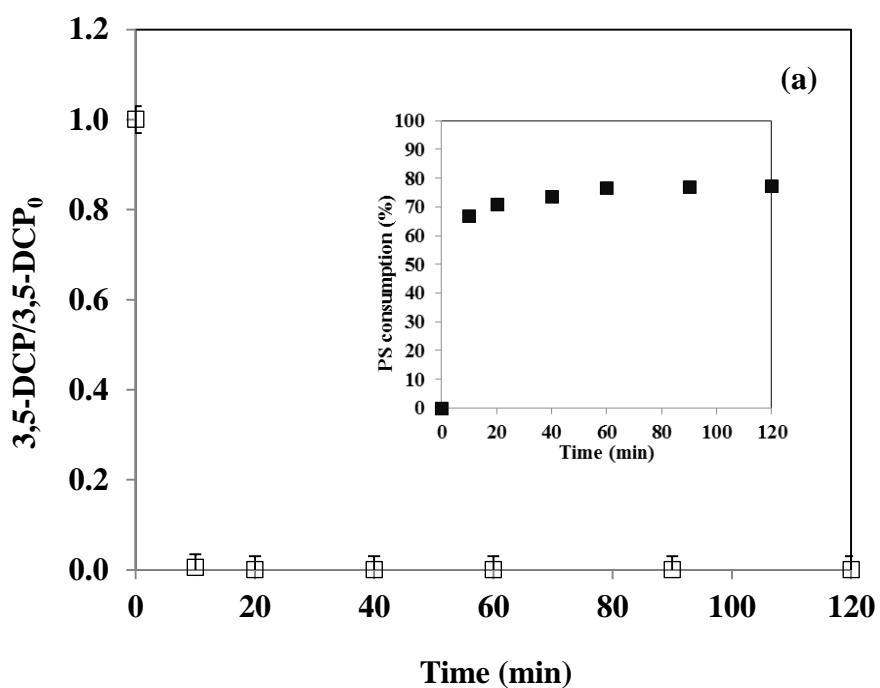
Figure 4.20 : Changes in normalized 3,5-DCP (a) and DOC (b) concentrations during ZVI/PS treatment in DW. 3,5-DCP=10 mg/L; PS=2.50 mM; DOC for 10 mg/L 3,5-DCP=4.42 mg/L; ZVI=1 g/L; pH=3.0. Figure 4.20 (a) insert shows the calculated PS consumptions (%) during ZVI/PS treatment of 10 mg/L 3,5-DCP in DW.

4.2.2 2,4-Dichloroaniline

4.2.2.1 Photolysis and homogeneous photochemical processes

Although UV photolysis would attack and directly decompose some organic molecules whose UV absorption coefficients are high, usually it occurs at very slow rates and does not end up with mineralization (Boucenna et al, 2019; Goi and Trapido, 2002). One of the ways to degrade more effectively these compounds is to combine UV-C with strong oxidizing agents. Therefore the capability of both UV-C and UV-C/PS in effective mineralization of 2,4-DCA was explored and their correlations with PS consumption and dechlorination extent were investigated.

Figure 4.21 depicts changes in normalized 2,4-DCA (a), DOC (b) and Cl$^-$ (c) concentrations during UV-C and UV-C/PS treatments (2,4-DCA=10 mg/L; PS=1.00 mM; pH=6.0). From Figure 4.21 (a), it is apparent that complete 2,4-DCA removal was achieved in 80 min UV-C photolysis indicating that mere UV-C was effective in 2,4-DCA removal. Upon addition of 1.00 mM PS to working solution, an appreciable enhancement in the 2,4-DCA degradation rate was evident such that practically complete 2,4-DCA degradation was achieved after 10 min UV-C/PS treatment as a consequence of accelerated SO$_4^{\bullet-}$ production. According to Figure 4.21 (b), although complete 2,4-DCA degradation was obtained during UV-C photolysis, negligible mineralization was observed after 120 min UV-C photolysis treatment. It can be interpreted that the degradation of 2,4-DCA during only UV-C, might transform it into other organic contaminants which were recalcitrant to further oxidation. On the other hand, after only 40 min UV-C/PS treatment of 2,4-DCA, appreciable mineralization (~93%) accompanied with almost complete PS consumption was achieved. However, DOC removal slowed down and practically stopped after 40 min treatment, most probably due to complete oxidant consumption and the accumulation of oxidation intermediates (Liang and Su, 2009). This was consistent with the study reported by Dan et al. (2020), who investigated the degradation of 4.6 mg/L sulfachloropyridazine by UV-C/PS (4 mM PS) treatment in which sulfachloropyridazine could be completely degraded after 120 min. The results also showed that the products of sulfachloropyridazine degradation were not recalcitrant and the level of mineralization of sulfachloropyridazine could be close to 90% or more when the reaction time and/or PS concentration was increased (Dan et al, 2020).
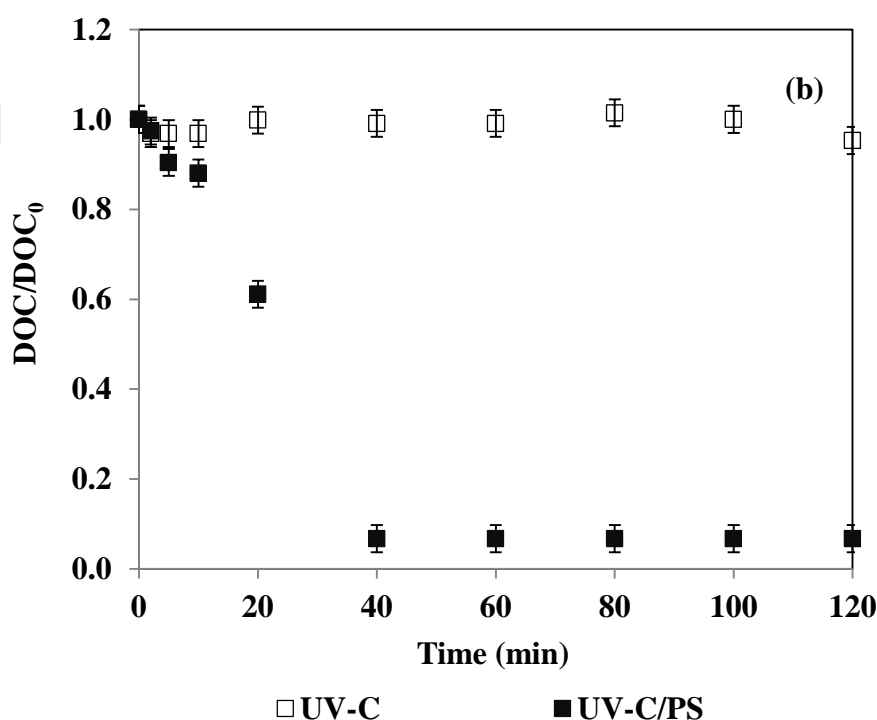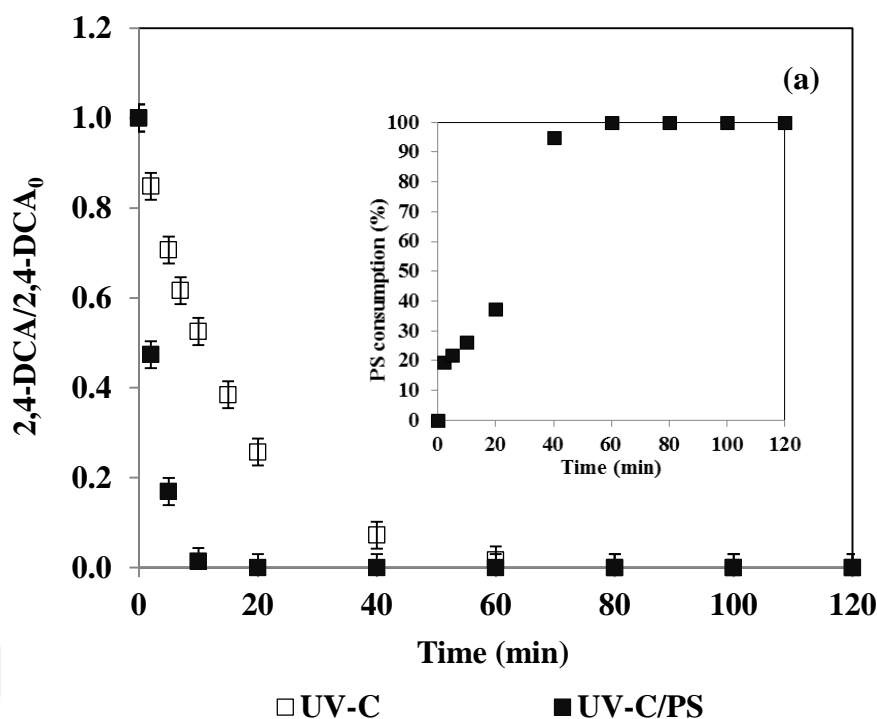
Figure 4.21 : Changes in normalized 2,4-DCA (a), DOC (b) and Cl⁻ (c) concentrations during UV-C and UV-C/PS treatments of 2,4-DCA in DW. The theoretically expected maximum Cl⁻ concentration after full oxidation of 2,4-DCA is 4.38 mg/L. 2,4-DCA=10 mg/L; PS=1.00 mM; DOC for 10 mg/L 2,4-DCA=4.44 mg/L; UV-C intensity=0.5 W/L; pH=6.0. Figure 4.21 (a) insert shows the calculated PS consumptions (%) during UV-C/PS treatment of 10 mg/L 2,4-DCA in DW.
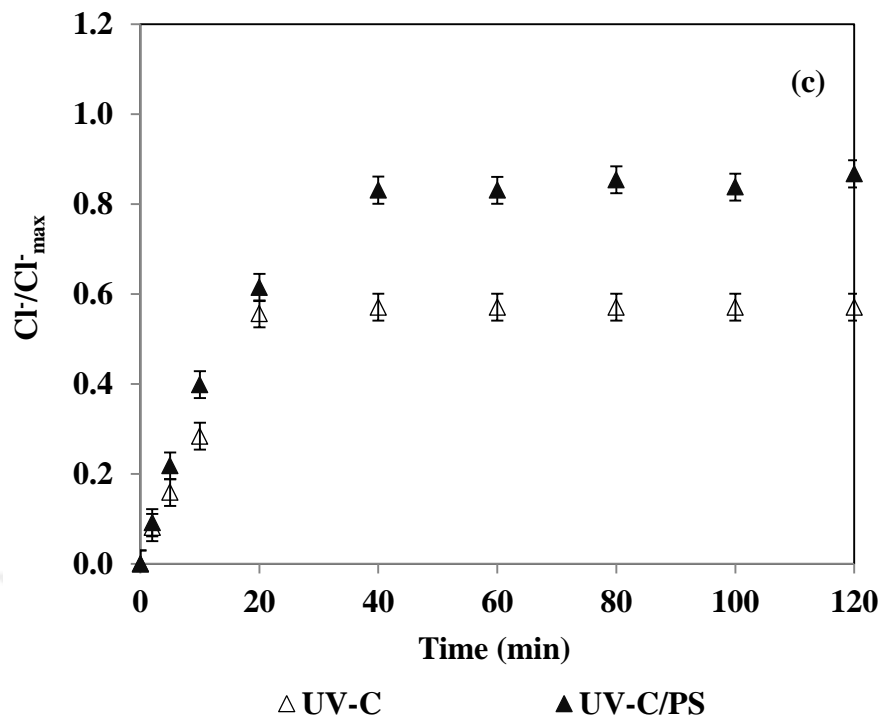
Figure 4.21 (continued) : Changes in normalized 2,4-DCA (a), DOC (b) and Cl⁻ (c) concentrations during UV-C and UV-C/PS treatments of 2,4-DCA in DW. The theoretically expected maximum Cl⁻ concentration after full oxidation of 2,4-DCA is 4.38 mg/L. 2,4-DCA=10 mg/L; PS=1.00 mM; DOC for 10 mg/L 2,4-DCA=4.44 mg/L; UV-C intensity=0.5 W/L; pH=6.0. Figure 4.21 (a) insert shows the calculated PS consumptions (%) during UV-C/PS treatment of 10 mg/L 2,4-DCA in DW.

As it was mentioned before, it has previously been demonstrated that the degradation of CAs can also be accompanied with Cl⁻ release to the reaction solution during their treatment (Yao et al, 2019). Figure 4.20 (c) delineates Cl⁻ release during UV-C and UV-C/PS treatment of 10 mg/L 2,4-DCA at an initial PS concentration of 1.00 mM at pH 6.0. According to Figure 4.21 (c) it is obvious that for both treatments similar trends were observed. Dechlorination was stopped after 20 min and 40 min treatments such that Cl⁻ concentrations reached 2.44 mg/L and 3.64 mg/L for UV-C and UV-C/PS, respectively. Obtained experimental findings indicated that during UV-C treatment, 2,4 DCA degradation and dechlorination proceeded simultaneously, since 74% 2,4-DCA was removed after 20 min. These results also revealed that dechlorination is one of the initial stages of 2,4 DCA removal by UV-C.

4.2.2.2 Heterogeneous catalytic experiments

Figure 4.22 demonstrates changes in normalized 2,4-DCA (a) and DOC (b) concentrations during ZVI/PS (PS=2.50 mM; pH=3.0) treatment. The insert in

94

Figure 4.22 (a) depicts PS consumption (%) during ZVI/PS treatment of 10 mg/L 2,4-DCA in DW. As it can be seen in Figure 4.22 (a), it is evident that 95% 2,4-DCA degradation was observed in first 10 min ZVI/PS. Beyond this treatment time, no further 2,4-DCA degradation was observed. This could be attributed to the depletion of the oxidant PS in working solution after 20 min (inset in Figure 4.22 (a)) or scavenging of the formed $SO_4^{\bullet-}$ according to equations 2.11-13. Similar trend was also evident for the DOC removal; after 10 min treatment, 30% DOC removal was observed and no appreciable change was observed until 120 min treatment. These findings revealed that the formation of $SO_4^{\bullet-}$ through ZVI activation with PS plays a major role in effective 2,4-DCA degradation and mineralization. Similarly, in the study of Wu et al. (2020) degradation and mineralization of nine typical pharmaceuticals and personal care products including bisphenol A, indomethacin, norfloxacin, tetracycline, paracetamol, carbamazepine, phenacetin, sulfamethoxazole and sulfamethazine with initial 50 mg/L for each target pollutant from water were investigated by ZVI/PS coupled with Fenton (ZVI/PS-Fenton) in the presence of 1 mM PS and 0.5 mM H_2O_2 with initial ZVI concentration of 2 mM and pH of 6.8. Experiment results indicated that although ZVI/PS-Fenton process could result in significantly degradations for all nine target pollutants in the range of 77% to 100%, it was not capable in effective mineralization degree of these pollutants except bisphenol A. Entire mineralization could not be achieved by the ZVI/PS-Fenton and only bisphenol A could be oxidized to mineral form in a significant manner (89% TOC removal), while the other pollutants were partially dismantled to smaller organic fragments, with a mineralization degree varying from 4% to 26%. In that study, the differences in degradation of nine pharmaceutical compounds were attributed to diverse physicochemical properties of each compound under studied conditions. For examples those compounds with primary and secondary amino or amidic groups were more refractory to degradation by PS (Wu et al, 2020).
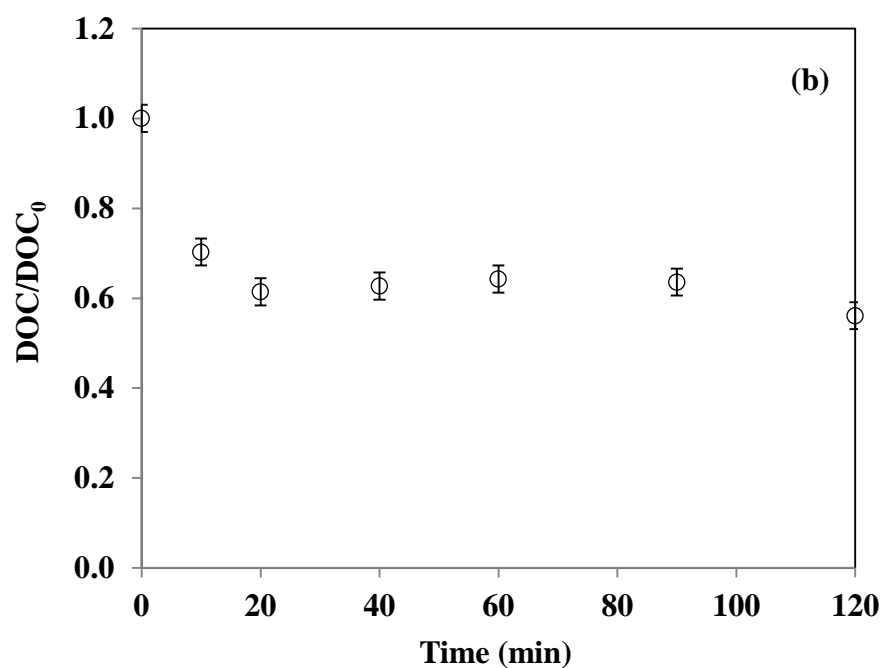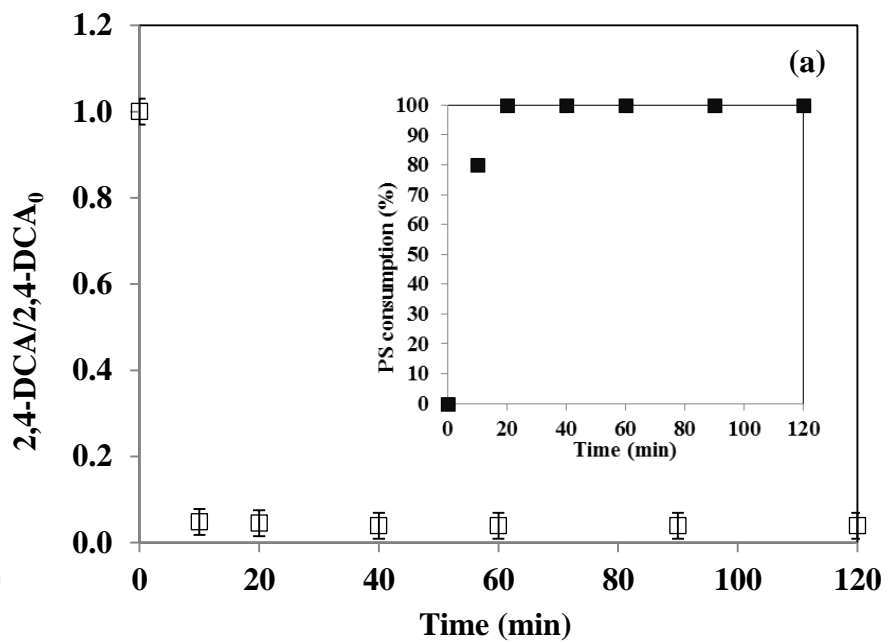
Figure 4.22 : Changes in normalized 2,4-DCA (a) and DOC (b) concentrations during ZVI/PS treatment in DW. 2,4-DCA=10 mg/L; PS=2.50 mM; DOC for 10 mg/L 2,4-DCA=4.44 mg/L; ZVI=1 g/L; pH=3.0. Figure 4.22 (a) insert shows the calculated PS consumptions (%) during ZVI/PS treatment of 10 mg/L 2,4-DCA in DW.

As it was shown in treatability experiments in DW part, unlike 3,5-DCP, 2,4-DCA could be removed near completely both initial pH=3.0 and pH=5.0 after 120 min ZVI/PS treatment in the presence of 0.50 mM PS. Therefore, in order to evaluate the efficiency of PS activation (PS=0.50 mM) by ZVI, dissolved/released Fe concentrations were also monitored for 2 mg/L 2,4-DCA after 120 min of treatment for both initial of pH=3.0 and pH=5.0.

Experimental findings demonstrated that the ZVI/air/H$^+$ treatment resulted in only 0.22 mg/L released Fe concentration after 120 min at pH 5.0 while, upon PS addition (PS=0.50 mM) the Fe concentration in the reaction solution slightly increased to 0.24 mg/L after 120 min ZVI/PS (pH=5.0). On the other hand, further pH decrease from 5.0 to 3.0 significantly enhanced the dissolution of Fe ions. The ultimately released Fe concentrations was measured as 12 mg/L for where complete removal of 2,4-DCA and PS consumptions were achieved. Fe concentrations positively correlated with PS consumption and pollutant removals during ZVI/PS treatment.

4.2.3 Iprodione

4.2.3.1 Photolysis and homogeneous photochemical processes

Figure 4.23 presents time-dependent changes in IPR (a), DOC (b), and PS (c) abatements as well as Cl$^-$ release (d) during UV-C/PS treatment of 10 mg/L IPR in DW. According to Figure 4.23 (a) and (b), although 92% IPR removal was obtained after 120-min UV-C treatment, no mineralization (DOC removal) was observed for this run, revealing that UV-C alone (in the absence of active oxidants) was not capable of efficiently degrading UV-C photolysis products of IPR. From Figure 4.23 (b) it is clear that UV-C/PS treatment in the presence of 0.30 mM PS was effective both in terms of IPR and its organic carbon abatements and DOC removals increased remarkably from no removal via UV-C photolysis to 78% through UV-C/PS treatment (PS=0.30 mM). It can be concluded that the addition of PS changed the reaction mechanism from direct UV-C photolysis of IPR to photochemical oxidation of IPR through the generation and intermediacy of mainly SO$_4^{\bullet-}$ which resulted in an appreciable mineralization. Upon comparison of Figure 4.23 (a) and the insert in Figure 4.23 (a), it can be seen that practically 100% IPR removal was obtained after 10 min UV-C/PS corresponding to 33% PS consumption. Despite the almost complete degradation of IPR at this particular treatment time (10 min), only 13% of

the initial DOC was removed, speaking for IPR degradation to some organic degradation intermediates. However, after 10-min UV-C/PS treatment, PS consumptions further increased at the expense of DOC removal until 60 min, since obviously the oxidation of IPR degradation products continued as long as active oxidants are available and/or products being resistant to further oxidation might form in the reaction solution.

Advanced oxidation and mineralization of halogenated organic pollutants has been associated with the release of organically bound halogen atoms in the form of free ions as already been reported in the scientific literature (Chen et al, 2019; Karci et al, 2012; Krebel et al, 2011). Figure 4.23 (c) displays Cl^- release being observed during UV-C photolysis and UVC/PS (0.30 mM; pH=6.2) treatment of IPR. As is evident in Figure 4.23(c), Cl^- concentration linearly increased at a slow rate during UV-C photolysis, and 1.77 mg/L of Cl^- was detected at the end of the reaction (120 min). On the other hand, dechlorination was relatively rapid in the first 20 min of UV-C/PS treatment corresponding to the fast transformation of IPR and its primary degradation products. After 20-min UV-C/PS treatment of IPR with 0.30 mM the Cl^- concentrations reached 1.50 mg/L, corresponding to 70% the maximum possible (theoretical) Cl^- release being expected from IPR, respectively (2.15 mg/L). This observation was also in accord with the study of Wang and Chu (2012) where the degradation of 2,4,5-trichlorophenoxyacetic acid was investigated by Fe(II)-catalyzed activation of Oxone (peroxymonosulfate). It was concluded that the Cl^- release profile -a rapid initial formation rate leveling off at a later stage-suggested the persistence of carboxylic acid and/or other aliphatic products bearing chlorine atoms towards further mineralization. The relationship between IPR degradation and Cl^- release during UV/H_2O_2 treatment was previously reported by (Lopez-Alvarez et al, 2016). In that work, dechlorination of IPR proceeded parallel to its degradation suggesting a $SO_4^{\bullet-}$ attack into the carbon-chloride bond. In another related study, Cl^- release was reported as the first step of UV-C photolysis of IPR as a consequence of the substitution of chlorine atom by a hydroxyl group (Lassalle et al, 2014).
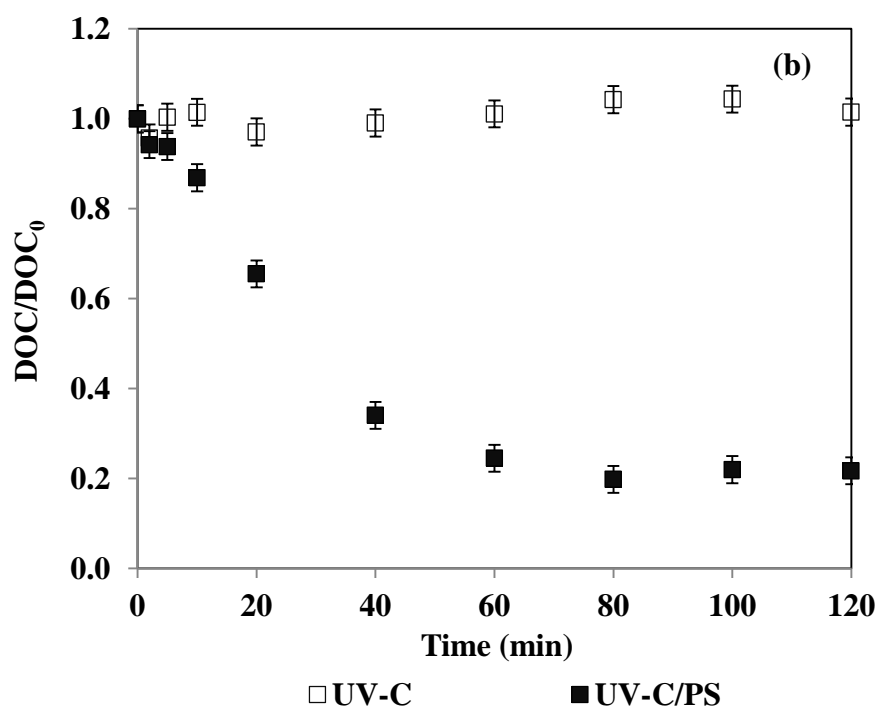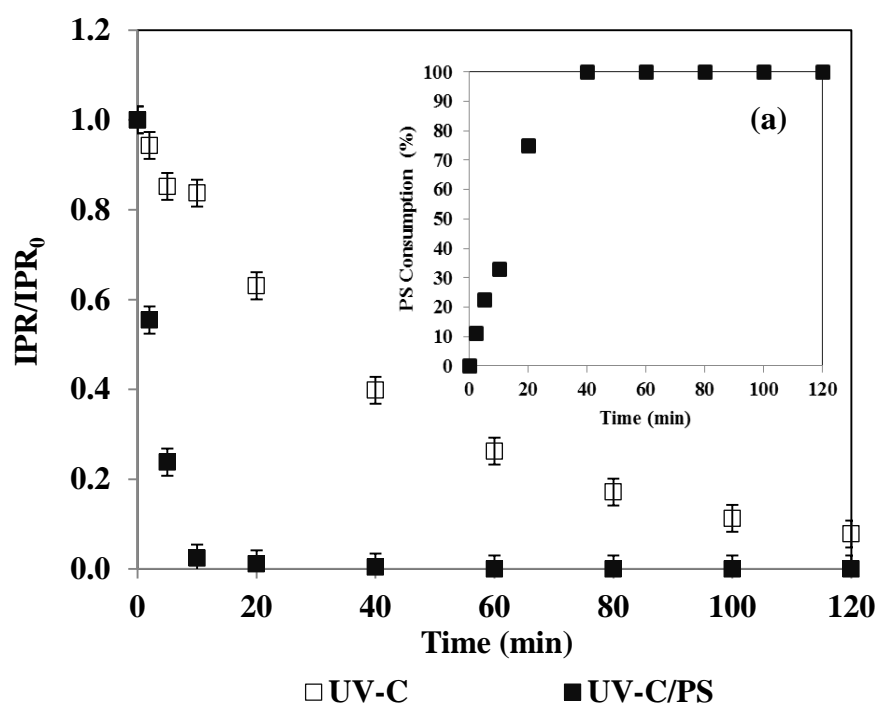
Figure 4.23 : Changes in IPR (a), DOC (b), and Cl⁻ (c) during UV-C/PS treatment of IPR in DW. The theoretically expected maximum Cl⁻ concentration after full oxidation of IPR is 2.15 mg/L. IPR = 10 mg/L; DOC of 10 mg/L IPR=4.3 mg/L; UV-C intensity=0.5 W/L; pH=6.2. Figure 4.23 (a) insert shows the calculated PS consumptions (%) during UV-C/PS treatment of 10 mg/L IPR in DW.
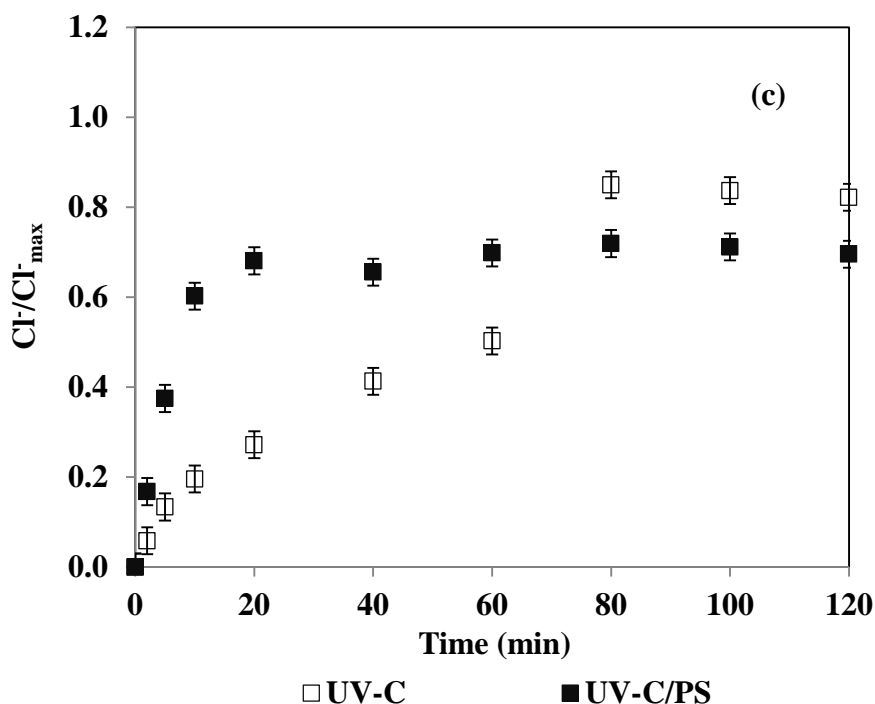
Figure 4.23 (continued) : Changes in IPR (a), DOC (b), and Cl$^-$ (c) during UV-C/PS treatment of IPR in DW. The theoretically expected maximum Cl$^-$ concentration after full oxidation of IPR is 2.15 mg/L. IPR = 10 mg/L; DOC of 10 mg/L IPR=4.3 mg/L; UV-C intensity=0.5 W/L; pH=6.2. Figure 4.23 (a) insert shows the calculated PS consumptions (%) during UV-C/PS treatment of 10 mg/L IPR in DW.

4.2.3.2 Heterogeneous catalytic experiments

Zero-valent iron activated persulfate oxidation process

Figure 4.24 depicts changes in normalized IPR (a) and DOC (b) during ZVI/PS (PS=2.50 mM; pH=3.0). The insert in Figure 4.24 (a) demonstrates PS consumption (%) during ZVI/PS treatment of 10 mg/L IPR in DW. According to Figure 4.24 (a), during the first 10 min of ZVI/PS treatment of IPR, 97% IPR degradation was obtained accompanied with almost 77% PS consumption and no mineralization. Upon comparison of Figure 4.24 (a) and 4.24 (b), it can be seen that while practically complete IPR was achieved after 10 min ZVI/PS treatment, no mineralization was observed suggesting formation of the intermediates which were recalcitrant to further oxidation. However, after 10 min ZVI/PS treatment, DOC removal efficiency started to increased and reached 10% and 17% after 20 min and 40 min ZVI treatment, respectively. Obtained results revealed that prolonged ZVI/PS treatment led to only 21% DOC removal after 120 min treatment.

100
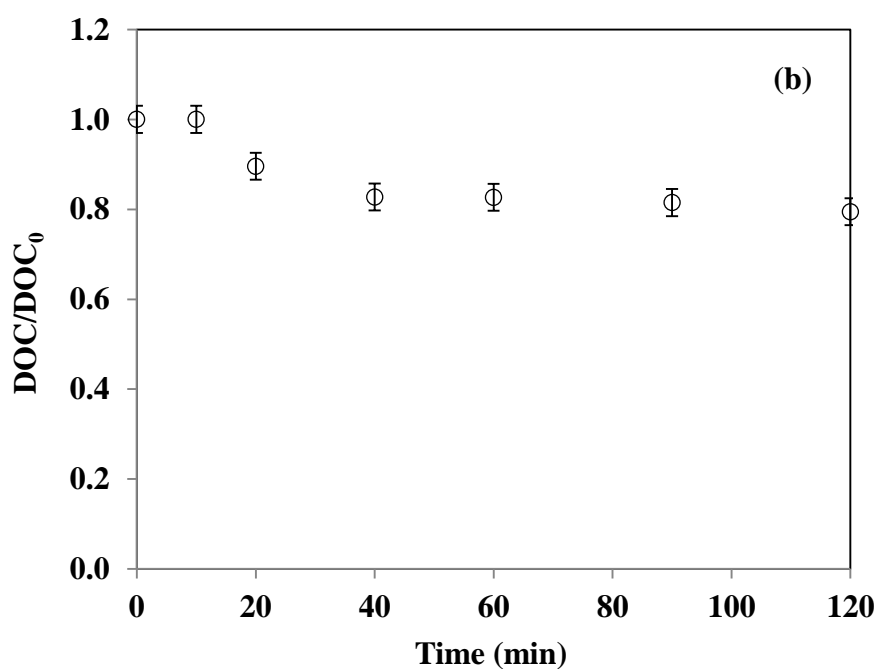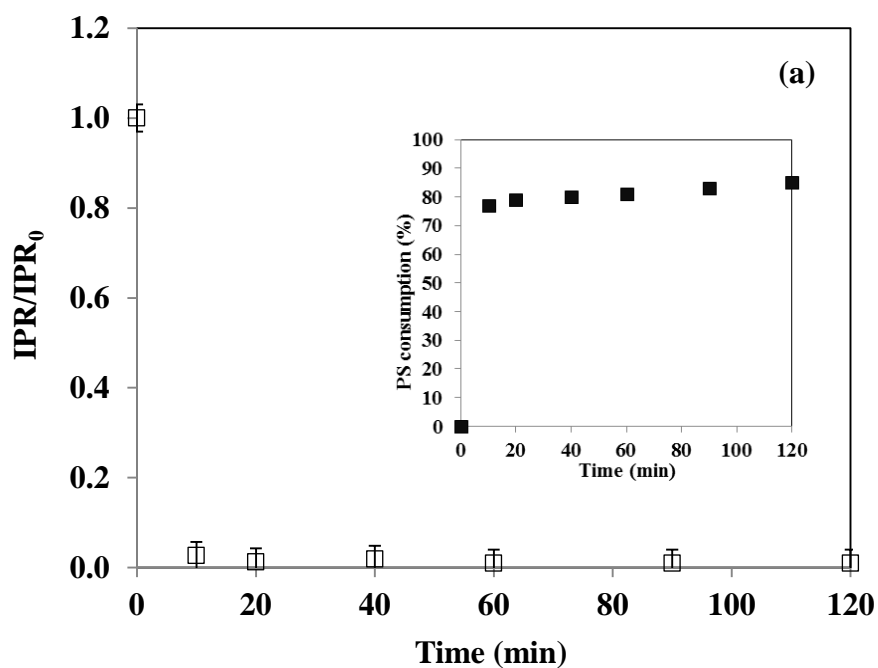
Figure 4.24 : Changes in normalized IPR (a) and DOC (b) concentrations during ZVI/PS treatment in DW. IPR=10 mg/L; PS=2.50 mM; DOC for 10 mg/L IPR=4.3 mg/L; ZVI=1 g/L; pH=3.0. Figure 4.24 (a) insert shows the calculated PS consumptions (%) during ZVI/PS treatment of 10 mg/L IPR in DW.

The degree of Fe release and PS consumption was also followed during ZVI/PS (PS=0.50 mM, pH=3.0) treatment of 2 mg/L IPR. According to Table 4.6, complete IPR degradation was achieved during the first 10 min of ZVI/PS treatment accompanied with 13% of PS consumption. As it can be seen in Table 4.6, more corrosion on ZVI surface resulted in more Fe releases from the particle surface to the reaction bulk and consequently resulted in more PS consumption ($SO_4^{\bullet-}$ generation). The ultimately released Fe concentration was measured 129 µg/L where almost complete IPR degradation and PS consumptions were achieved. Fe concentrations positively correlated with PS consumption and micropollutant removals during ZVI/PS treatment.

Table 4.6 : IPR and released Fe concentrations as well as PS consumption (%) during ZVI/PS treatment of IPR. IPR=2 mg/L; PS=0.50 mM; ZVI=1 g/L; pH=3.0.

Time (min)	IPR (mg/L)	Fe (µg/L)	PS Consumption (%)
5	0.16	<10	10
10	0	<10	13
30	0	<10	20
60	0	88	68
120	0	129	95

Zero-valent aluminum-activated persulfate oxidation process

Figure 4.25 presents changes in normalized IPR (a) and DOC (b) concentrations during ZVA/PS (PS=2.50 mM; pH=3.0) treatment of 10 mg/L IPR in DW. The insert in Figure 4.25 (a) depicts PS consumption (%) during ZVA/PS treatment of 10 mg/L IPR in DW. From Figure 4.25, it is evident that for the first 60 min ZVA/PS treatment, IPR removal was slow such that only 12% IPR removal was achieved accompanied with 25% PS consumption. With the progress of the treatment, IPR removal proceeded faster and reached 65% after 120 min treatment accompanied with 33% PS consumption and poor mineralization. The observed quite low and partially PS consumption (33%) during 120 min ZVA/PS treatment of IPR can be

explained by considering the fact that IPR degradation was attributed not only to $SO_4^{\bullet-}$ but also to $HO^{\bullet}$ derived from the reaction of H_2O with $SO_4^{\bullet-}$ as (equation 2.8) well as sequential single electron transfer from ZVA to O_2 . However, due to the lower diffusion rate of O_2, whether O_2 is involved in the reaction was closely related to the degree of ZVA corrosion (Ren et al, 2018). It should be taken into account that direct application of ZVA in water/wastewater treatments is accompanied with Al release into the environment and hence the assessment of its concentration in the reaction medium is very essential. Table 4.7 presents IPR and released Al concentration as well as PS consumption during ZVA/PS (PS=0.50 mM; pH=3.0) treatment of 2 mg/L IPR in DW. During ZVA/PS treatment, it is expected that the $SO_4^{\bullet-}$ formation relies on the activation of PS by ZVA that results in Al ion release. According to Table 4.7, throughout the treatment period, with IPR degradation, Al ion concentration increased gradually without evidence of an induction period at any stage of the oxidation reaction which can be attributed to the acidic pH environment that hindered ZVA passivation so that continuous $SO_4^{\bullet-}$ and/or $HO^{\bullet}$ formation and subsequent pollutant degradation occurred via oxidation reactions (Arslan-Alaton et al, 2018b). Al ion concentration reached a maximum value of 499 µg/L at the end of 120 min.

Table 4.7 : IPR and released Al concentrations as well as PS consumption (%) during ZVA/PS treatment of IPR. IPR=2 mg/L; PS=0.50 mM; ZVA=1 g/L; pH=3.0.

| Time (min)	IPR (mg/L)	Al (µg/L)	PS Consumption (%)
5	1.90	-	-
10	1.87	299	5
30	1.79	324	7
60	1.49	353	10
120	0	499	15
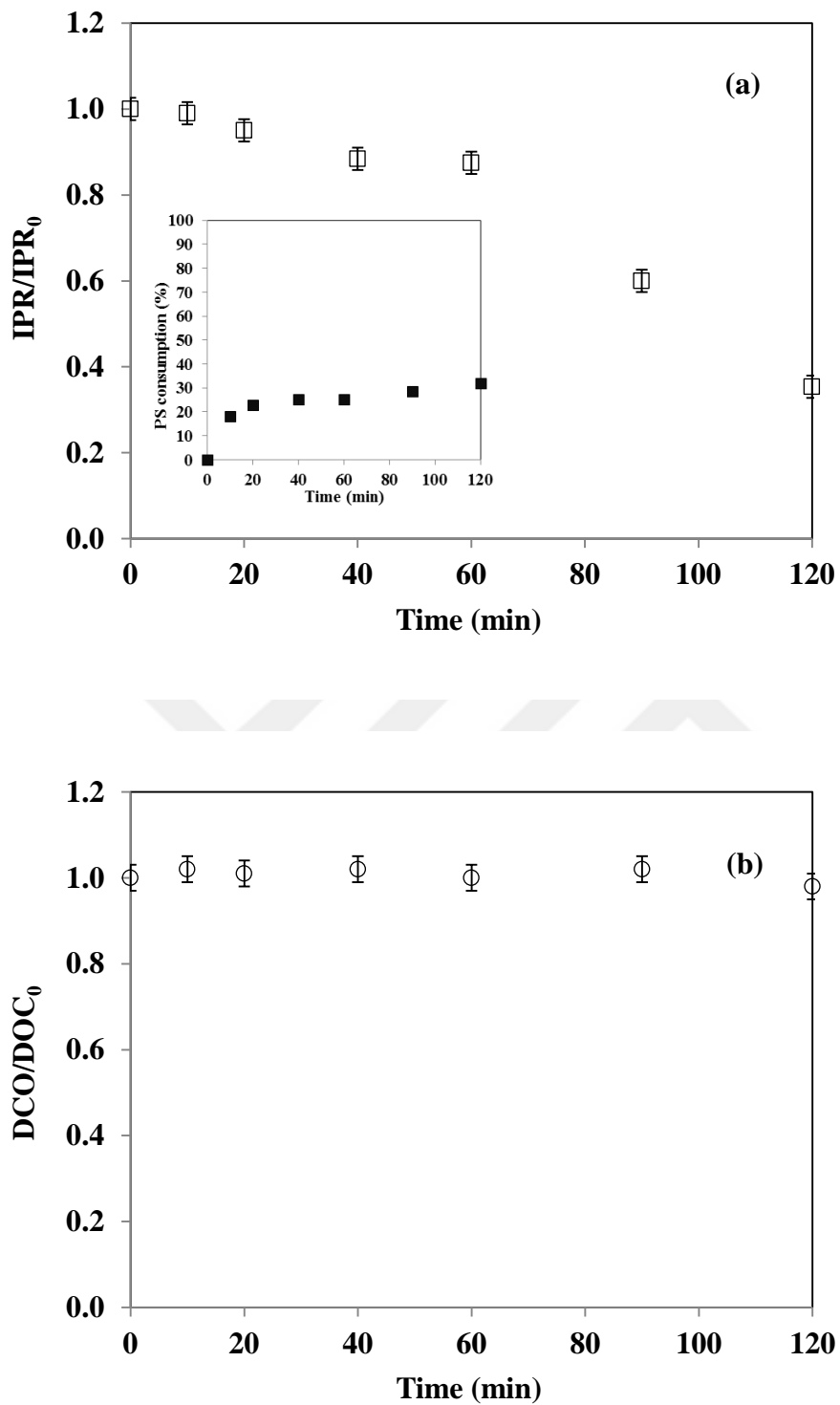
Figure 4.25 : Changes in normalized IPR (a) and DOC (b) concentrations during ZVA/PS treatment in DW. IPR=10 mg/L; PS=2.50 mM; DOC for 10 mg/L IPR=4.3 mg/L; ZVA=1 g/L; pH=3.0. Figure 4.25 (a) insert shows the calculated PS consumptions (%) during ZVA/PS treatment of 10 mg/L IPR in DW.

4.3 Treatability of the Model Industrial Micropollutants in Synthetic Tertiary Treated Urban Wastewater

In order to elucidate the oxidation of each model industrial micropollutant (3,5-DCP, 2,4-DCA and IPR) in a more complex effluent matrix through selected oxidation experiments (UV-C/PS and/or ZVI/PS and/or ZVA/PS), additional experiments were conducted in SWW mimicking tertiary treated urban wastewater. In addition to model industrial micropollutant abatement, the degree of mineralization of each micropollutant in terms of DOC removal efficiencies and rates was investigated. Table 4.8 presents the selected treatments processes and initial reaction conditions for each model industrial micropollutant.

Table 4.8 : Initial reaction conditions of selected treatment-processes for each model industrial micropollutant in SWW.

Pollutant	Selected treatment-processes	Reaction conditions and treatment time
3,5-DCP	UV-C	3,5-DCP=2 mg/L; pH=6.8; t=120 min
	UV-C/PS	3,5-DCP=2 mg/L; PS=0.09 mM; pH=6.8; t=120 min
	ZVI/PS	3,5-DCP=2 mg/L; PS=1.50 mM; pH=3.0; t=120 min
2,4-DCA	UV-C	2,4-DCA=2 mg/L; pH=6.8; t=120 min
	UV-C/PS	2,4-DCA=2 mg/L; PS=0.30 mM; pH=6.8; t=120 min
	ZVI/PS	2,4-DCA=2 mg/L; PS=1.50 mM; pH=5.0; t=120 min
IPR	UV-C	IPR=2 mg/L; pH=6.8; t=120 min
	UV-C/PS	IPR=2 mg/L; PS=0.09 mM; pH=6.8; t=120 min
	ZVI/PS	IPR=2 mg/L; PS=1.50 mM; pH=3.0; t=120 min
	ZVA/PS	IPR=2 mg/L; PS=1.50 mM; pH=3.0; t=120 min

4.3.1 3,5-Dichlorophenol

4.3.1.1 Ultraviolet-C and Ultraviolet-C-activated persulfate oxidation processes

Figure 4.26 presents changes in normalized 3,5-DCP (a) and DOC (b) values through UV-C and UV-C/PS (PS=0.09 mM) treatments at an initial concentration of 2 mg/L 3,5-DCP in SWW. As it can be seen from Figure 4.26 (a) complete 3,5-DCP removal was observed after 60 min by UV-C/PS while degradation of 3,5-DCP through UV-C photolysis was slower reaching complete degradation after 100 min. Pseudo-first order 3,5-DCP degradation rate constants in SWW were calculated as 0.0486 min^{-1} and 0.0773 min^{-1} for UV-C photolysis and UV-C/PS processes, respectively. These values were appreciably lower than the rate constants calculated for 3,5-DCP treatments in DW (even with lower PS concentrations; 0.030 mM, 0.050 mM and 0.075 mM) which can be ascribed to the complexity of SWW as compared to DW.

The presence of various organic and inorganic constituents in the SWW might have different but mainly inhibitory effects on UV-C and UV-C/PS treatment of 3,5-DCP. For example humic acid as one of typical dissolved organic compounds in water, absorbs UV photons at 200 nm-300 nm, thereby decreasing UV transmittance and availability for PS (Frontistis 2019; Chen et al. 2019). The inhibitory effect of humic acid on UV/PS treatment was also reported in a recent related work (Fu et al. 2019) where the apparent degradation rate constant of three non-steroidal anti-inflammatory drugs decreased by increasing humic acid concentration resulting in UV photon absorption of humic acid and thereby, fewer available photons to activate PS. Parallel to 3,5-DCP, changes in normalized DOC being observed during UV-C and UV-C/PS treatments is comparatively shown in Figure 4.26 (b). As it can be seen from Figure 4.26 (b), only 14% and 26% DOC (overall) removals were achieved at the end of 120 min for UV-C and UV-C/PS treatments, respectively. Insignificant mineralization may be related to the formation of intermediates which are not oxidized to mineral compounds and have long oxidation pathway (Ghanbari et al, 2016). Limited mineralization of degradation products by UV/PS also reported in previous studies (Gao et al, 2012; Gao et al, 2015). For instance, in a former related study (Fu et al, 2019), mineralization of diclofenac, ibuprofen and naproxen in UV-C/PS treatment were investigated and despite of over 99% removals of all three drugs during 30 min, mineralization was only 27%.
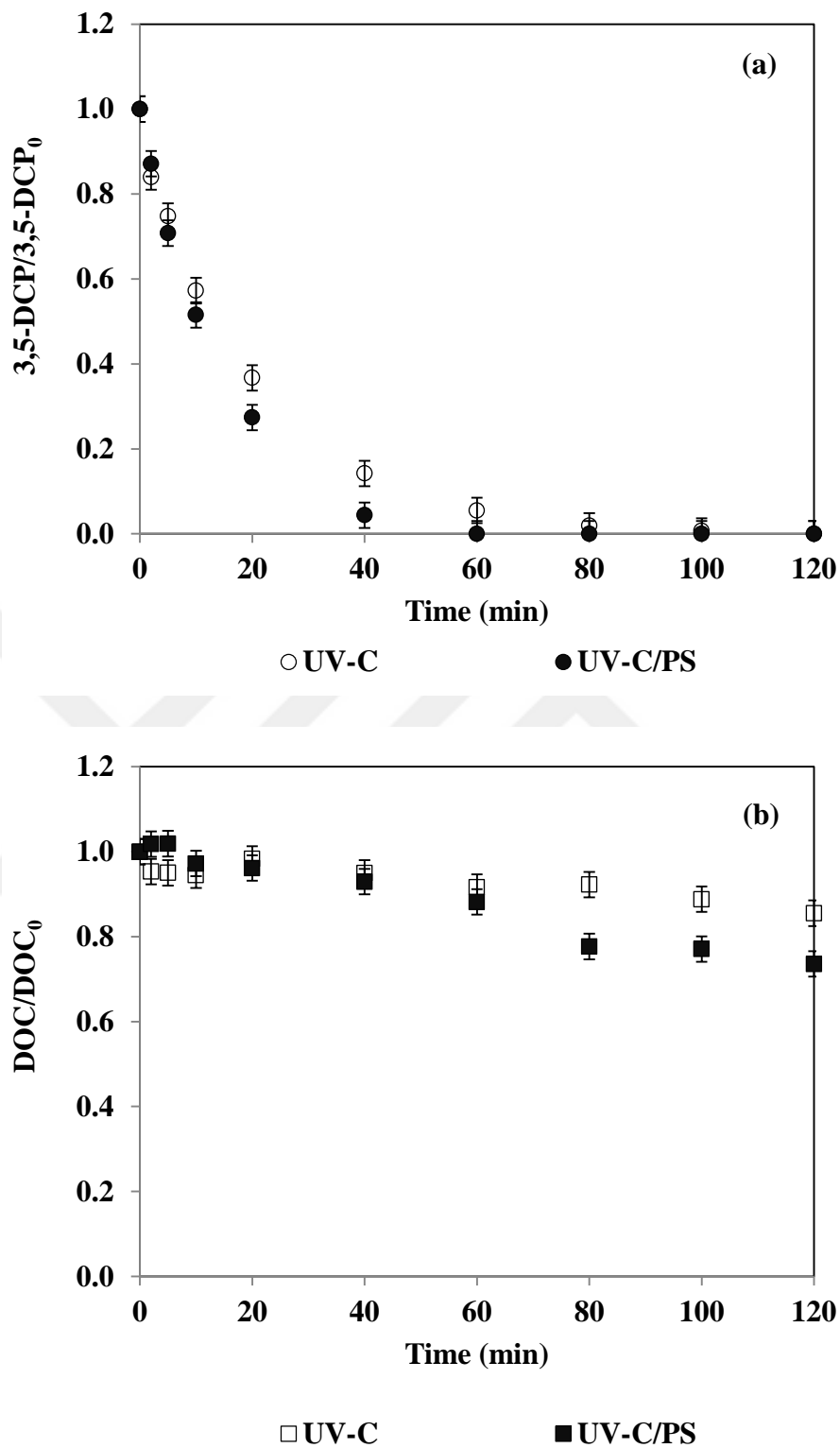
Figure 4.26 : Changes in normalized 3,5-DCP (a) and DOC (b) values during UV-C and UV-C/PS treatments in SWW. 3,5-DCP=2 mg/L; PS=0.09 mM; DOC=12.6 mg/L; UV-C intensity=0.5 W/L; pH=6.8.

4.3.1.2 Zero-valent iron-activated persulfate oxidation process

Figure 4.27 depicts changes in normalized 3,5-DCP and DOC concentrations during ZVI/PS (PS=1.50 mM; pH=3.0) treatment in SWW with initial 3,5-DCP concentration 2 mg/L. As can be seen from Figure 4.27 complete removals were achieved after 20 min as a consequence of ferrous ion production which can catalyze PS to produce $SO_4^{\bullet-}$ (Hussain et al, 2014; Liang and Lai, 2008) through equations 2.2-5. Such high efficiency of ZVI/PS treatment system in target micropollutant removal can be ascribed to the multivalent oxidation states of Fe which may enhance the electron transfer, causing high catalytic reactivity (Hussain et al, 2014). Although obtained results showed complete micropollutant removal, mineralization efficiency of 3,5-DCP solution at the end of treatment (120 min) was 41%. DOC removal of 3,5-DCP solution in SWW decreased compared to DW (50%) revealing the presence of organic/inorganic compounds in SWW has an inhibitory effect on 3,5-DCP mineralization.

Figure 4.27 : Changes in normalized 3,5-DCP and DOC concentrations during ZVI/PS treatments in SWW. 3,5-DCP=2 mg/L; DOC=12.6 mg/L; PS=1.50 mM; ZVI=1 g/L, pH=3.0.

4.3.2 2,4-Dichloroaniline

4.3.2.1 Ultraviolet-C and Ultraviolet-C-activated persulfate oxidation processes

Figure 4.28 shows changes in normalized 2,4-DCA (a) and DOC (b) through UV-C and UV-C/PS (PS=0.30 mM) treatments at an initial concentration of 2 mg/L 2,4-DCA. From Figure 4.28 (a), it could be demonstrated that UV-C photolysis of 2,4-DCA, even in the absence of PS, resulted in 98% 2,4-DCA removal only after 20 min whereas no effective mineralization was observed (Figure 4.28 (b)). Upon addition of 0.30 mM PS to the SWW, complete removal was achieved after 10 min and DOC removal was appreciably improved from 7% removal to 57% through 120 min UV-C photolysis and UV-C/PS treatment, respectively as a consequence of $SO_4^{\bullet-}$ production (Figure 4.28 (a) and (b)). In fact, the addition of PS shifted the reaction mechanism from UV-C photolysis to advanced oxidation of 2,4-DCA through $SO_4^{\bullet-}$ production showing a more effective and powerful mechanism than UV-C treatment alone in terms of DOC removal. Similar results were also reported in a former related study (Xu et al, 2016), in which mineralization of sucralose (a new non-nutritive artificial sweetener) was examined in synthetic sewage. Poor mineralization (7% TOC removal) was observed during UV photolysis of sucralose while the mineralization efficiency of sucralose was significantly improved during UV-C/PS treatment using 2.520 mM PS as a consequence of reactive radical ($SO_4^{\bullet-}$) production such that caused a TOC removal of 93% in 60 min at pH of 7.

UV-C/PS treatment of 2,4-DCA resulted to partially DOC removal and this may be attributed to the formation of intermediates which are not oxidized to mineral compounds and more recalcitrant compared to the original pollutant. Partial mineralization during electrochemical oxidation of 2,4-DCA was reported in a former related study (Kádár et al, 2001). In that study, electrochemical oxidation of 2,4-DCA did not lead to complete mineralization but to the formation of chlorinated products chlorinated 4-amino-diphenylamines as well as chlorinated anilines (Kádár et al, 2001).
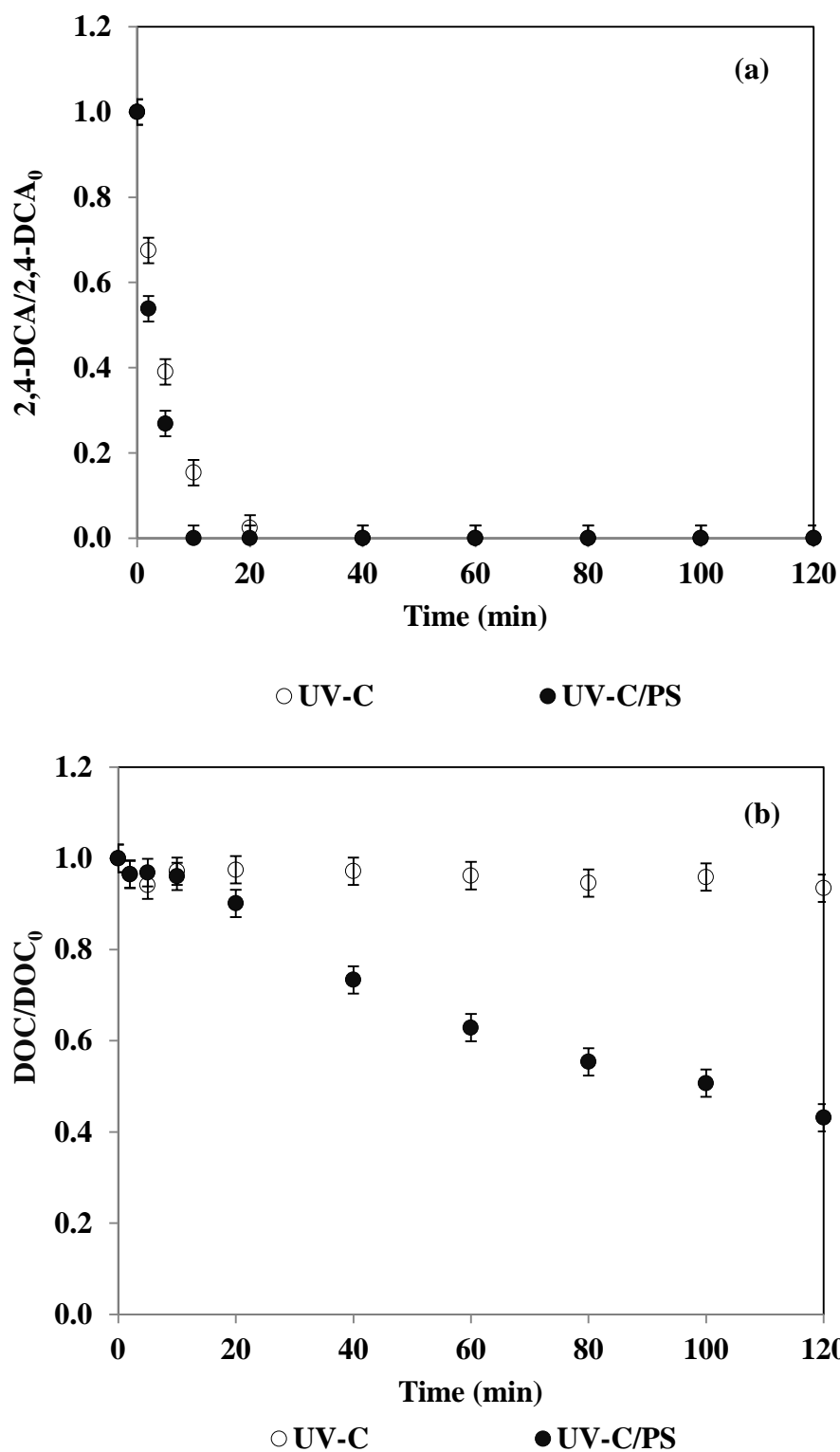
Figure 4.28 : Changes in normalized 2,4-DCA (a) and DOC (b) values during UV-C and UV-C/PS treatments in SWW. 2,4-DCA=2 mg/L; PS=0.30 mM; DOC= 12.3 mg/L; UV-C intensity=0.5 W/L; pH=6.8.

4.3.2.2 Zero-valent iron-activated persulfate oxidation processes

Figure 4.29 depicts changes in normalized 2,4-DCA and DOC concentrations during ZVI/PS (PS=1.50 mM; pH=5.0) treatment in SWW. As it was mentioned before, in ZVI/PS, it is proposed that $SO_4^{\bullet-}$ is generated by Fe^{2+} mediated activation of PS (Deng et al, 2014; Li et al, 2014a). However, presence of other organic and inorganic SWW compositions can decrease the available $SO_4^{\bullet-}$ through scavenging reactions. Obtained results revealed that 2,4-DCA could be effectively degraded by ZVI/PS treatment such that complete 2,4-DCA removal was achieved after 40 min ZVI/PS treatment in SWW.
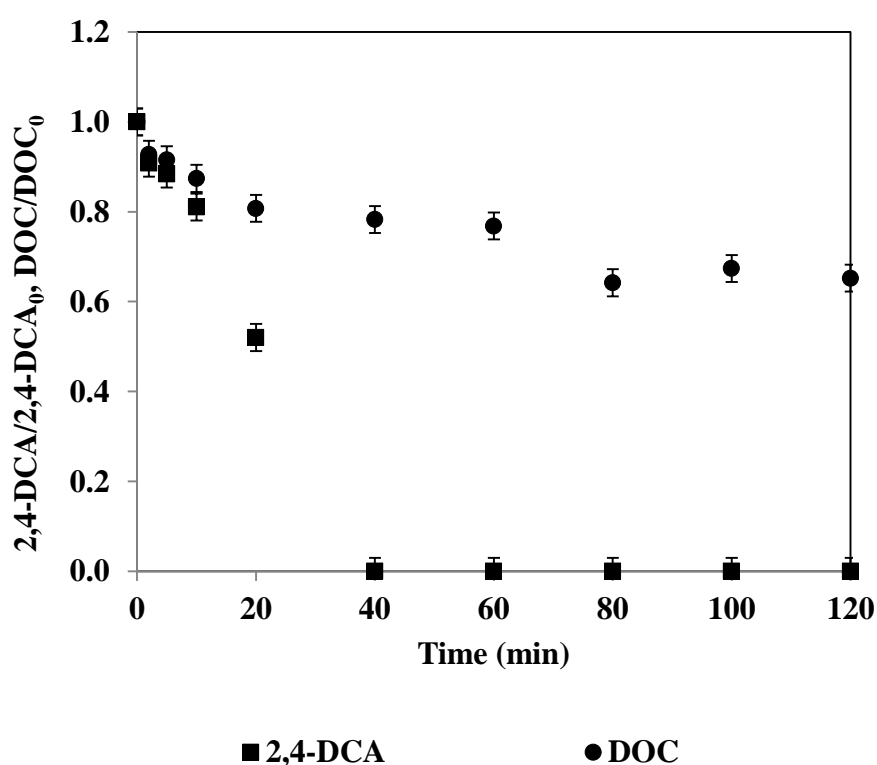
Figure 4.29 : Changes in normalized 2,4-DCA and DOC concentrations during ZVI/PS treatments in SWW. 2,4-DCA=2 mg/L; DOC=12.3 mg/L; PS=1.50 mM; ZVI=1 g/L, pH=5.0**.**

Figure 4.29 also presents the changes in normalized DOC concentration during ZVI/PS treatment of 2,4-DCA. Partially mineralization was observed after 80 min treatment and then no appreciable changed in normalized DOC was observed beyond this treatment time. Although complete 2,4-DCA was achieved only after 40 min treatment, with the progress of treatment only 35% DOC removal was obtained (120 min) that was a lower DOC removal compared to DW (44% DOC removal) indicating that oxidation of the intermediates was inhibited in the presence of organic

and inorganic SWW compositions. This inhibition can be attributed to the competitive scavenging of $SO_4^{\bullet-}$ by these reactive moieties in organic SWW composition (Zhao et al, 2016)

4.3.3 Iprodione

4.3.3.1 Ultraviolet-C and Ultraviolet-C-activated persulfate oxidation processes

Figure 4.30 shows changes in normalized IPR (a) and DOC (b) through UV-C and UV-C/PS (PS=0.09 mM) treatments at an initial concentration of 2 mg/L IPR. UV-C photolysis of IPR resulted in 92% IPR removal after 120 min (Figure 4.30 (a)) although no DOC removal was observed at the end of treatment time (Figure 4.30 (b)) indicating that the use of UV-C treatment alone was not sufficient in the effective degradation of IPR intermediate photolysis products. The degradation of IPR through UV-C/PS caused complete IPR removal after 80 min whereas DOC removal was only 24% after 120 min treatment indicating UV-C/PS (PS=0.09 mM) treatment was not also capable of efficient mineralization of IPR and its degradation products in SWW. Pseudo-first order IPR degradation rate constants in SWW were calculated as 0.0583 min^{-1} for UV-C/PS process showing IPR removal rate decreased in SWW as compared with DW. This observation is at least partially attributable to the competition between PS and inorganic/organic SWW components for UV-C light absorption which leads to fewer available photons to generate $SO_4^{\bullet-}$ and thereby these components hindering PS photo activation (Fu et al, 2019). Similarly, in a recent study (Li et al. 2018), indomethacin degradation by UV/PS was dramatically inhibited by increment in fulvic acid concentrations from 1 mg/L to 10 mg/L due to the light attenuation effect since the UV-vis absorption spectra of different fulvic acid concentrations overlapped dramatically with indomethacin. Moreover, fulvic acid also retarded indomethacin degradation through quenching of free radicals. At the same time, inorganic and organic water/wastewater components such as chloride, bicarbonate, carbonate, nitrate, phosphate, and sulfate can act as free radical scavengers inhibiting the oxidation of IPR.
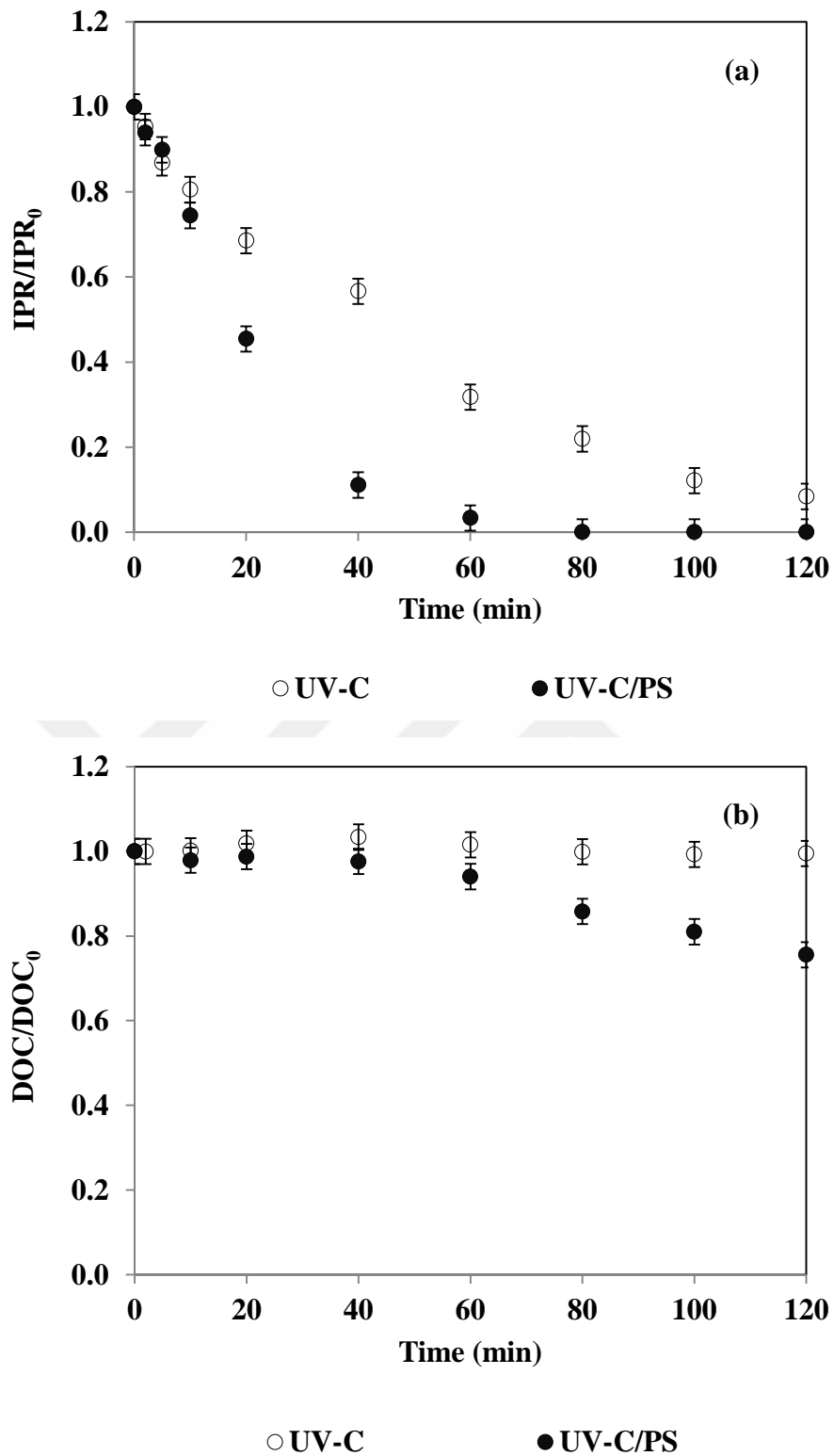
Figure 4.30 : Changes in normalized IPR (a) and DOC (b) values during UV-C and UV-C/PS treatments in SWW. IPR=2 mg/L; PS=0.09 mM; DOC=11.4 mg/L; UV-C intensity=0.5 W/L; pH=6.8.

4.3.3.2 Zero-valent iron-activated persulfate oxidation processes

Figure 4.31 depicts changes in presents changes in normalized IPR and DOC values through ZVI/PS (PS=1.50 mM) treatment at initial solution pH of 3.0 and initial concentration of 2mg/L of IPR in SWW. From Figure 4.31, IPR was completely removed after 20 min ZVI/PS treatment; however, its mineralization was partially and limited to 30% at the end of 20 min ZVI/PS treatment. Beyond this treatment time, no appreciable mineralization was observed. As can be seen in Figure 4.31, prolonged ZVI/PS treatment led to 40% DOC removal after 120 min and this treatment was more effective in mineralization of IPR compared to UV-C/PS and ZVA/PS (as will be explained in following section). This can be described by considering that Fe has two oxidation states -Fe(II) and Fe(III)- that can undergo a series of redox (Fenton and Fenton-like oxidation) and complexation reactions. Fe complexation of IPR's transformation products could enhance their oxidation by changing the solubility and availability of these substrates towards active oxidants. In this way, the removal of IPR and its organic carbon content would be removed more effectively.
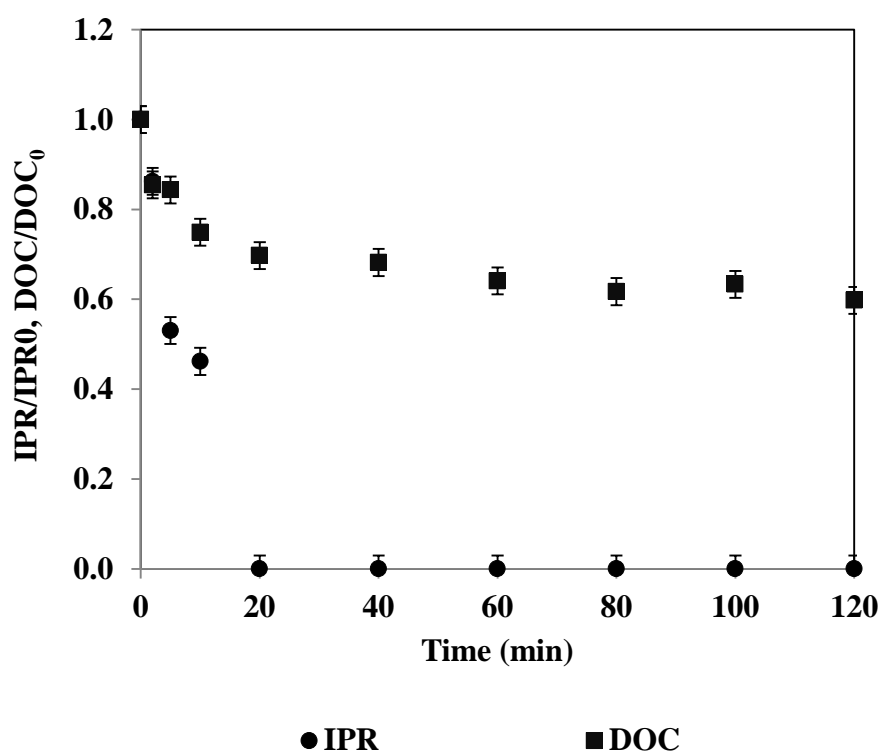
Figure 4.31 : Changes in normalized IPR and DOC concentrations during ZVI/PS treatments in SWW. IPR=2 mg/L; DOC=11.4 mg/L; PS=1.50 mM; ZVI=1 g/L, pH=3.0.

4.3.3.3 Zero-valent aluminum-activated persulfate oxidation process

Obtained results from baseline experiments in DW showed that only IPR was removed completely after 120 min ZVA/PS treatment. Therefore ZVA/PS as a selected oxidation process was chosen to elucidate treatability of IPR in SWW. Figure 4.32 presents changes in normalized IPR and DOC values through ZVA/PS (PS=1.50 mM) treatment at initial solution pH of 3.0 and at an initial concentration of 2mg/L of IPR in SWW. From Figure 4.32, poor IPR removal was observed during 120 min ZVA/PS treatment of SWW spiked with 2 mg/L IPR while ZVA/PS treatment of 2 mg/L of IPR in DW with initial PS concentration of 0.50 mM resulted in complete IPR removal in 120 min (data shown above). This observation can be ascribed to the complexity of SWW as compared to DW. The presence of various organic and inorganic constituents in the SWW led to inhibitory effects on ZVA/PS treatment of IPR.

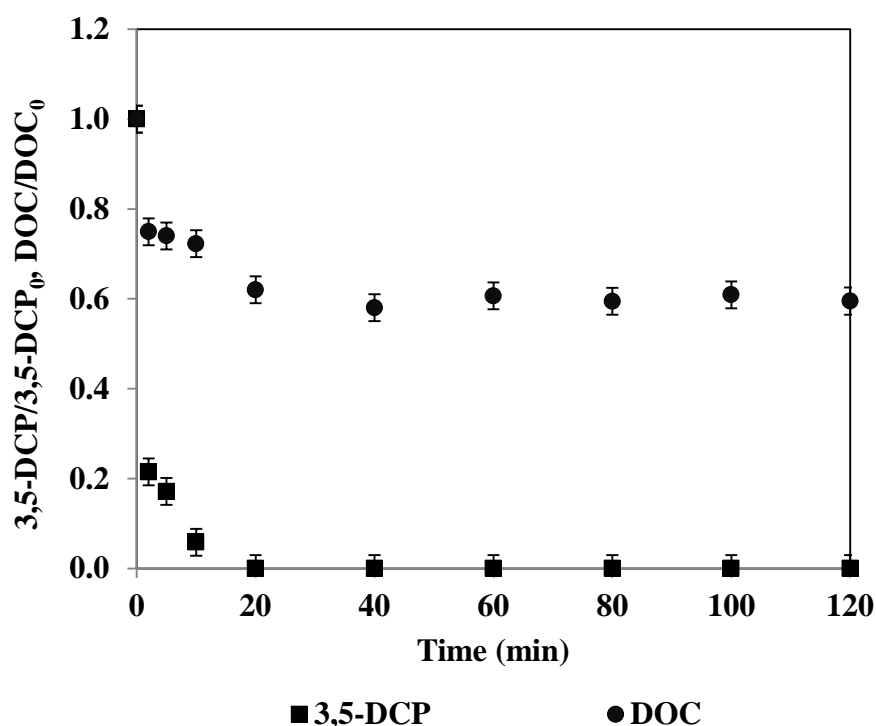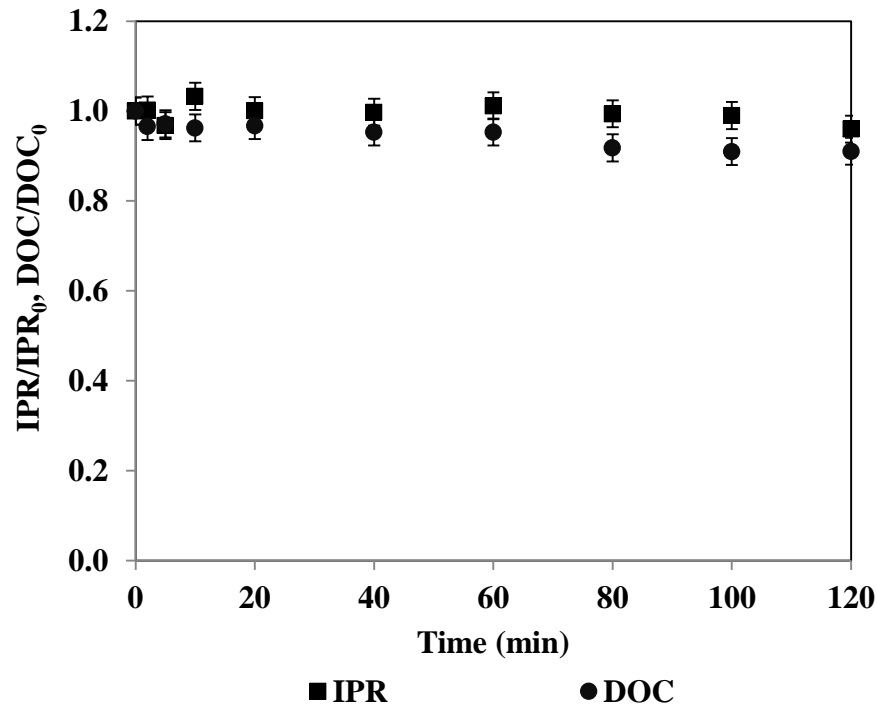**Figure 4.32 :** Changes in normalized IPR and DOC concentrations during ZVA/PS treatments in SWW. IPR=2 mg/L; DOC=11.96 mg/L; PS=1.50 mM; ZVA=1 g/L, pH=3.0.

Changes in normalized DOC values in SWW spiked with IPR were also followed during ZVA/PS treatment at pH 3.0 and poor mineralization was obtained after 120 min treatment. Similar to this result, in a former study (Arslan-Alaton et al, 2017c), it

was shown that presence of organic/inorganic compounds in wastewater samples such as humic acid (a major dissolved organic matter component in wastewater samples), had an inhibitory effect on the performance of the ZVA/PS oxidation system such that no iopamidol removal was observed during ZVA/PS treatment in the wastewater sample (Arslan-Alaton et al, 2017c). As it can be seen from Figure 4.32, practically no change in normalized DOC was observed (9%) indicating that the ingredients present in SWW might inhibit the oxidation process.

4.4 Toxicity

4.4.1 Acute toxicity

4.4.1.1 3,5-Dichlorophenol

Ultraviolet-C and Ultraviolet-C-activated persulfate oxidation processes

Figure 4.33 depicts changes in percent relative inhibitions values before and during UV-C (a) (pH=6.8) and UV-C/PS (b) (PS=0.09 mM; pH=6.8) on two different bioassays namely *V. fischeri* and *P. subcapitata* as well as 3,5-DCP abatements. As shown in Figure 4.33 (a) and (b) the original 3,5-DCP did not cause significant inhibition towards *V. fischeri* such that the original relative inhibition value for 2 mg/L 3,5-DCP was obtained as less than 10%. During UV-C and UV-C/PS treatments of 2 mg/L of 3,5-DCP, toxicity of 3,5-DCP treated samples on *V. fischeri* did not change appreciably (fluctuated between 3%-8%) indicating that the photobacteria *V. fischeri* was not sensitive also toward the possible evolved intermediates of 3,5-DCP during UV-C and UV-C/PS treatments. From Figure 4.33 (a) and (b), the responses of the test organisms were rather different; higher inhibition rates were observed on *P. subcapitata* than *V. fischeri*. As it can be seen from Figure 4.33 (b), the percent relative inhibition of the original 3,5-DCP on *P. subcapitata* was 20%. During UV-C/PS treatment, the inhibitory effect increased, reaching 33% and 34% after 10 min and 20 min treatment, respectively. The observed trend in the toxicity changes in the initial stages of UV-C photochemical treatment of CPs may be ascribed to the formation of substituted hydroxy- and phenoxy-derivates of phenols (Karci 2014). Prolonged UV-C/PS treatment resulted in a re-increase in acute toxicity to 47% after 80 min probably due to the possible evolved aldehydes, non-chlorinated carboxylic acids and chlorinated aliphatic by-

116

products suggesting the contribution of these oxidation products to toxicity at the end of reaction time (Fang et al, 2019; Fu et al, 2019; Karci et al, 2013a).
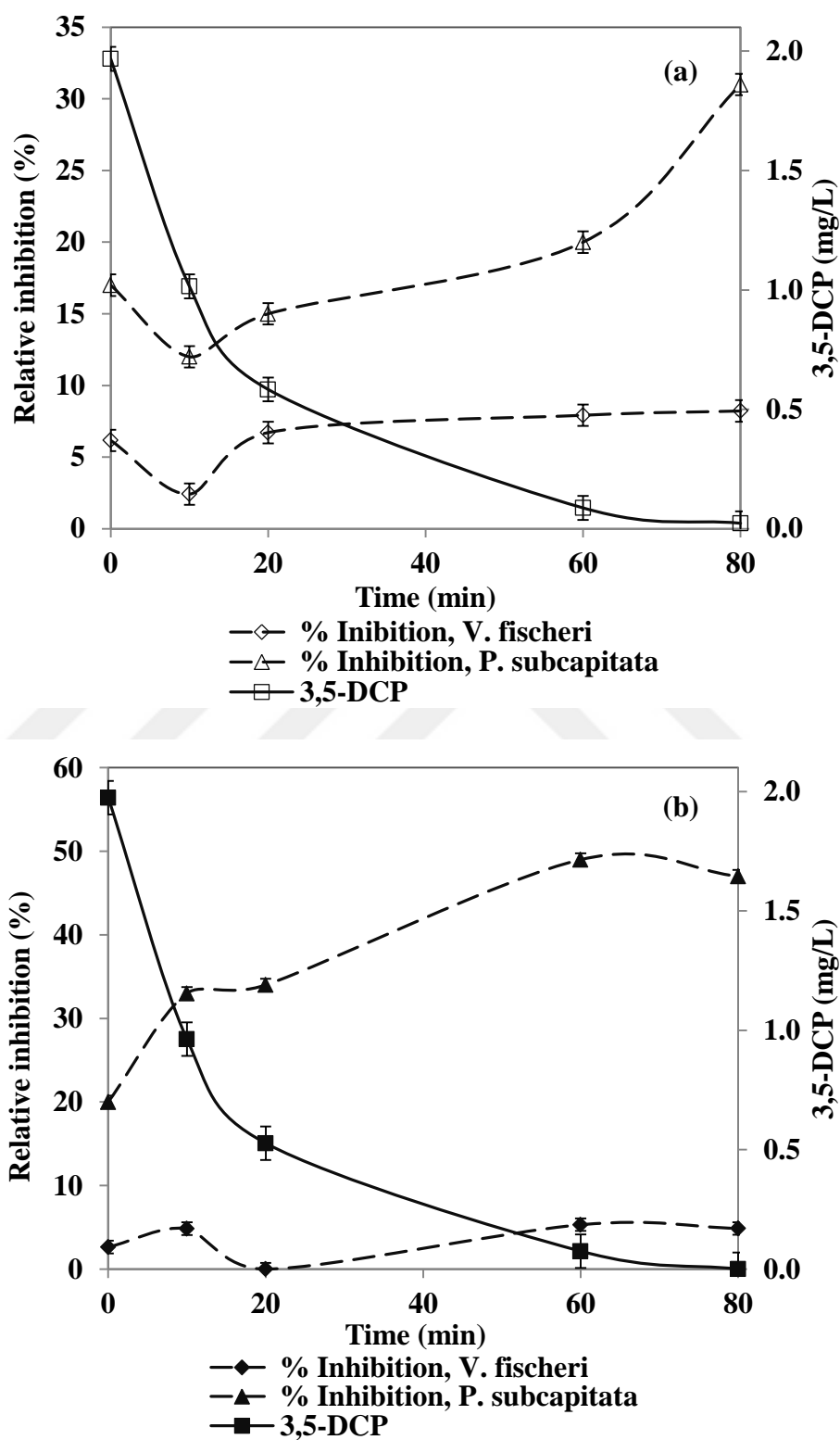
Figure 4.33 : Changes in percent relative inhibition values and 3,5-DCP concentrations during UV-C (a) and UV-C/PS (b) treatments of 3,5-DCP in SWW. 3,5-DCP=2 mg/L; PS=0.09 mM; UV-C intensity=0.5 W/L; pH=6.8.

The same trend was also observed in another study (Arslan-Alaton et al, 2018a), in which the treatability of iopamidol was explored in real tertiary treated municipal wastewater using the UV-C/PS treatment. In that work, the percent relative inhibition towards *P. subcapitata* increased remarkably from 15% to 63% after UV-C/PS application. This observation was ascribed to the formation of degradation products being more toxic than wastewater or wastewater spiked with iopamidol solution.

Zero-valent iron-activated persulfate oxidation processes

Figure 4.34 depicts changes in percent relative inhibition values before and during ZVI/PS (PS=1.50 mM; pH=3.0) treatment of 3,5-DCP in SWW on *V. fischeri* and *P. subcapitata* as well as 3,5-DCP abatements. As shown in Figure 4.34 the original 3,5-DCP did not cause appreciable inhibition towards *V. fischeri* (the original relative inhibition value for 2 mg/L 3,5-DCP was obtained 12%) as it was also shown in previous section. During ZVI/PS treatment of 3,5-DCP, the relative inhibition of treated samples on *V. fischeri* did not change appreciably (fluctuated between 10%-19%) indicating that *V. fischeri* was not sensitive also toward the possible evolved degradation products.
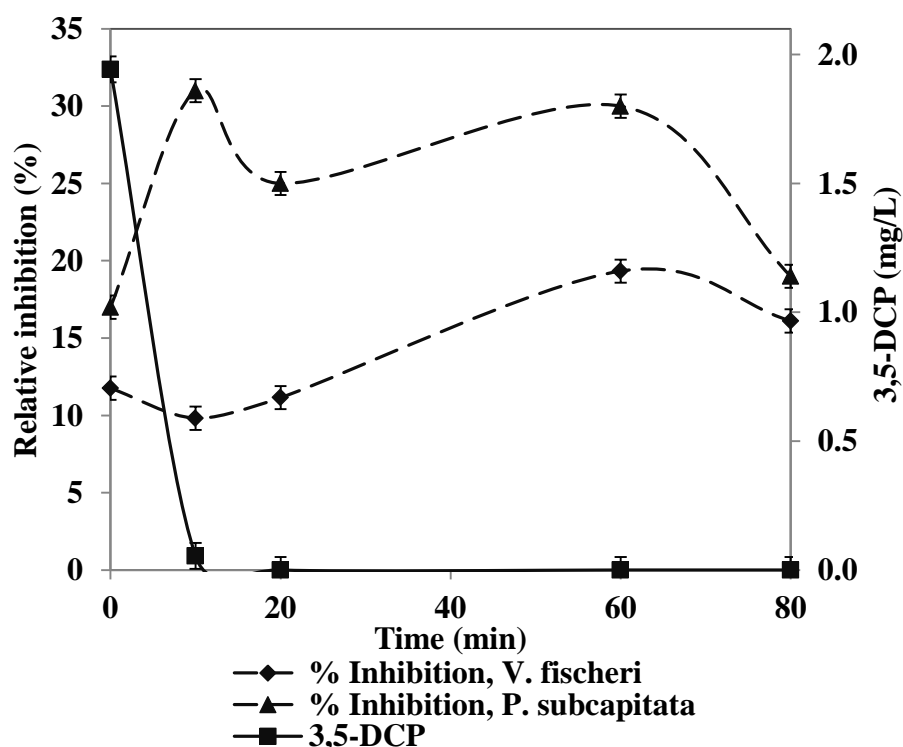
Figure 4.34 : Changes in percent relative inhibition values and 3,5-DCP concentrations during ZVI/PS treatment of 3,5-DCP in SWW. 3,5-DCP=2 mg/L; PS=1.50 mM; ZVI=1g/L; pH=3.0.

On the other hand, percent relative inhibition of 2 mg/L 3,5-DCP on *P. subcapitata* was obtained 17%, increased to 30% with 3,5-DCP abatement during the first 10 min of ZVI/PS treatment. This increment can be attributed to evolution of chlorinated aromatic intermediates of CPs during AOPs which have been reported in previous studies (Apak and Hugül, 1996; Czaplicka, 2004; Czaplicka, 2006). However after 80 min of ZVI/PS treatment of 3,5-DCP, toxicity of treated samples decreased to 19%.

4.4.1.2 2,4-Dichloroaniline

Ultraviolet-C and Ultraviolet-C-activated persulfate oxidation processes

Figure 4.35 presents changes in percent relative inhibition values before and during UV-C (a) and UV-C/PS (b) treatments of 2,4-DCA in SWW on *V. fischeri* and *P. subcapitata* as well as 2,4-DCA abatements. .As it can be seen from Figure 4.35 (a) and (b), the original 2,4-DCA sample caused no significant relative inhibition toward *V. fischeri* (<10%) whereas after 10 min and 20 min UV-C photolysis treatment of 2,4-DCA, relative inhibition toward *V. fischeri* reached to 33% and 34%, respectively. The increase in relative inhibition during the UV-C photolysis treatment of 2,4-DCA, might be ascribed to the generation of transformation products exerting higher toxicity than original 2,4-DCA. At the end of 80 min UV-C photolysis treatment, the relative inhibition toward *V. fischeri* decreased to 19%. The relative inhibition of 2,4-DCA treated samples on *P. subcapitata* increased to 33% after 20 min UV-C photolysis and decreased to 24% at the end of 80 min treatment.

As it can be seen from Figure 4.36 (a) and (b), the responses of the test organisms are rather different; the relative inhibition caused by the original 2,4-DCA was found as 25-28% on *P. subcapitata* while no significant relative inhibition on *V. fischeri* was observed (<10 %) indicating different sensitivities towards 2,4-DCA. These results emphasize the necessities of employing more than a single test organism in bioassays.
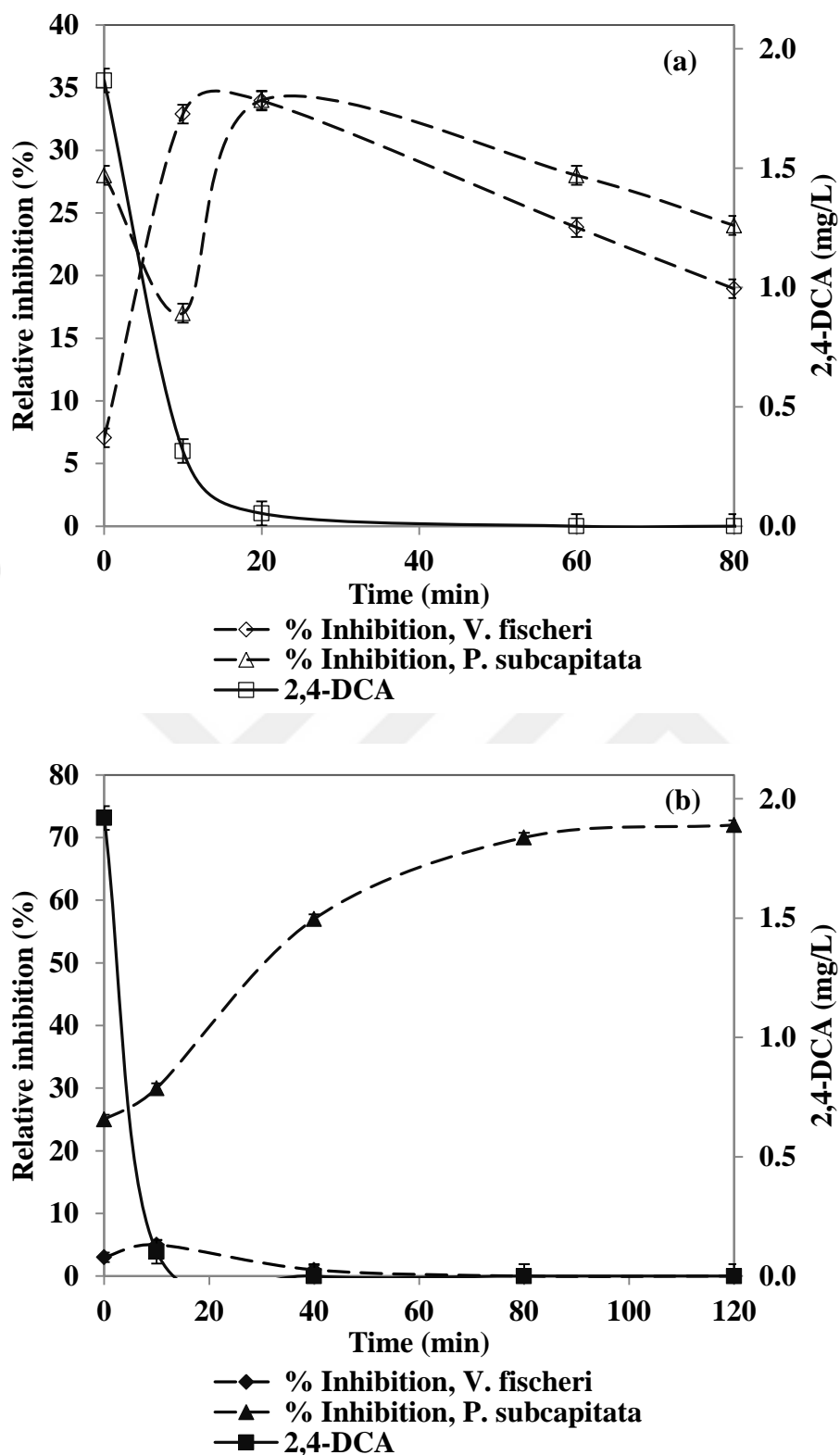
Figure 4.35 : Changes in percent relative inhibition values and 2,4-DCA concentrations during UV-C (a) and UV-C/PS (b) treatments of 2,4-DCA in SWW. 2,4-DCA =2 mg/L; PS=0.30 mM; UV-C intensity=0.5 W/L; pH=6.8.

No appreciable inhibition towards *V. fischeri* (<10%) was evident during UV-C/PS treatment of 2,4-DCA. In contrary to *V. fischeri* responses during UV-C/PS treatment

of 2,4-DCA, acute toxicity patterns of the bioassays conducted with *P. subcapitata* showed significant changes in relative inhibitions such that relative inhibition of 2,4-DCA increased during UV-C/PS treatment and reached to 72% after 120 min treatment. This increment in toxicity could be explained that 2,4-DCA degradation may produce some chlorinated intermediate compounds, which were more difficult to mineralize than 2,4-DCA and these intermediates organically may impart an additional toxicity to the reaction solutions (Liang et al, 2013). For example, in the former related works (Gosetti et al, 2010; Hussain et al, 2012) the identification of AOPs treated samples of 4-CA were investigated that the 4-CA degradation may produce some chlorinated intermediates (N-(4-chlorophenyl)-p-phenylene di-imine, 1-(4-chlorophenyl)-3- phenlurea and 5-chloro-2-((4-chlorophenyl) diazenyl) phenol) that may related to the increased toxicity. Besides, the formation of ring-opening products might be the most likely origin of the toxicity of UV-C/PS treated samples toward *P. subcapitata* based on 57% mineralization in terms of DOC removal at the end of treatment time (Liang et al, 2013).

Zero-valent iron-activated persulfate oxidation processes

Figure 4.36 shows changes in percent relative inhibition values before and during ZVI/PS treatment of 2,4-DCA in SWW on *V. fischeri* and *P. subcapitata* as well as 2,4-DCA abatements. As it can be seen from Figure 4.36, the original and treated samples of 2,4-DCA had no inhibition effect toward *V. fischeri* during ZVI/PS treatment.

The relative inhibition of original 2,4-DCA was found as 21% on *P. subcapitata* but during the first 10 min of ZVI/PS treatment of 2,4-DCA, the percentage relative inhibition toward *P. subcapitata* decreased to 7% and then remarkably increased to 68% which is corresponding to almost complete 2,4-DCA removal and ultimately decreased to 23% after 80 min treatment. This increment in relative inhibition can be ascribed to the formation of intermediates which are more toxic toward *P. subcapitata.*
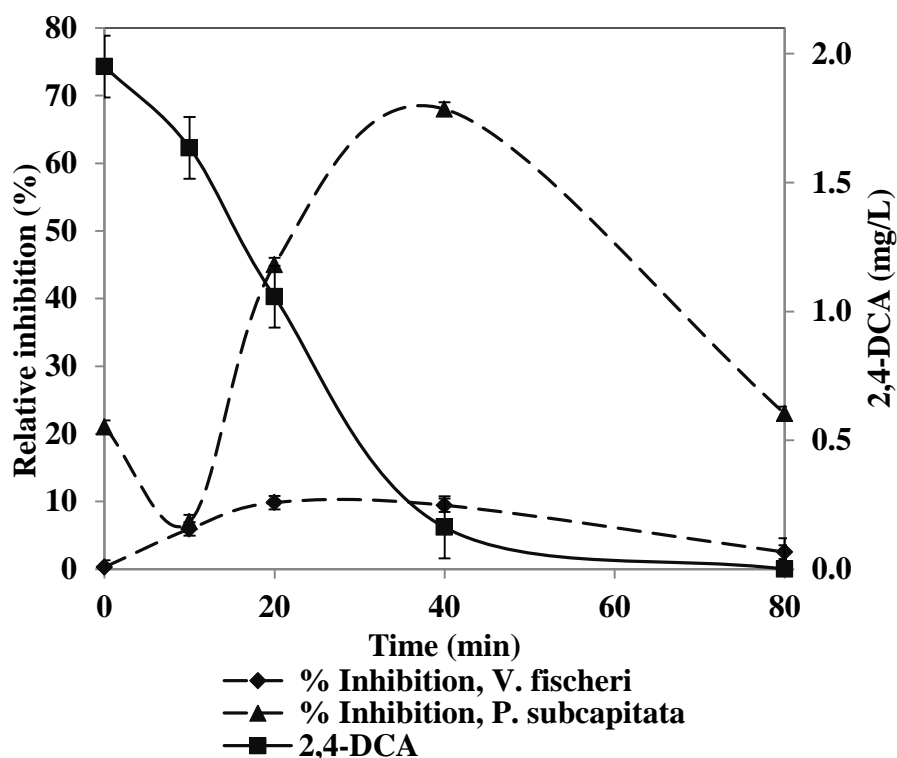
Figure 4.36 : Changes in percent relative inhibition values and 2,4-DCA concentrations during ZVI/PS treatment of 2,4-DCA in SWW. 2,4-DCA=2 mg/L; PS=1.50 mM; ZVI=1 g/L; pH=5.0.

4.4.1.3 Iprodione

Ultraviolet-C and Ultraviolet-C-activated persulfate oxidation processes

Figure 4.37 displays changes in percent relative inhibitions values as well as IPR before and during UV-C (a) and UV-C/PS (b) on two different bioassays namely *V. fischeri* and *P. subcapitata*. As shown in Figure 4.37 (a) and (b) the original IPR did not cause inhibition towards *V. fischeri* such that the original relative inhibition value for 2 mg/L IPR was obtained as less than 10%. Figure 4.37 displays changes in acute toxicity towards *V. fischeri* photobacteria in terms of percent relative inhibition of the luminescence intensities during UV-C/PS treatment of IPR in SWW as a function of treatment time. During the UV-C/PS treatment of IPR in SWW, the acute toxicity of the reaction solution started to decrease gradually to 4% after 120 min. The results of the present study demonstrated that the original IPR in the SWW sample as well as its UV-C/PS degradation products were practically non-toxic towards *V. fischeri*.

In a former related work (Lassalle et al, 2014), percent relative inhibition of original IPR and its photoproducts were investigated on *V. fischeri* after 15 min of incubation.

122

Results showed that photolyzed solution was significantly more toxic than original, in particular due to the formation of phenolic compounds (Lassalle et al, 2014).
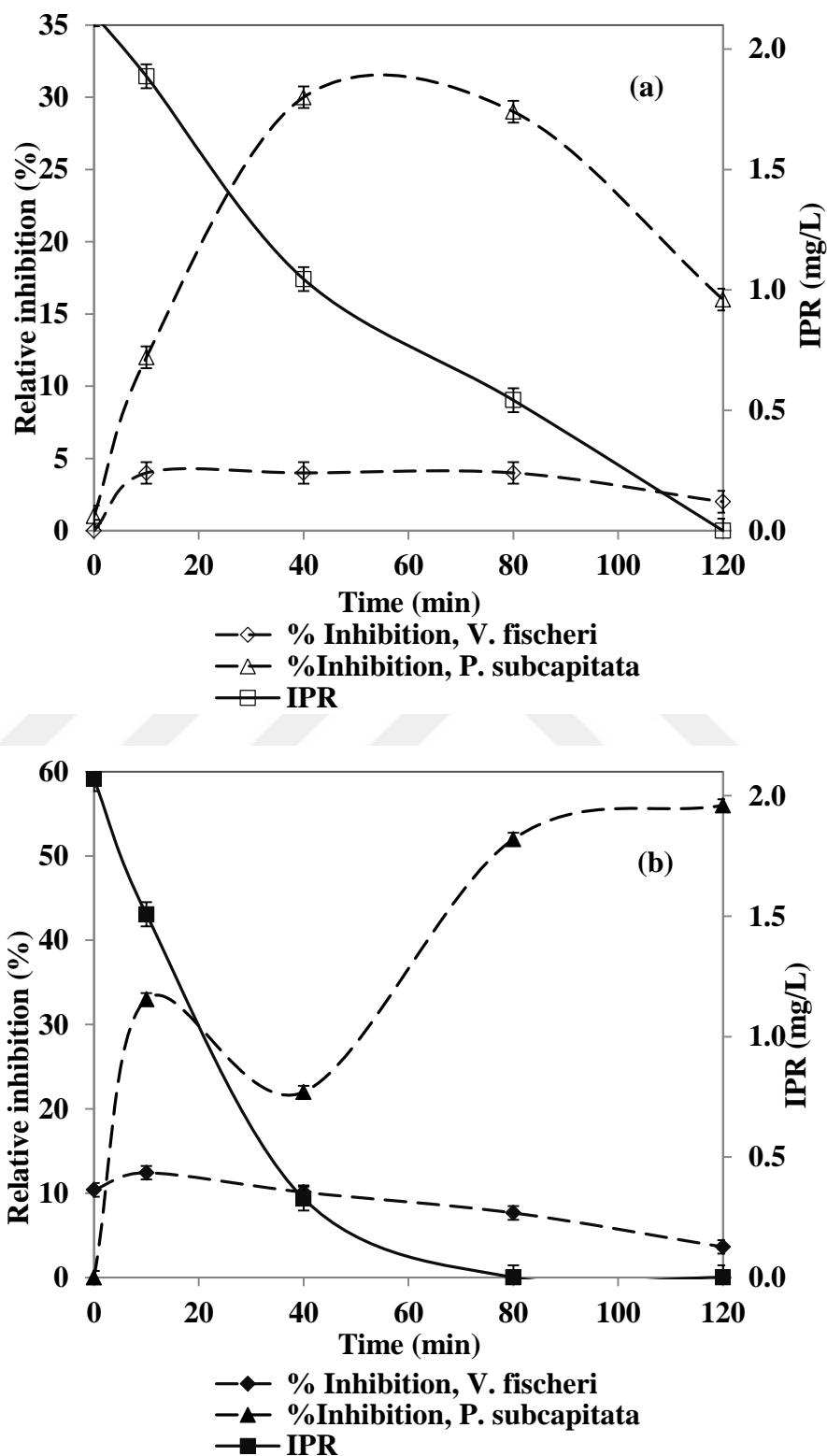
Figure 4.37 : Changes in percent relative inhibition values and IPR concentrations during UV-C (a) and UV-C/PS (b) treatments of IPR in SWW. IPR =2 mg/L; PS=0.09 mM; UV-C intensity=0.5 W/L; pH=6.8.

In another related work (Lopez-Alvarez et al, 2016), degradation of IPR through UV-C/H_2O_2 and toxicity of the photo-treated solutions employing *V. fischeri* were evaluated based on percentage change in $1/EC_{50}$. In that work complete IPR removal was reported after 160 min UV-C/H_2O_2 treatment and solution toxicity was reduced into 88 % after 240 min which was correspond to TOC removal 76%. This decrease in toxicity can be attributed to dechlorination as one of the first steps during IPR degradation as a consequence of $HO^{\bullet}$ attacks into carbon-chloride bond (Lopez-Alvarez et al, 2016).

As it can be seen from Figure 4.37 (a) and (b), the percent relative inhibition of the original IPR on *P. subcapitata* was calculated negligible. This observation might be attributed to IPR decomposition at pH of 8.1 adjusted for all samples (according to ISO 8692) before conducting *P. subcapitata* tests. Alkaline hydrolysis of IPR has already been reported in former works (Belafdal et al, 1986; Campos et al, 2015). The low percent relative inhibition of untreated IPR (original) demonstrated that neither IPR nor the possible hydrolyzed form of IPR have any inhibitory effect on *P. subcapitata*. The percent relative inhibition of the photolysis treated samples of IPR on *P. subcapitata* increased to 30% and 29% after 40 and 80 min treatment, respectively and finally after 120 min treatment decreased to 15%. The percent relative inhibition of the UV-C/PS treated IPR reached 56% after 120 min. This increment in toxicity could be attributed to the possible intermediates having kept a chlorine atom and are expected to induce a potential toxicity on *P. subcapitata* (Lassalle et al, 2014).

Zero-valent iron-activated persulfate oxidation processes
Figure 4.38 shows changes in percent relative inhibition values before and during ZVI/PS (PS=1.50 mM; pH=3.0) treatment of IPR in SWW on *V. fischeri* and *P. subcapitata*. As it can be seen from Figure 4.38, the original IPR sample had no inhibitory effect on *V. fischeri* and during the ZVI/PS treatment of IPR, the percentage relative inhibition of treated samples increased slightly to 11% after 120 min. Obtained toxicity results demonstrated that the original IPR in the SWW sample as well as its ZVI/PS intermediates were practically non-toxic towards *V. fischeri*. The percent relative inhibition of original IPR solution on *P. subcapitata* was calculated low (<10%). As it was mentioned above, the percent relative inhibition of original IPR solution might not be related to IPR because of its hydrolysis in alkaline

solution of pH 8.1 adjusted for all samples according to ISO 8692. As the treatment process progressed, a fluctuation occurred; however, the obtained percent relative inhibition values after 120 min reached to 40% indicating toxic degradation intermediates were formed during ZVI/PS treatment of IPR solution.
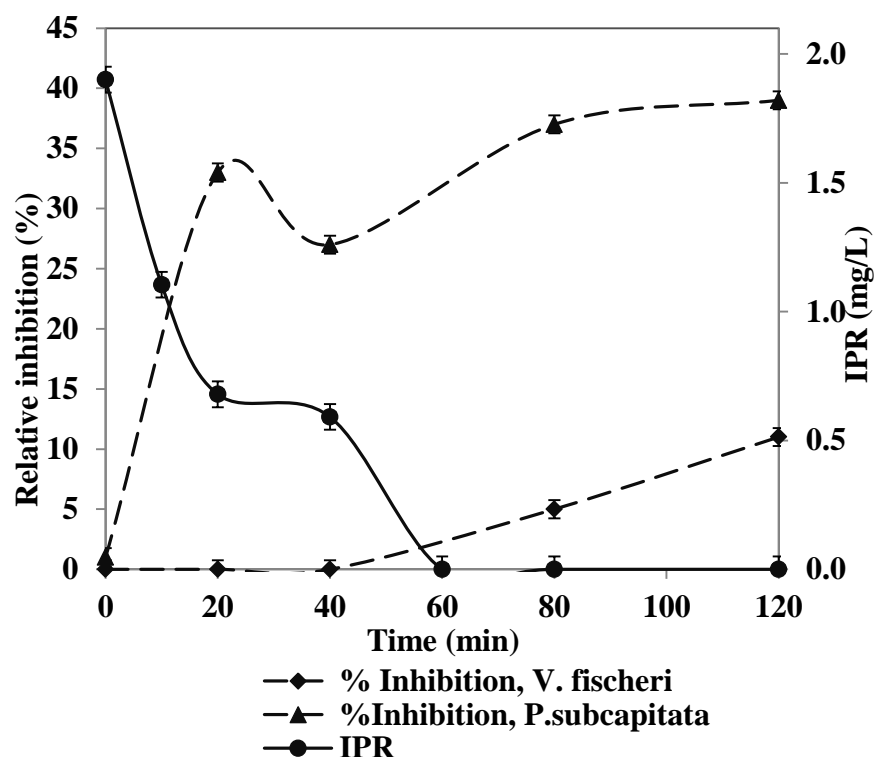
Figure 4.38 : Changes in percent relative inhibition values and IPR concentrations during ZVI/PS treatment of IPR in SWW. IPR=2 mg/L; PS=1.50 mM; ZVI=1g/L; pH=3.0.

Zero-valent aluminum-activated persulfate oxidation processes

Percent relative inhibition values of original IPR and ZVA/PS (PS=1.50 mM; pH=3.0) treated samples after 40 min and 120 min on *V. fischeri* and *P. subcapitata* were examined. The original IPR (2 mg/L) and ZVA/PS (PS=1.50 mM; pH=3.0) treated samples (after 40 min and 120 min treatment) had no inhibitory effect on *V. fischeri*. The percent relative inhibition value of original IPR samples on *P. subcapitata* was obtained as <10%; however, the inhibition did not change significantly for IPR's ZVA/PS treated samples after 40 min and 120 min treatment and remained less than 10%. This can be explained by considering IPR hydrolysis at alkaline pH such that hydrolysis half-life of IPR at pH of 9.0 is reported only 27 min (Stacy and Latin, 2020). Hence, a rapid IPR hydrolysis can be expected at pH of 8.1 adjusted for original IPR (untreated) and its ZVA/PS treated samples before

conducting *P. subcapitata* test. The treatability study of IPR by ZVA/PS in SWW (previous section) resulted in poor IPR removal and its mineralization, supports the acute toxicity finding in that unreacted IPR and its hydrolyzed forms, do not caused any inhibitor effect during 120 min ZVA/PS treatment.

4.4.2 Genotoxicity

It is well known that pollutant removal is not enough evidence to test the efficiency of certain applied treatment and in some cases, AOPs can transform the initial pollutant into more dangerous contaminants (Giraldo et al, 2010). In the case of halogenated organic molecules that could be degraded into hazardous compounds such as mono-, di- or trichloromethane and chlorobenzenes, which are known to be high carcinogenic molecules (Lopez-Alvarez et al, 2016). Mutagenicity was evaluated by Ames test (*S. typhimurium* TA 1535) of original and treated samples of each industrial micropollutant. Table 4.9 presents test number (Nr) of samples and initial reaction conditions of selected treatments for genetoxicity test in DW.

Table 4.9 : Test Nr. and initial reaction conditions of selected treatment-processes for genotoxicity test in DW.

Test Nr.	Treatment	Reaction conditions and treatment time
1	-	Original 3,5-DCP=2 mg/L
2	ZVI/PS	3,5-DCP=2 mg/L; PS=0.50 mM; pH=3.0; t=120 min
3	UV-C/PS	3,5-DCP=2 mg/L; PS=0.03 mM; pH=6.3; t=120 min
4	-	Original 2,4-DCA=2 mg/L
5	UV-C/PS	2,4-DCA=2 mg/L; PS=0.10 mM; pH=6.0; t=120 min
6	ZVI/PS	2,4-DCA=2 mg/L; PS=0.50 mM; pH=5.0; t=120 min
7	-	Original IPR=2 mg/L
8	UV-C/PS	IPR=2 mg/L; PS=0.03 mM; pH=6.2; t=120 min
9	ZVA/PS	IPR=2 mg/L; PS=0.50 mM; pH=3.0; t=120 min

Figure 4.39 presents Ames test plates after 48 h incubation and the number of colonies which have been formed on each plate for the original and treated samples of each model industrial micropollutant under above mentioned reaction conditions as well as their standard deviations (SD). As it can be seen in Figure 4.39 neither original model micropollutants nor treated samples after 120 min, had genotoxic activity according to the Ames test results. As mentioned before, *S. typhimurium* TA 1535 strain is mutant for the biosynthesis of histidine thereby it is unable to grow and form colonies in a medium lacking histidine. When these mutant bacterial cells treated with chemicals, which are mutagenic causes a reversal of mutation in bacterial cells, which enables bacteria to grow on a media lacking in histidine (Zhao et al, 2010b). Therefore, more potency of a chemical leads to more number of cells forming colonies on agar media. Due to the limited number of colonies (maximum 17) are formed on each samples plates, as seen also in Table 4.10, it can be concluded that neither origin model micropollutants nor treated samples were genotoxic.

Results of Ames mutagenicity of 3,5-DCP revealed that original 3,5-DCP, UV-C/PS-treated and ZVI/PS-treated samples were not mutagenic. This is supported by genotoxicity data that suggest that the CPs are not directly mutagenic (Jeffrey and Koplan, 1999). Limited information are available about mutagenicity of dichlorophenols. One of isomer of 3,5-DCP namely 2,4-dichlorphenol was mostly negative for mutagenic activity in *S. typhimurium* assays (Haworth et al, 1983; Jeffrey and Koplan, 1999; Probst et al, 1981). Obtained results from Ames mutagenicity of 2,4-DCA showed that the original 2,4-DCA, UV-C/PS-treated and ZVI/PS-treated samples were not mutagenic. A variety of in vitro genotoxicity tests including *S. typhimurium* test indicate that CAs are possibly genotoxic, although results are sometimes conflicting (Koenig et al, 2018). For example, it has been reported that CAs are mutagenic in the Ames assay in *S. typhimurium* strain TA98 with S9 metabolic activation (Boehncke et al, 2003). Due to lack of data, it is impossible to make any conclusion about 2,4-DCA's in vivo genotoxicity.
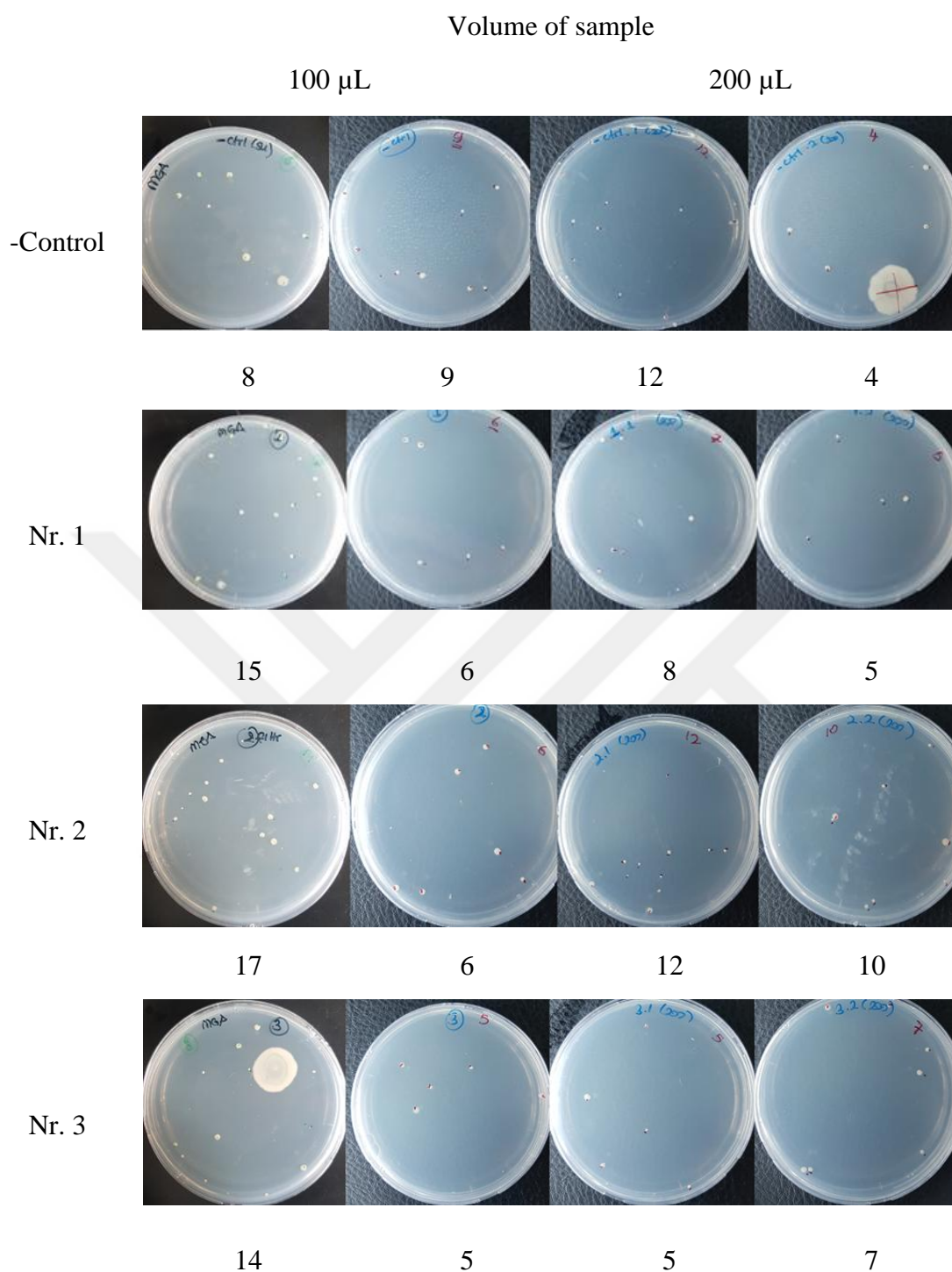
Figure 4.39 : Ames test plates after 48 h incubation. Test numbers are indicated next to the plate lines and the numbers of colonies are given below of each plate. Initial reaction conditions of each test are presented in Table 4.9.
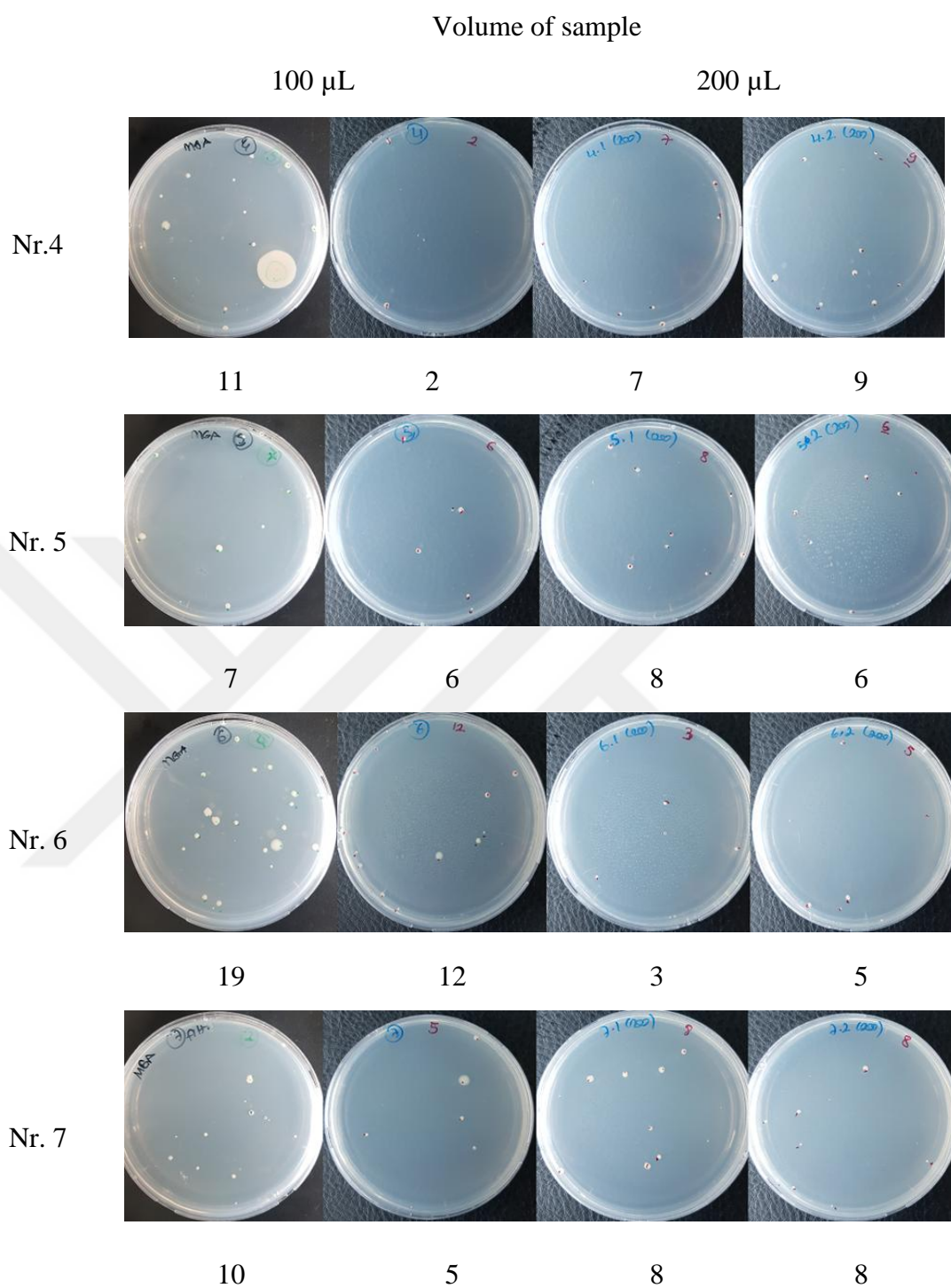
Figure 4.39 (continued) : Ames test plates after 48 h incubation. Test numbers are indicated next to the plate lines and the numbers of colonies are given below of each plate.

Volume of sample

100 µL		200 µL	

Nr.8

8 5 8 6

Nr. 9

8 10 9 6

+Control

>300 >300 >300 >300
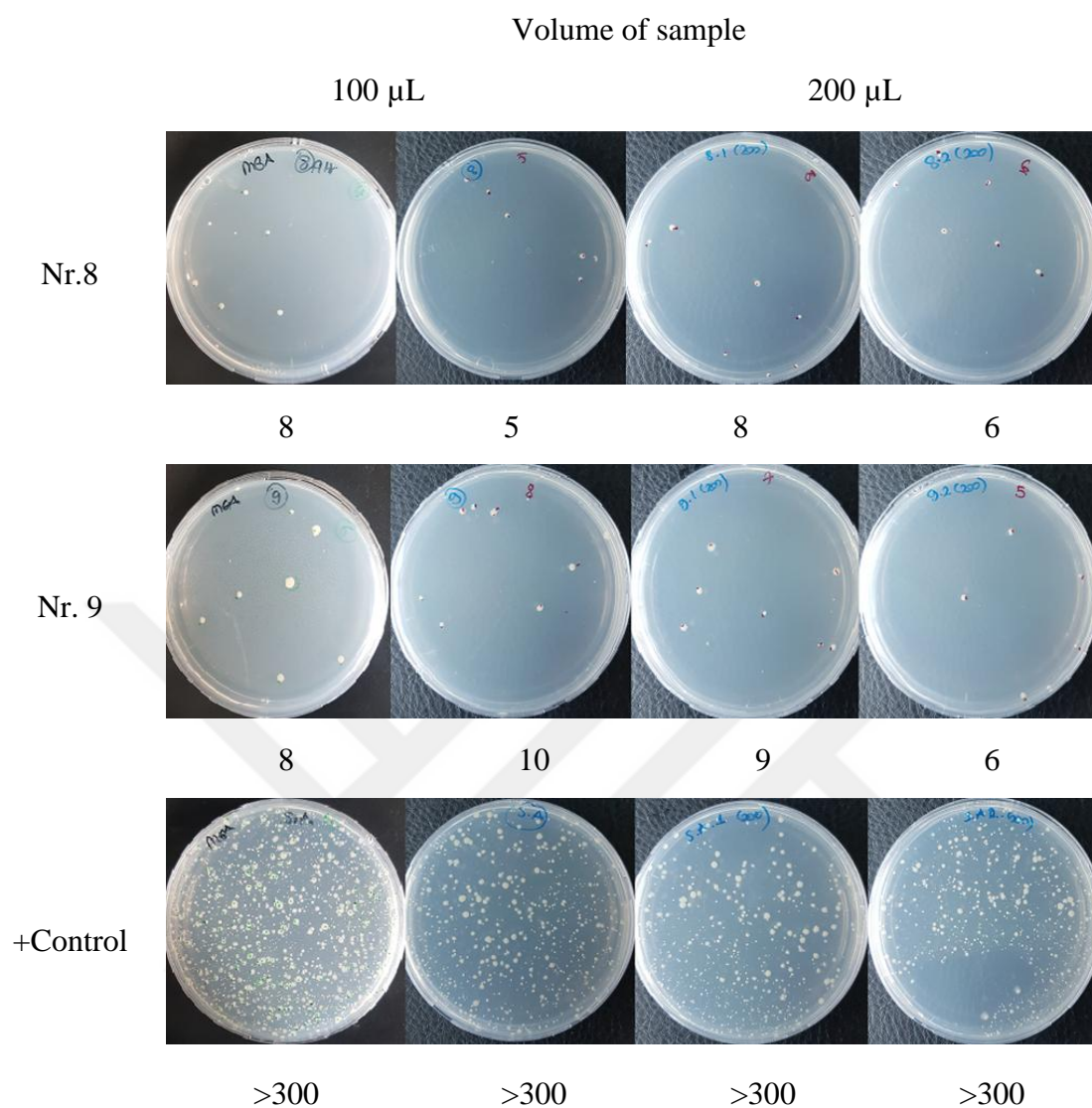
Figure 4.39 (continued) : Ames test plates after 48 h incubation. Test numbers are indicated next to the plate lines and the numbers of colonies are given below of each plate

.

Results of the Ames mutagenicity test indicated that the original IPR, UV-C/PS-treated and ZVA/PS-treated samples were not mutagenic. While original IPR was also reported to be non-mutagenic in the related scientific literatures (US EPA, 1998), its photodegradation products were estimated potentially mutagenic due to presence of hydroxyl groups on their aromatic rings (Lassalle et al, 2014).

Table 4.10 : Colony numbers and means of controls and samples.

Sample	100 µg/L				200 µg/L			
	Colony		Mean	S.D	Colony		Mean	S.D
-Control	8	9	8.5	0.5	12	4	8	4
Nr. 1	15	6	10.5	4.5	8	5	6.5	1.5
Nr. 2	17	6	11.5	5.5	12	10	11	1
Nr. 3	14	5	9.5	4.5	5	7	6	1
Nr. 4	11	2	6.5	4.5	7	9	8	1
Nr. 5	7	6	6.5	0.5	8	6	7	1
Nr. 6	19	12	15.5	3.5	3	5	4	1
Nr. 7	10	5	7.5	2.5	8	8	8	0
Nr. 8	8	5	6.5	1.5	8	6	7	1
Nr. 9	8	19	9	1	9	6	7.5	1.5
+Control	>300	>300	>300	-	>300	>300	>300	-

4.5 Degradation Products and Proposed Pathways

4.5.1 3,5-Dichlorophenol

4.5.1.1 Ultraviolet-C and Ultraviolet-C-activated persulfate oxidation processes

Generally speaking the degradation pathway of CPs through the better-known $HO^\bullet$-based AOPs involves C-Cl bond scission and subsequent $HO^\bullet$ attack at chlorine positions corresponding to the formation of dechlorinated and hydroxylated degradation products (Gomez et al, 2010; Karci et al, 2012). Similarly, the electron transfer and hydrogen abstraction are assumed to be the first step of CPs oxidation with $SO_4^{\bullet-}$. A $SO_4^{\bullet-}$-mediated attack on an aromatic ring leads to the formation of C-centered radicals via electron transfer from the organic compound. Thereafter, the C-centered radicals lead to the formation of aromatic hydroxylated intermediates such as hydroquinone, p-benzoquinone, catechol and phenol (Apak and Hugül, 1996; Czaplicka, 2004; Czaplicka, 2006). In the case of chloro-organics, chlorine atoms of benzene ring are released during the early stages of oxidation. Figure 4.40 displays changes in 3,5-DCP and DOC (a), hydroquinone (b) and Cl^- (c) concentrations during UV-C (pH=6.3) and UV-C/PS (PS=0.30 mM PS; pH=6.3) treatments of 10 mg/L 3,5-DCP in DW. As illustrated in Figure 4.40, the chlorine atoms of the aromatic ring were removed at the first stages of degradation. Among the above-mentioned hydroxylated intermediates that are expected during $SO_4^{\bullet-}$-mediated degradation of CPs, in the present study, only hydroquinone could be detected and quantified in the reaction solution during UV-C/PS treatment. As is evident from Figure 4.40 (b), hydroquinone was formed after 2 min UV-C/PS treatment, reaching its highest concentration of 0.24 mg/L after 5 min and disappeared after 15 min treatment. Previous related work also reported the oxidative cleavage of CPs led to aromatic and ultimately aliphatic carboxylic acids as the final organic degradation products of CPs (Abe and Tanaka, 1997; Androulaki et al, 2000). Considering previous related work, it was aimed at quantifying phthalic acid, lactic acid, acetic acid and eventually formic acid during UV-C/PS treatment of aqueous 3,5-DCP.
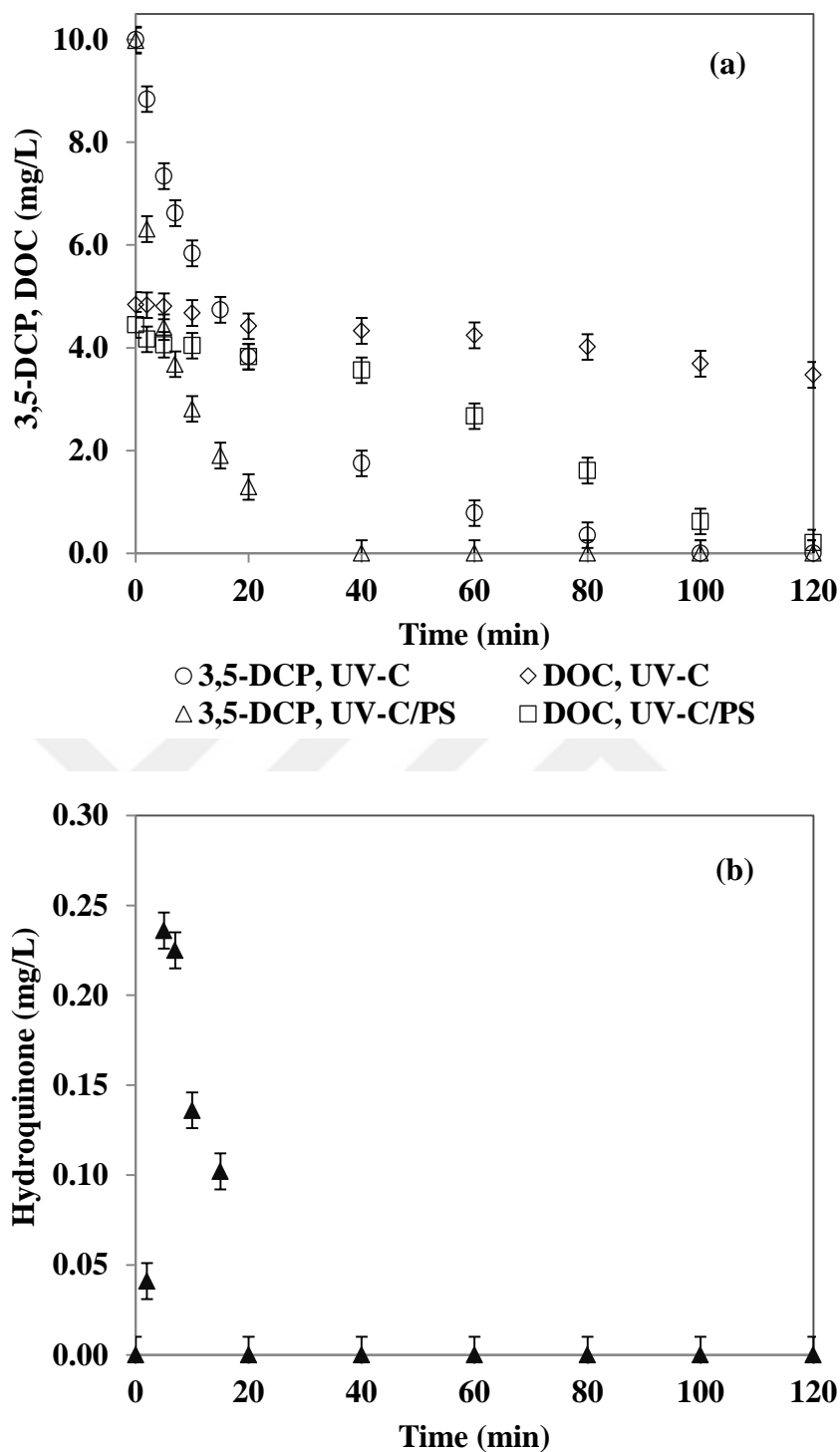
Figure 4.40 : Changes in 3,5-DCP and DOC (a), hydroquinone (b) and Cl⁻ (c) concentrations during UV-C and UV-C/PS treatments. Hydroquinone formation was observed only during UV-C/PS treatment. The theoretically expected maximum Cl⁻ concentration after full oxidation of 3,5-DCP is 4.35 mg/L. 3,5-DCP=10 mg/L; PS=0.30 mM; UV-C intensity=0.5 W/L; pH=6.3.
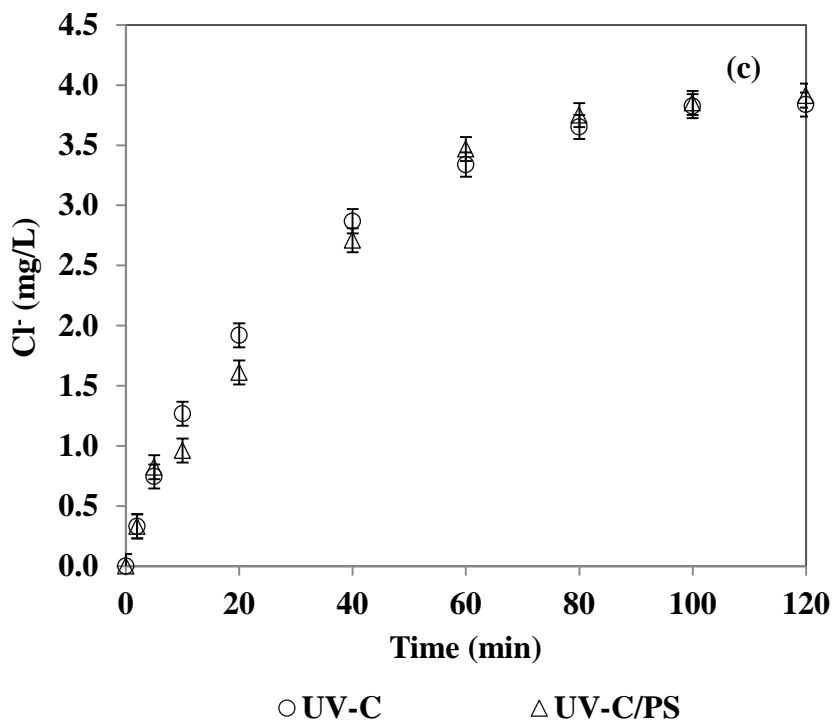
Figure 4.40 (continued) : Changes in 3,5-DCP and DOC (a), hydroquinone (b) and Cl⁻ (c) concentrations during UV-C and UV-C/PS treatments. Hydroquinone formation was observed only during UV-C/PS treatment. The theoretically expected maximum Cl⁻ concentration after full oxidation of 3,5-DCP is 4.35 mg/L. 3,5-DCP=10 mg/L; PS=0.30 mM; UV-C intensity=0.5 W/L; pH=6.3.

However, none of the above-mentioned acidic degradation products could be detected under the studied reaction conditions. On the other hand, oxidation of 3,5-DCP was accompanied by a rapid pH drop (data not shown) from 6.3 to 3.4 within the first 10 min of UV-C/PS treatment most probably due to formation of acidic oxidation intermediates (Olmez-Hanci et al, 2011) and beyond 10 min treatment no appreciable change in pH was observed. It might be concluded that during UV-C/PS treatment of aqueous 3,5-DCP first hydroxylation and dechlorination followed by fragmentation into relatively smaller, acidic degradation products occurred prior to ultimate oxidation (mineralization) to inorganics (Olmez-Hanci et al, 2011).

On the basis of detailed analysis of degradation intermediates, it might be proposed that the oxidation starts at the aromatic hydroxylation involving $HO^{\bullet}$ generated in the solution from $SO_4^{\bullet-}$ reaction with water through equations 2.8 and 2.9. The pathways of CPs degradation by $HO^{\bullet}$ were proposed in previous works (Cravotto et al, 2010; Kucharska and Naumczyk, 2009; Zhou et al, 2008) in which CPs degrade primarily chlororesorcinol, chlorocatechols and/or chlorinated benzenetriols with the

134

subsequent formation of various ring-opened products (several possible aliphatic by-products of CPs degradation such as maleic acid, fumaric acid, malonic acid, oxalic acid, acetic acid and formic acid). On the other hand, HO$^{\bullet}$ can also attack onto the C atom being occupied by the ─Cl group and substitute chlorine, resulting in Cl^{-} release (Karci, 2014). In fact generation of hydroquinone and catechol being originated from the HO$^{\bullet}$-mediated transformation of mono-CPs such as 2-CP, has been ascribed to this mechanistic pathway (Bertelli and Selli, 2006). Figure 4.41 depicts 3,5-DCP degradation pathway during UV-C and UV-C/PS. Dechlorination of 3,5-DCP followed by formation of hydroquinone and catechol can be proposed as a possible degradation pathway (Figure 4.41) which was also reported in former studies (Basu and Wei, 1998; Ghaly et al, 2001; Kang et al, 2002; Karci et al, 2012). Based on the results obtained by the UV-C and UV-C/PS treatment of 3,5-DCP a probable reaction mechanism can be assumed. The proposed degradation pathway (Figure 4.41) can involve SO$_4^{\bullet-}$ and/or HO$^{\bullet}$ attack on aromatic rings leads to phenol formation through dechlorination (pathway Nr. 1) and/or formation of chlorinated 1,4-hydroquinone (pathway Nr. 2). The formed phenol can undergo hydroxylation to form hydroquinone and/or catechol (pathways Nrs. 3 and 4). The pathways of CPs degradation by HO$^{\bullet}$ were proposed in previous works (Cravotto et al, 2010; Kucharska and Naumczyk, 2009; Zhou et al, 2008) in which CPs degrade primarily chlororesorcinol, chlorocatechols and/or chlorinated benzenetriols with the subsequent formation of various ring-opened products (several possible aliphatic by-products of CPs degradation such as maleic acid, fumaric acid, malonic acid, oxalic acid, acetic acid and formic acid). On the other hand, HO$^{\bullet}$ can also attack onto the C atom being occupied by the ─Cl group and substitute chlorine, resulting in Cl^{-} release (Karci, 2014). In fact generation of hydroquinone and catechol being originated from the HO$^{\bullet}$-mediated transformation of mono-CPs such as 2-CP, has been ascribed to this mechanistic pathway (Bertelli and Selli, 2006). Figure 4.41 depicts 3,5-DCP degradation pathway during UV-C and UV-C/PS. Dechlorination of 3,5-DCP followed by formation of hydroquinone and catechol can be proposed as a possible degradation pathway (Figure 4.41) which was also reported in former studies (Basu and Wei, 1998; Ghaly et al, 2001; Kang et al, 2002; Karci et al, 2012).

Figure 4.41 : Proposed reaction pathway for 3,5-DCP by UV-C and UV-C/PS treatment.

4.5.1.2 Zero-valent iron-activated persulfate oxidation processes

As mentioned above, ZVI appeared to be promising activators of PS through generating $SO_4^{\bullet-}$ (equations 2.2-5) which degrade contaminants more effectively than conventional activators such as ferrous ion (Li et al, 2014a). Recently, several researchers have used ZVI to activate PS to control the rate of $SO_4^{\bullet-}$ formation, therefore, enhancing the reaction efficiency (Li et al, 2014b; Li et al, 2017; Zhou et al, 2016). Generally, three main mechanisms have been proposed for the first step of $SO_4^{\bullet-}$ attack of aromatic compounds including radical adduct formation, hydrogen atom abstraction and single electron transfer (Luo et al, 2017). As mentioned previously, $SO_4^{\bullet-}$ attack on the aromatic ring leads to the formation of C-centered radicals via electron transfer from the organic compound and then the formed C-centered radicals lead to the formation of aforementioned aromatic hydroxylated intermediates (Olmez-Hanci and Arslan-Alaton, 2013). These aromatic intermediates may undergo subsequent ring cleavage reactions to yield carboxylic acids.

Dechlorination as a possible parallel pathway can proceed during chlorinated compounds degradation; however, due to high formed sulfate ions concentration during 3,5-DCP degradation by ZVI/PS, it was not possible to measure Cl⁻ released by IC. In order to investigate the degradation pathway of 3,5-DCP through ZVI/PS treatment, HPLC analysis were conducted to identify and monitor the evolved intermediates. Among aromatic hydroxylated intermediates (hydroquinone, benzoquinone, catechol, phenol and 4-CP) which were expected as 3,5-DCP degradation products, only hydroquinone could be identified through ZVI/PS treatment of 3,5-DCP. Figure 4.42 displays changes in 3,5-DCP and DOC (a), hydroquinone (b) and acetic acid (c) concentrations during ZVI/PS (PS=2.50 mM) treatment of 10 mg/L 3,5-DCP in DW at initial solution pH of 3.0. As illustrated in Figure 4.42 (b), hydroquinone as the only detected intermediate was formed after 10 min ZVI/PS treatment, reaching its highest concentration of 0.99 mg/L after 20 min and disappeared after 40 min treatment. Previous related works also reported the formation of hydroquinones through heterogeneous catalytic treatment of CPs with PS or PMS (Tian et al, 2019; Zhou et al, 2018). Tian et al. (2019) studied possible evolved intermediates during 2,4-DCP degradation through PMS activation over Mn_2O_3. They reported formation of chlorinated hydroquinones and chlorinated catechols as the result of substitution of chlorine atom by $HO^\bullet$ (Tian et al, 2019).

Acetic acid formation was evidenced as one of the major organic acid being formed as a result of subsequent ring-opening of the hydroxylated degradation products. The acetic acid concentration reached 19.6 mg/L after 10 min ZVI/PS treatment corresponding to complete 3,5-DCP removal and then increased to its highest concentration 42.0 mg/L after 20 min. Acetic acid concentration decreased dramatically to steady concentration of 2.3 mg/L after 40 min treatment.
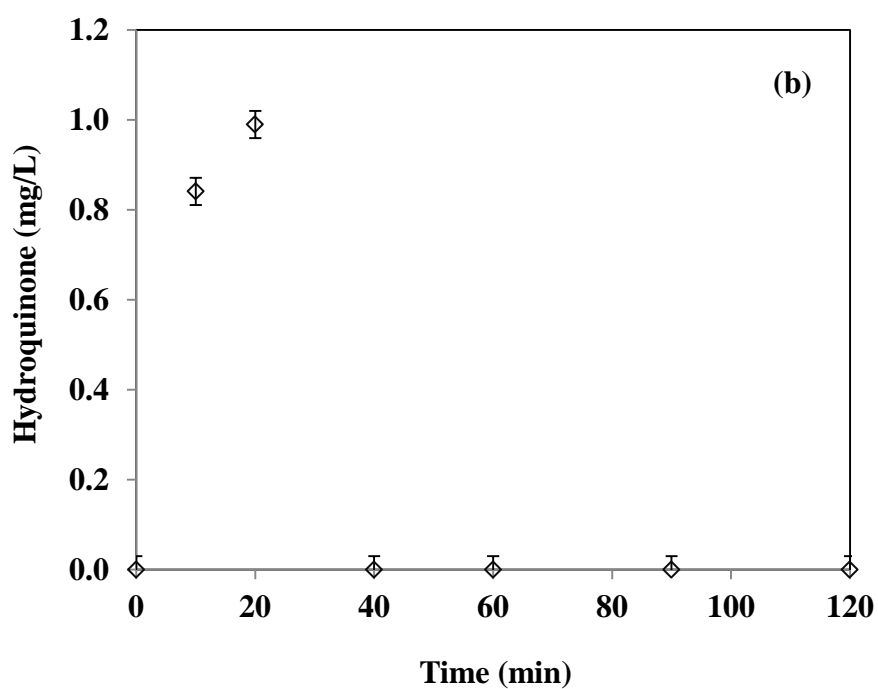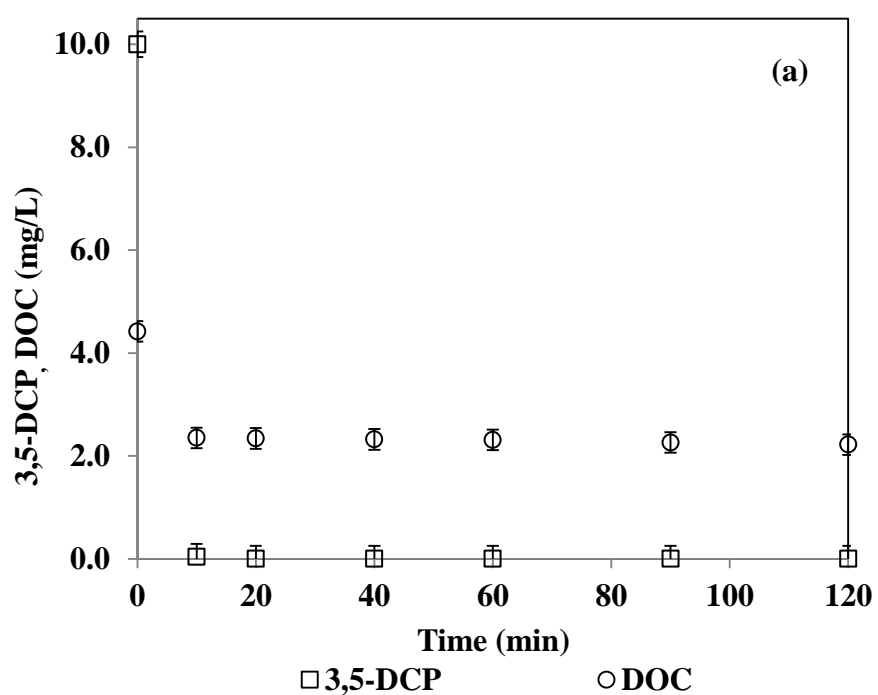
Figure 4.42 : Changes in 3,5-DCP and DOC (a), hydroquinone (b) and acetic acid (c) concentrations during ZVI/PS treatment. 3,5-DCP=10 mg/L; PS=2.50 mM; ZVI=1 g/L; pH=3.0.

138
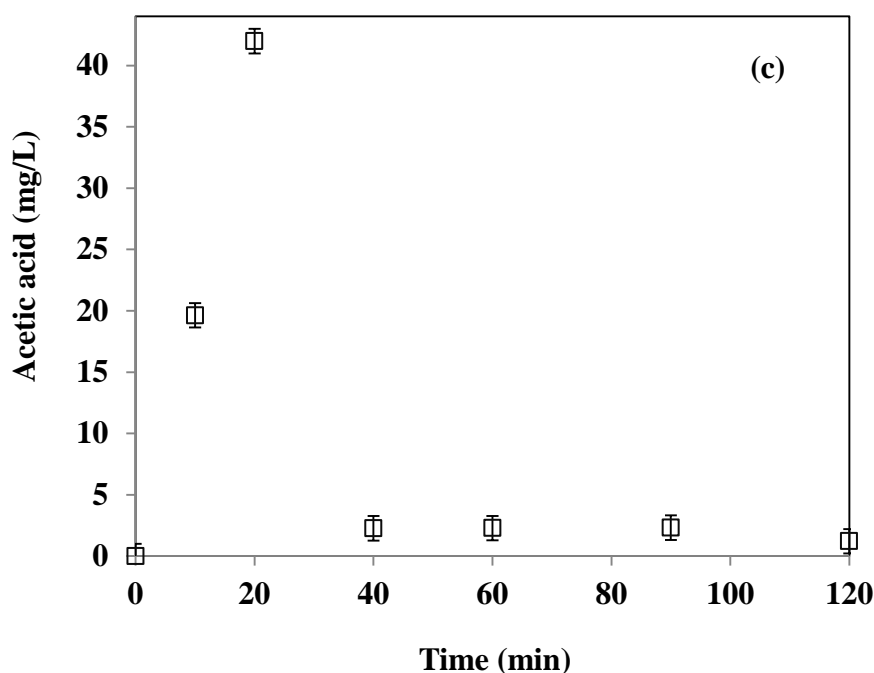
Figure 4.42 (continued) : Changes in 3,5-DCP and DOC (a), hydroquinone (b) and acetic acid (c) concentrations during ZVI/PS treatment. 3,5-DCP=10 mg/L; PS=2.50 mM; ZVI=1 g/L; pH=3.0.

The possible reaction mechanism for 3,5-DCP via ZVI/PS is proposed in Figure 4.43. Two possible pathways can occur during ZVI/PS treatment of 3,5-DCP. The first possible 3,5-DCP degradation pathway involves $SO_4^{\bullet-}$ or $HO^{\bullet}$ attacking the chlorines positions to produce phenol via dechlorination (pathway Nr. 1). Then the produced phenol can generate hydroxylated intermediates such as hydroquinones and catechol (pathway Nrs. 2 and 3). Further oxidation of these intermediates leads to C-C bond cleavage and ultimately formation of carboxylic acid. The second possible 3,5-DCP degradation pathway can be hydroxylation mechanism (pathway Nr. 4) in which several aromatic intermediates such as chlororesorcinols and chlorocetchols which would be degraded to chlorobenzoquinones as an aromatic compound and then organic acids including acetic acid (Ghorbanian et al, 2019). Formation of chlorobenzoquinones was also reported in a former related study (Zhou et al, 2011) where catalytic oxidation reaction of 3,5-DCP with H_2O_2 and Cu-Al hydrotalcite/clay composite has been investigated. In that study, 2,6-dichloro-1,4-benzoquinone was formed as the first step of 3,5-DCPoxidation by $HO^{\bullet}$ (Zhou et al, 2011). Quinone intermediates, serving as electron shuttles, could play an important catalytic role in the oxidation of aromatic compounds (Zhou et al, 2011). In a word, after chlorinated

139

quinones formed, the oxidation of CPs would be easier. Moreover, Leyva et al. (2003) also showed that at short reaction times, 4-CP was selectively oxidized to 1,4-benzoquinone and 2-CP to 2-chloro-1,4-benzoquinone by $HO^\bullet$ (Leyva et al, 2003). As the final stage quinone-related intermediates were further oxidized to smaller molecules after the aromatic ring was broken, and finally mineralized to carbon dioxide.

Zhou et al. (2018) studied identification of possible evolved intermediates of 2,4-DCP degradation during copper activation of PS and PMS. In that work various intermediates were identified including hydroquinone and chlorinated hydroquinone as a result of $SO_4^{\bullet-}$ or $HO^\bullet$ attack chlorobenzoquinone, 4-benzoquinone, 2-CP, phenol, catechol, resorcinol, and some aliphatic carboxylic acids, such as maleic acid and fumaric acid (Zhou et al, 2018).

Figure 4.43 : Proposed reaction pathway for 3,5-DCP by ZVI/PS treatment.

4.5.2 2,4-Dichloroaniline

4.5.2.1 Ultraviolet-C and Ultraviolet-C-activated persulfate oxidation processes

Generally, the first step in $SO_4^{\bullet-}$ oxidation of aromatic compounds is either electron transfer; hydrogen abstraction; or radical adduct formation (Luo et al, 2017). There are several studies proposing that the main reaction between aromatic compounds and $SO_4^{\bullet-}$ takes place by an initial electron transfer from the aromatic ring to $SO_4^{\bullet-}$ (Neta et al, 1977; O'Neill et al, 1975). Aromatic compounds containing electron

donating groups, such as $-NH_2$, $-NH$, $-OH$, $-O-$, $-O\text{-}CH_3$, and $-O\text{-}$, single electron transfer pathway could be a dominant reaction route and thermodynamically favorable (Luo et al, 2017). Besides an electron transfer mechanism, $SO_4^{\bullet-}$ can react with organic compounds through radical adduct formation and hydrogen atom abstraction. At the early stage of $SO_4^{\bullet-}$ reaction with aromatic compounds, short-lived $SO_4^{\bullet-}$ adducts can be formed as a result of $SO_4^{\bullet-}$ attack to the aromatic ring (Anipsitakis et al, 2006). Formation of C-centered radical as a result of electron transfer from the organic compound to $SO_4^{\bullet-}$ is also likely which leads to SO_4^{2-} release (Luo et al, 2017). Dioxygen radical adducts formation can also be possible via oxygen addition to the C-centered radicals or β-scission leading to the hydroxylated degradation products formation such as hydroquinones and catechols (Sharma et al, 2015). Hydroxylation may active the aromatic ring due to the elevated electron density derived from electron donating group ($-OH$), which favor further attack by electron species (Li et al, 2018). In this study, formation of evolved intermediates during UV-C and UV-C/PS treatment of 2,4-DCA was investigated by LC analysis. According to the analytical results, among expected aromatic degradation products such as hydroquinone, benzoquinone, catechol, phenol, aniline and nitrobenzene, only aniline was qualified during UV-C and UV-C/PS treatments of 2,4-DCA that could be formed via C-Cl bond cleavage (Hussain et al, 2012; Liang et al, 2013; Yuan et al, 2015). During UV-C and UV-C/PS treatments, some complex intermediate products were developed causing a change in the color of 2,4-DCA solution. The possible intermediate products could be *p*-benzoquinone, nitrosobenzene and nitrobenzene (Hussain et al, 2014) and then likely were consumed by reactions with $SO_4^{\bullet-}$ and/or $HO^{\bullet}$ and were transformed to other products. Acetic acid formation was monitor during both UV-C and UV-C/PS treatments; however, it was only qualified after 40 min UV-C/PS treatment. Low constant concentration of acetic acid and almost 93% DOC removal were observed after 120 min UV-C/PS treatment.

Cl^- was identified as one of the inorganic products during UV-C and UV-C/PS treatment of 2,4-DCA. As it can be seen from Figure 4.44 (a) and (d), during UV-C treatment, Cl^- concentration linearly increased for the first 20 min and remained constant until the end of the reaction (120 min) suggesting the formation of stable compounds being resistant to further oxidation. During UV-C/PS treatment

dechlorination proceeded for the first 20 min corresponding to 73% 2,4-DCA removal. After this point, the Cl⁻ concentration increased with a slow rate reaching to 3.8 mg/L at the end of the reaction.

The solution pH during the UV-C and UV-C/PS treatments was monitored. Generally, a drop of pH was observed for UV-C and UV-C/PS reaching to 4.4 and 3.2, respectively. Solution pH drop during UV-C/PS can be attributed to the generation of low molecular-weight organic acids in UV-C/PS oxidation processes such as carboxylic and formic acids as the end products during 2,4-DCA degradation (Chu et al, 2007).
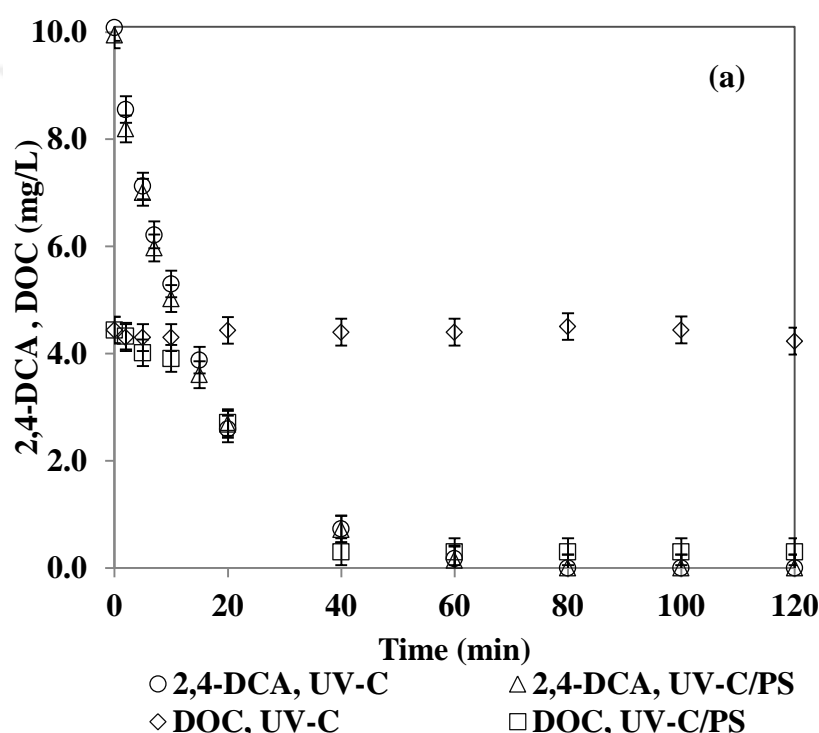
Figure 4.44 : Changes in 2,4-DCA and DOC (a), aniline (b), acetic acid (c) and Cl⁻ (d) concentrations during UV-C and UV-C/PS treatments. Acetic acid formation was observed only during UV-C/PS treatment. The theoretically expected maximum Cl⁻ concentration after full oxidation of 2,4-DCA is 4.38 mg/L. 2,4-DCA=10 mg/L; PS=0.30 mM; UV-C intensity=0.5 W/L; pH=6.0. Initial PS concentration to measure DOC removal, Cl⁻ release and acetic acid concentration was 1.00 mM.

Figure 4.44 (continued) : Changes in 2,4-DCA and DOC (a), aniline (b), acetic acid (c) and Cl⁻ (d) concentrations during UV-C and UV-C/PS treatments. Acetic acid formation was observed only during UV-C/PS treatment. The theoretically expected maximum Cl⁻ concentration after full oxidation of 2,4-DCA is 4.38 mg/L. 2,4-DCA=10 mg/L; PS=0.30 mM; UV-C intensity=0.5 W/L; pH=6.0. Initial PS concentration to measure DOC removal, Cl⁻ release and acetic acid concentration was 1.00 mM.

Figure 4.44 (continued) : Changes in 2,4-DCA and DOC (a), aniline (b), acetic acid (c) and Cl⁻ (d) concentrations during UV-C and UV-C/PS treatments. Acetic acid formation was observed only during UV-C/PS treatment. The theoretically expected maximum Cl⁻ concentration after full oxidation of 2,4-DCA is 4.38 mg/L. 2,4-DCA=10 mg/L; PS=0.30 mM; UV-C intensity=0.5 W/L; pH=6.0. Initial PS concentration to measure DOC removal, Cl⁻ release and acetic acid concentration was 1.00 mM.

Based on the results obtained by the UV-C and UV-C/PS treatment of 2,4-DCA a probable reaction mechanism can be assumed. The proposed degradation pathway (Figure 4.45) can involve $SO_4^{\bullet-}$ and/or $HO^{\bullet}$ attack on 2,4-DCA leading to 2-CA and 4-CA formation (pathway Nrs. 1 and 2). Further oxidation of the formed 2-CA can result aniline formation (pathway Nr. 3); one of the main intermediates of 2-CA oxidation as Winarno and Getoff (2002) reported. In that work photocatalytic degradation products of 2-CA was investigated in aqueous solution under various conditions (such as presence of oxygen, air and N_2O) and in addition to the aniline, phenol, 2-CP and a mixture of simple carboxylic acids have been identified (Winarno and Getoff, 2002b). Four degradation pathways can be assumed for 4-CA. The first degradation pathway of formed 4-CA can involve $SO_4^{\bullet-}$ and/or $HO^{\bullet}$ attack on 4-CA which leads to formation of 4-CP and replacement of amino group (pathway Nr. 4) (Nitoi et al, 2015).The second degradation pathway of the formed 4-CA can

144

encompass hydrogen abstraction mechanism with anilinyl-radical formation that is subsequently stabilized by dimerization to form dimeric intermediates products (pathway Nrs. 5 and 6) such as dichloroazobenzene as was reported in previous studies (Kumar and Mathur, 2006; Nitoi et al, 2015). Further $SO_4^{\bullet-}$ and/or $HO^{\bullet}$ attack on dichloroazobenzene leads to chloronitrobenzene (pathway Nr. 7) which is further oxidized to 4-CP (pathway Nr. 8) (Ishikawa et al, 1989). The third degradation pathway of the formed 4-CA is dechlorination which leads to aniline formation as was reported in previous studies (pathway Nr. 9) (Hussain et al, 2018; Nitoi et al, 2015; Santaballa and Vulliet, 2005) and then is oxidized to 4-aminophenol via $HO^{\bullet}$ attack on aromatic ring (pathway Nr. 10). The forth pathway of the formed 4-CA can be its photolysis to 4-aminophenol (pathway Nr. 11). These hydroxylated degradation intermediates (4-CP and 4-aminiphenol) can be oxidized to form benzoquinones (pathway Nr. 12) and carboxylic acids as reported in former studies (Bandara et al, 2001; Hussain et al, 2014; Hussain et al, 2018).
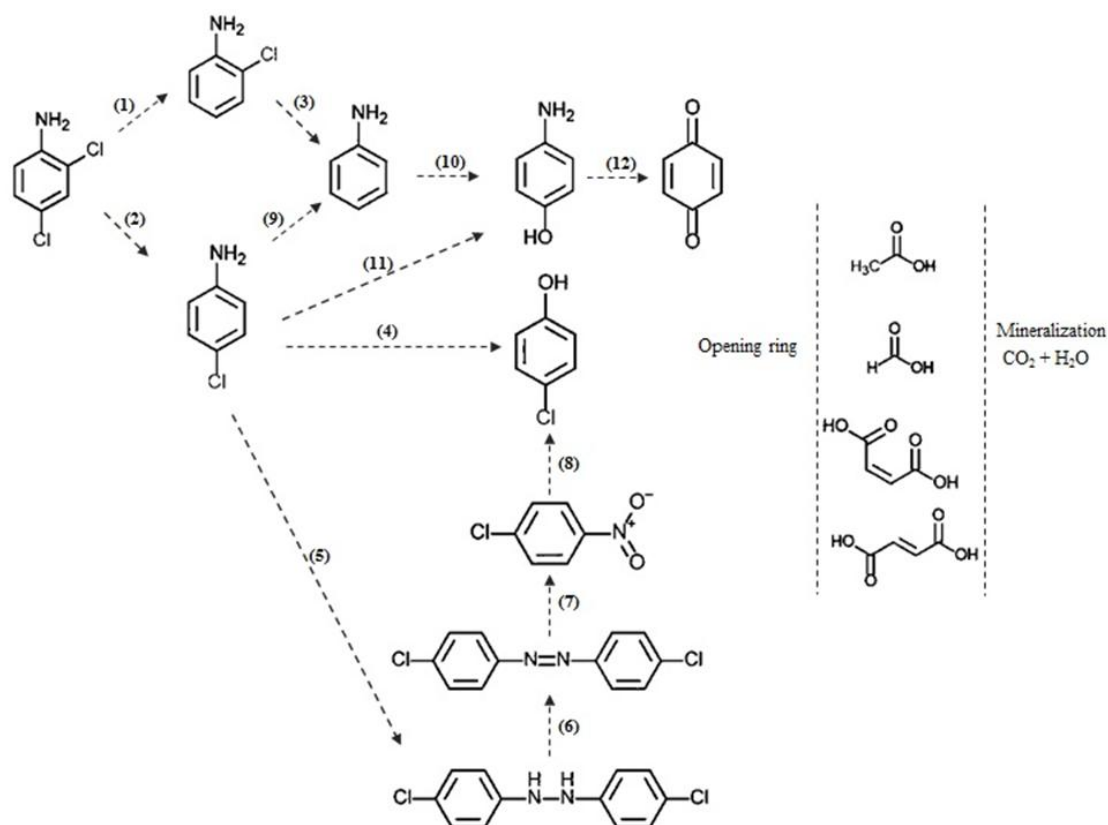
Figure 4.45 : Proposed reaction pathway for 2,4-DCA by UV-C and UV-C/PS treatment.

4.5.2.2 Zero-valent iron-activated persulfate oxidation processes

As mentioned above, ZVI activation of PS is a relatively cost-effective and efficient method in comparison to the other activation methods and therefore has received considerable attention in the PS-driven oxidation of contaminants (Hussain et al, 2012; Xiong et al, 2014). ZVI serves as a slow-releasing source of ferrous and the mechanism of heterogeneous ZVI treatment in the presence of PS involves direct electron transfer from the ZVI or surface-bound ferrous to PS, continuing with a homogenous Fenton-like redox reaction that involves $SO_4^{\bullet-}$ production in the reaction bulk (Hussain et al, 2012). The decomposition of PS in aqueous solution produced $SO_4^{\bullet-}$ and $HO^{\bullet}$ which can oxidize many organic pollutants into carbon dioxide (Dogan et al, 2016; Hussain et al, 2014; Hussain et al, 2012; Liang and Lai, 2008).

Figure 4.46 depicts changes in 2,4-DCA and DOC (a) as well as acetic acid (b) concentrations during ZVI/PS (PS=2.50 mM) treatment of 10 mg/L 2,4-DCA in DW at initial solution pH of 3.0. The degradation of 2,4-DCA was 99% only after 10 min. Dechlorination is expected during 2,4-DCA degradation; however, due to high formed sulfate ions concentration, it was not possible to measure Cl^- released by IC. Formation of aniline and nitrobenzene as two possible intermediates of 2,4-DCA and other hydroxylated intermediates (hydroquinone, benzoquinone, catechol, phenol and 4-CP) was investigated during ZVI/PS treatment; however, none of them was detected by LC analysis. Formation of aniline during CAs treatment by AOPs has been reported in previous works (Hussain et al, 2012; Mailhot et al, 2004; Winarno and Getoff, 2002b).

Dechlorination was observed in work of Liang et al (2013) and Yuan et al. (2015) in which 4-CA degradation in presence of PS as a strong oxidant was investigated by copper oxidate and ferrous sulfide ore particles, respectively. In those studies, 4-CA degradation was associated with the release of organically bound Cl atoms in the form of free Cl^- (Liang et al, 2013; Yuan et al, 2015).
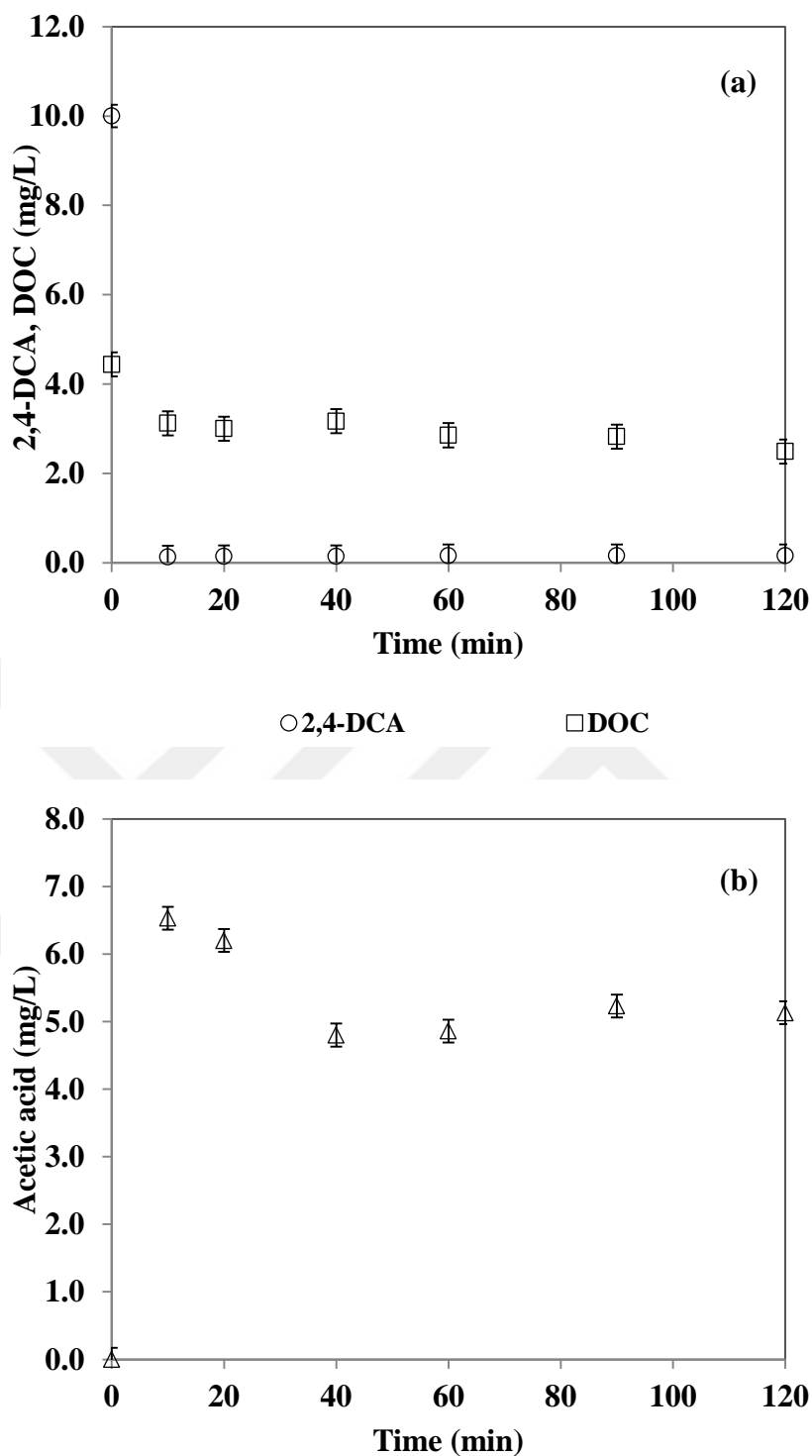
Figure 4.46 : Changes in 2,4-DCA and DOC (a) and acetic acid (b) concentrations during ZVI/PS treatment. 2,4-DCA=10 mg/L; PS=2.50 mM; ZVI=1 g/L; pH=3.0.

There is only limited literature exploring CAs degradation mechanism through AOPs (Hussain et al, 2012; Liang et al, 2013; Mailhot et al, 2004). However, the mechanisms of reactions are complicated, and the effectiveness of the process

depends also on other parameters, such as the place of chlorine atom substitution in the ring and the forms of CAs dependent on the pH value (Kádár et al, 2001).

Generally, in most PS oxidation treatment systems, both $SO_4^{\bullet-}$ and $HO^{\bullet}$ coexist during the PS oxidation and are responsible for the degradation of pollutants (Avetta et al, 2015; Ding et al, 2017; Fang et al, 2013; Yan et al, 2011). For instance, Anipsitakis and Dionysiou (2004) found that both $SO_4^{\bullet-}$ and $HO^{\bullet}$ were the major radical species in ferrous ion activated PS at pH of 2.8 (Anipsitakis and Dionysiou, 2004).

The degradation pathway of 2,4-DCA can be initiated by the attack of $SO_4^{\bullet-}$ and $HO^{\bullet}$ and release of organically bound Cl atoms in the form of free Cl- leading to 2-CA and/or 4-CA (pathway Nrs. 1 and 2) and aniline formation (pathway Nrs. 3 and 4). Further $HO^{\bullet}$ attack on the formed aniline can yield either 4-aminophenol (pathway Nr. 5) and then benzoquinone imine (pathway Nr. 6) or nitrobenzene (pathway Nr. 7). Oxidation of benzoquinone imine can lead to benzoquinone formation (pathway Nr. 8). Further degradation of nitrobenzene, as well as benzoquinone produced low molecular weight acids such as acetic acid (Hussain et al, 2014).
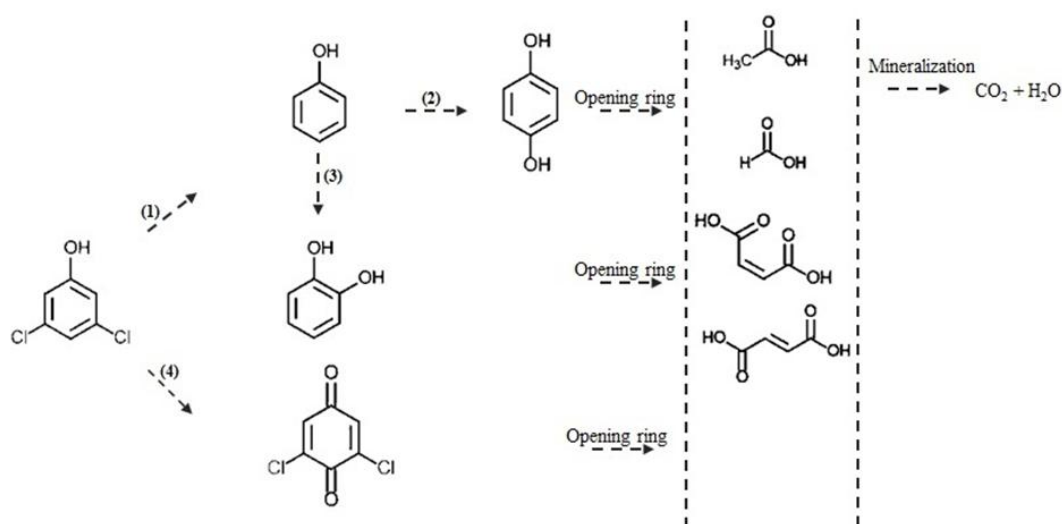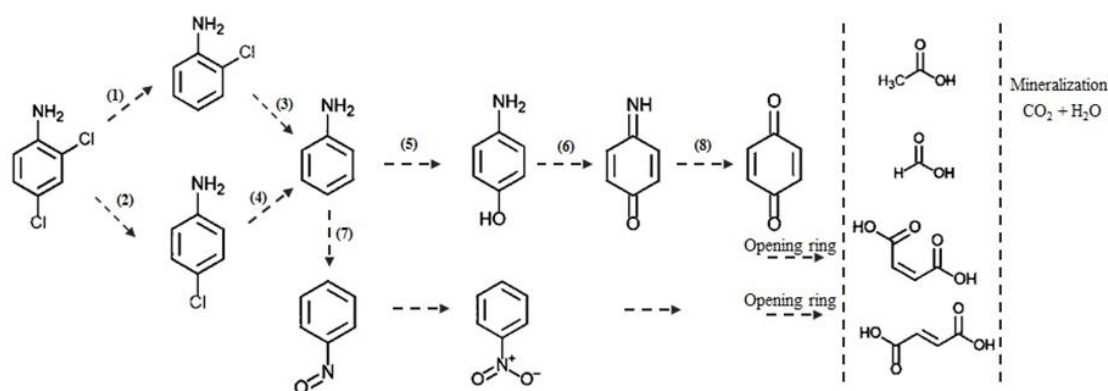

Figure 4.47 : Proposed reaction pathway for 2,4-DCA by ZVI/PS treatment.

4.5.3 Iprodione

4.5.3.1 Ultraviolet-C and Ultraviolet-C-activated persulfate oxidation processes

In previous studies it was demonstrated that $SO_4^{\bullet-}$ and $HO^{\bullet}$ could react with organic micropollutants via direct electron transfer and/or by addition/elimination reactions. Formation of $HO^{\bullet}$ adducts via hydrolysis was evidenced (Antoniou et al, 2010; Chen

et al, 2019; Sharma et al, 2015). Similarly, a $SO_4^{\bullet-}$-mediated attack on an aromatic ring or olefinic double bond can lead to the formation of short-lived $SO_4^{\bullet-}$ adducts. C-centered radical formation via electron transfer from the organic compound to $SO_4^{\bullet-}$ by releasing SO_4^{2-} is also possible due to the electrophilic nature of $SO_4^{\bullet-}$ as expected for $HO^{\bullet}$ (Antoniou et al, 2010; Chen et al, 2019; Sharma et al, 2015). The possibility of hydrogen abstraction cannot be ruled out though the efficiency of hydrogen abstraction from the organic compounds strongly depends on the nature, ring position and hydrogen-bond formation capacity of the substituted phenols (Burton et al, 1985; Thavasi et al, 2009). Oxygen addition to the C-centered radicals or β-scission will result in the formation of dioxygen radical adducts which would further be responsible for the formation of hydroxylated degradation products such as phenol, catechol, hydroquinone or benzoquinone (Sharma et al, 2015). Further oxidation of the hydroxylated byproducts would lead to ring-opening products including short-chain aliphatic acids and ultimately carbon dioxide. The above degradation pathway has generally been reported during degradation of organic pollutants with either $HO^{\bullet}$ or $SO_4^{\bullet-}$-based AOPs (Garcia-Segura et al, 2012; Karci et al, 2012; Skoumal et al, 2008). Acetic, formic, glyoxylic and oxalic acids are typically evidenced as the major organic degradation products of the later oxidation stages and their presence indicates the efficiency of the investigated AOP (Molkenthin et al, 2013). In addition to above mentioned possible degradation products, in the present study, the reaction solution was examined for 2,4-DCA during both UV-C and UV-C/PS treatments since one of DCAs was identified as a degradation product of IPR and appeared concomitantly with the disappearance of this fungicide (Wittke et al, 2001).

As aforementioned, there is only limited information available about the photodegradation products of IPR (Burrows et al, 2002; Lassalle et al, 2014; Schwack and Bourgeois, 1989; Schwack et al, 1995). In the present study, the identification of degradation products during IPR treatment with UV-C and UV-C/PS processes was carried out employing LC analyses and considering the above mentioned degradation pathway of IPR. According to the analytical findings, IPR degradation via UV-C/PS process yielded 2,4-DCA, hydroquinone, acetic and formic acids, while only 2,4-DCA was qualified during UV-C photolysis of IPR. 2,4-DCA that might be formed via C-N bond cleavage. During UV-C photolysis, the 2,4-DCA

149

concentration increased for the first 20 min of the reaction and reached its highest concentration as 0.12 mg/L after 20 min UV-C treatment. At the end of UV-C treatment (120 min), 2,4-DCA was still evidenced in the reaction solution. On the other hand, during UV-C/PS treatment of IPR, the 2,4-DCA concentration increased rapidly to 0.19 mg/L during the first 2 min of the reaction and disappeared after 20 min. From Figure 4.48 (b) and (d), it is apparent that 2,4-DCA formation and degradation profiles were in accord with the Cl$^-$ release data obtained for UV-C and UV-C/PS treatments. Degradation of 2,4-DCA proceeded parallel to dechlorination of IPR. Hydroquinone, acetic and formic acids were only evidenced for UV-C/PS treatment where the former was the most common hydroxylated degradation product being observed through the oxidation of aromatic organics and the latter two were the major organic acids being formed as a result of subsequent ring-opening of the hydroxylated degradation products. During UV-C/PS treatment of IPR, hydroquinone was measured at t=20 min and 60 min as 0.050 mg/L and 0.064 mg/L, respectively, and disappeared after 120 min. The acetic acid concentration reached 98 mg/L after 20 min UV-C/PS treatment when IPR was completely removed and decreased steadily to non-detectable levels after 40 min treatment (Figure 4.48 (c)). On the other hand, formic acid formation started right after 10 min and its concentration continued to increase to 26.3 mg/L after 40 min treatment. Thereafter, formic acid decreased at a slower rate compared to its formation rate reaching an ultimate concentration of 9.8 mg/L. The formation and degradation pattern of carboxylic acids were in agreement with the observed DOC abatement profiles. As was already evident from Figure 4.48 (a), DOC removal was initially fast but slowed down after 40 min treatment, which might be attributed to the (i) formation of degradation products (e.g. formic acid) being more resistant towards further oxidation (Oturan et al. 2000; Wang and Chu 2012) and (ii) depletion of oxidant PS as the reaction progressed. It should be also mentioned here that parallel to carboxylic acid formation a rapid decrease in pH from 6.0 to 3.5 (data not shown) occurred within the first 10 min of the oxidation reaction supporting the formation of acidic degradation products during photochemical IPR treatment. Based on the aromatic and aliphatic (carboxylic acid) degradation products identified in the present study and previous related studies, a reaction pathway was proposed for UV-C and UV-C/PS treatments of aqueous IPR as can be followed from Figure 4.48.
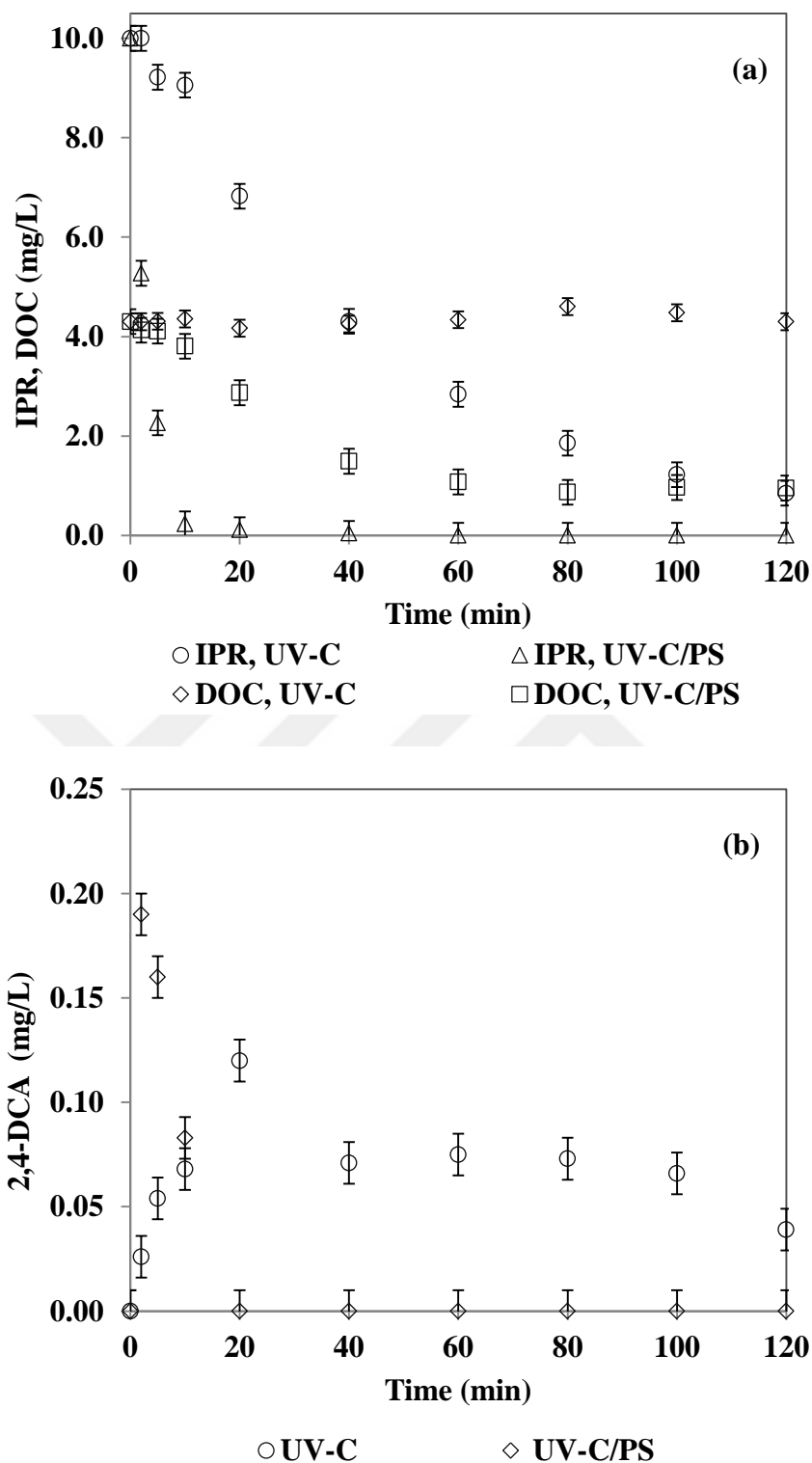
Figure 4.48 : Changes in IPR and DOC (a), 2,4-DCA (b), carboxylic acids (c) and Cl⁻ (d) concentrations during UV-C and UV-C/PS treatments. Carboxylic acids formation was observed only during UV-C/PS treatment. The theoretically expected maximum Cl⁻ concentration after full oxidation of IPR is 2.15 mg/L. IPR=10 mg/L; PS=0.30 mM; UV-C intensity=0.5 W/L; pH=6.2.
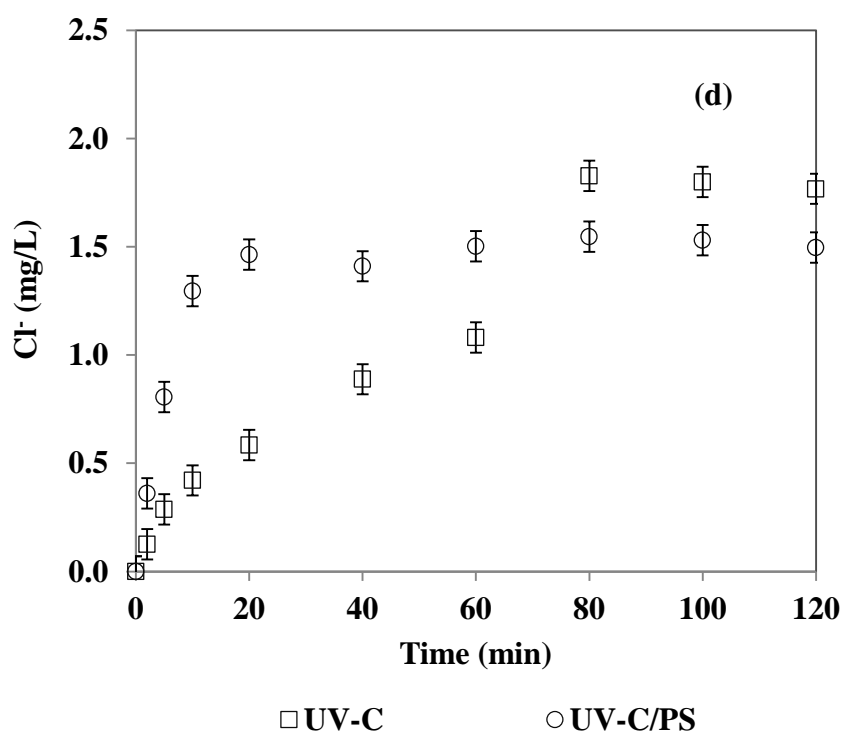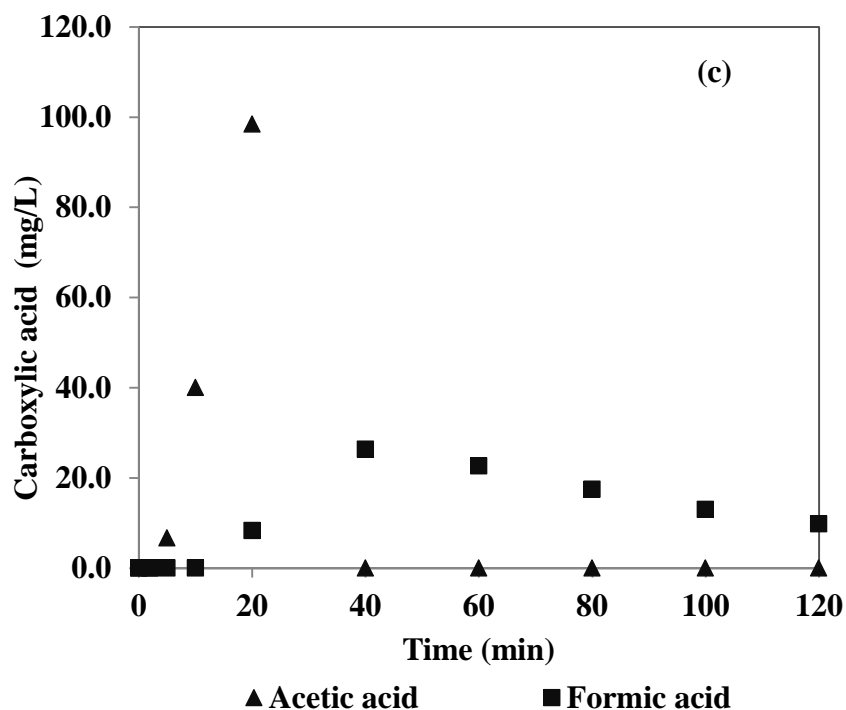
Figure 4.48 (continued) : Changes in IPR and DOC (a), 2,4-DCA (b), carboxylic acids (c) and Cl⁻ (d) concentrations during UV-C and UV-C/PS treatments. Carboxylic acids formation was observed only during UV-C/PS treatment. The theoretically expected maximum Cl⁻ concentration after full oxidation of IPR is 2.15 mg/L. IPR=10 mg/L; PS=0.30 mM; UV-C intensity=0.5 W/L; pH=6.2.

Considering the above mentioned results and taking into account of the previously reported degradation pathways of IPR, one possible degradation pathway can be assumed where the two chlorine atoms have been replaced by hydroxyl groups (pathway Nrs. 1 and 2). C-centered radical formation via electron transfer from the organic compound to $SO_4^{\bullet -}$ might also be possible (pathway Nr. 3). A $SO_4^{\bullet -}$ and/or $HO^{\bullet}$-mediated attack on an aromatic ring might lead the formation of short-lived $SO_4^{\bullet -}$ and/or $HO^{\bullet}$ adducts (pathway Nr. 4) and eventually 2,4-DCA formation that might be formed via C-N bond cleavage (pathway Nr. 5) (Figure 4.49).

The IPR degradation products during UV-C and UV-C/PS treatments were also analyzed by LC-MS at Boğaziçi University. The chromatographic profiles and retention time of UV-C and UV-C/PS treated samples of IPR are shown in Appendix; however, the type of the degradation products was not identified.

4.5.3.2 Zero-valent iron-activated persulfate oxidation processes

As aforementioned, $SO_4^{\bullet -}$ can be generated from the activation of PS by ZVI (Li et al, 2014a). Unlike metal ion activation of PS where in order to achieve complete pollutant degradation, excess ferrous salts are necessary and theses excess ferrous ion can react with even $SO_4^{\bullet -}$, ZVI can continuously release ferrous ions to activate PS (Li et al, 2014a).

In this study, formation of evolved intermediates during ZVI/PS treatment of IPR was investigated by LC analysis. Figure 4.50 depicts changes in IPR and DOC (a) hydroquinone (b) and carboxylic acids (lactic and acetic acids) (c) concentrations during ZVI/PS (PS=2.50 mM) treatment of 10 mg/L IPR in DW at initial solution pH of 3.0. As it can be seen from Figure 4.50 (a), 97% and almost near-complete IPR removals were achieved only after 10 min and 20 min ZVI/PS treatment, respectively. Dechlorination is expected during IPR degradation; however, due to high formed sulfate ions concentration, it was not possible to measure Cl$^-$ released by IC. Formation of 2,4-DCA, 4-CP, catechol, benzoquinone, phenol, formic acid and phthalic acid were investigated as possible intermediates during ZVI/PS treatment of IPR; however, none of them was detected by LC analysis. Hydroquinone was identified after 90 min ZVI/PS treatment as 0.44 mg/L and reaching to its highest concentration as 0.50 mg/L after 120 min. Hydroquinone accumulation during ZVI/PS treatment of IPR was higher compared to its UV-C/PS treatment.
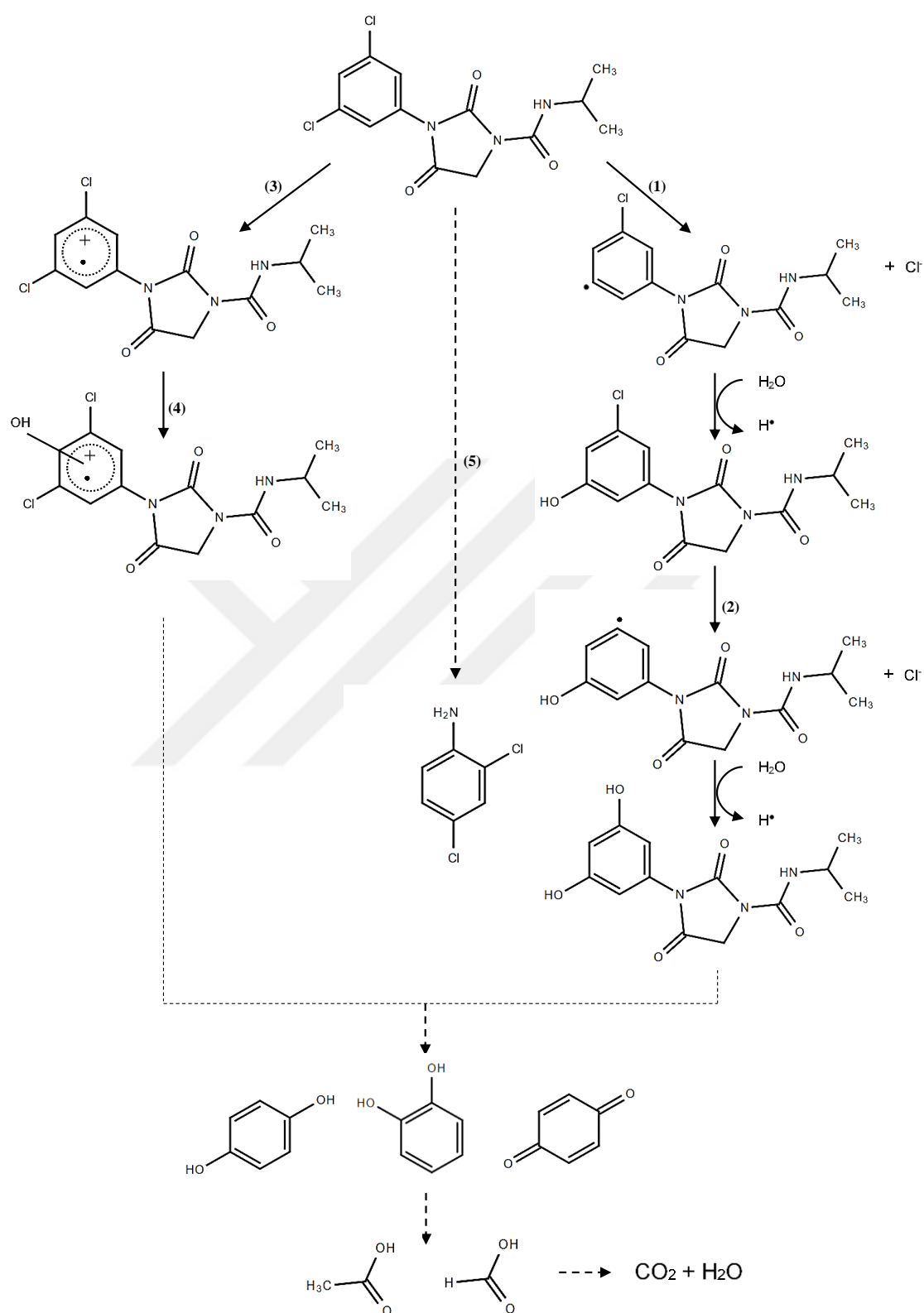
Figure 4.49 : Proposed reaction pathway for IPR degradation by UV-C and UV-C/PS treatments.

154
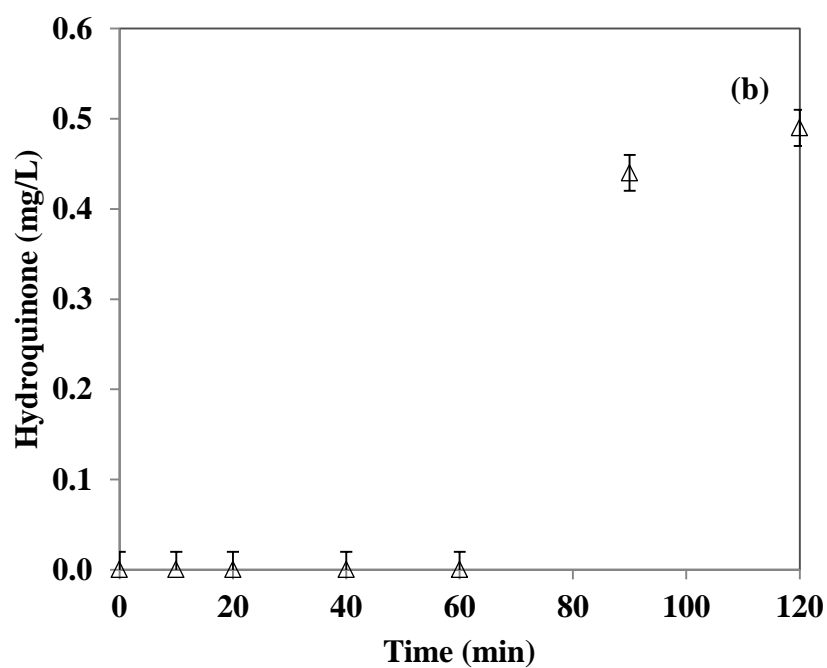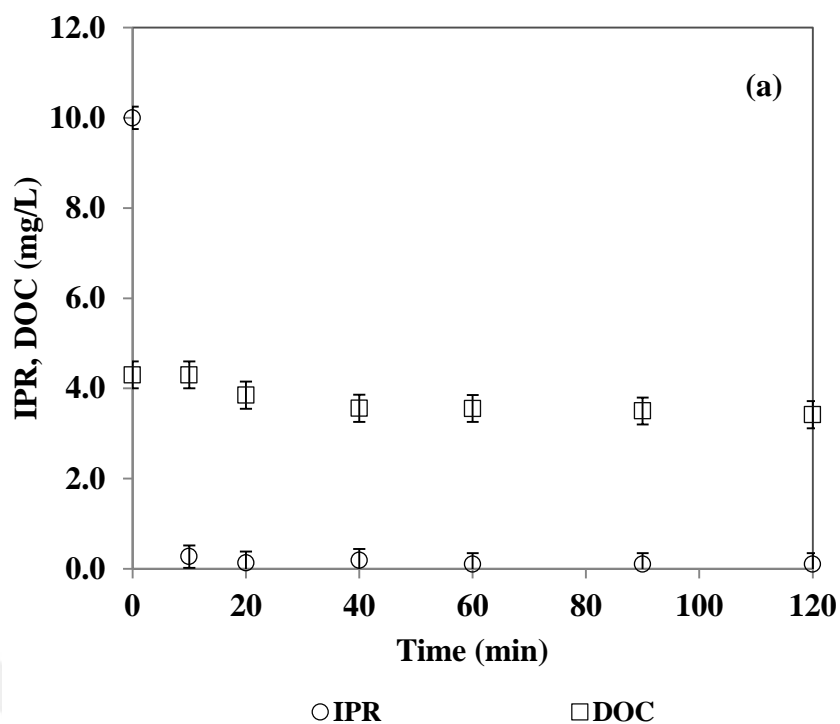
Figure 4.50 : Changes in IPR and DOC (a), hydroquinone (b) and carboxylic acids (c) concentrations during ZVI/PS treatment. IPR=10 mg/L; PS=2.50 mM; ZVI=1 g/L; pH=3.0.
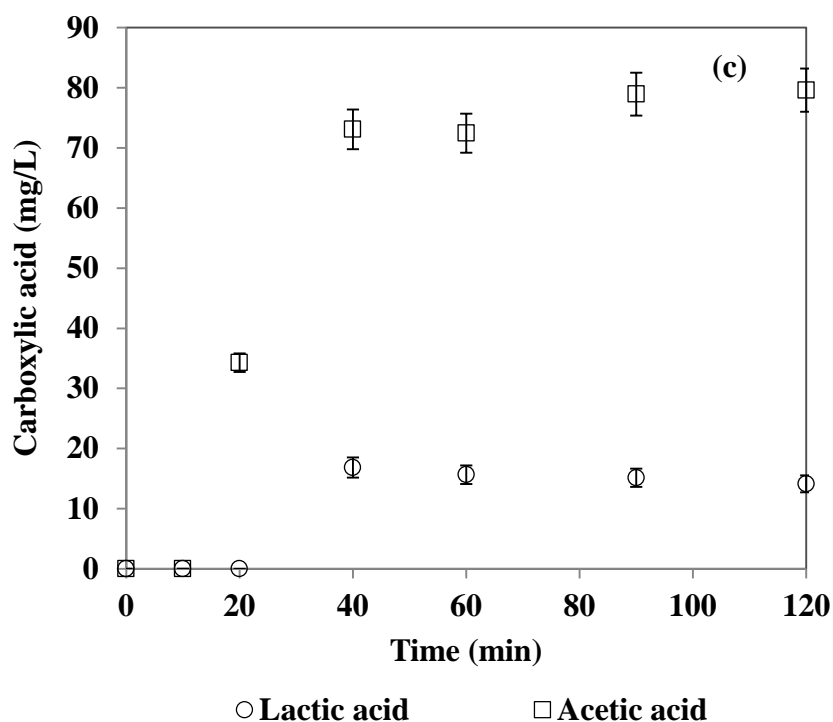
Figure 4.50 (continued) : Changes in IPR and DOC (a), hydroquinone (b) and carboxylic acids (c) concentrations during ZVI/PS treatment. IPR=10 mg/L; PS=2.50 mM; ZVI=1 g/L; pH=3.0.

As mentioned above, it was shown that $SO_4^{\bullet-}$ and $HO^{\bullet}$ could react with organic micropollutants through direct electron transfer and/or by addition/elimination reactions and form $HO^{\bullet}$ adducts via hydrolysis (Sharma et al, 2015). $SO_4^{\bullet-}$ adducts can be formed from $SO_4^{\bullet-}$ attack on an aromatic ring or olefinic double bond (Luo et al, 2017; Sharma et al, 2015). C-centered radical formation via electron transfer from the organic compound to $SO_4^{\bullet-}$ by releasing SO_4^{2-} is also possible due to the electrophilic nature of $SO_4^{\bullet-}$. Formation of radicals via hydrogen abstraction mechanism also is possible (Sharma et al, 2015). Oxygen addition to the C-centered radicals or β-scission will result in the formation of dioxygen radical adducts which would resulted in formation of hydroxylated degradation products and ultimately ring-opening products including short-chain aliphatic acids and carbon dioxide (Garcia-Segura et al, 2012; Skoumal et al, 2008). Limited information is currently available describing IPR degradation. Due to IPR is a dichloride organic molecule; the evolution of Cl^- was reported during photolytic and photochemical degradation of this pesticide (Lassalle et al, 2014; Lopez-Alvarez et al, 2016; Schwack et al, 1995). Cl^- release might be as result of $SO_4^{\bullet-}$ and/or $HO^{\bullet}$ attack into the carbon-chloride bond as one of the first steps during IPR degradation. The susceptibility of these

bonds has been also reported during the photodecomposition of IPR leading to the substitution of the Cl atoms by OH groups (Lassalle et al, 2014; Lopez-Alvarez et al, 2016) according to the mechanism described above in Figure 4.49.

5. CONCLUSIONS

Generally, industrial effluents are difficult to treat using traditional biological processes due to the high diversity in their compositions as well as probability of generation of toxic biotransformation products. AOPs including UV-C/PS, ZVI/PS and ZVA/PS can be considered as efficient solutions for partial and full degradation of a wide range of industrial micropollutants. Hence, the degradation of three model industrial micropollutants including 3,5-DCP, 2,4-DCA and IPR being chosen representatives of three main industrial micropollutants groups namely CPs, CAs and hydantoins through one homogenous photochemical and two heterogeneous catalytic oxidation processes, namely UV-C/PS and ZVI/PS-ZVA/PS treatments, respectively was investigated. A series of experiments was conducted at varying PS concentrations (0.00-1.00 mM) and pH values (1.5-11.0) to examine the effect of critical process parameters on the model industrial micropollutants removal in pure water (DW). Moreover, the degradation of the micropollutants and their mineralization were assessed in SWW to examine the performance of the PS-activated oxidation systems in a more complex water matrix under selected conditions and changes in acute toxicity as well as genotoxicity patterns were also investigated. Eventually, possible evolved degradation products of three model industrial micropollutants were examined in order to assess efficiency and safe use potential of selected AOPs. The major conclusions drawn from the present study could be listed for 3,5-DCP, 2,4-DCA and IPR individually as follows;

5.1 3,5-Dichlorophenol

Although, complete 3,5-DCP degradation was observed by UV-C photolysis of 3,5-DCP in DW, its mineralization was insignificant after 120 min treatment revealing that mere UV-C photolysis was not capable of efficient degradation of 3,5-DCP transformation products . On the other hand, UV-C/PS treatment of 3,5-DCP with the intermediacy of highly reactive $SO_4^{\bullet-}$ resulted in rapid and complete degradation of 3,5-DCP and efficient mineralization of 3,5-DCP (near 95 % DOC removal) at the

end of treatment time. Fast and complete degradation of 3,5-DCP was also obtained by ZVI/PS; however, the degree of mineralization of 3,5-DCP through ZVI/PS treatment was much lower compared to UV-C/PS and partial mineralization of 3,5-DCP (50% DOC removal) was obtained at the end of treatment time.

UV-C/PS that demonstrated superior treatment performance in DW, exhibited worse treatment performance than ZVI/PS when applied in SWW (26% DOC removal and 41% DOC removal by UV-C/PS and ZVI/PS, respectively). Obviously, the SWW composition inhibited the photochemical treatment process more seriously than the heterogeneous catalytic treatment. Ecotoxicological evaluation of original 3,5-DCP and its UV-C, UV-C/PS and ZVI/PS treated samples using *P. subcapitata* revealed that the phototransformation products of 3,5-DCP caused more inhibitory effect compared to ZVI/PS; the percentage relative inhibition of 31%, 47% and 19% was obtained after 80 min UV-C, UV-C/PS and ZVI/PS treatments, respectively suggesting ZVI/PS under selected conditions as an effective oxidation process for 3,5-DCP removal in SWW as a complex effluent medium.

Among hydroxylated intermediates that are expected during UV-C/PS treatment of 3,5-DCP, only hydroquinone could be quantified in the reaction. Dechlorination was observed during oxidation of 3,5-DCP followed by fragmentation into relatively smaller, acidic degradation products resulted to almost complete mineralization to inorganics. ZVI/PS treatment of 3,5-DCP also resulted in formation hydroquinone during the early stages of oxidation; however, hydroquinone was accumulated longer in working solution compared to UV-C/PS treatment and eventually degraded to non-detectable after 40 min treatment.

5.2 2,4-Dichloroaniline

Despite of complete 2,4-DCA degradation through UV-C photolysis treatment, poor mineralization (5% DOC removal) of 2,4-DCA was evidenced after 120 min treatment. On the other hand, UV-C/PS proved to be effective treatment to achieve not only complete degradation but also significant mineralization of 2,4-DCA (almost 93% DOC removal) at the end of treatment time. ZVI/PS treatment of 2,4-DCA resulted in almost complete 2,4-DCA degradation and its partial mineralization (44% DOC removal).

UV-C/PS treatment of 2,4-DCA in SWW resulted in partial mineralization (57%) after 120 min which was much lower compared to UV-C/PS treatment in DW revealing the presence of various organic and inorganic constituents in the SWW might have inhibitory effects on 2,4-DCA mineralization during UV-C/PS. Similarly, ZVI/PS treatment of 2,4-DCA in SWW resulted in partial mineralization of 2,4-DCA (35% DOC removal). Hence, it can be concluded that the treatment performance was strongly influenced by the SWW constituents and UV-C/PS treatment appeared to be the most sensitive to it and its efficiency in DOC removal decreased noticeably in more complex matrix compare to DW as a result of organic/inorganic competition of SWW constituents with PS for UV-C light absorption. The relative inhibition caused by the original 2,4-DCA was found as ~25% on *P. subcapitata* and reached 24%, 70% and 23% at the end of 80 min UV-C, UV-C/PS and ZVI/PS treatments. Upon comparison between the capability of the examined treatments in DOC removals in SWW and the inhibitory effect of transformation products on algal growth, ZVI/PS may be offered as a more feasible treatment option for the efficient removal of 2,4-DCA in real wastewater.

Formation of evolved intermediates during UV-C (pH=6.0) and UV-C/PS (PS=0.30 mM; pH=6.0) treatment of 2,4-DCA was investigated and among expected aromatic degradation products such as hydroquinone, *p*-benzoquinone, catechol, phenol, aniline and nitrobenzene, only aniline was qualified as a result of C-Cl bond cleavage. Aniline and nitrobenzene formation as two possible intermediates of 2,4-DCA was investigated during ZVI/PS treatment; however, none of them was detected by LC analysis. The degradation pathway of 2,4-DCA can be initiated by the attack of $SO_4^{\bullet-}$ and $HO^{\bullet}$ and release of organically bound Cl atoms in the form of free Cl^- leading to aniline formation. Further $SO_4^{\bullet-}$ and/or $HO^{\bullet}$ attack on the formed aniline can yield low molecular weight acids such as acetic acid.

5.3 Iprodione

UV-C photolysis of IPR resulted in 92% removal; however, no DOC removal was evidenced at the end of treatment time indicating the use of mere UV-C treatment did not result in mineralization of the IPR photolysis products. Although rapid IPR removal was achieved by UV-C/PS and ZVI/PS treatment, the degree of mineralization at the end of treatment time was completely different. While

appreciable mineralization (78%) was achieved after 120 min UV-C/PS treatment of IPR, its mineralization by ZVI/PS was limited to 21%. ZVA/PS treatment of IPR led to 65% IPR degradation and poor mineralization. Therefore, it can be concluded that UV-C/PS exhibited not only effective IPR degradation, but also appreciable mineralization of photoproduct of IPR in DW. However, in a complex wastewater matrix (in the presence of a variety of organic/inorganic constituents) its performance was different. While the experiments in DW marked the superior performance of the UV-C/PS for IPR removal and its mineralization, the oxidation performance of UV-C/PS decreased appreciably (only 24% DOC removal after 120 min) in a more complex water matrix (SWW). Practically complete degradation and partial but good mineralization of IPR (40% DOC removal) were observed with ZVI/PS being the most efficient process in SWW. The originally low toxicity of IPR (9% relative inhibition towards *V. fischeri*) gradually decreased to neglectable levels (4% relative inhibition) at the end of UV-C/PS treatment indicating that no inhibitory degradation products were formed during its photochemical treatment in SWW. The percentage relative inhibition of original IPR on *P. subcapitata* was calculated less than 10%. The percent relative inhibition of the UV-C/PS and ZVI/PS treated samples reached 56% and 39%, respectively after 120 min. In conclusion, ZVI/PS can be suggested as an efficient and toxicology safer treatment of IPR in complex water matrix.

Considering the experimental finings, the ZVI/PS treatment under selected conditions for each model industrial micropollutant, appears to be a better treatment option in SWW than the other studied PS-activated AOPs both in terms of oxidation (treatment) performance and ecotoxicological safety (toxicity values) and hence, may be considered as a more feasible treatment for the efficient removal of industrial micropollutants found in water or wastewater.

Based on the obtained results, the following recommendation can be suggested for future research;

- Treatability studies in real urban wastewater may help improving the current knowledge on the effect of water matrices on the generation of transformation products and any possible inhibitory effect on performance $SO_4^{\bullet-}$-based AOPs.

- AOPs integration with conventional wastewater treatment processes (aerobic/anaerobic biological) can be suggested; however, before their

applications, the chemical composition of the wastewater, scale of operation and ultimate treatment objectives should be considered.

- If the recommended ZVI/PS process is selected for further investigation in pilot- or real scale the following issues should to be taken into account;

  First, the need for pH adjustment in acidic pH values should be considered. Acidic pH values are required for ZVI/PS activation and that would be an additional serious operating cost in real scale application. Another limitation can be the inevitable need for iron solid catalyst removal at the end of the treatment by additional processes such as membrane filtration which needs more cost to design an effective filtration unit. Moreover, SO_4^{2-} and Fe release have to be controlled (whether below discharge limit values; $SO_4^{2-} <$ 500 mg/L, Fe < 0.2 mg/L).

REFERENCES

Abe, K., and Tanaka, K. (1997). Fe^{3+} and UV-enhanced ozonation of chlorophenolic compounds in aqueous medium, *Chemosphere, 35*, 2837-2847.

Acero, J. L., Benítez, F. J., Real, F. J., and Rodríguez, E. (2018). Degradation of selected emerging contaminants by UV-activated persulfate: Kinetics and influence of matrix constituents, *Separation and Purification Technology, 201*, 41-50.

Amor, C., Marchão, L., Lucas, M. S., and Peres, J. A. (2019). Application of advanced oxidation processes for the treatment of recalcitrant agro-industrial wastewater: A review, *Water, 11*, 205.

Androulaki, E., Hiskia, A., Dimotikali, D., Minero, C., Calza, P., Pelizzetti, E., and Papaconstantinou, E. (2000). Light induced elimination of mono-and polychlorinated phenols from aqueous solutions by $PW_{12}O_{40}^{3-}$. The case of 2,4,6-trichlorophenol, *Environmental Science and Technology, 34*, 2024-2028.

Anipsitakis, G. P., and Dionysiou, D. D. (2004). Radical generation by the interaction of transition metals with common oxidants, *Environmental Science and Technology, 38*, 3705-3712.

Anipsitakis, G. P., Dionysiou, D. D., and Gonzalez, M. A. (2006). Cobalt-mediated activation of peroxymonosulfate and sulfate radical attack on phenolic compounds. Implications of chloride ions, *Environmental Science and Technology, 40*, 1000-1007.

Antonaraki, S., Androulaki, E., Dimotikali, D., Hiskia, A., and Papaconstantinou, E. (2002). Photolytic degradation of all chlorophenols with polyoxometallates and H_2O_2, *Journal of Photochemistry and Photobiology A: Chemistry, 148*, 191-197.

Antoniou, M. G., de la Cruz, A. A., and Dionysiou, D. D. (2010). Intermediates and reaction pathways from the degradation of microcystin-LR with sulfate radicals, *Environmental Science and Technology, 44*, 7238-7244.

Apak, R., and Hugül, M. (1996). Photooxidation of some mono-, di-, and tri-chlorophenols in aqueous solution by hydrogen peroxide/UV combinations, *Journal of Chemical Technology and Biotechnology: International Research in Process, Environmental AND Clean Technology, 67*, 221-226.

APHA (2012). *Standard Methods for the Examination of Water and Wastewater*, American Public Health Association, Washington.

Araújo, K. C. d. F., Barreto, J. P. d. P., Cardozo, J. C., dos Santos, E. V., de Araújo, D. M., and Martínez-Huitle, C. A. (2018). Sulfate pollution: evidence for electrochemical production of persulfate by oxidizing sulfate released by the surfactant sodium dodecyl sulfate, *Environmental Chemistry Letters, 16*, 647-652.

Arslan-Alaton, I., Kolba, O., and Olmez-Hanci, T. (2018a). Removal of an X-Ray contrast chemical from tertiary treated wastewater: Investigation of persulfate-mediated photochemical treatment systems, *Catalysis Today, 313*, 134-141.

Arslan-Alaton, I., Olmez-Hanci, T., Dogan, M., and Ozturk, T. (2017a). Zero-valent aluminum-mediated degradation of Bisphenol A in the presence of common oxidants, *Water Science and Technology, 76*, 2455-2464.

Arslan-Alaton, I., Olmez-Hanci, T., Khoei, S., and Fakhri, H. (2017b). Oxidative degradation of Triton X-45 using zero valent aluminum in the presence of hydrogen peroxide, persulfate and peroxymonosulfate, *Catalysis Today, 280*, 199-207.

Arslan-Alaton, I., Olmez-Hanci, T., Korkmaz, G., and Sahin, C. (2017c). Removal of iopamidol, an iodinated X-ray contrast medium, by zero-valent aluminum-activated H_2O_2 and $S_2O_8^{2-}$, *Chemical Engineering Journal, 318*, 64-75.

Arslan-Alaton, I., Olmez-Hanci, T., and Ozturk, T. (2018b). Effect of inorganic and organic solutes on zero-valent aluminum-activated hydrogen peroxide and persulfate oxidation of bisphenol A, *Environmental science and pollution research, 25*, 34938-34949.

Ashauer, R., Hintermeister, A., Potthoff, E., and Escher, B. I. (2011). Acute toxicity of organic chemicals to *Gammarus pulex* correlates with sensitivity of *Daphnia magna* across most modes of action, *Aquatic Toxicology, 103*, 38-45.

Avetta, P., Pensato, A., Minella, M., Malandrino, M., Maurino, V., Minero, C., Hanna, K., and Vione, D. (2015). Activation of persulfate by irradiated magnetite: implications for the degradation of phenol under heterogeneous photo-Fenton-like conditions, *Environmental Science and Technology, 49*, 1043-1050.

Bandara, J., Mielczarski, J., Lopez, A., and Kiwi, J. (2001). 2. Sensitized degradation of chlorophenols on iron oxides induced by visible light: comparison with titanium oxide, *Applied Catalysis B: Environmental, 34*, 321-333.

Barzegar, G., Jorfi, S., Zarezade, V., Khatebasreh, M., Mehdipour, F., and Ghanbari, F. (2018). 4-Chlorophenol degradation using ultrasound/peroxymonosulfate/nanoscale zero valent iron: reusability, identification of degradation intermediates and potential application for real wastewater, *Chemosphere, 201*, 370-379.

Basu, S., and Wei, I. W. (1998). Advanced chemical oxidation of 2,4,6 trichlorophenol in aqueous phase by Fenton's Reagent-Part II: Effects of various reaction parameters on the treatment reaction, *Chemical Engineering Communications, 164*, 139-151.

Belafdal, O., Bergon, M., and Calmon, J. P. (1986). Mechanism of hydantoin ring opening in iprodione in aqueous media, *Pesticide science, 17*, 335-342.

Bellucci, M., Ofiţeru, I., Head, I., Curtis, T., and Graham, D. (2013). Nitrification in hybrid bioreactors treating simulated domestic wastewater, *Journal of applied microbiology, 115*, 621-630.

Benitez, F. J., Beltran-Heredia, J., Acero, J. L., and Rubio, F. J. (2000). Contribution of free radicals to chlorophenols decomposition by several advanced oxidation processes, *Chemosphere, 41*, 1271-1277.

Bernabeu, A., Vercher, R., Santos-Juanes, L., Simón, P., Lardín, C., Martínez, M., Vicente, J., González, R., Llosá, C., and Arques, A. (2011). Solar photocatalysis as a tertiary treatment to remove emerging pollutants from wastewater treatment plant effluents, *Catalysis Today, 161*, 235-240.

Bertelli, M., and Selli, E. (2006). Reaction paths and efficiency of photocatalysis on TiO$_2$ and of H$_2$O$_2$ photolysis in the degradation of 2-chlorophenol, *Journal of Hazardous Materials, 138*, 46-52.

Bessergenev, V., Mateus, M., Morgado, I., Hantusch, M., and Burkel, E. (2017). Photocatalytic reactor, CVD technology of its preparation and water purification from pharmaceutical drugs and agricultural pesticides, *Chemical Engineering Journal, 312*, 306-316.

Boehncke, A., Kielhorn, J., Konnecker, G., Pohlenz-Michel, C., and Mangelsdorf, I. (2003). *4-Chloroaniline CICADS Report 48*, Geneva.

Bokare, A. D., and Choi, W. (2009). Zero-valent aluminum for oxidative degradation of aqueous organic pollutants, *Environmental Science and Technology, 43*, 7130-7135.

Boon, N., Goris, J., De Vos, P., Verstraete, W., and Top, E. M. (2001). Genetic diversity among 3-chloroaniline and aniline degrading strains of the *Comamonadaceae*, *Applied and Environmental Microbiology, 67*, 1107-1115.

Boucenna, A., Oturan, N., Chabani, M., Bouafia-Chergui, S., and Oturan, M. A. (2019). Degradation of Nystatin in aqueous medium by coupling UV-C irradiation, H$_2$O$_2$ photolysis, and photo-Fenton processes, *Environmental science and pollution research, 26*, 23149-23161.

Boule, P., Guyon, C., and Lemaire, J. (1984). Photochemistry and environment: VI. Direct phototransformation of chlorophenols and interactions with phenol on UV exposure in aqueous solution, *Toxicological and Environmental Chemistry, 7*, 97-110.

Bu, L., Zhou, S., Shi, Z., Deng, L., Li, G., Yi, Q., and Gao, N. (2016). Degradation of oxcarbazepine by UV-activated persulfate oxidation: kinetics, mechanisms, and pathways, *Environmental science and pollution research, 23*, 2848-2855.

Burrows, H. D., Santaballa, J., and Steenken, S. (2002). Reaction pathways and mechanisms of photodegradation of pesticides, *Journal of photochemistry and photobiology B: Biology, 67*, 71-108.

Burton, G. W., Doba, T., Gabe, E., Hughes, L., Lee, F., Prasad, L., and Ingold, K. U. (1985). Autoxidation of biological molecules. 4. Maximizing the antioxidant activity of phenols, *Journal of the American Chemical Society, 107*, 7053-7065.

Buxton, G. V., Greenstock, C. L., Helman, W. P., and Ross, A. B. (1988). Critical review of rate constants for reactions of hydrated electrons, hydrogen atoms and hydroxyl radicals ($^\bullet$OH/$^\bullet$O$^-$ in aqueous solution, *Journal of physical and chemical reference data, 17*, 513-886.

Cabras, P., Meloni, M., Pirisi, F. M., and Cabitza, F. (1985). Behavior of acylanilide and dicarboximidic fungicide residues on greenhouse tomatoes, *Journal of agricultural and food chemistry, 33*, 86-89.

Camiletti, B. X., Asensio, C. M., Gadban, L. C., Pecci, M. d. l. P. G., Conles, M. Y., and Lucini, E. I. (2016). Essential oils and their combinations with iprodione fungicide as potential antifungal agents against withe rot (*Sclerotium cepivorum Berk*) in garlic (*Allium sativum L.*) crops, *Industrial Crops and Products, 85*, 117-124.

Campos, M., Perruchon, C., Vasilieiadis, S., Menkissoglu-Spiroudi, U., Karpouzas, D., and Diez, M. (2015). Isolation and characterization of bacteria from acidic pristine soil environment able to transform iprodione and 3,5-dichloraniline, *International Biodeterioration and Biodegradation, 104*, 201-211.

Causserand, C., Aimar, P., Cravedi, J.-P., and Singlande, E. (2005). Dichloroaniline retention by nanofiltration membranes, *Water research, 39*, 1594-1600.

Černá, M., Hájek, V., Stejskalová, E., Dobiáš, L., Zudová, Z., and Rössner, P. (1991). Environmental genotoxicity monitoring using *Salmonella typhimurium* strains as indicator system, *Science of the Total Environment, 101*, 139-147.

Chang, S.-j., and Liu, Y.-c. (2007). Degradation mechanism of 2,4,6-trinitrotoluene in supercritical water oxidation, *Journal of Environmental Sciences, 19*, 1430-1435.

Chen, C. Y., Ko, C. W., and Lee, P. I. (2007). Toxicity of substituted anilines to Pseudokirchneriella subcapitata and quantitative structure-activity relationship analysis for polar narcotics, *Environmental Toxicology and Chemistry: An International Journal, 26*, 1158-1164.

Chen, J., Gao, N., Lu, X., Xia, M., Gu, Z., Jiang, C., and Wang, Q. (2016). Degradation of 2,4-dichlorophenol from aqueous using UV activated persulfate: kinetic and toxicity investigation, *Royal Society of Chemistry Advances, 6*, 100056-100062.

Chen, L., Cai, T., Cheng, C., Xiong, Z., and Ding, D. (2018). Degradation of acetamiprid in UV/H_2O_2 and UV/persulfate systems: A comparative study, *Chemical Engineering Journal, 351*, 1137-1146.

Chen, T., Ma, J., Zhang, Q., Xie, Z., Zeng, Y., Li, R., Liu, H., Liu, Y., Lv, W., and Liu, G. (2019). Degradation of propranolol by UV-activated persulfate oxidation: Reaction kinetics, mechanisms, reactive sites, transformation pathways and Gaussian calculation, *Science of the Total Environment, 690*, 878-890.

Chen, W.-S., and Su, Y.-C. (2012). Removal of dinitrotoluenes in wastewater by sono-activated persulfate, *Ultrasonics sonochemistry, 19*, 921-927.

Chen, Y., Xie, P., Wang, Z., Shang, R., and Wang, S. (2017). UV/persulfate preoxidation to improve coagulation efficiency of *Microcystis aeruginosa*, *Journal of Hazardous Materials, 322*, 508-515.

Chu, W., Choy, W., and So, T. (2007). The effect of solution pH and peroxide in the TiO_2-induced photocatalysis of chlorinated aniline, *Journal of Hazardous Materials, 141*, 86-91.

Cravedi, J. P., Boudry, G., Baradat, M., Rao, D., and Debrauwer, L. (2001). Metabolic fate of 2,4-dichloroaniline, prochloraz and nonylphenol diethoxylate in rainbow trout: a comparative in vivo/in vitro approach, *Aquatic Toxicology, 53*, 159-172.

Cravotto, G., Binello, A., Di Carlo, S., Orio, L., Wu, Z.-L., and Ondruschka, B. (2010). Oxidative degradation of chlorophenol derivatives promoted by microwaves or power ultrasound: a mechanism investigation, *Environmental science and pollution research, 17*, 674-687.

Crincoli, K. R., Green, C., and Huling, S. G. (2020). Sulfate radical scavenging by mineral surfaces in persulfate-driven oxidation systems: reaction rate constants and implications, *Environmental Science and Technology, 54*, 1955-1962.

Criquet, J., and Leitner, N. K. V. (2011). Electron beam irradiation of aqueous solution of persulfate ions, *Chemical Engineering Journal, 169*, 258-262.

Crossland, N. (1990). A review of the fate and toxicity of 3,4-dichloroaniline in aquatic environments, *Chemosphere, 21*, 1489-1497.

Cuerda-Correa, E. M., Alexandre-Franco, M. F., and Fernández-González, C. (2020). Advanced oxidation processes for the removal of antibiotics from water. An overview, *Water, 12*, 102.

Czaplicka, M. (2004). Sources and transformations of chlorophenols in the natural environment, *Science of the Total Environment, 322*, 21-39.

Czaplicka, M. (2006). Photo-degradation of chlorophenols in the aqueous solution, *Journal of Hazardous Materials, 134*, 45-59.

Czaplicka, M., and Kaczmarczyk, B. (2006). Infrared study of chlorophenols and products of their photodegradation, *Talanta, 70*, 940-949.

Dalzell, D., Alte, S., Aspichueta, E., De la Sota, A., Etxebarria, J., Gutierrez, M., Hoffmann, C., Sales, D., Obst, U., and Christofi, N. (2002). A comparison of five rapid direct toxicity assessment methods to determine toxicity of pollutants to activated sludge, *Chemosphere, 47*, 535-545.

Dan, J., Wang, Q., Mu, K., Rao, P., Dong, L., Zhang, X., He, Z., Gao, N., and Wang, J. (2020). Degradation of sulfachloropyridazine by UV-C/persulfate: kinetics, key factors, degradation pathway, *Environmental Science: Water Research and Technology*.

Dean, J. A. (1997) Lange's handbook of chemistry. 14th edn. McGraw-Hill, New York

Deblonde, T., Cossu-Leguille, C., and Hartemann, P. (2011). Emerging pollutants in wastewater: a review of the literature, *International journal of hygiene and environmental health, 214*, 442-448.

Deng, J., Shao, Y., Gao, N., Deng, Y., Tan, C., and Zhou, S. (2014). Zero-valent iron/persulfate (Fe^0/PS) oxidation acetaminophen in water, *International Journal of Environmental Science and Technology, 11*, 881-890.

Derbalah, A. S. H., Nakatani, N., and Sakugawa, H. (2003). Distribution, seasonal pattern, flux and contamination source of pesticides and nonylphenol residues in Kurose River water, Higashi-Hiroshima, Japan, *Geochemical Journal, 37*, 217-232.

Dewil, R., Mantzavinos, D., Poulios, I., and Rodrigo, M. A. (2017). New perspectives for advanced oxidation processes, *Journal of environmental management, 195*, 93-99.

Ding, D., Liu, C., Ji, Y., Yang, Q., Chen, L., Jiang, C., and Cai, T. (2017). Mechanism insight of degradation of norfloxacin by magnetite nanoparticles activated persulfate: identification of radicals and degradation pathway, *Chemical Engineering Journal, 308*, 330-339.

Dogan, M., Ozturk, T., Olmez-Hanci, T., and Arslan-Alaton, I. (2016). Persulfate and hydrogen peroxide-activated degradation of bisphenol A with nano-scale zero-valent iron and aluminum, *Journal of Advanced Oxidation Technologies, 19*, 266-275.

Dogliotti, L., and Hayon, E. (1967). Flash photolysis of per [oxydi] sulfate ions in aqueous solutions. The sulfate and ozonide radical anions, *The Journal of Physical Chemistry, 71*, 2511-2516.

Dong, H., Hou, K., Qiao, W., Cheng, Y., Zhang, L., Wang, B., Li, L., Wang, Y., Ning, Q., and Zeng, G. (2019). Insights into enhanced removal of TCE utilizing sulfide-modified nanoscale zero-valent iron activated persulfate, *Chemical Engineering Journal, 359*, 1046-1055.

Dong, S., Zhai, X., Pi, R., Wei, J., Wang, Y., and Sun, X. (2020). Efficient degradation of naproxen by persulfate activated with zero-valent iron: performance, kinetic and degradation pathways, *Water Science and Technology*.

Du, L., Xu, W., Liu, Y., Li, X., Huang, D., and Wu, S. (2020). Removal of sulfamethoxazole in aqueous solutions by iron-based advanced oxidation processes: performances and mechanisms, *WATER AIR AND SOIL POLLUTION, 231*.

Du, Y., Zhou, M., and Lei, L. (2007). The role of oxygen in the degradation of *p*-chlorophenol by Fenton system, *Journal of Hazardous Materials, 139*, 108-115.

Đurkić, T., Jazić, J. M., Watson, M., Bašić, B., Prica, M., Tubić, A., Maletić, S., and Agbaba, J. (2020). Application of UV-activated persulfate and peroxymonosulfate processes for the degradation of 1,2,3-trichlorobenzene in different water matrices, *Environmental science and pollution research,*1-15.

EC (2001). Decision No 2455/2001/EC of the European Parliament and of the Council of 20 November 2001, establishing the list of priority substances in the field of water policy and amending Directive 2000/60/EC, Official Journal of the European Communities, Brussels.

EC (2017). Regulation EU 2091 concerning the non-renewal of approval of the active substance iprodione, in accordance with regulation (EC) No 1107/2009 of the European Parliament and of the council concerning the placing of plant protection products on the market, and amending commission implementing regulation (EU) No 540/2011, Brussels.

EFSA (2016). Peer review of the pesticide risk assessment of the active substance iprodione, *European Food Safety Authority Journal, 14*, 4609-4640.

Escher, B. I., Lawrence, M., Macova, M., Mueller, J. F., Poussade, Y., Robillot, C., Roux, A., and Gernjak, W. (2011). Evaluation of contaminant removal of reverse osmosis and advanced oxidation in full-scale operation by combining passive sampling with chemical analysis and bioanalytical tools, *Environmental Science and Technology, 45*, 5387-5394.

Fang, C., Lou, X., Huang, Y., Feng, M., Wang, Z., and Liu, J. (2017). Monochlorophenols degradation by UV/persulfate is immune to the presence of chloride: illusion or reality?, *Chemical Engineering Journal, 323*, 124-133.

Fang, G.-D., Dionysiou, D. D., Al-Abed, S. R., and Zhou, D.-M. (2013). Superoxide radical driving the activation of persulfate by magnetite nanoparticles: implications for the degradation of PCBs, *Applied Catalysis B: Environmental, 129*, 325-332.

Fang, Z., Chelme-Ayala, P., Shi, Q., Xu, C., and El-Din, M. G. (2018). Degradation of naphthenic acid model compounds in aqueous solution by UV activated persulfate: influencing factors, kinetics and reaction mechanisms, *Chemosphere, 211*, 271-277.

Fang, Z., Huang, R., Chelme-Ayala, P., Shi, Q., Xu, C., and El-Din, M. G. (2019). Comparison of UV/persulfate and UV/H_2O_2 for the removal of naphthenic acids and acute toxicity towards *Vibrio fischeri* from petroleum production process water, *Science of the Total Environment, 694*, 133686.

Farré, M., and Barceló, D. (2003). Toxicity testing of wastewater and sewage sludge by biosensors, bioassays and chemical analysis, *Trends in Analytical Chemistry, 22*, 299-310.

Fatta-Kassinos, D., Dionysiou, D. D., and Kümmerer, K. (2016) Advanced treatment technologies for urban wastewater reuse (the handbook of environmental chemistry) vol 45. 1 edn. Springer International Publishing, Switzerland

Fattahi, N., Assadi, Y., Hosseini, M. R. M., and Jahromi, E. Z. (2007). Determination of chlorophenols in water samples using simultaneous dispersive liquid–liquid microextraction and derivatization followed by gas chromatography-electron-capture detection, *Journal of Chromatography A, 1157*, 23-29.

Federal Register (1979). In priority pollutant list promulgated by the US EPA under authority of the clean water act of 1977, Federal Register, Washington.

Fernandez, J., Maruthamuthu, P., Renken, A., and Kiwi, J. (2004). Bleaching and photobleaching of Orange II within seconds by the oxone/Co^{2+} reagent in Fenton-like processes, *Applied Catalysis B: Environmental, 49*, 207-215.

Frontistis, Z. (2019). Degradation of the nonsteroidal anti-inflammatory drug piroxicam from environmental matrices with UV-activated persulfate, *Journal of Photochemistry and Photobiology A: Chemistry, 378*, 17-23.

Fu, Y., Gao, X., Geng, J., Li, S., Wu, G., and Ren, H. (2019). Degradation of three nonsteroidal anti-inflammatory drugs by UV/persulfate: degradation mechanisms, efficiency in effluents disposal, *Chemical Engineering Journal, 356*, 1032-1041.

Gao, Y.-q., Gao, N.-y., Deng, Y., Yang, Y.-q., and Ma, Y. (2012). Ultraviolet (UV) light-activated persulfate oxidation of sulfamethazine in water, *Chemical Engineering Journal, 195*, 248-253.

Gao, Y.-q., Gao, N.-y., Deng, Y., Yin, D.-q., and Zhang, Y.-s. (2015). Degradation of florfenicol in water by UV/$Na_2S_2O_8$ process, *Environmental science and pollution research, 22*, 8693-8701.

Gao, Y.-q., Zhang, J., Zhou, J.-q., Li, C., Gao, N.-y., and Yin, D.-q. (2020). Persulfate activation by nano zero-valent iron for the degradation of metoprolol in water: influencing factors, degradation pathways and toxicity analysis, *Royal Society of Chemistry Advances, 10*, 20991-20999.

Garcia-Segura, S., El-Ghenymy, A., Centellas, F., Rodríguez, R. M., Arias, C., Garrido, J. A., Cabot, P. L., and Brillas, E. (2012). Comparative degradation of the diazo dye Direct Yellow 4 by electro-Fenton, photoelectro-Fenton and photo-assisted electro-Fenton, *Journal of Electroanalytical Chemistry, 681*, 36-43.

Ghaly, M. Y., Härtel, G., Mayer, R., and Haseneder, R. (2001). Photochemical oxidation of *p*-chlorophenol by UV/H_2O_2 and photo-Fenton process. A comparative study, *waste management, 21*, 41-47.

Ghanbari, F., Moradi, M., and Gohari, F. (2016). Degradation of 2,4,6-trichlorophenol in aqueous solutions using peroxymonosulfate/activated carbon/UV process via sulfate and hydroxyl radicals, *Journal of Water Process Engineering, 9*, 22-28.

Ghauch, A., Baalbaki, A., Amasha, M., El Asmar, R., and Tantawi, O. (2017). Contribution of persulfate in UV-254 nm activated systems for complete degradation of chloramphenicol antibiotic in water, *Chemical Engineering Journal, 317*, 1012-1025.

Ghorbanian, Z., Asgari, G., Samadi, M. T., and Seid-mohammadi, A. (2019). Removal of 2,4 dichlorophenol using microwave assisted nanoscale zero-valent copper activated persulfate from aqueous solutions: Mineralization, kinetics, and degradation pathways, *Journal of Molecular Liquids, 296*, 111873.

Giraldo, A. L., Penuela, G. A., Torres-Palma, R. A., Pino, N. J., Palominos, R. A., and Mansilla, H. D. (2010). Degradation of the antibiotic oxolinic acid by photocatalysis with TiO_2 in suspension, *Water research, 44*, 5158-5167.

Girit, B., Dursun, D., Olmez-Hanci, T., and Arslan-Alaton, I. (2015). Treatment of aqueous bisphenol A using nano-sized zero-valent iron in the presence of hydrogen peroxide and persulfate oxidants, *Water Science and Technology, 71*, 1859-1868.

Gogate, P. R., and Pandit, A. B. (2004). A review of imperative technologies for wastewater treatment I: oxidation technologies at ambient conditions, *Advances in Environmental Research, 8*, 501-551.

Goi, A., and Trapido, M. (2002). Hydrogen peroxide photolysis, Fenton reagent and photo-Fenton for the degradation of nitrophenols: a comparative study, *Chemosphere, 46*, 913-922.

Gomez, M., Murcia, M., Gomez, E., Gomez, J., Dams, R., and Christofi, N. (2010). Enhancement of 4-chlorophenol photodegradation with KrCl excimer UV lamp by adding hydrogen peroxide, *Separation Science and Technology, 45*, 1603-1609.

Gosetti, F., Bottaro, M., Gianotti, V., Mazzucco, E., Frascarolo, P., Zampieri, D., Oliveri, C., Viarengo, A., and Gennaro, M. C. (2010). Sun light degradation of 4-chloroaniline in waters and its effect on toxicity. A high performance liquid chromatography–Diode array–Tandem mass spectrometry study, *Environmental pollution, 158*, 592-598.

Grabke, A., Fernández-Ortuño, D., Amiri, A., Li, X., Peres, N. A., Smith, P., and Schnabel, G. (2014). Characterization of iprodione resistance in *Botrytis cinerea* from strawberry and blackberry, *Phytopathology, 104*, 396-402.

Grabner, G., and Richard, C. (2005) Mechanisms of direct photolysis of biocides based on halogenated phenols and anilines vol 2M. Environmental Photochemistry Part II (the Handbook of Environmental Chemistry). Springer, Berlin, Heidelberg. doi:https://doi.org/10.1007/b138183

Gsponer, H. E., Previtali, C. M., and García, N. A. (1987). Kinetics of the photosensitized oxidation of polychlorophenols in alkaline aqueous solution, *Toxicological and Environmental Chemistry, 16*, 23-37.

Guan, Y.-H., Ma, J., Li, X.-C., Fang, J.-Y., and Chen, L.-W. (2011). Influence of pH on the formation of sulfate and hydroxyl radicals in the UV/peroxymonosulfate system, *Environmental Science and Technology, 45*, 9308-9314.

Guo, W., Zhao, Q., Du, J., Wang, H., Li, X., and Ren, N. (2020). Enhanced removal of sulfadiazine by sulfidated ZVI activated persulfate process: Performance, mechanisms and degradation pathways, *Chemical Engineering Journal, 388*, 124303.

Gupta, P., Mathur, N., Bhatnagar, P., Nagar, P., and Srivastava, S. (2009). Genotoxicity evaluation of hospital wastewaters, *Ecotoxicology and Environmental Safety, 72*, 1925-1932.

Han, Q., Dong, W., Wang, H., Ma, H., Liu, P., Gu, Y., Fan, H., and Song, X. (2019). Degradation of tetrabromobisphenol a by ozonation: Performance, products, mechanism and toxicity, *Chemosphere, 235*, 701-712.

Hassan, S. H., Van Ginkel, S. W., Hussein, M. A., Abskharon, R., and Oh, S.-E. (2016). Toxicity assessment using different bioassays and microbial biosensors, *Environment international, 92*, 106-118.

Haworth, S., Lawlor, T., Mortelmans, K., Speck, W., and Zeiger, E. (1983). *Salmonella* mutagenicity test results for 250 chemicals, *Environmental mutagenesis, 5*, 3-49.

Hayat, W., Zhang, Y., Hussain, I., Du, X., Du, M., Yao, C., Huang, S., and Si, F. (2019). Efficient degradation of imidacloprid in water through iron activated sodium persulfate, *Chemical Engineering Journal, 370*, 1169-1180.

Hepperle, J., Dörk, D., Barth, A., Taşdelen, B., and Anastassiades, M. (2015). Studies to improve the extraction yields of incurred pesticide residues from crops using the QuEChERS method, *Journal of the Association of Official Analytical Chemists International, 98*, 450-463.

Hofmann, J., Freier, U., Wecks, M., and Demund, A. (2005). Degradation of halogenated organic compounds in ground water by heterogeneous catalytic oxidation with hydrogen peroxide, *Topics in catalysis, 33*, 243-247.

Hongsawat, P., and Vangnai, A. S. (2011). Biodegradation pathways of chloroanilines by *Acinetobacter baylyi* strain GFJ2, *Journal of Hazardous Materials, 186*, 1300-1307.

Hori, H., Yamamoto, A., Hayakawa, E., Taniyasu, S., Yamashita, N., Kutsuna, S., Kiatagawa, H., and Arakawa, R. (2005). Efficient decomposition of environmentally persistent perfluorocarboxylic acids by use of persulfate as a photochemical oxidant, *Environmental Science and Technology, 39*, 2383-2388.

Hou, S., Ling, L., Shang, C., Guan, Y., and Fang, J. (2017). Degradation kinetics and pathways of haloacetonitriles by the UV/persulfate process, *Chemical Engineering Journal, 320*, 478-484.

Huang, C., Dong, C., and Tang, Z. (1993). Advanced chemical oxidation: its present role and potential future in hazardous waste treatment, *waste management, 13*, 361-377.

Huang, J., Yi, S., Zheng, C., and Lo, I. M. (2019). Persulfate activation by natural zeolite supported nanoscale zero-valent iron for trichloroethylene degradation in groundwater, *Science of the Total Environment, 684*, 351-359.

Huie, R. E., and Clifton, C. L. (1989). Rate constants for hydrogen abstraction reactions of the sulfate radical, $SO_4^{\bullet-}$ Alkanes and ethers, *International Journal of Chemical Kinetics, 21*, 611-619.

Hussain, I., Zhang, Y., and Huang, S. (2014). Degradation of aniline with zero-valent iron as an activator of persulfate in aqueous solution, *The Royal Society of Chemistry Advances, 4*, 3502-3511.

Hussain, I., Zhang, Y., Huang, S., and Du, X. (2012). Degradation of *p*-chloroaniline by persulfate activated with zero-valent iron, *Chemical Engineering Journal, 203*, 269-276.

Hussain, I., Zhang, Y., Li, M., Huang, S., Hayat, W., He, L., Du, X., Liu, G., and Du, M. (2018). Heterogeneously degradation of aniline in aqueous solution using persulfate catalyzed by magnetic $BiFeO_3$ nanoparticles, *Catalysis Today, 310*, 130-140.

Hwang, H. M., Hodson, R., and Lee, R. (1986). Degradation of phenol and chlorophenols by sunlight and microbes in estuarine water, *Environmental Science and Technology, 20*, 1002-1007.

Imai, A., Fukushima, T., Matsushige, K., Kim, Y.-H., and Choi, K. (2002). Characterization of dissolved organic matter in effluents from wastewater treatment plants, *Water research, 36*, 859-870.

Ishikawa, S., Baba, K., Hanada, Y., Uchimura, Y., and Kido, K. (1989). Photodecomposition of o-chloroaniline in aqueous solution with low pressure mercury lamp, *Bulletin of Environmental Contamination and Toxicology, 42*.

ISO 8692 (2012). *Water Quality Freshwater Algal Growth Inhibition Test with Unicellular Green Algae*, ISO, Geneva.

ISO 11348-3 (2007). *Water Quality —Determination of the Inhibitory Effect of Water Samples on the Light Emission of Vibrio fischeri* (*luminescent bacteria test*) Part 3: Method Using Freeze-Dried Bacteria, ISO, Geneva.

ISO 17294-2 (2003). *Water Quality—Application of Inductively Coupled Plasma Mass Spectrometry* (*ICP-MS*)—Part 2: Determination of 62 Elements, ISO, Geneva.

Jaffrezic-Renault, N., and Dzyadevych, S. V. (2008). Conductometric microbiosensors for environmental monitoring, *Sensors, 8*, 2569-2588.

Jeffrey, P., and Koplan, M. (1999). Toxicological Profile for chlorophenols. US Department of Health and Human Services, *Public Health Service Agency for Toxic Substances and Disease Registry*.

Jen, J.-F., Chang, C.-T., and Yang, T. C. (2001). On-line microdialysis–high-performance liquid chromatographic determination of aniline and 2-chloroaniline in polymer industrial wastewater, *Journal of Chromatography A, 930*, 119-125.

Jurado-Sanchez, B., Ballesteros, E., and Gallego, M. (2012). Occurrence of aromatic amines and N-nitrosamines in the different steps of a drinking water treatment plant, *Water research, 46*, 4543-4555.

Kádár, M., Nagy, Z., Karancsi, T., and Farsang, G. (2001). The electrochemical oxidation of 4-chloroaniline, 2,4-dichloroaniline and 2,4,6-trichloroaniline in acetonitrile solution, *Electrochimica acta, 46*, 1297-1306.

Kang, C., Peng, F., Guo, J., Guo, P., and Xue, H. (2009) Degradation of acetic acid by UV/H_2O_2 reaction. Paper presented at the 2009 3rd International Conference on Bioinformatics and Biomedical Engineering, Beijing, China, 11-13 June

Kang, N., Lee, D. S., and Yoon, J. (2002). Kinetic modeling of Fenton oxidation of phenol and monochlorophenols, *Chemosphere, 47*, 915-924.

Kaonga, C., Chidya, R., Kosamu, I., Abdel-Dayem, S., Mapoma, H., Thole, B., Mbewe, R., and Sakugawa, H. (2018). Trends in usage of selected fungicides in Japan between 1962 and 2014: a review, *International Journal of Environmental Science and Technology, 15*, 1801-1814.

Karci, A. (2014). Degradation of chlorophenols and alkylphenol ethoxylates, two representative textile chemicals, in water by advanced oxidation processes: the state of the art on transformation products and toxicity, *Chemosphere, 99*, 1-18.

Karci, A., Arslan-Alaton, I., and Bekbolet, M. (2013a). Advanced oxidation of a commercially important nonionic surfactant: Investigation of degradation products and toxicity, *Journal of Hazardous Materials, 263*, 275-282.

Karci, A., Arslan-Alaton, I., Olmez-Hanci, T., and Bekbolet, M. (2013b). Degradation and detoxification of industrially important phenol derivatives in water by direct UV-C photolysis and H_2O_2/UV-C process: a comparative study, *Chemical Engineering Journal, 224*, 4-9.

Karci, A., Arslan-Alaton, I., Olmez-Hanci, T., and Bekbölet, M. (2012). Transformation of 2,4-dichlorophenol by H_2O_2/UV-C, Fenton and photo-Fenton processes: oxidation products and toxicity evolution, *Journal of Photochemistry and Photobiology A: Chemistry, 230*, 65-73.

Katsumata, H., Oda, Y., Kaneco, S., Suzuki, T., and Ohta, K. (2012). Determination of aniline derivatives in water samples after preconcentration with oxidized multiwalled carbon nanotubes as solid-phase extraction disk, *Frontiers of Chemical Science and Engineering, 6*, 270-275.

Khan, S., Sohail, M., Han, C., Khan, J. A., Khan, H. M., and Dionysiou, D. D. (2020). Degradation of highly chlorinated pesticide, lindane, in water using UV/persulfate: kinetics and mechanism, toxicity evaluation, and synergism by H_2O_2, *Journal of Hazardous Materials, 402*, 123558.

Khatri, J., Nidheesh, P., Singh, T. A., and Kumar, M. S. (2018). Advanced oxidation processes based on zero-valent aluminium for treating textile wastewater, *Chemical Engineering Journal, 348*, 67-73.

Kilemade, M., and Mothersill, C. (2000). An in vitro assessment of the toxicity of 2,4-dichloroaniline using rainbow trout primary epidermal cell cultures, *Environmental Toxicology and Chemistry: An International Journal, 19*, 2093-2099.

Kim, C., Ahn, J.-Y., Kim, T. Y., Shin, W. S., and Hwang, I. (2018). Activation of persulfate by nanosized zero-valent iron (NZVI): mechanisms and transformation products of NZVI, *Environmental Science and Technology, 52*, 3625-3633.

Kimura, Z.-i., Hirano, Y., Matsuzawa, Y., and Hiraishi, A. (2016). Effects of 3,5-dichlorophenol on excess biomass reduction and bacterial community dynamics in activated sludge as revealed by a polyphasic approach, *Journal of bioscience and bioengineering, 122*, 467-474.

Koenig, C. M., Beevers, C., Pant, K., and Young, R. R. (2018). Assessment of the mutagenic potential of *para*-chloroaniline and aniline in the liver, spleen, and bone marrow of Big Blue[®] rats with micronuclei analysis in peripheral blood, *Environmental and molecular mutagenesis, 59*, 785-797.

Kolthoff, I., and Miller, I. (1951). The chemistry of persulfate. I. The kinetics and mechanism of the decomposition of the persulfate ion in aqueous medium1, *Journal of the American Chemical Society, 73*, 3055-3059.

Könnecker, G., Boehncke, A., and Schmidt, S. (2003). Ecotoxicological assessment of *p*-chloroaniline- Fate and effects in aquatic systems, *Fresenius Environmental Bulletin, 12*, 589-593.

Krebel, M., Kusic, H., Koprivanac, N., Meixner, J., and Bozic, A. L. (2011). Treatment of chlorophenols by UV-based processes: correlation of oxidation by-products, wastewater parameters, and toxicity, *Journal of Environmental Engineering, 137*, 639-649.

Kreuger, J. (1998). Pesticides in stream water within an agricultural catchment in southern Sweden, 1990–1996, *Science of the Total Environment, 216*, 227-251.

Kronholm, J., Jyske, P., and Riekkola, M.-L. (2000). Oxidation efficiencies of potassium persulfate and hydrogen peroxide in pressurized hot water with and without preheating, *Industrial and Engineering Chemistry Research, 39*, 2207-2213.

Kucharska, M., and Naumczyk, J. (2009). Degradation of selected chlorophenols by advanced oxidation processes, *Environment Protection Engineering, 35*, 47-55.

Kumar, A., and Mathur, N. (2006). Photocatalytic degradation of aniline at the interface of TiO_2 suspensions containing carbonate ions, *Journal of colloid and interface science, 300*, 244-252.

Lacorte, S. l., Perrot, M.-C., Fraisse, D., and Barceló, D. (1999). Determination of chlorobenzidines in industrial effluent by solid-phase extraction and liquid chromatography with electrochemical and mass spectrometric detection, *Journal of Chromatography A, 833*, 181-194.

Lassalle, Y., Jellouli, H., Ballerini, L., Souissi, Y., Nicol, É., Bourcier, S., and Bouchonnet, S. (2014). Ultraviolet–vis degradation of iprodione and estimation of the acute toxicity of its photodegradation products, *Journal of Chromatography A, 1371*, 146-153.

Latorre, J., Reineke, W., and Knackmuss, H.-J. (1984). Microbial metabolism of chloroanilines: enhanced evolution by natural genetic exchange, *Archives of microbiology, 140*, 159-165.

Lau, T. K., Chu, W., and Graham, N. J. (2007). The aqueous degradation of butylated hydroxyanisole by $UV/S_2O_8^{2-}$: study of reaction mechanisms via dimerization and mineralization, *Environmental Science and Technology, 41*, 613-619.

Lee, Y.-M., Lee, G., and Zoh, K.-D. (2021). Benzophenone-3 degradation via UV/H_2O_2 and UV/persulfate reactions, *Journal of Hazardous Materials, 403*, 123591.

Lente, G., and Espenson, J. H. (2004). A kinetic study of the early steps in the oxidation of chlorophenols by hydrogen peroxide catalyzed by a water-soluble iron (III) porphyrin, *New Journal of Chemistry, 28*, 847-852.

Leyva, E., Crispin, I., Moctezuma, E., and Leyva, S. (2003). Selective chemical oxidation or reduction of chlorophenols with potassium nitrosodisulfonate, *Arkivoc, 11*, 203-212.

Li, H., Wan, J., Ma, Y., Huang, M., Wang, Y., and Chen, Y. (2014a). New insights into the role of zero-valent iron surface oxidation layers in persulfate oxidation of dibutyl phthalate solutions, *Chemical Engineering Journal, 250*, 137-147.

Li, H., Wan, J., Ma, Y., Wang, Y., and Huang, M. (2014b). Influence of particle size of zero-valent iron and dissolved silica on the reactivity of activated persulfate for degradation of acid orange 7, *Chemical Engineering Journal, 237*, 487-496.

Li, R., Gao, Y., Jin, X., Chen, Z., Megharaj, M., and Naidu, R. (2015a). Fenton-like oxidation of 2,4-DCP in aqueous solution using iron-based nanoparticles as the heterogeneous catalyst, *Journal of colloid and interface science, 438*, 87-93.

Li, R., Jin, X., Megharaj, M., Naidu, R., and Chen, Z. (2015b). Heterogeneous Fenton oxidation of 2,4-dichlorophenol using iron-based nanoparticles and persulfate system, *Chemical Engineering Journal, 264*, 587-594.

Li, R., Kong, J., Liu, H., Chen, P., Su, Y., Liu, G., and Lv, W. (2018). Removal of indomethacin using UV–vis/peroxydisulfate: kinetics, toxicity, and transformation pathways, *Chemical Engineering Journal, 331*, 809-817.

Li, X., Zhou, M., Pan, Y., and Xu, L. (2017). Pre-magnetized Fe^0/persulfate for notably enhanced degradation and dechlorination of 2,4-dichlorophenol, *Chemical Engineering Journal, 307*, 1092-1104.

Liang, C., and Guo, Y.-y. (2010). Mass transfer and chemical oxidation of naphthalene particles with zerovalent iron activated persulfate, *Environmental Science and Technology, 44*, 8203-8208.

Liang, C., and Lai, M.-C. (2008). Trichloroethylene degradation by zero valent iron activated persulfate oxidation, *Environmental Engineering Science, 25*, 1071-1078.

Liang, C., Lin, Y.-T., and Shin, W.-H. (2009). Persulfate regeneration of trichloroethylene spent activated carbon, *Journal of Hazardous Materials, 168*, 187-192.

Liang, C., and Su, H.-W. (2009). Identification of sulfate and hydroxyl radicals in thermally activated persulfate, *Industrial and Engineering Chemistry Research, 48*, 5558-5562.

Liang, C., Wang, Z.-S., and Bruell, C. J. (2007). Influence of pH on persulfate oxidation of TCE at ambient temperatures, *Chemosphere, 66*, 106-113.

Liang, H.-y., Zhang, Y.-q., Huang, S.-b., and Hussain, I. (2013). Oxidative degradation of *p*-chloroaniline by copper oxidate activated persulfate, *Chemical Engineering Journal, 218*, 384-391.

Lin, C.-C., and Chen, Y.-H. (2018). Feasibility of using nanoscale zero-valent iron and persulfate to degrade sulfamethazine in aqueous solutions, *Separation and Purification Technology, 194*, 388-395.

Lin, Y.-T., Liang, C., and Chen, J.-H. (2011). Feasibility study of ultraviolet activated persulfate oxidation of phenol, *Chemosphere, 82*, 1168-1172.

Liu, J., Zhao, Z., Shao, P., and Cui, F. (2015). Activation of peroxymonosulfate with magnetic Fe_3O_4–MnO_2 core–shell nanocomposites for 4-chlorophenol degradation, *Chemical Engineering Journal, 262*, 854-861.

Liu, W., Zhang, H., Cao, B., Lin, K., and Gan, J. (2011). Oxidative removal of bisphenol A using zero valent aluminum–acid system, *Water research, 45*, 1872-1878.

Liu, Y., He, X., Fu, Y., and Dionysiou, D. D. (2016). Kinetics and mechanism investigation on the destruction of oxytetracycline by UV-254 nm activation of persulfate, *Journal of Hazardous Materials, 305*, 229-239.

Lominchar, M. A., Rodríguez, S., Lorenzo, D., Santos, N., Romero, A., and Santos, A. (2018). Phenol abatement using persulfate activated by nZVI, H_2O_2 and NaOH and development of a kinetic model for alkaline activation, *Environmental technology, 39*, 35-43.

Lopez-Alvarez, B., Villegas-Guzman, P., Peñuela, G. A., and Torres-Palma, R. A. (2016). Degradation of a toxic mixture of the pesticides carbofuran and iprodione by UV/H$_2$O$_2$: evaluation of parameters and implications of the degradation pathways on the synergistic effects, *Water, Air, and Soil Pollution, 227*, 215.

Loutfy, N., Malhat, F., Kamel, E., and Saber, A. (2015). Residual pattern and dietary intake of iprodione on grapes under Egyptian field conditions: A prelude to risk assessment profile, *Human and Ecological Risk Assessment: An International Journal, 21*, 265-279.

Lu, X., Shao, Y., Gao, N., Chen, J., Zhang, Y., Xiang, H., and Guo, Y. (2017). Degradation of diclofenac by UV-activated persulfate process: Kinetic studies, degradation pathways and toxicity assessments, *Ecotoxicology and Environmental Safety, 141*, 139-147.

Luo, S., Wei, Z., Dionysiou, D. D., Spinney, R., Hu, W.-P., Chai, L., Yang, Z., Ye, T., and Xiao, R. (2017). Mechanistic insight into reactivity of sulfate radical with aromatic contaminants through single-electron transfer pathway, *Chemical Engineering Journal, 327*, 1056-1065.

Luo, T., Wan, J., Ma, Y., Wang, Y., and Wan, Y. (2019). Sulfamethoxazole degradation by an Fe (II)-activated persulfate process: insight into the reactive sites, product identification and degradation pathways, *Environmental Science: Processes and Impacts, 21*, 1560-1569.

Luo, Y., Guo, W., Ngo, H. H., Nghiem, L. D., Hai, F. I., Zhang, J., Liang, S., and Wang, X. C. (2014). A review on the occurrence of micropollutants in the aquatic environment and their fate and removal during wastewater treatment, *Science of the Total Environment, 473*, 619-641.

Lutze, H. V., Kerlin, N., and Schmidt, T. C. (2015). Sulfate radical-based water treatment in presence of chloride: formation of chlorate, inter-conversion of sulfate radicals into hydroxyl radicals and influence of bicarbonate, *Water research, 72*, 349-360.

Mahdi-Ahmed, M., and Chiron, S. (2014). Ciprofloxacin oxidation by UV-C activated peroxymonosulfate in wastewater, *Journal of Hazardous Materials, 265*, 41-46.

Mailhot, G., Hykrdová, L., Jirkovský, J. r., Lemr, K., Grabner, G., and Bolte, M. (2004). Iron (III)-photoinduced degradation of 4-chloroaniline in aqueous solution, *Applied Catalysis B: Environmental, 50*, 25-35.

McCarty, P. L. (1980). Organics in water—an engineering challenge, *Journal of the Environmental Engineering Division, 106*, 1-17.

Meinero, S., and Zerbinati, O. (2006). Oxidative and energetic efficiency of different electrochemical oxidation processes for chloroanilines abatement in aqueous medium, *Chemosphere, 64*, 386-392.

Messele, S. A., Bengoa, C., Stüber, F. E., Giralt, J., Fortuny, A., Fabregat, A., and Font, J. (2019). Enhanced degradation of phenol by a fenton-like system (Fe/EDTA/H$_2$O$_2$) at circumneutral pH, *Catalysts, 9*, 474.

Meusel, M., and Gütschow, M. (2004). Recent developments in hydantoin chemistry. A review, *Organic preparations and procedures international, 36*, 391-443.

Meylan, W. M., and Howard, P. H. (1991). Bond contribution method for estimating Henry's law constants, *Environmental Toxicology and Chemistry: An International Journal, 10*, 1283-1293.

Mico, M. M., Chourdaki, S., Bacardit, J., and Sans, C. (2010). Comparison between ozonation and photo-fenton processes for pesticide methomyl removal in advanced greenhouses, *Ozone: Science and Engineering, 32*, 259-264.

Miklos, D. B., Remy, C., Jekel, M., Linden, K. G., Drewes, J. E., and Hübner, U. (2018). Evaluation of advanced oxidation processes for water and wastewater treatment–A critical review, *Water research, 139*, 118-131.

Miller, G. C., Zisook, R., and Zepp, R. (1980). Photolysis of 3,4-dichloroaniline in natural waters, *Journal of agricultural and food chemistry, 28*, 1053-1056.

Miñambres, G. G., Conles, M. Y., Lucini, E. I., Verdenelli, R. A., Meriles, J. M., and Zygadlo, J. A. (2010). Application of thymol and iprodione to control garlic white rot (*Sclerotium cepivorum*) and its effect on soil microbial communities, *World Journal of Microbiology and Biotechnology, 26*, 161.

Minière, M., Boutin, O., and Soric, A. (2018). Evaluation of degradation and kinetics parameters of acid orange 7 through wet air oxidation process, *The Canadian Journal of Chemical Engineering, 96*, 2450-2454.

Ministry of Agriculture and Forestry (2018). Official list of banned active substances, Republic of Turkey Ministry of Agriculture and Forestry, Ankara.

Mirzaei, A., Chen, Z., Haghighat, F., and Yerushalmi, L. (2017). Removal of pharmaceuticals from water by homo/heterogonous Fenton-type processes–A review, *Chemosphere, 174*, 665-688.

Mitchell, S. M., Ullman, J. L., Teel, A. L., Watts, R. J., and Frear, C. (2013). The effects of the antibiotics ampicillin, florfenicol, sulfamethazine, and tylosin on biogas production and their degradation efficiency during anaerobic digestion, *Bioresource technology, 149*, 244-252.

Molkenthin, M., Olmez-Hanci, T., Jekel, M. R., and Arslan-Alaton, I. (2013). Photo-Fenton-like treatment of BPA: effect of UV light source and water matrix on toxicity and transformation products, *Water research, 47*, 5052-5064.

Mortelmans, K., and Zeiger, E. (2000). The Ames *Salmonella*/microsome mutagenicity assay, *Mutation research/fundamental and molecular mechanisms of mutagenesis, 455*, 29-60.

Muneer, M., Kanjal, M. I., Saeed, M., Javed, T., Haq, A. U., Den, N. Z. U., Jamal, M. A., Ali, S., and Iqbal, M. (2020). High energy radiation induced degradation of reactive yellow 145 dye: A mechanistic study, *Radiation Physics and Chemistry,*109115.

Neamtu, M., Yediler, A., Siminiceanu, I., Macoveanu, M., and Kettrup, A. (2004). Decolorization of disperse red 354 azo dye in water by several oxidation processes—a comparative study, *Dyes and pigments, 60*, 61-68.

Neta, P., Huie, R. E., and Ross, A. B. (1988). Rate constants for reactions of inorganic radicals in aqueous solution, *Journal of physical and chemical reference data, 17*, 1027-1284.

Neta, P., Madhavan, V., Zemel, H., and Fessenden, R. W. (1977). Rate constants and mechanism of reaction of sulfate radical anion with aromatic compounds, *Journal of the American Chemical Society, 99*, 163-164.

Nidheesh, P., Khatri, J., Singh, T. A., Gandhimathi, R., and Ramesh, S. (2018). Review of zero-valent aluminium based water and wastewater treatment methods, *Chemosphere, 200*, 621-631.

Nie, M., Yan, C., Li, M., Wang, X., Bi, W., and Dong, W. (2015). Degradation of chloramphenicol by persulfate activated by Fe^{2+} and zerovalent iron, *Chemical Engineering Journal, 279*, 507-515.

Nitoi, I., Oancea, P., Cristea, I., Constsntin, L., and Nechifor, G. (2015). Kinetics and mechanism of chlorinated aniline degradation by TiO_2 photocatalysis, *Journal of Photochemistry and Photobiology A: Chemistry, 298*, 17-23.

O'Neill, P., Steenken, S., and Schulte-Frohlinde, D. (1975). Formation of radical cations of methoxylated benzenes by reaction with OH radicals, Ti^{2+}, Ag^{2+}, and $SO_4^{\bullet-}$ in aqueous solution. An optical and conductometric pulse radiolysis and in situ radiolysis electron spin resonance study, *Journal of Physical Chemistry, 79*, 2773-2779.

Oh, S.-Y., Kang, S.-G., and Chiu, P. C. (2010). Degradation of 2,4-dinitrotoluene by persulfate activated with zero-valent iron, *Science of the Total Environment, 408*, 3464-3468.

Oh, S.-Y., Kim, H.-W., Park, J.-M., Park, H.-S., and Yoon, C. (2009). Oxidation of polyvinyl alcohol by persulfate activated with heat, Fe^{2+}, and zero-valent iron, *Journal of Hazardous Materials, 168*, 346-351.

Oller, I., Malato, S., and Sánchez-Pérez, J. (2011). Combination of advanced oxidation processes and biological treatments for wastewater decontamination—a review, *Science of the Total Environment, 409*, 4141-4166.

Olmez-Hanci, T., and Arslan-Alaton, I. (2013). Comparison of sulfate and hydroxyl radical based advanced oxidation of phenol, *Chemical Engineering Journal, 224*, 10-16.

Olmez-Hanci, T., Arslan-Alaton, I., and Basar, G. (2011). Multivariate analysis of anionic, cationic and nonionic textile surfactant degradation with the H_2O_2/UV-C process by using the capabilities of response surface methodology, *Journal of Hazardous Materials, 185*, 193-203.

Olmez-Hanci, T., Arslan-Alaton, I., and Dursun, D. (2014a). Investigation of the toxicity of common oxidants used in advanced oxidation processes and their quenching agents, *Journal of Hazardous Materials, 278*, 330-335.

Olmez-Hanci, T., Arslan-Alaton, I., and Genc, B. (2014b). Degradation of the nonionic surfactant Triton™ X-45 with $HO^{\bullet}$ and $SO_4^{\bullet-}$–based advanced oxidation processes, *Chemical Engineering Journal, 239*, 332-340.

Olmez-Hanci, T., Dalmaz, B., Arslan-Alaton, I., Kabdaşlı, I., and Tünay, O. (2010). Kinetic modeling and toxicity assessment of diethyl phthalate treated by H_2O_2/UV-C process, *Ozone: Science and Engineering, 32*, 238-243.

Omirou, M., Vryzas, Z., Papadopoulou-Mourkidou, E., and Economou, A. (2009). Dissipation rates of iprodione and thiacloprid during tomato production in greenhouse, *Food Chemistry, 116*, 499-504.

Othmen, K., and Boule, P. (1999). Photochemical behaviour of dichloroanilines in water and formation of aminochlorophenoxazones, *Journal of Photochemistry and Photobiology A: Chemistry, 121*, 161-167.

Othmen, K., Boule, P., Szczepanik, B., Rotkiewicz, K., and Grabner, G. (2000). Photochemistry of 4-chloroaniline in solution. Formation and kinetic properties of a new carbene, 4-iminocyclohexa-2,5-dienylidene, *The Journal of Physical Chemistry A, 104*, 9525-9534.

Paasivirta, J., Heinola, K., Humppi, T., Karjalainen, A., Knuutinen, J., Mäntykoski, K., Paukku, R., Piilola, T., Surma-Aho, K., and Tarhanen, J. (1985). Polychlorinated phenols, guaiacols and catechols in environment, *Chemosphere, 14*, 469-491.

Padmanabhan, J., Parthasarathi, R., Subramanian, V., and Chattaraj, P. (2006). Theoretical study on the complete series of chloroanilines, *The Journal of Physical Chemistry A, 110*, 9900-9907.

Pandiyan, T., Rivas, O. M. n., Martínez, J. O., Amezcua, G. B., and Martínez-Carrillo, M. (2002). Comparison of methods for the photochemical degradation of chlorophenols, *Journal of Photochemistry and Photobiology A: Chemistry, 146*, 149-155.

Pang, Y., Zhou, Y., Luo, K., Zhang, Z., Yue, R., Li, X., and Lei, M. (2019). Activation of persulfate by stability-enhanced magnetic graphene oxide for the removal of 2,4-dichlorophenol, *Science of the Total Environment,*135656.

Parvez, S., Venkataraman, C., and Mukherji, S. (2006). A review on advantages of implementing luminescence inhibition test *(Vibrio fischeri)* for acute toxicity prediction of chemicals, *Environment international, 32*, 265-268.

Pascal-Lorber, S., Rathahao, E., Cravedi, J.-p., and Laurent, F. (2003). Uptake and metabolic fate of [^{14}C]-2,4-dichlorophenol and [^{14}C]-2,4-dichloroaniline in wheat (*Triticum aestivum*) and soybean (*Glycine max*), *Journal of agricultural and food chemistry, 51*, 4712-4718.

Pasinszki, T., and Krebsz, M. (2020). Synthesis and application of zero-valent iron nanoparticles in water treatment, environmental remediation, catalysis, and their biological fffects, *Nanomaterials, 10*, 917.

Pera-Titus, M., García-Molina, V., Baños, M. A., Giménez, J., and Esplugas, S. (2004). Degradation of chlorophenols by means of advanced oxidation processes: a general review, *Applied Catalysis B: Environmental, 47*, 219-256.

Pérez-Lucas, G., Aliste, M., Vela, N., Garrido, I., Fenoll, J., and Navarro, S. (2020). Decline of fluroxypyr and triclopyr residues from pure, drinking and leaching water by photo-assisted peroxonation, *Process Safety and Environmental Protection*.

Peternel, I., Koprivanac, N., and Grcic, I. (2012). Mineralization of *p*-chlorophenol in water solution by AOPs based on UV irradiation, *Environmental technology, 33*, 27-36.

Probst, G. S., McMahon, R. E., Hill, L., Thompson, C. Z., Epp, J., and Neal, S. (1981). Chemically-induced unscheduled DNA synthesis in primary rat hepatocyte cultures: A comparison with bacterial mutagenicity using 218 compounds, *Environmental mutagenesis, 3*, 11-32.

Rajeswari, R., and Kanmani, S. (2009). Degradation of pesticide by photocatalytic ozonation process and study of synergistic effect by comparison with photocatalysis and UV/ozonation processes, *Journal of Advanced Oxidation Technologies, 12*, 208-214.

Ratti, M., Canonica, S., McNeill, K., Erickson, P. R., Bolotin, J., and Hofstetter, T. B. (2015). Isotope fractionation associated with the direct photolysis of 4-chloroaniline, *Environmental Science and Technology, 49*, 4263-4273.

Ren, T., Yang, S., Jiang, Y., Sun, X., and Zhang, Y. (2018). Enhancing surface corrosion of zero-valent aluminum (ZVAl) and electron transfer process for the degradation of trichloroethylene with the presence of persulfate, *Chemical Engineering Journal, 348*, 350-360.

Ren, T., Yang, S., Wu, S., Wang, M., and Xue, Y. (2019). High-energy ball milling enhancing the reactivity of microscale zero-valent aluminum toward the activation of persulfate and the degradation of trichloroethylene, *Chemical Engineering Journal, 374*, 100-111.

Rizzo, L. (2011). Bioassays as a tool for evaluating advanced oxidation processes in water and wastewater treatment, *Water research, 45*, 4311-4340.

Rodríguez-Chueca, J., García-Cañibano, C., Lepistö, R.-J., Encinas, Á., Pellinen, J., and Marugán, J. (2019). Intensification of UV-C tertiary treatment: Disinfection and removal of micropollutants by sulfate radical based Advanced Oxidation Processes, *Journal of Hazardous Materials, 372*, 94-102.

Rodríguez-Delgado, M., Orona-Navar, C., García-Morales, R., Hernandez-Luna, C., Parra, R., Mahlknecht, J., and Ornelas-Soto, N. (2016). Biotransformation kinetics of pharmaceutical and industrial micropollutants in groundwaters by a laccase cocktail from *Pycnoporus sanguineus* CS43 fungi, *International Biodeterioration and Biodegradation, 108*, 34-41.

Rodriguez, I., Turnes, M., Mejuto, M., and Cela, R. (1996). Determination of chlorophenols at the sub-ppb level in tap water using derivatization, solid-phase extraction and gas chromatography with plasma atomic emission detection, *Journal of Chromatography A, 721*, 297-304.

Rodriguez, S., Vasquez, L., Costa, D., Romero, A., and Santos, A. (2014). Oxidation of Orange G by persulfate activated by Fe (II), Fe (III) and zero valent iron (ZVI), *Chemosphere, 101*, 86-92.

Sadick, M. (2002). Understanding the puzzle of 'well-characterized biotechnology products', *Current opinion in biotechnology, 13*, 275-278.

Santaballa, J., and Vulliet, E. (2005). On the mechanism of TiO_2-photocatalyzed degradation of aniline derivatives, *Journal of Photochemistry and Photobiology A: Chemistry, 175*, 192-200.

Schafers, C., and Nagel, R. (1991). Effects of 3,4-dichloroaniline on fish populations. Comparison between r-and K-strategists: a complete life cycle test with the guppy (*Poecilia reticulata*), *Archives of Environmental Contamination and Toxicology, 21*, 297-302.

Schwack, W., and Bourgeois, B. (1989). Fungicides and photochemistry: Iprodione, procymidone, vinclozolin 1. Photodehalogenation, *Zeitschrift für Lebensmittel-Untersuchung und Forschung, 188*, 346-347.

Schwack, W., Bourgeois, B., and Walker, F. (1995). Fungicides and photochemistry photodegradation of the dicarboximide fungicide iprodione, *Chemosphere, 31*, 2993-3000.

Schwarzenbach, R. P., Escher, B. I., Fenner, K., Hofstetter, T. B., Johnson, C. A., Von Gunten, U., and Wehrli, B. (2006). The challenge of micropollutants in aquatic systems, *Science, 313*, 1072-1077.

Sequinatto, L., Reichert, J. M., Santos, D. R. d., Reinert, D. J., and Copetti, A. C. C. (2013). Occurrence of agrochemicals in surface waters of shallow soils and steep slopes cropped to tobacco, *Química Nova, 36*, 768-772.

Sharma, A., Ahmad, J., and Flora, S. (2018). Application of advanced oxidation processes and toxicity assessment of transformation products, *Environmental research, 167*, 223-233.

Sharma, J., Mishra, I., Dionysiou, D. D., and Kumar, V. (2015). Oxidative removal of Bisphenol A by UV-C/peroxymonosulfate (PMS): kinetics, influence of co-existing chemicals and degradation pathway, *Chemical Engineering Journal, 276*, 193-204.

Shimizu, T. (1986). Studies on the use of hydantoin-related compounds as slow release fertilizers, *Soil Science and Plant Nutrition, 32*, 373-382.

Sithole, B. B., and Williams, D. T. (1986). Halogenated phenols in water at forty Canadian potable water treatment facilities, *Journal of the Association of Official Analytical Chemists, 69*, 807-810.

Skoumal, M., Arias, C., Cabot, P. L., Centellas, F., Garrido, J. A., Rodríguez, R. M., and Brillas, E. (2008). Mineralization of the biocide chloroxylenol by electrochemical advanced oxidation processes, *Chemosphere, 71*, 1718-1729.

Smith, J. H., Bomberger, D. C., and Haynes, D. L. (1980). Prediction of the volatilization rates of high-volatility chemicals from natural water bodies, *Environmental Science and Technology, 14*, 1332-1337.

Song, B., Zeng, G., Gong, J., Liang, J., Xu, P., Liu, Z., Zhang, Y., Zhang, C., Cheng, M., and Liu, Y. (2017). Evaluation methods for assessing effectiveness of in situ remediation of soil and sediment contaminated with organic pollutants and heavy metals, *Environment international, 105*, 43-55.

St-Jean, G. (2003). Automated quantitative and isotopic (^{13}C) analysis of dissolved inorganic carbon and dissolved organic carbon in continuous-flow using a total organic carbon analyser, *Rapid communications in mass spectrometry, 17*, 419-428.

Stacy, T., and Latin, R. (2020). The influence of water pH on efficacy of fungicides for turf disease control, *Crop, Forage and Turfgrass Management, 6*, 20007.

Stamatis, N., Hela, D., and Konstantinou, I. (2010). Occurrence and removal of fungicides in municipal sewage treatment plant, *Journal of Hazardous Materials, 175*, 829-835.

Starling, M. C. V., Souza, P. P., Le Person, A., Amorim, C. C., and Criquet, J. (2019). Intensification of UV-C treatment to remove emerging contaminants by UV-C/H_2O_2 and UV-C/$S_2O_8^{2-}$: Susceptibility to photolysis and investigation of acute toxicity, *Chemical Engineering Journal, 376*, 120856.

Stolper, P., Fabel, S., Weller, M. G., Knopp, D., and Niessner, R. (2008). Whole-cell luminescence-based flow-through biodetector for toxicity testing, *Analytical and bioanalytical chemistry, 390*, 1181-1187.

Strömqvist, J., and Jarvis, N. (2005). Sorption, degradation and leaching of the fungicide iprodione in a golf green under Scandinavian conditions: measurements, modelling and risk assessment, *Pest Management Science, 61*, 1168-1178.

Tan, C., Gao, N., Deng, Y., An, N., and Deng, J. (2012). Heat-activated persulfate oxidation of diuron in water, *Chemical Engineering Journal, 203*, 294-300.

Tan, C., Gao, N., Deng, Y., Zhang, Y., Sui, M., Deng, J., and Zhou, S. (2013). Degradation of antipyrine by UV, UV/H_2O_2 and UV/PS, *Journal of Hazardous Materials, 260*, 1008-1016.

Temiz, K., Olmez-Hanci, T., and Arslan-Alaton, I. (2016). Zero-valent iron-activated persulfate oxidation of a commercial alkyl phenol polyethoxylate, *Environmental technology, 37*, 1757-1767.

Thavasi, V., Bettens, R. P. A., and Leong, L. P. (2009). Temperature and solvent effects on radical scavenging ability of phenols, *The Journal of Physical Chemistry A, 113*, 3068-3077.

Tian, N., Tian, X., Nie, Y., Yang, C., Zhou, Z., and Li, Y. (2019). Enhanced 2,4-dichlorophenol degradation at pH 3–11 by peroxymonosulfate via controlling the reactive oxygen species over Ce substituted 3D Mn_2O_3, *Chemical Engineering Journal, 355*, 448-456.

Trapido, M., Hirvonen, A., Veressinina, Y., Hentunen, J., and Munter, R. (1997). Ozonation, ozone/UV and UV/H_2O_2 degradation of chlorophenols, *Ozone: Science and Engineering, 19*, 75-96.

Trapp, S., Zambrano, K. C., Kusk, K. O., and Karlson, U. (2000). A phytotoxicity test using transpiration of willows, *Archives of Environmental Contamination and Toxicology, 39*, 154-160.

Tufail, A., Price, W. E., and Hai, F. I. (2020). A critical review on advanced oxidation processes for the removal of trace organic contaminants: A voyage from individual to integrated processes, *Chemosphere, 260*, 127460.

Tugcu, G., Ertürk, M. D., and Saçan, M. T. (2017). On the aquatic toxicity of substituted phenols to Chlorella vulgaris: QSTR with an extended novel data set and interspecies models, *Journal of Hazardous Materials, 339*, 122-130.

US EPA (1998). Reregistration Eligibility Document for Iprodione LB, Case 2335, US EPA, Washington DC.

Valentovic, M., Ball, J., Anestis, D., and Rankin, G. (1995). Comparison of the *in vitro* toxicity of dichloroaniline structural isomers, *Toxicology in vitro, 9*, 75-81.

Villegas, E., Pomeranz, Y., and Shellenberger, J. (1963). Colorimetric determination of persulfate with alcian blue, *Analytica Chimica Acta, 29*, 145-148.

Villemur, R. (2013). The pentachlorophenol-dehalogenating *Desulfitobacterium hafniense strain* PCP-1, *Philosophical Transactions of the Royal Society B: Biological Sciences, 368*, 20120319.

Wacławek, S., Lutze, H. V., Grübel, K., Padil, V. V., Černík, M., and Dionysiou, D. D. (2017). Chemistry of persulfates in water and wastewater treatment: a review, *Chemical Engineering Journal, 330*, 44-62.

Wang, J., and Wang, S. (2018). Activation of persulfate (PS) and peroxymonosulfate (PMS) and application for the degradation of emerging contaminants, *Chemical Engineering Journal, 334*, 1502-1517.

Wang, J., and Zhuan, R. (2020). Degradation of antibiotics by advanced oxidation processes: an overview, *Science of the Total Environment, 701*, 135023.

Wang, J. L., and Xu, L. J. (2012). Advanced oxidation processes for wastewater treatment: formation of hydroxyl radical and application, *Critical Reviews in Environmental Science and Technology, 42*, 251-325.

Wang, Q., Shao, Y., Gao, N., Chu, W., Shen, X., Lu, X., Chen, J., and Zhu, Y. (2016). Degradation kinetics and mechanism of 2,4-Di-tert-butylphenol with UV/persulfate, *Chemical Engineering Journal, 304*, 201-208.

Wang, Y., Chen, S.-y., Yang, X., Huang, X.-f., Yang, Y.-h., He, E.-k., Wang, S., and Qiu, R.-l. (2017). Degradation of 2,2′,4,4′-tetrabromodiphenyl ether (BDE-47) by a nano zerovalent iron-activated persulfate process: the effect of metal ions, *Chemical Engineering Journal, 317*, 613-622.

Wegman, R., and De Korte, G. (1981). Aromatic amines in surface waters of the Netherlands, *Water research, 15*, 391-394.

Węgrzyn, G., and Czyż, A. (2003). Detection of mutagenic pollution of natural environment using microbiological assays, *Journal of applied microbiology, 95*, 1175-1181.

Wei, X., Gao, N., Li, C., Deng, Y., Zhou, S., and Li, L. (2016). Zero-valent iron (ZVI) activation of persulfate (PS) for oxidation of bentazon in water, *Chemical Engineering Journal, 285*, 660-670.

Weng, C.-H., and Tao, H. (2018). Highly efficient persulfate oxidation process activated with Fe^0 aggregate for decolorization of reactive azo dye Remazol Golden Yellow, *Arabian journal of chemistry, 11*, 1292-1300.

Weng, C.-H., and Tsai, K.-L. (2016). Ultrasound and heat enhanced persulfate oxidation activated with Fe^0 aggregate for the decolorization of CI Direct Red 23, *Ultrasonics sonochemistry, 29*, 11-18.

Winarno, E. K., and Getoff, N. (2002a). Comparative studies on the degradation of aqueous 2-chloroaniline by O_3 as well as by UV-light and γ-rays in the presence of ozone, *Radiation Physics and Chemistry, 65*, 387-395.

Winarno, E. K., and Getoff, N. (2002b). Photo-induced decomposition of 2-chloroaniline in aqueous solution, *Zeitschrift für Naturforschung C, 57*, 512-515.

Wittke, K., Hajimiragha, H., Dunemann, L., and Begerow, J. (2001). Determination of dichloroanilines in human urine by GC–MS, GC–MS–MS, and GC–ECD as markers of low-level pesticide exposure, *Journal of Chromatography B: Biomedical Sciences and Applications, 755*, 215-228.

Wu, J., Wang, B., Cagnetta, G., Huang, J., Wang, Y., Deng, S., and Yu, G. (2020). Nanoscale zero valent iron-activated persulfate coupled with Fenton oxidation process for typical pharmaceuticals and personal care products degradation, *Separation and Purification Technology, 239*, 116534.

Wu, S., He, H., Li, X., Yang, C., Zeng, G., Wu, B., He, S., and Lu, L. (2018). Insights into atrazine degradation by persulfate activation using composite of nanoscale zero-valent iron and graphene: Performances and mechanisms, *Chemical Engineering Journal, 341*, 126-136.

Xiao, R., Luo, Z., Wei, Z., Luo, S., Spinney, R., Yang, W., and Dionysiou, D. D. (2018). Activation of peroxymonosulfate/persulfate by nanomaterials for sulfate radical-based advanced oxidation technologies, *Current opinion in chemical engineering, 19*, 51-58.

Xiao, S., Cheng, M., Zhong, H., Liu, Z., Liu, Y., Yang, X., and Liang, Q. (2020). Iron-mediated activation of persulfate and peroxymonosulfate in both homogeneous and heterogeneous ways: a review, *Chemical Engineering Journal, 384*, 123265.

Xie, L., Gomes, T., Solhaug, K. A., Song, Y., and Tollefsen, K. E. (2018). Linking mode of action of the model respiratory and photosynthesis uncoupler 3,5-dichlorophenol to adverse outcomes in *Lemna minor*, *Aquatic Toxicology, 197*, 98-108.

Xie, P., Ma, J., Liu, W., Zou, J., Yue, S., Li, X., Wiesner, M. R., and Fang, J. (2015). Removal of 2-MIB and geosmin using UV/persulfate: contributions of hydroxyl and sulfate radicals, *Water research, 69*, 223-233.

Xiong, X., Sun, B., Zhang, J., Gao, N., Shen, J., Li, J., and Guan, X. (2014). Activating persulfate by Fe^0 coupling with weak magnetic field: performance and mechanism, *Water research, 62*, 53-62.

Xu, M., Deng, J., Cai, A., Ma, X., Li, J., Li, Q., and Li, X. (2020a). Comparison of UVC and UVC/persulfate processes for tetracycline removal in water, *Chemical Engineering Journal, 384*, 123320.

Xu, M., Deng, J., Cai, A., Ye, C., Ma, X., Li, Q., Zhou, S., and Li, X. (2020b). Synergistic effects of UVC and oxidants (PS vs. Chlorine) on carbamazepine attenuation: Mechanism, pathways, DBPs yield and toxicity assessment, *Chemical Engineering Journal,*127533.

Xu, Y., Lin, Z., and Zhang, H. (2016). Mineralization of sucralose by UV-based advanced oxidation processes: UV/PDS versus UV/H$_2$O$_2$, *Chemical Engineering Journal, 285*, 392-401.

Yan, J., Lei, M., Zhu, L., Anjum, M. N., Zou, J., and Tang, H. (2011). Degradation of sulfamonomethoxine with Fe$_3$O$_4$ magnetic nanoparticles as heterogeneous activator of persulfate, *Journal of Hazardous Materials, 186*, 1398-1404.

Yang, Q., Ma, Y., Chen, F., Yao, F., Sun, J., Wang, S., Yi, K., Hou, L., Li, X., and Wang, D. (2019). Recent advances in photo-activated sulfate radical-advanced oxidation process (SR-AOP) for refractory organic pollutants removal in water, *Chemical Engineering Journal, 378*, 122149.

Yang, S., Wang, P., Yang, X., Shan, L., Zhang, W., Shao, X., and Niu, R. (2010). Degradation efficiencies of azo dye Acid Orange 7 by the interaction of heat, UV and anions with common oxidants: persulfate, peroxymonosulfate and hydrogen peroxide, *Journal of Hazardous Materials, 179*, 552-558.

Yang, Y., Lu, X., Jiang, J., Ma, J., Liu, G., Cao, Y., Liu, W., Li, J., Pang, S., and Kong, X. (2017). Degradation of sulfamethoxazole by UV, UV/H$_2$O$_2$ and UV/persulfate (PDS): formation of oxidation products and effect of bicarbonate, *Water research, 118*, 196-207.

Yangin-Gomec, C., Olmez-Hanci, T., Arslan-Alaton, I., Khoei, S., and Fakhri, H. (2018). Iopamidol degradation with ZVI-and ZVA-activated chemical oxidation: Investigation of toxicity, anaerobic inhibition and microbial communities, *Journal of environmental chemical engineering, 6*, 7318-7326.

Yao, C., Zhang, Y., Du, M., Du, X., and Huang, S. (2019). Insights into the mechanism of non-radical activation of persulfate via activated carbon for the degradation of *p*-chloroaniline, *Chemical Engineering Journal, 362*, 262-268.

Yeber, M. C., Díaz, L., and Fernández, J. (2010). Catalytic activity of the SO$_4^{\bullet-}$ radical for photodegradation of the azo dye Cibacron Brilliant Yellow 3 and 3,4-dichlorophenol: Optimization by application of response surface methodology, *Journal of Photochemistry and Photobiology A: Chemistry, 215*, 90-95.

Yen, J.-H., Lin, K.-H., and Wang, Y.-S. (2002). Acute lethal toxicity of environmental pollutants to aquatic organisms, *Ecotoxicology and Environmental Safety, 52*, 113-116.

Yi, W., Law, S., and Wetzstein, H. (2003). Pollen tube growth in styles of apple and almond flowers after spraying with pesticides, *The Journal of Horticultural Science and Biotechnology, 78*, 842-846.

Yu, X.-Y., Bao, Z.-C., and Barker, J. R. (2004). Free radical reactions involving Cl$^{\bullet}$, Cl$_2^{-\bullet}$, and SO$_4^{-\bullet}$ in the 248 nm photolysis of aqueous solutions containing S$_2$O$_8^{2-}$and Cl, *The Journal of Physical Chemistry A, 108*, 295-308.

Yuan, Y., Tao, H., Fan, J., and Ma, L. (2015). Degradation of *p*-chloroaniline by persulfate activated with ferrous sulfide ore particles, *Chemical Engineering Journal, 268*, 38-46.

Zadorozhnaya, O., Kirsanov, D., Buzhinsky, I., Tsarev, F., Abramova, N., Bratov, A., Muñoz, F. J., Ribó, J., Bori, J., and Riva, M. C. (2015). Water pollution monitoring by an artificial sensory system performing in terms of *Vibrio fischeri* bacteria, *Sensors and Actuators B: Chemical, 207*, 1069-1075.

Zhang, H., Cao, B., Liu, W., Lin, K., and Feng, J. (2012). Oxidative removal of acetaminophen using zero valent aluminum-acid system: efficacy, influencing factors, and reaction mechanism, *Journal of Environmental Sciences, 24*, 314-319.

Zhang, H., Choi, H. J., and Huang, C.-P. (2005). Optimization of Fenton process for the treatment of landfill leachate, *Journal of Hazardous Materials, 125*, 166-174.

Zhang, M., Ren, Y., Jiang, W., Wu, C., Zhou, Y., Wang, H., Ke, Z., Gao, Q., Liu, X., and Qiu, J. (2020). Comparative genomic analysis of iprodione-degrading *Paenarthrobacter* strains reveals the iprodione catabolic molecular mechanism in *Paenarthrobacter sp.* strain YJN-5, *Environmental Microbiology*.

Zhang, Y. Q., Du, X. Z., and Huang, W. L. (2011). Temperature effect on the kinetics of persulfate oxidation of *p*-chloroaniline, *Chinese Chemical Letters, 22*, 358-361.

Zhao, J., Zhang, Y., Quan, X., and Chen, S. (2010a). Enhanced oxidation of 4-chlorophenol using sulfate radicals generated from zero-valent iron and peroxydisulfate at ambient temperature, *Separation and Purification Technology, 71*, 302-307.

Zhao, L., Ji, Y., Kong, D., Lu, J., Zhou, Q., and Yin, X. (2016). Simultaneous removal of bisphenol A and phosphate in zero-valent iron activated persulfate oxidation process, *Chemical Engineering Journal, 303*, 458-466.

Zhao, Z., Zhang, L., Wu, J., Fan, C., and Shang, J. (2010b). Assessment of the potential mutagenicity of organochlorine pesticides (OCPs) in contaminated sediments from Taihu Lake, China, *Mutation Research/Genetic Toxicology and Environmental Mutagenesis, 696*, 62-68.

Zhou, P., Zhang, J., Zhang, Y., Zhang, G., Li, W., Wei, C., Liang, J., Liu, Y., and Shu, S. (2018). Degradation of 2,4-dichlorophenol by activating persulfate and peroxomonosulfate using micron or nanoscale zero-valent copper, *Journal of Hazardous Materials, 344*, 1209-1219.

Zhou, S., Gu, C., Qian, Z., Xu, J., and Xia, C. (2011). The activity and selectivity of catalytic peroxide oxidation of chlorophenols over Cu–Al hydrotalcite/clay composite, *Journal of colloid and interface science, 357*, 447-452.

Zhou, T., Li, Y., Ji, J., Wong, F.-S., and Lu, X. (2008). Oxidation of 4-chlorophenol in a heterogeneous zero valent iron/H_2O_2 Fenton-like system: Kinetic, pathway and effect factors, *Separation and Purification Technology, 62*, 551-558.

Zhou, T., Zou, X., Mao, J., and Wu, X. (2016). Decomposition of sulfadiazine in a sonochemical Fe^0-catalyzed persulfate system: parameters optimizing and interferences of wastewater matrix, *Applied Catalysis B: Environmental, 185*, 31-41.

APPENDICES

APPENDIX A : Control experiments.

APPENDIX B : Changes in pH values during UV-C/PS treatment of IPR.

APPENDIX C : Changes in PS concentration and pH during UV-C/PS and ZVI/PS.

APPENDIX D : Acute toxicity tests with green microalgae *P. subcapitata.*

APPENDIX E : The analysis of IPR degradation products by LC-MS.

.

APPENDIX A: Control experiments.
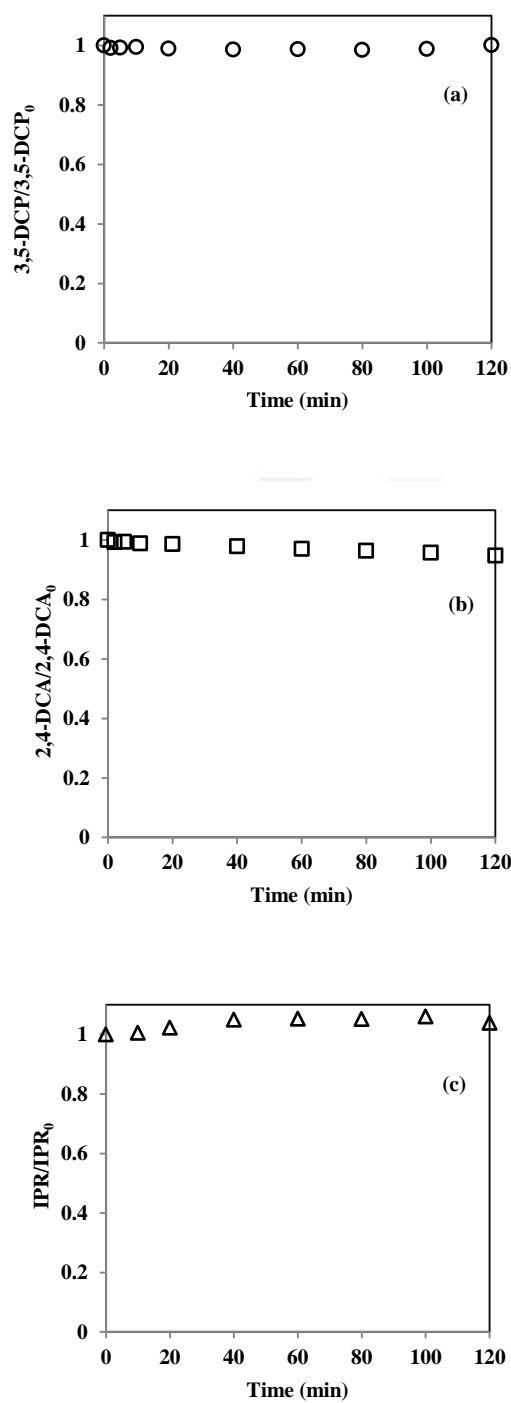
Figure A.1 : Normalized 3,5-DCP (a), 2,4-DCA (b) and IPR (c) concentrations during PS control experiment with initial pH of 6.3, 6.0 and 6.2, respectively. Each micropollutant concentration 2 mg/L; PS=1.0 mM.
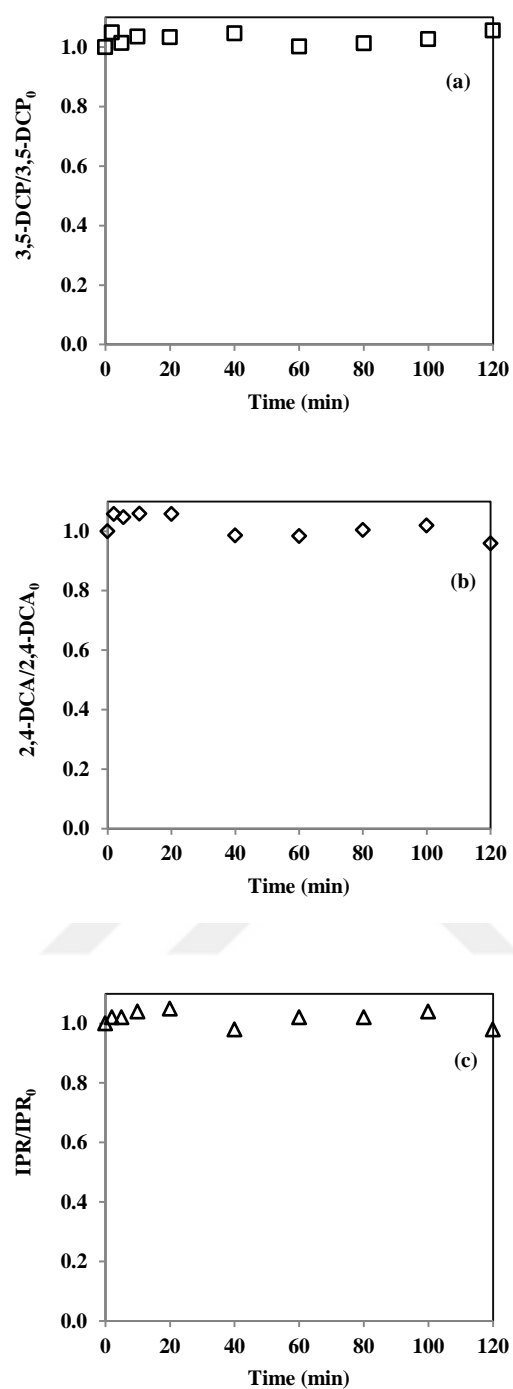
Figure A.2 : Normalized 3,5-DCP (a), 2,4-DCA (b) and IPR (c) concentrations during ZVI control experiment. Each micropollutant concentration 2 mg/L; ZVI= 1 g/L; pH=5.0.
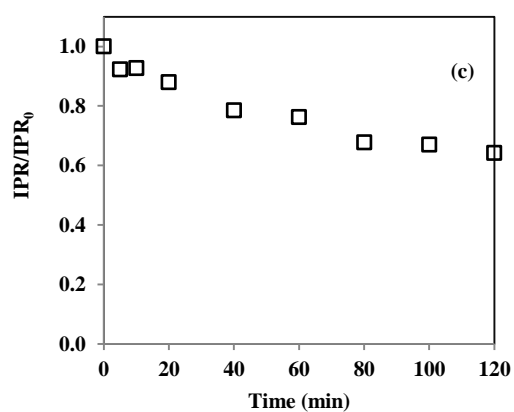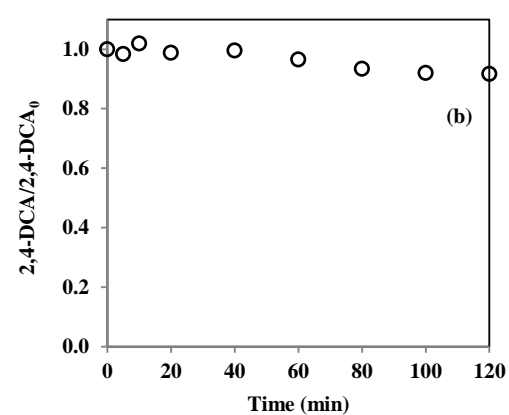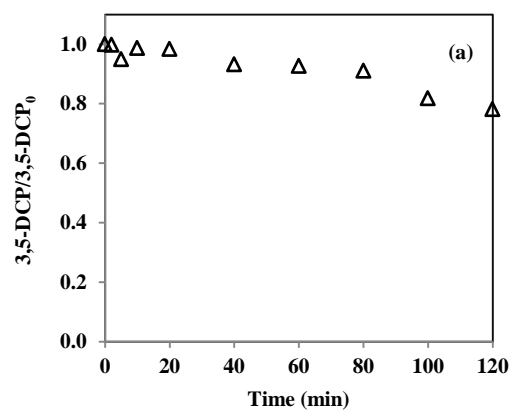
Figure A.3 : Normalized 3,5-DCP (a), 2,4-DCA (b) and IPR (c) concentrations during ZVA control experiment. Each micropollutant concentration 2 mg/L; ZVA= 1 g/L; pH=3.0.

Figure B.1 : Changes in pH values during UV-C/PS treatment of IPR at varying initial PS concentrations (IPR=2 mg/L; pH=6.2; UV-C intensity=0.5 W/L).

APPENDIX C: Changes in PS concentration and pH during UV-C/PS and ZVI/PS.

Table C.1 : Changes in PS concentration and pH during UV-C/PS and ZVI/PS treatments of 2 mg/L 3,5-DCP in SWW. Initial condition for UV-C/PS: PS=0.09 mM; UV-C intensity=0.5 W/L; pH=6.8. Initial condition for ZVI/PS treatment: PS=1.50 mM; ZVI= 1 g/L; pH=3.0.

Time (min)	UV-C/PS		ZVI/PS	
	PS (mM)	pH	PS (mM)	pH
0	0.09	6.8	1.50	3.0
2	0.09	5.0	-	-
5	0.07	3.9	-	-
10	0.06	3.9	-	-
20	0.05	3.4	1.47	-
40	0.02	3.1	0.26	-
60	0.02	3.0	0.43	-
80	0.02	3.1	0.35	-
100	0.02	3.1	0.26	-
120	0.02	3.0	0.27	2.8

APPENDIX D: Acute toxicity tests with green microalgae *P. subcapitata.*

Table D.1 : Biomass readings of original 3,5-DCP and its UV-C treated samples in SWW for 72 h incubation period. 3,5-DCP=2 mg/L; UV-C intensity=0.5 W/L; pH=6.8.

Sample	Biomass Reading, 0 h	Biomass Reading, 24 h	Biomass Reading, 48 h	Biomass Reading, 72 h	Average, 72 h	Growth Rate, 72 h	% Inhibition, 72 h
SWW	0.034	0.046	0.170	0.163			
SWW	0.036	0.050	0.169	0.188	0.168	0.022	-
SWW	-	-	0.179	0.153			
0 min	0.065	0.076	0.202	0.228	0.239	0.018	17
0 min	0.066	0.081	0.198	0.250			
10 min	-	-	0.173	0.214			
10 min	0.066	0.089	0.208	0.317	0.272	0.019	12
10 min	0.070	0.093	0.217	0.286			
20 min	0.059	0.078	0.170	0.242	0.248	0.019	15
20 min	0.071	0.086	0.176	0.253			

Table D.1 (continued) : Biomass readings of original 3,5-DCP and its UV-C treated samples in SWW for 72 h incubation period. 3,5-DCP=2 mg/L; UV-C intensity=0.5 W/L; pH=6.8.

Sample	Biomass Reading, 0 h	Biomass Reading, 24 h	Biomass Reading, 48 h	Biomass Reading, 72 h	Average, 72 h	Growth Rate, 72 h	% Inhibition, 72 h
60 min	0.058	0.070	0.134	0.196	0.243	0.017	20
60 min	0.070	0.091	0.165	0.290			
80 min	0.081	0.083	0.159	0.215	0.226	0.015	31
80 min	0.073	0.080	0.174	0.237			

Table D.2 : Biomass readings of original 3,5-DCP and its UV-C/PS treated samples in SWW for 72 h incubation period. 3,5-DCP=2 mg/L; PS=0.09 mM; UV-C intensity=0.5 W/L; pH=6.8.

Sample	Biomass Reading, 0 h	Biomass Reading, 24 h	Biomass Reading, 48 h	Biomass Reading, 72 h	Average, 72 h	Growth Rate, 72 h	% Inhibition, 72 h
0 min	0.030	0.049	0.135	0.225			
0 min	0.034	0.050	0.155	0.242	0.231	0.027	20
0 min	0.033	0.049	0.148	0.226			
10 min	0.033	0.045	0.104	0.193			
10 min	0.043	0.054	0.107	0.192	0.195	0.023	33
10 min	0.038	0.047	0.117	0.200			
20 min	0.038	0.045	0.100	0.167			
20 min	0.031	0.043	0.094	0.182	0.181	0.023	34
20 min	0.038	0.050	0.113	0.195			

Table D.2 (continued) : Biomass readings of original 3,5-DCP and its UV-C/PS treated samples in SWW for 72 h incubation period. 3,5-DCP=2 mg/L; PS=0.09 mM; UV-C intensity=0.5 W/L; pH=6.8.

Sample	Biomass Reading, 0 h	Biomass Reading, 24 h	Biomass Reading, 48 h	Biomass Reading, 72 h	Average, 72 h	Growth Rate, 72 h	% Inhibition, 72 h
60 min	0.026	0.028	0.068	0.107			
60 min	0.031	0.033	0.064	0.103	0.106	0.017	49
60 min	0.034	0.031	0.068	0.107			
80 min	0.026	0.027	0.055	0.099	0.098	0.018	47
80 min	0.028	0.031	0.060	0.097			

Table D.3 : Biomass readings of original 3,5-DCP and its ZVI/PS treated samples in SWW for 72 h incubation period. 3,5-DCP= 2 mg/L; PS=1.50 mM; ZVI=1 g/L; pH=3.0.

Sample	Biomass Reading, 0 h	Biomass Reading, 24 h	Biomass Reading, 48 h	Biomass Reading, 72 h	Average, 72 h	Growth Rate, 72 h	% Inhibition, 72 h
SWW+STS	0.070	0.115	0.707	0.887			
SWW+STS	0.074	0.123	0.692	0.852	0.819	0.034	-
SWW+STS	0.069	0.116	0.690	0.719			
0 min	0.046	0.077	0.201	0.351			
0 min	0.038	0.078	0.179	0.291	0.318	0.028	17
0 min	0.042	0.066	0.175	0.313			
10 min	0.026	0.060	0.102	0.193			
10 min	0.038	0.054	0.104	0.178	0.178	0.024	31
10 min	0.034	0.064	0.111	0.163			
20 min	0.023	0.046	0.099	0.178			
20 min	0.035	0.058	0.114	0.192	0.189	0.025	25
20 min	0.033	0.070	0.119	0.197			

Table D.3 (continued) : Biomass readings of original 3,5-DCP and its ZVI/PS treated samples in SWW for 72 h incubation period. 3,5-DCP= 2 mg/L; PS=1.50 mM; ZVI=1 g/L; pH=3.0.

Sample	Biomass Reading, 0 h	Biomass Reading, 24 h	Biomass Reading, 48 h	Biomass Reading, 72 h	Average, 72 h	Growth Rate, 72 h	% Inhibition, 72 h
60 min	0.043	0.079	0.168	0.222			
60 min	0.037	0.062	0.151	0.241	0.240	0.024	30
60 min	0.050	0.085	0.162	0.256			
80 min	0.027	0.066	0.130	0.201	0.218	0.028	19
80 min	0.033	0.065	0.144	0.235			

Table D.4 : Biomass readings of original 2,4-DCA and its UV-C treated samples in SWW for 72 h incubation period. 2,4-DCA=2 mg/L; UV-C intensity=0.5 W/L; pH=6.8.

Sample	Biomass Reading, 0 h	Biomass Reading, 24 h	Biomass Reading, 48 h	Biomass Reading, 72 h	Average, 72 h	Growth Rate, 72 h	% Inhibition, 72 h
SWW	0.051	0.059	0.170	0.163			
SWW	0.034	0.046	0.169	0.188	0.168	0.020	-
SWW	0.036	0.050	0.179	0.153			
0 min	0.066	0.084	0.212	0.196			
0 min	-	0.061	0.186	0.179	0.207	0.014	28
0 min	0.083	0.088	0.235	0.246			
10 min	0.055	0.067	0.109	0.207			
10 min	0.091	0.100	0.134	0.260	0.226	0.016	17
10 min	0.062	0.076	0.114	0.212			
20 min	0.064	0.071	0.101	0.194			
20 min	0.077	0.086	0.115	0.197	0.205	0.013	34
20 min	0.099	0.106	0.131	0.223			

Table D.4 (continued) : Biomass readings of original 2,4-DCA and its UV-C treated samples in SWW for 72 h incubation period. 2,4-DCA=2 mg/L; UV-C intensity=0.5 W/L; pH=6.8.

Sample	Biomass Reading, 0 h	Biomass Reading, 24 h	Biomass Reading, 48 h	Biomass Reading, 72 h	Average, 72 h	Growth Rate, 72 h	% Inhibition, 72 h
60 min	0.087	0.091	0.171	0.246	0.257	0.014	28
60 min	0.097	0.104	0.178	0.268			
80 min	0.090	0.098	0.162	0.232			
80 min	0.067	0.086	0.165	0.241	0.251	0.015	24
80 min	0.099	0.113	0.200	0.279			

Table D.5 : Biomass readings of original 2,4-DCA and its UV-C/PS treated samples in SWW for 72 h incubation period. 2,4-DCA=2 mg/L; PS=0.30 mM; UV-C intensity=0.5 W/L; pH=6.8.

Sample	Biomass Reading, 0 h	Biomass Reading, 24 h	Biomass Reading, 48 h	Biomass Reading, 72 h	Average, 72 h	Growth Rate, 72 h	% Inhibition, 72 h
SWW+STS	0.048	0.064	0.190	0.180	0.192	0.019	-
SWS+STS	0.050	0.069	0.193	0.204			
10 min	0.085	0.093	0.163	0.227			
10 min	0.109	0.125	0.213	0.303	0.253	0.013	30
10 min	-	-	0.153	0.229			
40 min	0.092	0.098	0.116	0.131			
40 min	0.054	0.066	0.103	0.126	0.131	0.008	57
40 min	0.072	0.085	0.124	0.137			

Table D.5 (continued) : Biomass readings of original 2,4-DCA and its UV-C/PS treated samples in SWW for 72 h incubation period. 2,4-DCA=2 mg/L; PS=0.30 mM; UV-C intensity=0.5 W/L; pH=6.8.

Sample	Biomass Reading, 0 h	Biomass Reading, 24 h	Biomass Reading, 48 h	Biomass Reading, 72 h	Average, 72 h	Growth Rate, 72 h	% Inhibition, 72 h
80 min	0.056	0.060	0.079	0.084	0.078	0.006	70
80 min	0.048	0.046	0.069	0.072			
120 min	0.047	0.051	0.070	0.075			
120 min	0.070	0.064	0.076	0.083	0.081	0.005	72
120 min	0.049	0.048	0.064	0.085			

Table D.6 : Biomass readings of original 2,4-DCA and its ZVI/PS treated samples in SWW for 72 h incubation period. 2,4-DCA=2 mg/L; PS=1.50 mM; ZVI=1 g/L; pH=5.0.

Sample	Biomass Reading, 0 h	Biomass Reading, 24 h	Biomass Reading, 48 h	Biomass Reading, 72 h	Average, 72 h	Growth Rate, 72 h	% Inhibition, 72 h
SWW+STS	0.046	0.085	0.211	0.201	0.204	0.020	-
SWW+STS	0.052	0.092	0.219	0.206			
0 min	-	-	0.194	0.198			
0 min	0.067	0.097	0.244	0.240	0.241	0.016	21
0 min	0.089	0.118	0.280	0.286			
10 min	0.093	0.109	0.281	-			
10 min	0.063	0.094	0.271	0.276	0.293	0.018	7
10 min	-	0.092	0.280	0.309			
20 min	0.046	0.072	0.089	0.093	0.104	0.011	45
20 min	0.049	0.078	0.098	0.115			

Table D.6 (continued) : Biomass readings of original 2,4-DCA and its ZVI/PS treated samples in SWW for 72 h incubation period. 2,4-DCA=2 mg/L; PS=1.50 mM; ZVI=1 g/L; pH=5.0.

Sample	Biomass Reading, 0 h	Biomass Reading, 24 h	Biomass Reading, 48 h	Biomass Reading, 72 h	Average, 72 h	Growth Rate, 72 h	% Inhibition, 72 h
40 min	0.061	0.076	0.068	0.076	0.095	0.006	68
40 min	0.059	0.077	0.075	0.114			
80 min	-	-	0.132	0.159			
80 min	0.066	0.107	0.174	0.244	0.223	0.015	23
80 min	0.082	0.114	0.187	0.266			

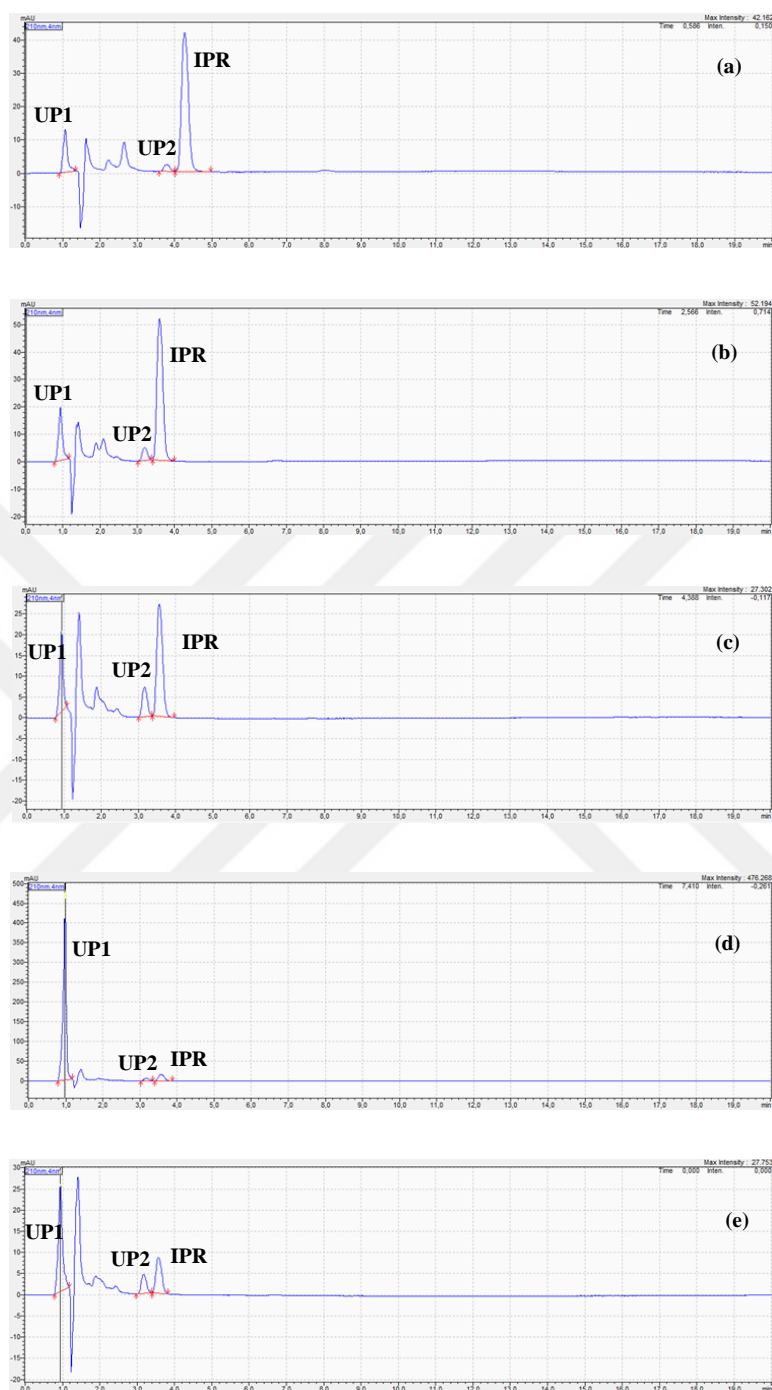**APPENDIX E:** The analysis of IPR degradation products by LC-MS.

Figure E.1 : UV-C photolysis of aqueous solution of IPR 10 mg/L for 10 min (a), 20 min (b), 60 min (c), 90 min (d) and 120 min (e). IPR=10 mg/L; pH=6.2; UV-C intensity=0.5 W/L.

Table E.1 : Retention times and main ions of IPR and its photoproducts.

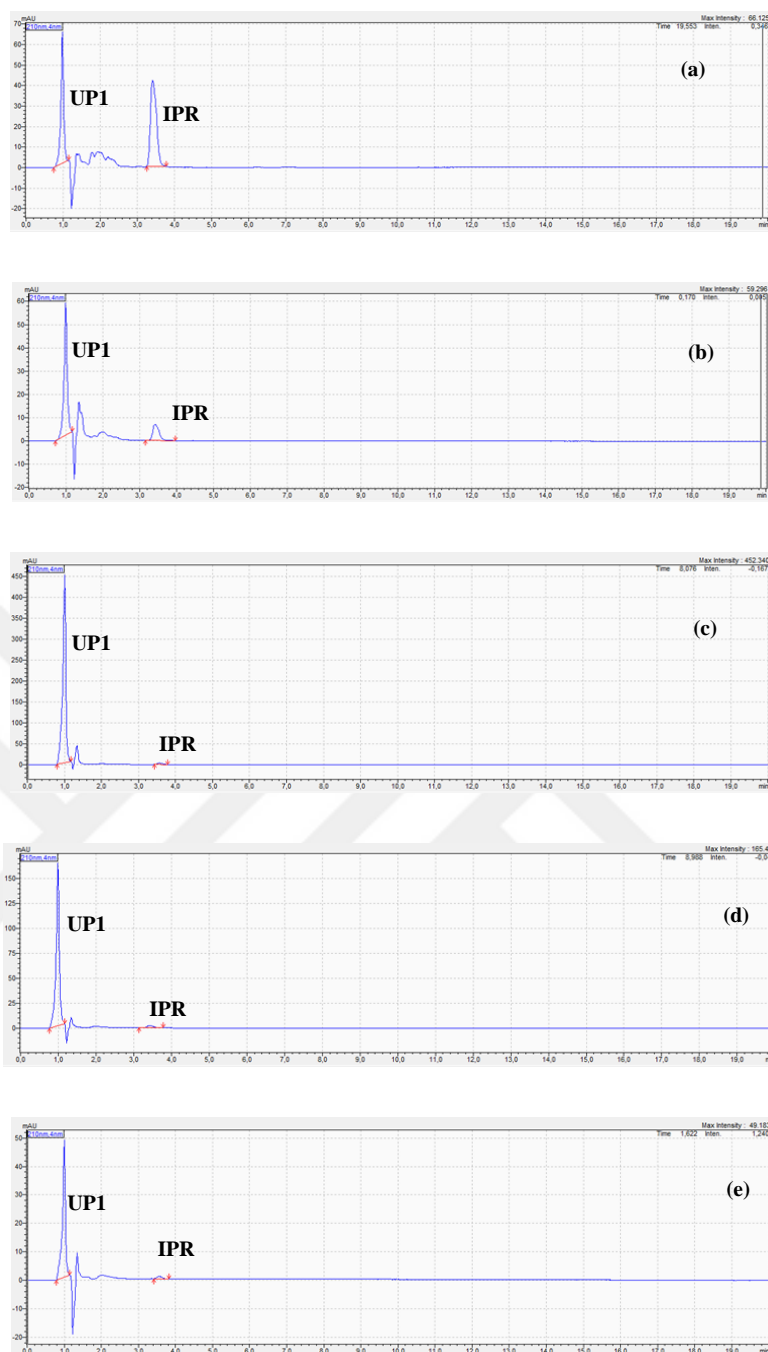| Compound	Retention time (min)	Ion (m/z)
UP1	1.0	106.1
		130.15
		284.5
UP2	3.2	187.10
		325.35
		130.15
		187.15
IPR	3.5	231.15
		295.2
		330.25

Figure E.2 : UV-C/PS treated aqueous solution of IPR 10 mg/L for 2 min (a), 10 min (b), 20 min (c), 60 min (d) and 120 min (e). IPR=10 mg/L; PS=0.30 mM; pH=6.2; UV-C intensity=0.5 W/L.

Table E.2 : Retention times and main ions of IPR and its UV-C/PS degradation products.

Compound	Retention time (min)	Ion (m/z)
UP1	1.0	106.1
		130.15
		284.5
IPR	3.5	130.15
		288
		295.3
		325.4
		373.45

CURRICULUM VITAE

Name Surname   **:** Bahareh MONTAZERI

EDUCATION:

B.Sc.   **:** 2008, Shiraz University, Faculty of Engineering, Chemical Engineering

M.Sc.   **:** 2013, University of Tehran, Faculty of Engineering, Chemical Engineering

PUBLICATIONS, PRESENTATIONS AND PATENTS ON THE THESIS:

- **Montazeri, B.**, Ucun O. K., Arslan-Alaton, I., and Olmez-Hanci, T. (2021) Iprodione removal by UV-light-, zero-valent iron- and zero-valent aluminium-activated persulfate oxidation processes in pure water and simulated tertiary treated urban wastewater, *Water*, *13*, 1679.
- **Montazeri, B.**, Ucun, O. K., Arslan-Alaton, I., and Olmez-Hanci, T. (2020) UV-C-activated persulfate oxidation of a commercially important fungicide: case study with iprodione in pure water and simulated tertiary treated urban wastewater, *Environmental Science and Pollution Research*, *27*, 22169–22183.
- Ucun, O. K., **Montazeri, B.**, Arslan-Alaton, I., and Olmez-Hanci, T. (2020) Degradation of 3,5-dichlorophenol by UV-C photolysis and UV-C-activated persulfate oxidation process in pure water and simulated tertiary treated urban wastewater, *Environmental Technology*, 1-12.
- Ucun, O. K., **Montazeri, B.**, Arslan-Alaton, I., and Olmez-Hanci, T. (2021) Treatment of industrial contaminants with zero-valent iron- and zero-valent aluminium-activated persulfate: a case study with 3,5-dichlorophenol and 2,4-dichloroaniline, *Turkish Journal of Chemistry*, *45*, 269-281.
- **Montazeri, B.**, Arslan-Alaton, I., Ucun, O. K., and Olmez-Hanci, T. (2019) Iprodione removal by Ultraviolet C-activated persulfate oxidation: assessment of reaction kinetics and degradation products, *6th European Conference on Environmental Applications of Advanced Oxidation Processes (EAAOP-6)*, Portorose, Slovenia, 26-30 June 2019.

- Ucun, O. K., **Montazeri, B.**, Arslan-Alaton, I., and Olmez-Hanci, T. (2019) Comparison of persulfate activation in heterogeneous and photochemical homogenous advanced oxidation systems for different water matrices bearing 3,5-dichlorophenol, *10th IWA International Symposium on Waste Management Problems in Agro-Industries (AGRO'2019)*, Rhode, Greece, 19-21 June 2019.

OTHER PUBLICATIONS, PRESENTATIONS AND PATENTS:

- **Montazeri, B.**, and Sarrafzadeh, M. H. (2016) Microbial Community from MTBE-Contaminated Soil for Aerobic Biodegradation of MTBE *Journal of Geoscience and Environment Protection* 4:93-99.
- **Montazeri, B.**, and Sarrafzadeh, M. H. (2014) Study of MTBE biodegradation in aerobic condition, *15th Iranian National Congress of Chemical Engineering (IChEC 2015)*, 17-19 February, 2015.